# Neural derivatives from human embryonic stem cells: a cellular and molecular model for studying the role of Orthodenticle homeobox2 in medulloblastoma progression

by

**Ravinder Kaur**

A Thesis submitted to the Faculty of Graduate Studies of

The University of Manitoba

In the partial fulfilment of the requirement of the degree of

**DOCTOR OF PHILOSOPHY**

Department of Biochemistry and Medical Genetics

University of Manitoba

Winnipeg, Manitoba, Canada

# Abstract:

Medulloblastoma (MB) is the most common malignant primary pediatric brain tumor and is divided into 4 subtypes based on different genomic alterations and gene expression profiles. This extensive heterogeneity has made it difficult to assess the functional relevance of genes to malignant progression. For example, expression of the transcription factor, Orthodenticle homeobox2 (*OTX2*) is frequently upregulated in multiple MB variants; however, its role may be subtype-specific. We recently demonstrated that neural precursors derived from transformed human embryonic stem cells (trans-hENs), but not their normal counterparts (hENs), resemble Groups 3 and 4 MBs. These trans-hENs also have >10-fold expression of OTX2. Therefore, we hypothesize that OTX2 has cell context-dependent functions in MB and using both normal and trans-hENs, we can delineate its specific roles in MB progression.

Parallel experiments with MB cells revealed that OTX2 exerts inhibitory effects on hEN and sonic hedgehog (SHH) MB cells by regulating growth, self-renewal and migration *in vitro* and tumor growth *in vivo*. Overexpression of OTX2 was accompanied by a decrease in expression of pluripotent genes such as *SOX2*. This was supported by exogenous introduction of SOX2 in OTX2+ SHH MB and hENs that rescued the OTX2 induced cellular deficits including self-renewal and cell migration. In contrast, OTX2 is oncogenic and promotes self-renewal of trans-hENs and Group 3 and 4 MBs by modulating expression of genes related to neurodevelopment and axonal guidance. OTX2 may play a central role in regulating the balance between self-renewal and differentiation in these aggressive MB cells.

Our studies underscore the value of hESC derivatives as alternatives to cell lines and heterogeneous patient samples for investigating the contribution of key developmental regulators to MB progression. Using the neural derivatives of hESCs, we have demonstrated a novel role

for OTX2 in self-renewal and migration of hENs and MB cells. Moreover, our results reveal a cell context-dependent link between OTX2 and pluripotent genes. The association between OTX2 and axonal guidance genes is important for its oncogenic role and may potentially be exploited for managing drug resistant stem cell and highly motile cellular populations in the most aggressive Group 3 and 4 MB subtypes.

# Acknowledgements

I am able to accomplish this work due to the support and guidance of many wonderful people. So, I would like to thank all of you who supported me unconditionally and made this thesis possible. First and foremost, I would like to thank my supervisor, Dr. Tamra Ogilvie for her continuous support and guidance during my entire graduate program. I am highly grateful to Dr. Ogilvie for recognizing my research potential and providing me this opportunity to work on this project. Dr Ogilvie's mentorship was not only limited to the laboratory research; she also provided guidance for developing research writing and presentation skills. Her continuous encouragement and constructive criticism helped me to accomplish the requirements of my graduate program.

I would like to take the opportunity to thank the members of my PhD advisory committee whose constructive support and guidance helped me to shape my research. I gratefully acknowledge, Dr. Mark Nachtigal, for allowing me to use his laboratory equipment, especially the PCR machine. I greatly admire his support and appreciate his guidance during my graduate program. My special thanks goes to Dr. Soheila Karimi for her consistent encouragement, support and for recognizing my research capabilities. I would like to thank Dr. Afshin Raouf for his valuable suggestions during the course of my research.

I would like to thank Dr. David Eisenstat, Adjunct Professor, University of Alberta, for accepting as an external examiner and for providing a critical review on my PhD thesis.

I sincerely acknowledge the support from Dr. Louise Simard, Professor and Department Head, University of Manitoba.

Now, I would like to acknowledge the people who helped me to achieve this stage with their expertise. I owe appreciation and gratitude to Ms. Ludivine Morrison for providing the initial laboratory training in different techniques such as cell culture, Western Blot and flow cytometry. Her tremendous help during my graduate program made me able to accomplish my research successfully. Beside these laboratory skills, I have learned organizational and management skills from her. I convey my thanks to Mr. Christopher Aiken for conducting all the *in vivo* experiments for my thesis. His patience for performing day-long surgeries and for providing training on intracranial transplantation experiments deserve great appreciation. I would like to thank Ms. Nazanin Tatari for performing immunocytochemical staining for my thesis. I would also like to thank my other labmates Ms. Lisa Liang and Ms. Margaret Stromecki for their friendly support and help whenever needed.

I would specifically like to express my thanks to the members of Dr. Shravanti Rampalli's laboratory at Centre for Inflammation and Tissue Homeostasis, Institute for Stem Cell Biology and Regenerative Medicine (inStem), India, for conducting initial chromatin immunoprecipitation studies and helping me to optimize the procedure for my research.

I sincerely convey my thanks to Dr. Mojgan Rastegar, University of Manitoba for allowing me to use her sonicator for chromatin immunoprecipitation assays. I would like to thank Robby

Zachariah for helping me with the chromatin immunoprecipitation assay and I would like to express my warm appreciation to Carl Olson for providing help whenever needed.

I would like to thank Ms. Cheryl Camia, Technician in Dr. David Merz's Laboratory for helping with the plasmid amplification procedure.

I would like to thank Elizabeth Henson from Dr. Spencer Gibson's laboratory for providing the required material as well as helping me with the luminometer for the luciferase assay.

I would like to thank Mr. Monroe Chan at the Flow Cytometry Facility for technical support.

I express my special thanks to Dr. Eftekhar Eftekharpour for his unconditional support and guidance that always filled me with self-confidence and positive energy.

My huge and warm thanks to Vasu, Pritima Vichi, Robby, Sanjida and Samantha for their friendly support. I cannot forget the coffee time spent with Nazanin. I would like to convey my thanks to the past and present members of our department office, Tuntun Sarkar, Jan Middleton, Nadia Burtniak, Cathy Webber and Philip Dufresne for their support in administrative work.

Finally, the unconditional and infinite support and encouragement of my family members need special mention. I would like to thank my parents for providing me strength during stressful conditions. Very special thanks to my mother and father in-laws for providing a helping hand for taking care of my daughter and giving me ample time to focus on my research. I convey special acknowledgement to my sisters and all other family members who always made me stress free. Words would not be sufficient to express my thanks and love to my little angel, Gurnaz Bahia, who always makes me feel full of life.

My last but the most important expression of gratitude and thanks goes to my husband-Nav. His encouragement always made me to feel strong and lifted my spirit during all the adversities. Without his unconditional love and support, I would not have made this thesis possible. Finally, I bow to the blessings of the almighty.

# Table of Content

# List of Tables

# List of Figures

# List of Abbreviations

| | |
|---|---|
| 7AAD | 7-Amino actinomycin D |
| ABC | ATP-binding cassette |
| AGCC | Affymetrix Genechip® Command Console® Software |
| Ahd2 | Aldehyde dehydrogenase family 1 subfamily A1 gene |
| ALL | Acute lymphoblastic leukemia |
| ANOVA | Analysis of variance |
| APC | Adenomatous polyposis coli |
| APC | Allophycocyanin |
| ARL | Anterior rhombic lip |
| AT/RT | Atypical rhabdoid teratoid tumor |
| ATCC | American type culture collection |
| ATOH1 | Atonal homologue 1 |
| 5-azaC | 5-Azacytidine |
| BSA | Bovine serum albumin |
| BET | Bromodomain and extraterminal domain family |
| bFGF | Basic fibroblast growth factor |
| BrdU | Bromodeoxyuridine |
| cc | Cubic centimeter |
| CDC | Cell division cycle |
| CDK | Cyclin dependent kinase |
| cDNA | Complementary DNA |
| CGNPs | Cerebral granular neural precursors |
| CHD7 | Chromodomain helicase DNA binding protein 7 |
| ChIP | Chromatin immunoprecipitation |
| CIHH | Congenital idiopathic hypogonadotropic hypogonadism |
| CK1 | Casein kinase |
| CMV | Cytomegalovirus |
| CNTN | Contactin |
| cRNA | Complementary RNA |
| CSF | Cerebral spinal fluid |
| CTNNB1 | β-catenin gene |
| DDX3X | DEAD-box RNA helicase |
| DIPGs | Diffuse intrinsic pontine gliomas |
| DMEM | Dulbecco's modified eagle medium |
| DNA | Deoxy-ribonucleic acid |
| DPBS | Dulbecco's phosphate-buffered saline |
| dpc | Day post-coitum |
| DSH | Dishevelled |
| ECR2 | Evolutionary conserved enhancer element2 |
| EDTA | Ethylenediaminetetraacetic acid |
| EGF | Epidermal growth factor |
| EGL | External granular layer |
| EFN | Ephrin ligand |
| EMEM | Eagle's minimum essential media |

| | |
|---|---|
| En1/2 | Engrailed-1/2 |
| EPH | EPH receptor for EPH/ephrin signaling |
| FACS | Fluorescent activated cell sorting |
| FBS | Fetal bovine serum |
| FDA | Food and drug administration |
| FGF8 | Fibroblast growth factor 8 |
| FOS | FBJ murine osteosarcoma virus oncogene homolog |
| FZD | Frizzled |
| GABA | Gamma-Aminobutyric acid |
| GAP43 | Growth associated protein 43 |
| GAPDH | Glyceraldehyde 3-phosphate dehydrogenase |
| Gbx2 | Gastrulation brain homoebox 2 |
| GFP | Green fluorescent protein |
| Gli1/2/3 | Glioma-associated oncogene family transcription factors |
| GnRH | Gonadotrophin releasing hormone |
| Grg4 | Groucho-related-gene family |
| GSK-3β | Glycogen synthase kinase |
| GTPase | Guanosine triphosphatase |
| HD | Huntington disease |
| hENs | Human embryonic neural precursors |
| HEPES | 4-(2-hydroxyethyl)-1-piperazineethanesulfonic acid |
| HES | Hairy and enhancer of split |
| hESCs | Human embryonic stem cells |
| hGFAP | Human glial fibrillary acidic protein |
| IGL | Internal granular layer |
| IPA | Ingenuity pathway analysis |
| iPSCs | Induced pluripotent stem cells |
| JAKMIP2 | Janus kinase microtubule interacting protein 2 |
| KD | Knockdown |
| KDM | Lysine specific demethylase |
| Kg | Kilogram |
| KMT | Lysine specific methyltransferase |
| L1CAM | L1 cell adhesion molecule |
| Lefty | Left-right determination factors |
| LentiORF | Lentiviral open reading frame |
| LiCl | Lithium chloride |
| Lmx1a | LIM homeodomain transcription factor 1 alpha |
| MAP | Microtubule-associated proteins |
| Mash1 | Mammalian achaete scute homolog-1 (also known as Ascl1) |
| MATH 1 | A basic helix-loop-helix transcription factor |
| MB | Medulloblastoma |
| MBEN | Medulloblastoma with extensive nodularity |
| mDA | Mesencephalon/midbrain dopaminergic neurons |
| Mdkk1 | Mouse dickkopf-related protein 1 |
| miRNA | MicroRNA |
| ml | Millilitre |

| | |
|---|---|
| mg | Milligram |
| µg | Microgram |
| µl | Microliter |
| mm | Millimeter |
| µm | Micrometer |
| µM | Micromolar |
| MLL | Mixed-lineage leukemia |
| MMP | Matrix metalloproteinase |
| MOI | Multiplicity of infection |
| MRI | Magnetic resonance imaging |
| mTOR | Mammalian target of rapamycin |
| MYC | Myelocytomatosis |
| NaCl | Sodium chloride |
| $NaHCO_3$ | Sodium bicarbonate |
| NCAM | Neural cell adhesion molecule |
| NEUROD | Neuronal differentiation gene |
| Ngn2 | Neurogenin2 |
| Ng | Nanogram |
| nM | Nanomolar |
| NOD SCID | Nonobese diabetic/severe combined immunodeficiency |
| OCT4/POU5F1 | POU class 5 homeobox 1 |
| OCT | Optimum cutting temperature |
| OTX2 | Orthodenticle homeobox2 |
| PCA | Principal component analysis |
| PDGFRA | Platelet-derived growth factor receptor α |
| PE | Phycoerythrin |
| PI3K/Akt | Phosphatidylinositol 3-kinase and protein kinase B |
| PLC | Phospholipase C |
| pLOC | Precision lentiORF collection |
| PNETs | Primitive neuro-ectodermal tumors |
| PR | Photoreceptor |
| PS | Phosphatidylserine |
| Ptch1 | Patched 1 |
| PTEN | Phosphatase and tensin homolog |
| qPCR | Quantitative real time polymerase chain reaction |
| RFP | Red fluorescent protein |
| RHOA | Ras homolog gene family, member A |
| RNA | Ribo-nucleic acid |
| RPE | Retinal pigmented epithelium |
| RT | Room temperature |
| SCL/TAL1 | Stem cell leukemia/T-cell acute lymphocytic leukemia 1 |
| SDS | Sodium dodecyl sulphate |
| SEMA | Semaphorin |
| SHH | Sonic hedgehog |
| shRNA | Short hairpin RNA |
| siRNA | Small interference RNA |

| | |
|---|---|
| SMARCA4 | ATP-dependent helicase SWI/SNF related, matrix associated actin dependent regulator of chromatin subfamily a, member 4 |
| Smo | Smoothened |
| SnRNA | Small nuclear RNA |
| SOX2/6 | Sex determining region Y-box 2/6 |
| SPGA | Secrete-Pair™ Gaussia Luciferase Assay |
| SSEA3 | Stage specific embryonic antigen 3 |
| Sufu | Suppressor of fused |
| TBS | Tris buffer saline |
| TCF/LEFs | T cell factor/lymphoid enhancer factors |
| TE | Tris EDTA buffer |
| TIMP4 | Tissue inhibitor of metalloproteinases |
| TP53 | Tumor protein 53 |
| Trans-hENs | Transformed human embryonic neural precursors |
| Trans-hESCs | Transformed human embryonic stem cells |
| TSS | Transcription start site |
| UNC | Uncoordinated |
| VTA | Ventricular zone |
| VZ | Ventral tegmental area |
| v/v | Volume/volume |
| w/v | Weight/volume |
| WNT | Wingless/Integrated |
| Zfp503 | A zinc finger protein503 or Nolz1 |

# List of Copyright Material

1. **Kaur R**, Aiken C, Morrison LC, Rao R, Del Bigio MR, Rampalli S, Werbowetski-Ogilvie T. 2015. OTX2 exhibits cell-context dependent effects on cellular and molecular properties of human embryonic neural precursors and Medulloblastoma cells. *Disease Models and Mechanisms*, 8(10): 1295-1309.

# CHAPTER 1: INTRODUCTION

## 1.1 Overview

Medulloblastoma (MB) is the most common malignant primary pediatric brain tumor. It consists of four molecular subtypes: wingless (WNT), sonic hedgehog (SHH), Group 3 and Group 4 that are distinguished based on different genetic alterations, gene expression profiles and response to treatment (Figure 1.1). However, the functional relevance of frequently dysregulated and mutated genes to MB progression is poorly understood. For example, a homeodomain transcription factor, orthodenticle homeobox2 (*OTX2*) is frequently amplified and overexpressed in multiple MB subgroups; however, it may function in a subgroup-specific manner. Our goal is to understand the context-dependent role of OTX2 in regulating the features of MB brain tumor cells representing the different subgroups. To achieve this, I aimed to utilize neural precursors derived from normal and transformed human embryonic stem cells (hESCs) as a cellular model for investigating the role of OTX2 in MB (Werbowetski-Ogilvie et al. 2009; Werbowetski-Ogilvie et al. 2012). In our laboratory, the characteristics of both normal (hENs) and transformed human embryonic neural precursors (trans-hENs) have been well studied using *in vitro* and *in vivo* techniques. It has been shown that the trans-hENs, but not their normal counterparts, mimic Group 3 and 4 MBs both *in vitro* and *in vivo*. These trans-hENs also exhibit >12 fold overexpression of *OTX2* (Werbowetski-Ogilvie et al. 2012). These properties make them a relevant and comparative cellular system for studying specific functions of OTX2.

To provide a comprehensive overview of my research project, I will first discuss the genetic, molecular and cellular heterogeneity within the MB subgroups. I will briefly explain the features of each molecular subgroup and associated treatment options. In the second part of the introduction, I will describe the known functions of OTX2 in normal brain development as well as in neuronal cell fate specifications. Finally, I will discuss the potential of hESCs and induced pluripotent stem cells (iPSCs) for modelling various human diseases. I will then describe the

studies from our laboratory demonstrating the use of neural derivatives from hESCs as a model system for investigating gene functions related to MB.

### 1.2 Medulloblastoma

Central nervous system tumors are the second most prevalent cancers in children after leukaemia and account for nearly 20% of all new cases (Canadian Cancer Society Statistics, 2015). These constitute a group of highly malignant cancers that manifest early during development such as MB, primitive neuro-ectodermal tumors (PNETs) and atypical rhabdoid teratoid tumor (AT/RT) (Mehta et al. 2011) (Pui et al. 2011; Siegel, Naishadham, and Jemal 2012). Current treatments such as surgery, cranio-spinal radiotherapy and chemotherapy have improved 5-years overall survival rates up to 70-80% in patients with standard-risk disease (Packer et al. 2006; Gajjar et al. 2006; Tarbell et al. 2013). However, 5-year event-free survival remains at 25-40% in high-risk patients (Pizer and Clifford 2009; Taylor et al. 2005). In these high-risk patients, MB often recur as a consequence of tumor cell infiltration into the brain following neurosurgery and/or metastasis through the cerebrospinal fluid (CSF) at the time of diagnosis (Northcott et al. 2012; Lau et al. 2012; Ramaswamy et al. 2013). Despite a multitude of therapies including resection, radiation and high-dose chemotherapy, the majority of patients typically suffer from permanent cognitive, developmental, neuroendocrine and physical dysfunctions attributed to the treatment related long-term toxicities on their developing nervous systems (Northcott et al. 2012). In fact, studies have shown that 47% of MB patients who underwent surgical resection exhibit long-term difficulties with psychological functioning as well as problems with driving and independent living (Zeltzer et al. 2008; Frange et al. 2009). High-risk patients with metastatic disease undergo complete craniospinal radiation treatment

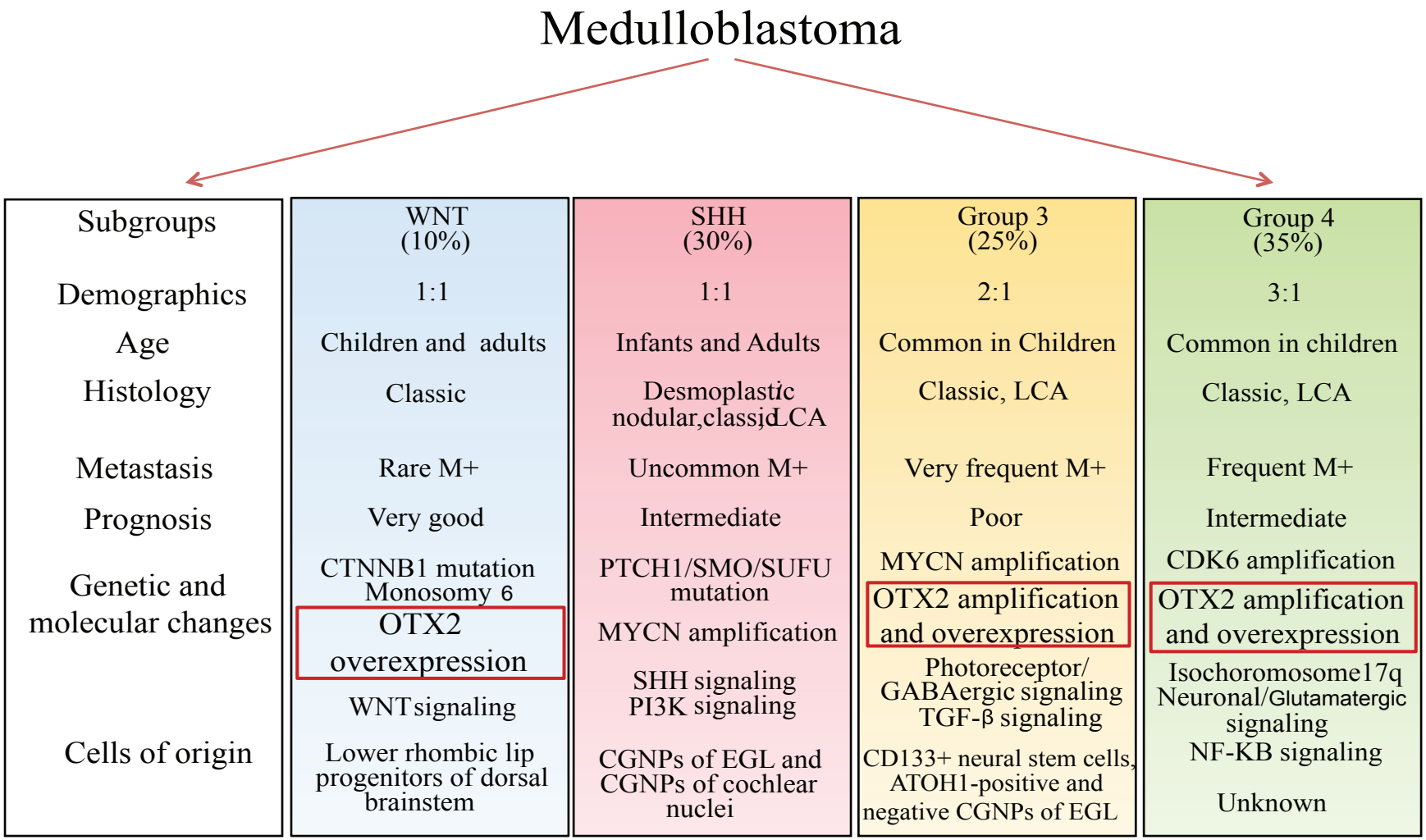


**Figure 1.1: Molecular subgroups of medulloblastoma:** WNT, SHH, Group 3 and Group 4 based on different genetic alterations, gene expression profiles and cells of origin. OTX2 amplifications and/or overexpression are more commonly linked to aggressive Group 3 and 4 tumors (Adapted from Taylor et al. 2012 and Faria et al. 2013).

that may result in serious cognitive deficits in intellectual function, academic achievement and learning delays (Palmer, Reddick, and Gajjar 2007).

Recent advances in genomic sequencing and microarray technologies have not only revolutionized our understanding of pediatric brain tumor heterogeneity but also identified underlying genetic and molecular events that contribute to the development of these tumors (Taylor et al. 2012; Northcott et al. 2012). For example, high throughput genomic studies have shown that MB is not a single disease. Instead, it consists of 4 molecular subtypes: WNT, SHH, Group 3 and Group 4. These variants can be distinguished based on the differences in their demographic distribution, clinical features at the time of diagnosis, genomic alterations, gene expression profiles, cell of origin and response to treatment (Taylor et al. 2012) (Figure 1.1). Recent update to the WHO classification now divide MB into 5 groups: WNT activated, SHH-activated with tumor suppressor (TP)53-mutant and SHH-activated TP53-wildtype, non-WNT/non SHH Group 3 and Group 4 tumors (Louis et al. 2016). These subgroups will likely continue to be evolved as we learn more about the biology of different subgroups.

### 1.2.1 WNT subgroup

The WNT subgroup is named after the upregulated WNT signaling pathway that accompanies this rare MB type and accounts for approximately 10% of MB cases. This subgroup is known for its excellent prognosis with >90% of patients surviving long-term (Gajjar and Robinson 2014; DeSouza et al. 2014; Taylor et al. 2012).

#### 1.2.1.1 Demographic distribution

WNT tumors have equal distribution between males and females (1:1) with a slight male to female predominance (Taylor et al. 2012). These tumors commonly occur in children older than 3 years with a peak incident rate at 10-12 years of age and are rarely observed in infants (Northcott et al. 2011; Northcott et al. 2012; Gajjar and Robinson 2014). WNT MBs are located in the midline of brain, occupy the fourth ventricle and infiltrate the brain stem but rarely metastasize (Gajjar and Robinson 2014).

#### 1.2.1.2 Histology

Mostly, WNT MBs comprise classic histological features; however, tumors with large cell anaplastic features have been observed, albeit rarely (Gilbertson and Ellison 2008). Classic histological features include the presence of small, undifferentiated round or ellipsoid cells with high nuclear-to-cytoplasmic ratio and round to oval or triangular hyperchromatic nuclei (Gilbertson and Ellison 2008; DeSouza et al. 2014). Around 40% of classic MBs that exhibit neuronal differentiation are associated with neuroblastic rosettes known as "Homer-Wright rosettes" in which tumor cell nuclei are arranged in a circular manner around fine tangled cytoplasmic processes (Gilbertson and Ellison 2008). Immunostaining for nuclear beta-catenin is used to identify WNT tumors (DeSouza et al. 2014).

#### 1.2.1.3 Genetic and molecular alterations

As the name suggests, WNT tumors are identified by genetic and molecular changes in the genes associated with the WNT signaling pathway. WNT/β- catenin signaling has an important role in defining the midbrain-hindbrain boundary during brain development (Thomas

and Capecchi 1990; McMahon et al. 1992; Ikeya et al. 1997), regulating self-renewal of neural precursors during neurogenesis (Lie et al. 2005) and playing a role in synaptogenesis (Hall, Lucas, and Salinas 2000; Rosso and Inestrosa 2013). There are canonical and non-canonical WNT signaling pathways. The canonical WNT signaling is β-catenin dependent but the non-canonical WNT pathways such as planar cell polarity and WNT-$Ca^{2+}$pathway are independent of β-catenin (Gomez-Orte et al. 2013). As the canonical WNT signaling is mainly associated with WNT MBs, I will describe the normal WNT signaling pathway as well as the associated genetic and molecular events in the components of WNT signaling that contribute to the development of WNT MBs.

Briefly, the canonical WNT pathway is mediated by a cytoplasmic protein β-catenin. The stability of β-catenin is regulated by a destruction complex consisting of multiple proteins such as dishevelled (DSH), AXIN, adenomatous polyposis coli (APC), glycogen synthase kinase (GSK-3β) and casein kinase (CK1) (Baryawno et al. 2010; Manoranjan et al. 2012; DeSouza et al. 2014) (Figure 1.2A). In the absence of WNT ligands, the destruction complex triggers the phosphorylation of β-catenin by GSK-3β and CK1 with subsequent ubiquitination and degradation of β-catenin (Chenn 2008). On the other hand, activation of the WNT pathway by binding of WNT ligands to the extracellular domain of both LDL-receptor-related protein 5/6 (LRP) and frizzled (FZD) receptors results in nuclear accumulation of β-catenin. In the nucleus, β-catenin interacts with the family of transcription factors known as T cell factor/lymphoid enhancer factors (TCF/LEFs). These factors form a complex with Groucho and histone acetylases and remain suppressed (Baryawno et al. 2010; Manoranjan et al. 2012; DeSouza et al. 2014). Once activated by β-catenin, the TCF/LEFs complex increase the transcription of target genes such as cyclin D1 (Shtutman et al. 1999; Tetsu and McCormick 1999) and

myelocytomatosis (*MYC*) (He et al. 1998; Chenn 2008), involved in regulating cellular functions such as cell division, proliferation and cell-cell adhesion (Manoranjan et al. 2012) (Figure 1.2A).

In contrast to its normal function, aberrant activation of WNT/β-catenin signaling is typically attributed to mutations in the *APC* (Huang et al. 2000), β-catenin (*CTNNB1*) (Northcott et al. 2012; Robinson et al. 2012; Jones et al. 2012; Pugh et al. 2012), *AXIN1* (Baeza et al. 2003) and *AXIN2* genes (Koch et al. 2007). These mutations may predispose to the primary brain tumor MB. More than 90% of WNT MBs harbour a point mutation on exon 3 of the *CTNNB1* gene and this promotes the stabilization as well as nuclear localization of β-catenin leading to constitutive activation of WNT signaling (Northcott et al. 2012; Gajjar and Robinson 2014; Schroeder and Gururangan 2014) (Figure 1.2B). Deletion of one copy of chromosome 6 is also a frequent event in WNT MBs (Northcott et al. 2012; Gajjar and Robinson 2014; Schroeder and Gururangan 2014). Therefore, both nuclear staining for β-catenin and monosomy 6 are commonly used to diagnose WNT MBs (DeSouza et al. 2014). In addition to the mutations in WNT signaling pathway members, an autosomal dominant condition known as "Turcot syndrome" may also increase the risk of developing colorectal cancer and brain tumors such as MB (Northcott et al. 2012; Schroeder and Gururangan 2014). Turcot syndrome has two subtypes and individuals with the type II syndrome may develop MB as a result of an inactivating germline mutation in *APC*. *APC* mutations lead to a truncated protein that lacks regulatory activity causing nuclear accumulation of β-catenin and constitutive activation of WNT signaling (Northcott et al. 2012; da Silva et al. 2013; Huang et al. 2000). *APC* mutations also occur in a small fraction of sporadic MBs that usually lack β-catenin mutation (Huang et al. 2000), indicating that mutations in these two genes are mutually exclusive events in MB. Additional mutations in genes such as DEAD-box RNA helicase (*DDX3X*), which functions to enhance the transactivating ability of β-catenin,

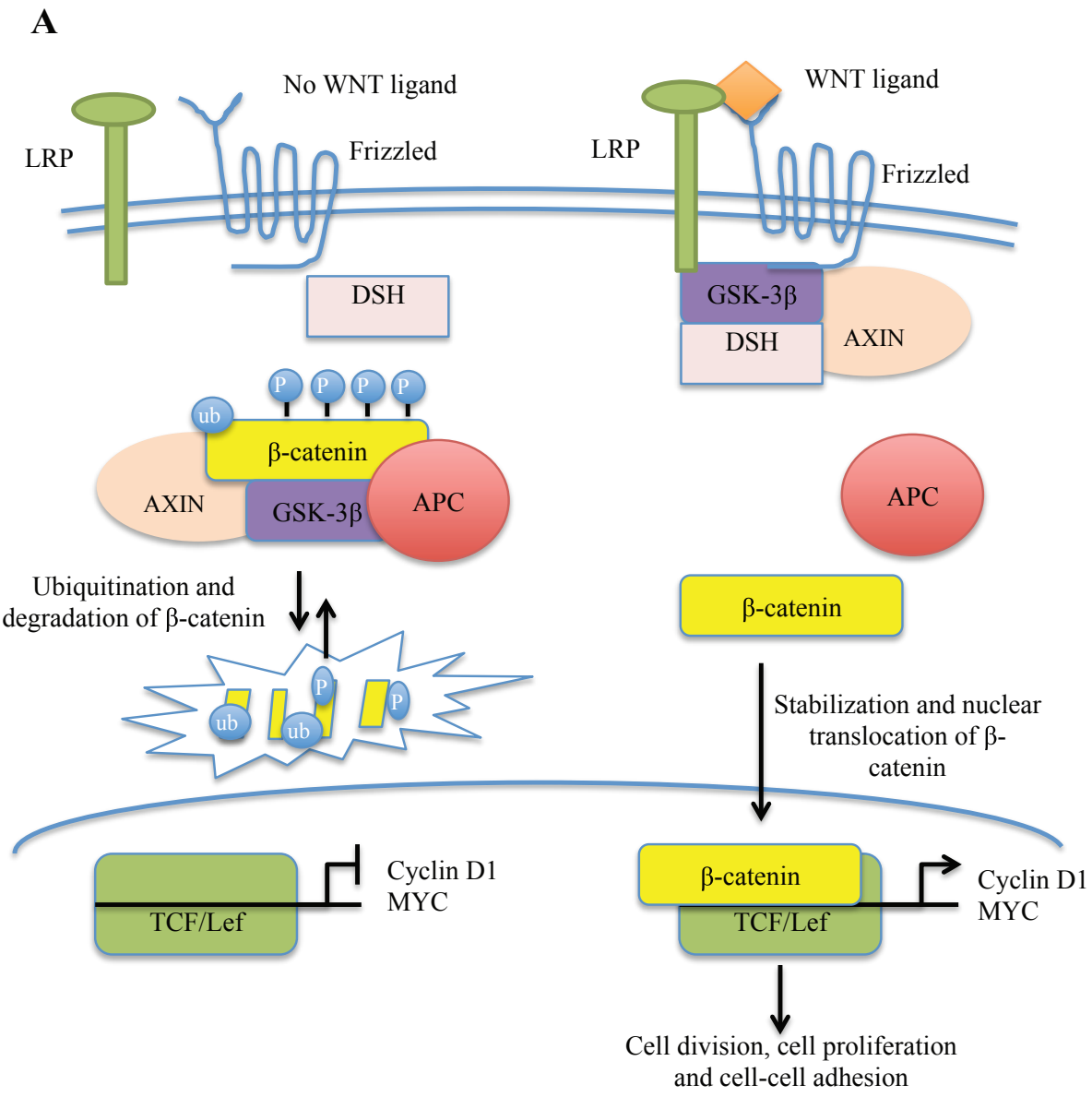


**Figure 1.2A: Normal WNT signaling pathway:** The WNT pathway functions via the cytoplasmic protein β-catenin. β-catenin is degraded in the cell by a complex of proteins such as adenomatous polyposis coli (APC), AXIN and glycogen synthase kinase (GSK)-3β. Binding of WNT ligand to the frizzled receptor (FZD) triggers the stabilization and nuclear translocation of β-catenin with subsequent activation of downstream target genes such as Cyclin D1 and MYC for controlling cellular functions (DeSouza et al. 2014).

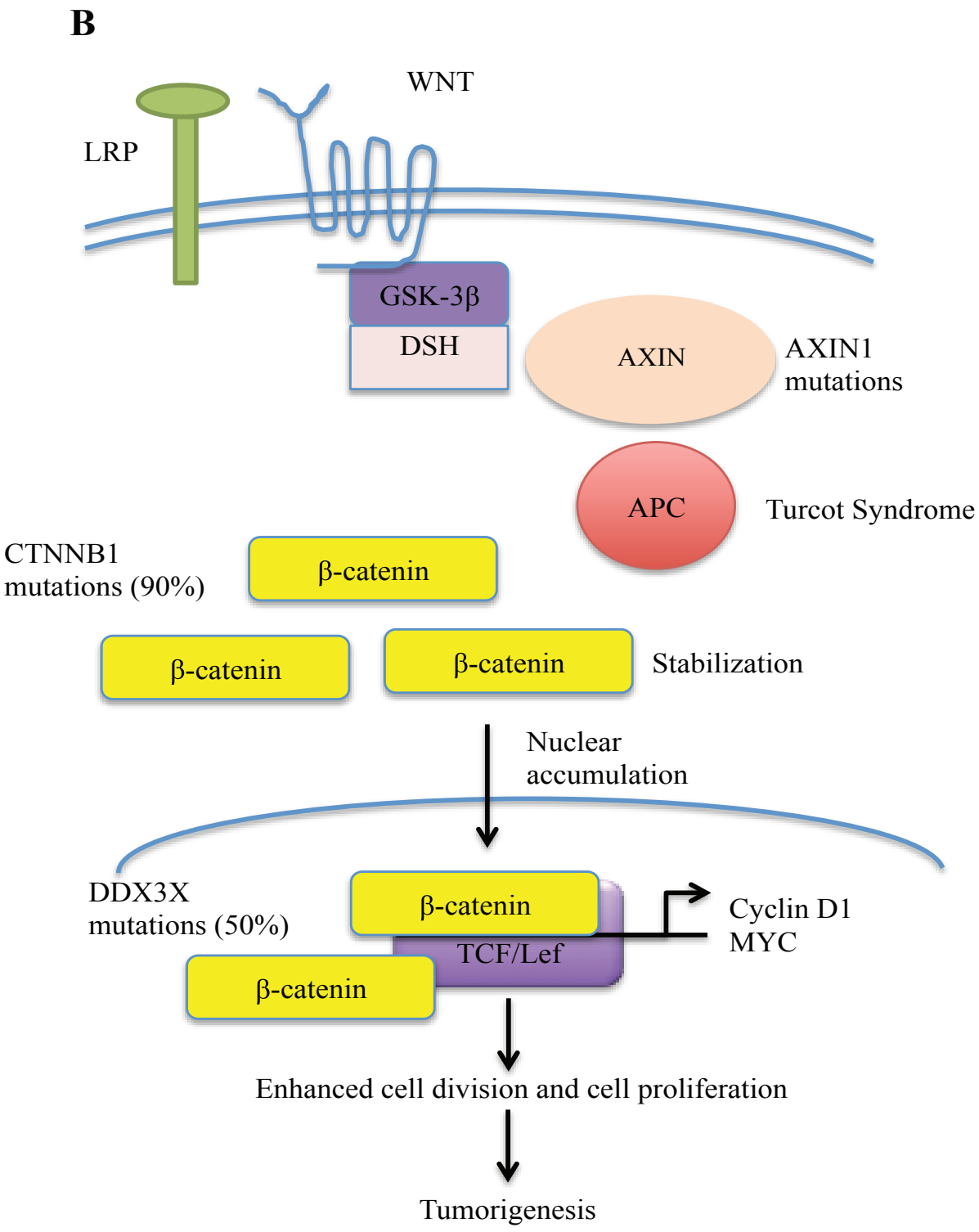


**Figure 1.2B: Aberrant WNT signaling pathway:** Mutations in components of the WNT signaling pathway result in aberrant activation leading to increased expression of target genes and abnormal cellular functions.

are observed in 50% of WNT MB cases. Finally, mutations in ATP-dependent helicase SWI/SNF related, matrix associated actin dependent regulator of chromatin subfamily a, member 4 (*SMARCA4*) (26.3%) and *TP53* (12.5%) have also been identified in WNT MB cases.

#### 1.2.1.4 Neural progenitors as cells of origin for WNT MB

Gibson et al. have shown that the MB subtypes have distinct cells of origin and WNT tumors are thought to arise from the lower rhombic lip progenitors of the dorsal brainstem. An activating mutation in the *Ctnnb1* gene that encodes the cytoplasmic protein, β-catenin, disrupts the normal differentiation and migration of these progenitor cells on the dorsal brainstem and results in an abnormal accumulation of cells (Gibson et al. 2010). When *Ctnnb1* mutation is compounded with *Trp53* deletion, mice develop tumors that recapitulate the anatomical location and gene expression profiles of human WNT MBs (Gibson et al. 2010).

#### 1.2.1.5 Treatment options

Standard surgical resection, radiation and chemotherapy are being used to treat WNT MBs (DeSouza et al. 2014). However, the 5-year survival rate is much better for WNT tumors; thus, reduced radiation and chemotherapy are recommended for patients with non-metastatic disease following confirmation of WNT subgroup identity (Northcott et al. 2012). In order to develop more specific treatments for WNT tumors, a complete understanding of the genes and signaling pathways involved in tumor progression will be necessary. For example, molecular cross-talk between WNT and the phosphatidylinositol 3-kinase/a serine/threonine kinase also known as protein kinase B (PI3K/Akt) pathway plays a major role in the pathophysiology of WNT tumors. Targeting WNT signaling may therefore not be sufficient for therapeutic

interventions. For example, Baryawno et al, have shown that small molecule inhibitors targeting PI3K/Akt signaling activate GSK-3β and cytoplasmic degradation of β-catenin, which in turn reduced the expression of Cyclin D1 and *MYC* (Baryawno et al. 2010). This led to decreased growth of established MBs in xenograft mouse models (Baryawno et al. 2010). Recently, a naturally occurring anti-tumor compound called cantharidin has been identified in beetles with anti-tumor properties, and has been shown to reduce intracranial tumor growth in mice by inhibiting WNT signaling (Cimmino et al. 2012). This compound is known to inhibit phosphatase 1 and 2A, which function to induce the stabilization of β-catenin (Yang et al. 2003). Although patients with WNT MBs have a better long-term survival, more targeted treatments may eliminate the therapy related side effects.

### 1.2.2 SHH subgroup

SHH MB accounts for almost 30% of cases and is one of the most well studied MB subtypes. These tumors have an intermediate prognosis with an overall survival rate of 75%, which may differ according to the age of the patient, metastatic status and underlying molecular abnormalities (Kool et al. 2012; Cho et al. 2011; Ellison et al. 2011; Northcott et al. 2011). Patients with recurrent disease have a much worse prognosis (Robinson et al. 2015).

#### 1.2.2.1 Demographic distribution

SHH MBs have similar male to female incidence rates with a slight predominance in males (Taylor et al. 2012). These tumors are more common in infants and adults but children aged 4-15 years are typically less affected by this disease (Taylor et al. 2012). SHH tumors

mostly originate in cerebellar hemispheres but some do arise in the midline of the brain (Gibson et al. 2010; Grammel et al. 2012).

#### 1.2.2.2 Histology

SHH MBs exhibit mostly desmoplastic histological features with few cases of classic and large cell anaplastic histology (Northcott et al. 2012). Desmoplastic MB consists of pericellular deposition of reticulin and is often immunopositive for synaptophysin, indicative of neuronal differentiation (Gilbertson and Ellison 2008; Northcott et al. 2012). A nodular phenotype is also observed consisting of differentiated neural cells, negligible proliferation, scattered apoptotic cells and internodular desmoplasia (Gilbertson and Ellison 2008). Some nodular/desmoplastic tumors acquire large and numerous nodules and are termed as medulloblastoma with extensive nodularity (MBEN). MBENs arise in infants under 3 years of age and typically have a good prognosis (Giangaspero et al. 1999; Ellison 2002; Gilbertson and Ellison 2008). A few cases of SHH MBs also show the presence of large cells with round nuclei or classic histology (Gajjar and Robinson 2014; DeSouza et al. 2014).

#### 1.2.2.3 Genetic and molecular alterations

Many transgenic, knockout and conditional knockout mouse models have been generated for understanding the genetic and molecular events that contribute to the development and/or progression of SHH MBs. Nearly all the genetic manipulations in SHH pathway genes such as deletion of Patched1 (*Ptch1*), activation of Smoothened (*Smo*) and deletion of Suppressor of fused (*Sufu*) lead to the perturbation of the SHH signaling pathway and consequent neoplastic transformation of normal cells. Human SHH MBs typically display high levels of downstream

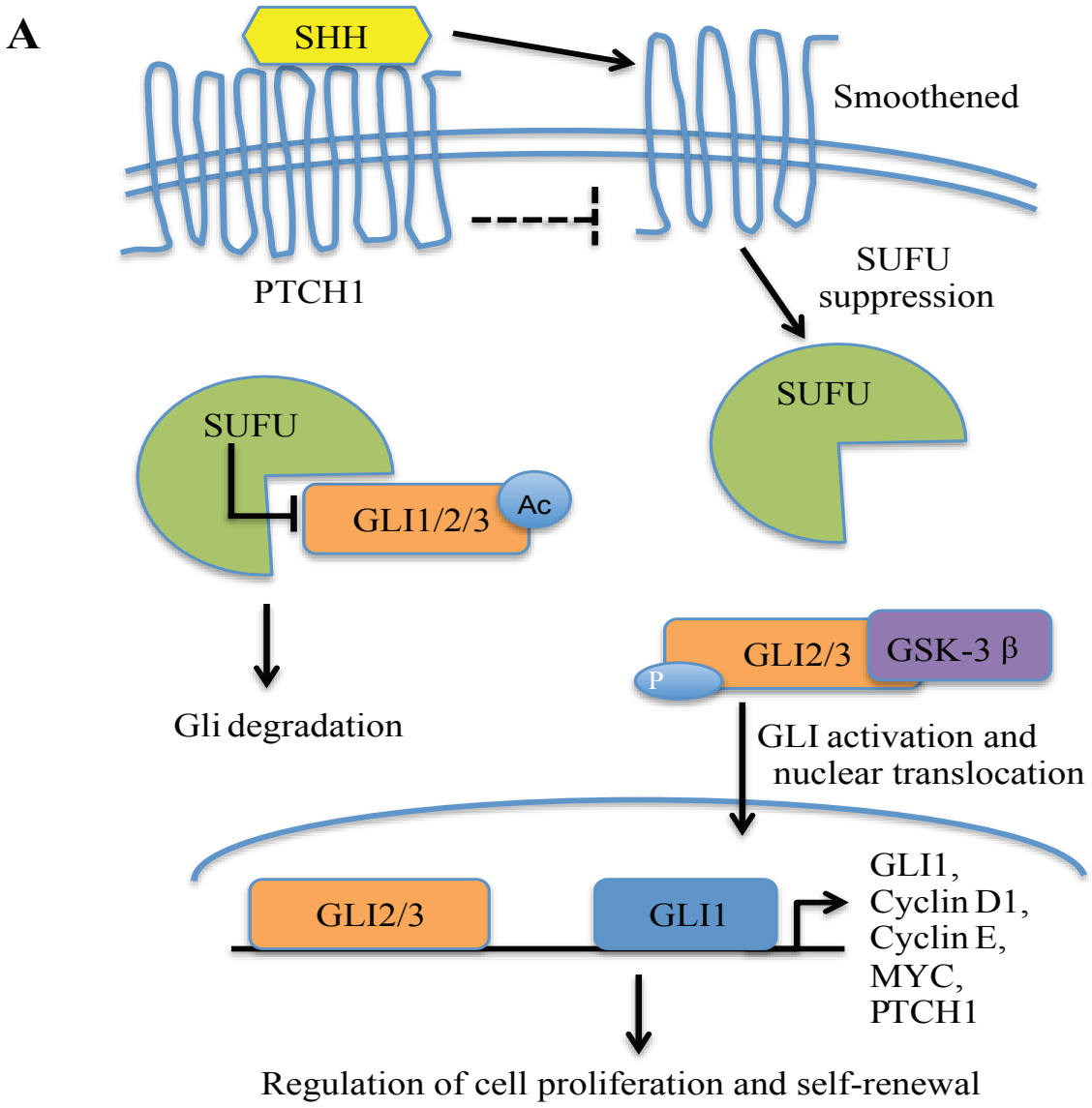


**Figure 1.3A: Normal sonic hedgehog (SHH) signaling pathway:** SHH signaling is crucial for the proliferation of cerebellar granule neural precursors (CGNPs) of the external granular layer (EGL) of the developing cerebellum. In an inactive state, the transmembrane protein PTCH1 suppresses SMO. Binding of SHH ligand secreted by Purkinje cells, underneath the EGL, relieves PTCH1-mediated inhibition of SMO, thereby initiating a cascade of events such as activation and nuclear translocation of GLI proteins followed by expression of downstream target genes such as cyclin D1, cyclin E and MYC that regulate cell proliferation and self-renewal of CGNPs.

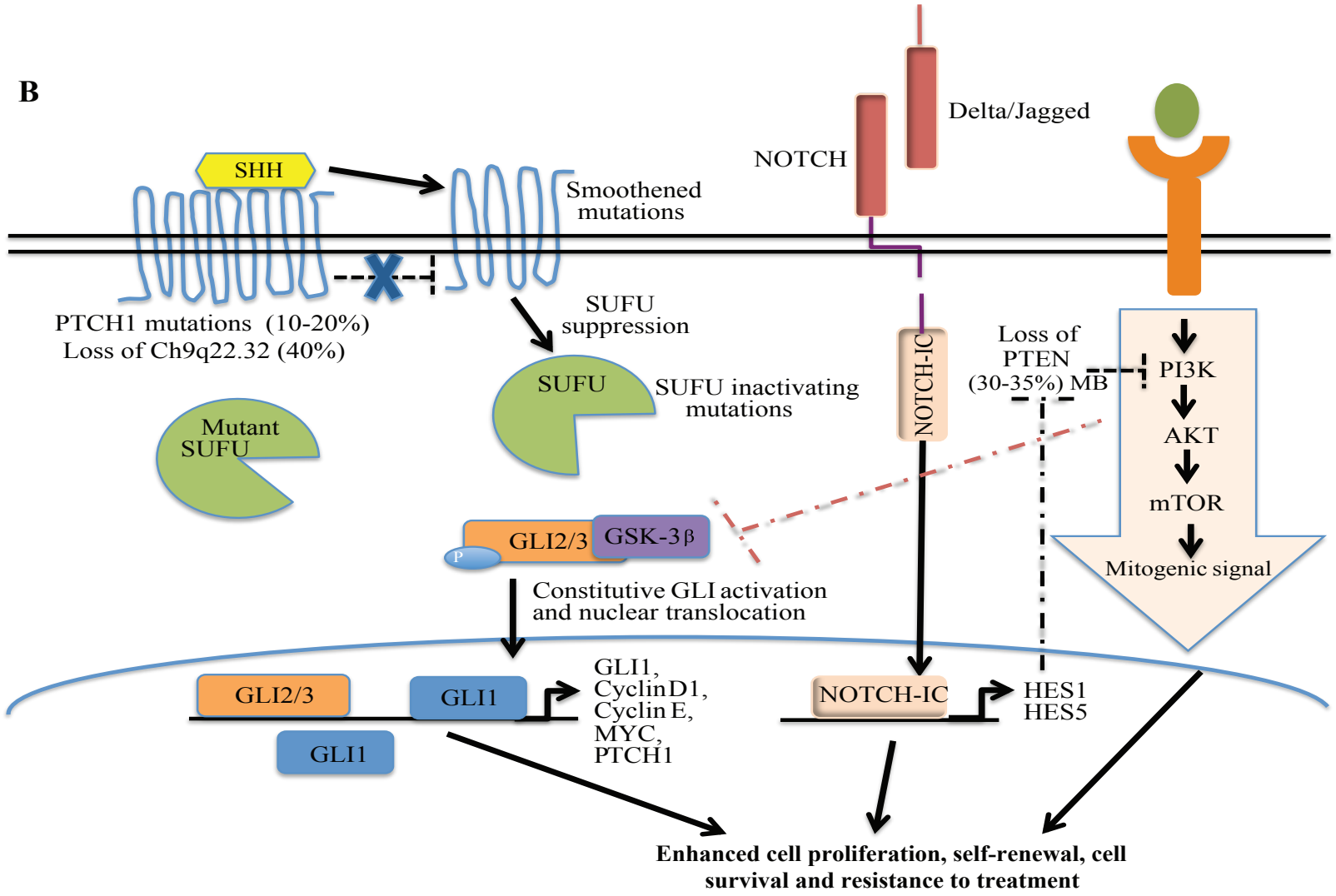


**Figure 1.3B: Cross-talk between SHH, PI3K and NOTCH pathways in SHH MB cells**: Activating or inactivating mutations in genes involved in regulating SHH signaling lead to constitutive activation of the pathway resulting in an elevated expression of target genes. Other signaling pathways such as PI3K and NOTCH are also important for the progression of SHH MB tumors and are also involved in treatment resistance (Hallahan et al. 2004; Dijkgraaf et al. 2011; Metcalfe et al. 2013).

targets of SHH signaling such as GLI1 and MYC (Hallahan et al. 2004; Oliver et al. 2005; Hatton et al. 2008). SHH signaling is critical for the proliferation of cerebellar granular neural precursors (CGNPs) in the external granular layer (EGL) of the developing cerebellum (Kenney, Cole, and Rowitch 2003; Vaillant and Monard 2009) (Figure 1.4A-B). SHH ligands are secreted by the Purkinje cells and bind to the receptor complex composed of the transmembrane proteins PTCH1 and SMO on CGNPs. SHH signaling is mediated through the primary cilium, a microtubule-based organelle, present on the CGNPs. The components of SHH signaling are brought together into and out of the cilium via active transport depending on the presence or absence of SHH ligand (Hassounah, Bunch, and McDermott 2012). Binding of the SHH ligand initiates a cascade of events including relieving the PTCH1-mediated inhibition of SMO activity followed by suppression of SUFU's proteolytic activity. This leads to enhanced stability and transcriptional activity of the glioma-associated oncogene family of transcription factors, GLI1, GLI2 and GLI3 (Manoranjan et al. 2012). Among the GLI proteins, GLI3 can act as either a repressor or activator. Activation of SHH signaling inhibits the cleavage of GLI3 into a truncated repressor protein. Further translocation of activated GLI2 and GLI3 induces the transcription of another GLI protein, GLI1. The primary cilia contribute to the posttranslational processing of GLI proteins into repressor or activator forms by modulating the localization of PTCH1 or through SUFU (Humke et al. 2010). GLI1 expression initiates a positive feed-forward mechanism, which induces the transcription of target genes such as *GLI1*, *Cyclin D1*, *Cyclin E* and *MYC* (Kenney, Cole, and Rowitch 2003; Stecca and Ruiz i Altaba 2005; Vaillant and Monard 2009; Manoranjan et al. 2012). In the absence of the SHH ligand, the transcription of these target genes that promote the proliferation of CGNPs is suppressed (Kenney, Cole, and Rowitch 2003; Manoranjan et al. 2012; Vaillant and Monard 2009) (Figure 1.3A).

The association between SHH signaling and MB was first identified in patients with nevoid basal cell carcinoma also known as Gorlin syndrome (Gorlin 1995; Hahn et al. 1996). Patients with Gorlin syndrome exhibit inactivating germline mutations in *PTCH1* and are usually prone to developing basal cell carcinoma or MB (Kenney, Cole, and Rowitch 2003; Gilbertson and Ellison 2008; Vaillant and Monard 2009; Manoranjan et al. 2012). *PTCH1* mutations account for 10-20% of sporadic SHH MBs (Pietsch et al. 1997; Xie et al. 1997). Chromosome 9q22.32, where the *PTCH1* gene is situated, is deleted in 40% of SHH MB cases (Gilbertson and Ellison 2008). Like *PTCH1*, *PTCH2* is another transmembrane protein that can bind to the SHH ligand. Expression of *PTCH2* is increased in approximately 30% of human MB cases and is associated with poor prognosis (Lee et al. 2006). Several studies have characterized *PTCH1* as a tumor suppressor gene (Briggs et al. 2008; Ayrault et al. 2009). Goodrich et al. developed the first and the most widely used sporadic mouse model of MB by introducing a germline deletion of the *Ptch1* (*Ptch1*+/-) allele. These mice developed tumors in CGNPs of the EGL within 15-25 weeks with a penetrance rate of 14-20% (Goodrich et al. 1997). However, these mice exhibit accelerated tumor growth with greater penetrance (95-100%) on a p53 null background (Wetmore, Eberhart, and Curran 2000). As *p53* mutations are found in only around 21% of SHH MB cases (Schroeder and Gururangan 2014), the mouse models developed on a p53 null background may be less useful for studying SHH tumors that lack p53 mutations.

Many reports have identified inactivating mutations and/or activating mutations in other components of the SHH signaling such as *SUFU* and *SMO* (Pietsch et al. 1997; Taylor et al. 2002). Mouse models carrying deletion of a single or both alleles of *SUFU* or transgenic *SMO* mice develop SHH MB at varying frequencies (Taylor et al. 2002; Hallahan et al. 2004; Oliver et al. 2005; Hatton et al. 2008). Collectively, these genomic changes lead to constitutive activation

of SHH signaling and elevated expression of downstream targets such as GLI1 and MYC (Figure 1.3B). As primary cilia are very critical in SHH signaling, mutations in pathway components upstream or downstream of cilium may have opposing effects on the development of MB tumors (Han et al. 2009). For example, mouse models driven by constitutively active SMO, an upstream molecule of SHH signaling, require intact cilium for MB development. In contrast, tumor growth driven by constitutively active GLI2, a downstream effector, needs complete removal of primary cilia in order to induce tumorigenesis (Han et al. 2009).

Several lines of evidence have identified the importance of other signaling pathways such as PI3K (Dijkgraaf et al. 2011; Buonamici et al. 2010) (Metcalfe et al. 2013) and NOTCH in initiation, maintenance and progression of SHH MBs (Hallahan et al. 2004; Fan et al. 2006). In the PI3K/AKT/PKB pathway, PI3K catalyzes the synthesis of PI-3,4,5-triphosphate from PI-4,5-diphosphate. PI-3,4,5-triphosphate acts as a second messenger and recruits AKT/PKB to the plasma membrane. Further phosphorylation of AKT/PKB activates downstream effectors such as mammalian target of rapamycin (mTOR) and GSK-3β, which are important for controlling cellular functions (Vivanco and Sawyers 2002; Panhuysen et al. 2004; Hartmann et al. 2006). Phosphatase and tensin homolog (PTEN), a negative regulator of PI3K, tightly controls the intracellular level of PI-3,4,5-triphosphate and therefore, acts as a tumor suppressor gene in MB. Deletions or mutations in *PTEN* have been detected in 30-35% of MB cases and contribute to an overactivation of PI3K/AKT signaling (Inda et al. 2004; Hartmann et al. 2006) (Figure 1.3B).

Similar to SHH signaling, NOTCH signaling is also important for the proliferation of CGNPs by activating hairy and enhancer of split (HES) family genes (Hallahan et al. 2004). NOTCH signaling is important in SHH MBs and can be activated by SHH signaling or by overexpression or amplification of genes coding NOTCH1, NOTCH2 receptor proteins and the

downstream targets HES1 and HES5 (Fan et al. 2004; Hallahan et al. 2004). Fan et al. have described the differential roles of NOTCH2 and NOTCH1 receptors in regulating different cell populations within SHH MB tumors as well as in normal cerebellar development (Fan et al. 2004). NOTCH2 is important for the proliferation of progenitor cell types within SHH MB; however, NOTCH1 is expressed in postmitotic differentiating cells (Fan et al. 2004). Pharmacologic inhibition of NOTCH pathway results in a significant reduction in the CD133+ cell population, demonstrating its role in maintaining the stem cell fraction of SHH MB tumors (Fan et al. 2006). However, Hatton et al. have shown that the complete deletion of *Notch1*, *Notch2* or *Hes5* genes had no affect on the initiation, engraftment or maintenance of SHH MBs in SmoA1-driven transgenic mouse models (Hatton et al. 2010). These conflicting results regarding the role of NOTCH signaling in pathology of SHH MBs require further investigation.

#### 1.2.2.4 Cerebellar granule neural precursors as ells of origin for SHH MB

CGNPs of the upper rhombic lip of the developing cerebellum serve as the cells of origin for SHH MBs (Wechsler-Reya and Scott 1999; Marino et al. 2000; Oliver et al. 2005; Schuller et al. 2008; Yang et al. 2008; Gibson et al. 2010). During cerebellar development, a series of events involving progenitor cell proliferation and migration take place throughout the embryonic and postnatal period (Vaillant and Monard 2009). In the first phase of cerebellar development, the ventricular zone (VZ) and anterior rhombic lip (ARL) generate the Purkinje cells and granule cells, respectively. In the second postnatal phase, CGNPs of the EGL proliferate to expand its cell population and migrate to form a more definitive internal granular layer (ten Donkelaar et al. 2003) (Figure 1.4A). However, increased activation of SHH signaling can results in neoplastic transformation of the CGNPs (Gilbertson and Ellison 2008; Manoranjan et al. 2012) (Figure 1.4B).

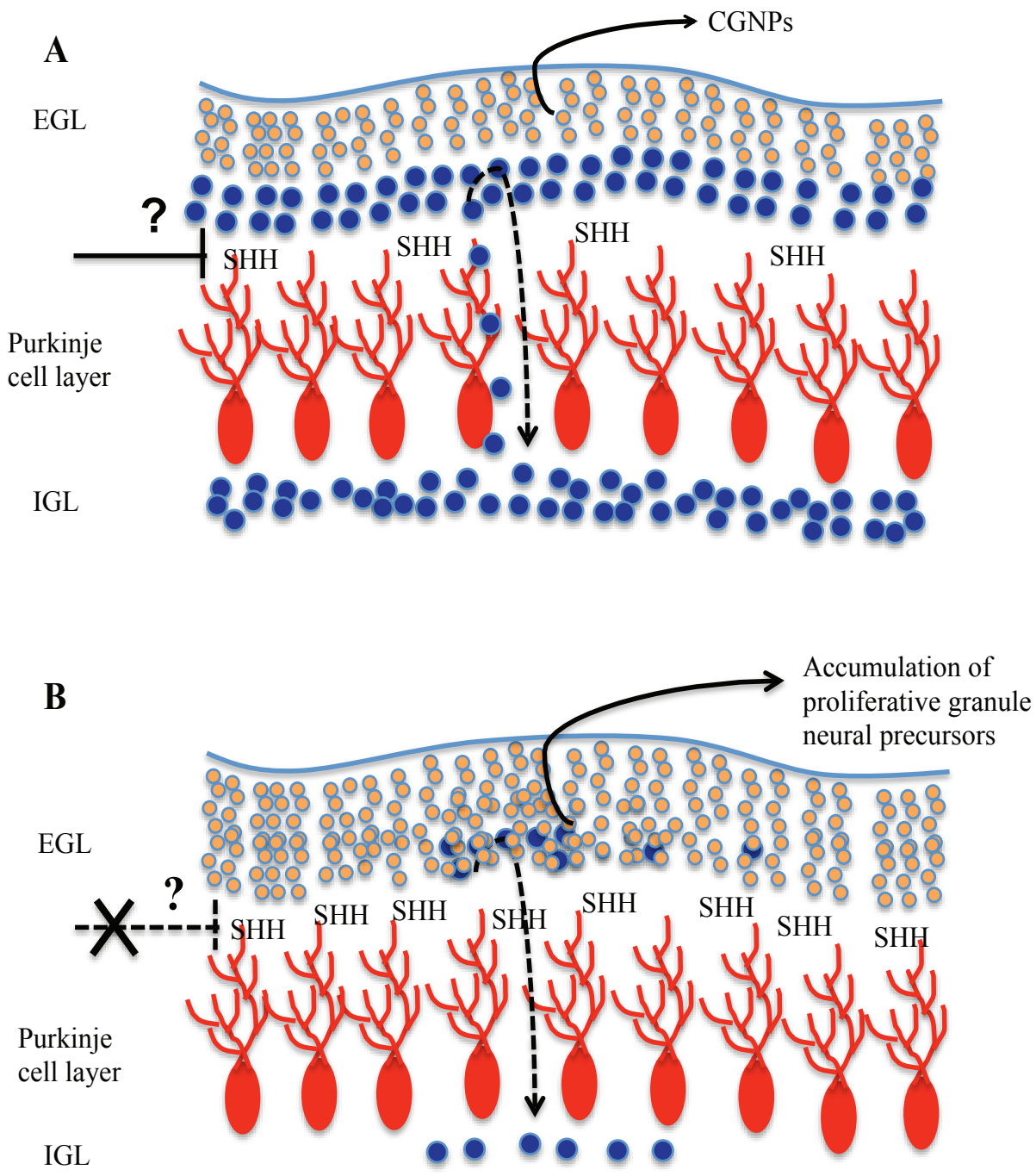


**Figure 1.4: Cells of origin for the Sonic hedgehog (SHH) medulloblastoma subgroup:** (A) During cerebellar development, cerebellar granule neural precursors (CGNPs) of the external granular layer (EGL) proliferate and migrate to form the definite internal granular layer (IGL). (B) However, increased activation of SHH signaling induces neoplastic transformation resulting in enhanced proliferation, self-renewal and survival of CGNPs, which are thought to be the cells of origin for SHH MBs (Romer and Curran 2005).

Recently, Grammel et al. have found that constitutive activation of SHH signaling in human glial fibrillary acidic protein (hGFAP) and MATH 1-positive (a basic helix-loop-helix transcription factor expressed in proliferating CGNPs) CGNPs derived from cochlear nuclei (a derivative of the auditory lower rhombic lip) of the brainstem can also induce SHH-associated MB development in mice (Grammel et al. 2012). These tumors resemble human SHH-associated MBs that are situated close to the cochlear nuclei (Grammel et al. 2012). Additionally, neural stem cells residing in the VZ are also susceptible to developing SHH-dependent MBs (Yang et al. 2008). Conditional deletion of the *Ptch1* allele in neural stem cells of the VZ leads to continuous expansion of these cells; however, only stem cells that differentiate to the granule lineage keep dividing and develop tumors in mouse models (Yang et al. 2008). These studies demonstrated that dysregulation of the SHH signaling pathway can induce tumor formation in both lineage restricted CGNPs and multipotent stem cells.

#### 1.2.2.5 Treatment options

Discovery of both naturally occurring and synthetic compounds that inhibit SHH pathway activation has improved the treatment outcome in patients with SHH MBs. For example, the first naturally occurring small molecule inhibitor, cyclopamine, a steroidal alkaloid isolated from corn lily, suppresses SHH signaling by binding to SMO and inhibiting the growth of cultured MB cells and xenografts (Taipale et al. 2000; Berman et al. 2002). However, the binding affinity of cyclopamine to SMO is relatively low. Moreover, studies have shown differential responsiveness of SHH MB cells to cyclopamine treatment based on the expression levels of CD133 (Enguita-German et al. 2010; Wang et al. 2012). CD133+ cancer stem cells

within SHH MBs are thought to be responsible for treatment resistance and tumor recurrence (Enguita-German et al. 2010).

A cell-based screen has identified a small molecule inhibitor named benzimidazole derivative, HH-Antag691, a semisynthetic cyclopamine analog. This drug binds to Smo with a higher affinity than cyclopamine and exhibits reduced toxicity (Romer et al. 2004). HH-Antag691 can decrease tumor growth by suppressing Gli1 expression and can effectively cross the blood-brain barrier by inhibiting the ATP-binding cassette (ABC) transporter, which is highly expressed at the blood-brain barrier (Romer et al. 2004; Zhang, Laterra, and Pomper 2009). Unfortunately, HH-Antag691 treatment induced permanent defects in bone structure in young mice, underscoring serious safety concerns regarding the potential use of this drug in young patients such as those children with SHH MB (Kimura, Ng, and Curran 2008).

Recently, a SMO inhibitor, Vismodegib (GDC-0449), has gained attention and is currently being utilized in advanced clinical trials for treating refractory, locally advanced or metastatic basal cell carcinoma and MB tumors (Robarge et al. 2009; Von Hoff et al. 2009; LoRusso et al. 2011; Gajjar et al. 2013; Sharpe et al. 2015). However, GDC-0449 treatment has been shown to induce a de novo mutation at D473H, an asparatic acid residue in SMO and the site of GDC-0449's action. As a result, tumor cells become resistant to this drug (Dijkgraaf et al. 2011).

As SHH tumors also exhibit upregulation of other signaling pathways such as NOTCH and PI3K, it might be possible that cells recovered from SHH pathway inhibitor treatment and become resistant by switching their dependence to these additional pathways for continuous growth. To overcome treatment-related resistance, a combinatory approach of targeting more than one pathway would be beneficial. For example, genes related to PI3K signaling are

commonly dysregulated in SHH MB and are responsible for inducing drug resistance in tumor cells (Dijkgraaf et al. 2011; Buonamici et al. 2010; Metcalfe et al. 2013). Targeting PI3K signaling in combination with SMO inhibitors has been shown to enhance efficacy and improve survival (Dijkgraaf et al. 2011; Buonamici et al. 2010; Metcalfe et al. 2013). Furthermore, a phase II Pediatric Brain Tumor Consortium study by Robinson et al, recently demonstrated that the activity of SMO inhibitors depend on the genomic alterations within the tumor (Robinson et al. 2015). In this study, adults with SHH MB and loss of heterozygosity of PTCH1 showed enhanced progression-free survival. However, SHH MB tumors also exhibiting diffuse staining for P53, which is associated with dominant-negative DNA-binding domain mutations in *P53*, had reduced progression free survival following vismodegib treatment. In contrast, the response in patients with recurrent non-SHH MB was poor (Robinson et al. 2015). Saridegib, another potent SMO inhibitor was found to be effective in cells with D473H point mutations. A preclinical study has shown a fivefold increase in lifespan in mice treated with saridegib without inducing any de novo genetic mutations (Lee et al. 2012).

Similar to PI3K, NOTCH signaling is upregulated along with SHH signaling in SmoA1 mouse models (Hallahan et al. 2004). Targeting the NOTCH signaling pathway using gamma-secretase inhibitors (ϒ-secretase inhibitors) resulted in decreased proliferation and increased apoptosis in xenograft models of SHH MB (Hallahan et al. 2004). This also reduced the population of $CD133^{+}$ cancer stem cells by five-fold (Fan et al. 2006). However, these findings were in contrast with the observation made by Hatton et al, who demonstrated that targeting the NOTCH pathway is not beneficial in SHH-driven MB (Hatton et al. 2010) and future studies focusing on more effective doses of anti-NOTCH therapies are required. Other drugs such as arsenic trioxide (GLI inhibitor), 5-azaC (DNA methylation agent) and valproic acid (histone

deacetylase inhibitor) have been the subject of phase II clinical trials, either alone or in combination, for treatment of SHH MB and are showing tumor inhibition with prolonged survival (Berman et al. 2002; Beauchamp et al. 2011; Ecke et al. 2009).

Although recent treatment options have increased the overall survival in patients with SHH MBs, existing heterogeneity within tumors and emerging resistance underscore the complexity of tumor biology. In addition, careful consideration of the relevant model system is also key for determining the cell-type-specific response to treatments. For example, Hambardzumyan et al have shown that the preclinical trials for radiation therapy using p53-deficient mouse models may provide inconsistent results (Hambardzumyan et al. 2008). They have observed a p53-dependent apoptotic cell death of proliferating cells in bulk tumors from SHH MB mouse models with wild type p53. However, the nestin-expressing stem cells of the periventricular niche underwent p53-dependent cell cycle arrest and re-entered the cell cycle at 72 hours via radiation-induced PI3K/Akt pathway activation (Hambardzumyan et al. 2008). Hence, inhibition of PI3K/Akt signaling before radiation treatment could be an approach to sensitize the cells of the perivascular niche to radiation-induced apoptosis (Hambardzumyan et al. 2008). These findings demonstrate that various genes and pathways are involved in regulating the properties of different cellular subpopulations within SHH tumors resulting in variable responses to treatment.

### 1.2.3 Group 3

Group 3 is the most aggressive form of MB with a 5-year survival rate of less than 50% (Schroeder and Gururangan 2014). It accounts for nearly 25-28% of all MB cases. These tumors

are commonly metastatic (40-45%) and exhibit the worst outcome (Kool et al. 2012; Northcott et al. 2012; Gajjar and Robinson 2014).

#### 1.2.3.1 Demographic distribution

Group 3 MBs are more common in males than females (2:1) with a higher incident rate in infants and children than adults (Northcott et al. 2012; Gajjar and Robinson 2014; DeSouza et al. 2014). These tumors have the worst outcomes in infants, with 5-year and 10-year survival rates of 45% and 39%, respectively compared to children (Gajjar and Robinson 2014).

#### 1.2.3.2 Histology

This aggressive MB subgroup exhibits the highest prevalence (40%) of large cell/anaplastic histology with no incidence of desmoplastic/nodular histological features (Gilbertson and Ellison 2008). Large cell MBs constitute large uniform cells with vesicular nuclei and a prominent single nucleolus (Gilbertson and Ellison 2008). Regions of anaplasia are defined by increased nuclear size with nuclear pleomorphism, nuclear moulding and tumor cell wrapping on one another (Louis et al. 2007; Gilbertson and Ellison 2008). Both large cell and anaplastic variants are characterized by high mitotic activity, the presence of apoptotic bodies and a worse prognosis (Haberler et al. 2006; Giangaspero et al. 2006; Louis et al. 2007).

#### 1.2.3.3 Genetic and molecular alterations

The most frequent genomic aberration in Group 3 MB includes amplification of *MYC* (16.7%) and the homoeodomain transcription factor, *OTX2* (7.7%) (Herms et al. 2000; Boon, Eberhart, and Riggins 2005; Adamson et al. 2010; Northcott et al. 2012). *MYC* amplification is

limited to Group 3 MB and is mutually exclusive from *OTX2* amplifications. This suggests that different mechanisms might be involved in pathogenesis of Group 3 tumors (Taylor et al. 2012; Northcott et al. 2012; Gajjar and Robinson 2014). Additional mutations in genes involved in chromatin remodelling such as *SMARCA4*, lysine specific methyltransferase 2D (*KMT2D*) and chromodomain-helicase-DNA binding protein 7 (*CHD7*) are associated with Group 3 MBs (Gajjar and Robinson 2014). Some cases of Group 3 tumors are also associated with mutations in lysine specific demethylase (KDM) gene family members (Robinson et al. 2012).

A high level of genomic instability is associated with Group 3 MBs and these tumors are often recognized by isochromosome 17q (i17q), which occurs as a result of loss of 17p and gain of 17q (Griffin et al. 1988). Additional chromosomal aberrations such as gains of 1q, 7 and deletion of 10q, 11 and 16q are also observed in Group 3 tumors (Kool et al. 2012). The *PTEN* gene, a negative regulator of PI3K/Akt signaling, is located on chromosome 10q and deletion of 10q may upregulate this pathway in Group 3 MBs. Tetraploidy (54% cases) and chromothripsis (massive chromosomal rearrangement) are also frequent occurrences in these tumors (Jones et al. 2012; Northcott et al. 2012). All these genetic and molecular changes make Group 3 a biologically complex subgroup. There is very little understanding of the functional relevance of these changes to disease progression and this has hampered the identification of novel therapeutic targets. Therefore, further studies investigating the functional relevance of genes related to the progression of Group 3 MBs are warranted.

#### 1.2.3.4 Lineage restricted neural precursors and neural stem cells as cells of origin for Group 3 MB

To date, there are only two published reports demonstrating that the lineage restricted CGNPs of the EGL and prominin 1-positive ($CD133^+$) neural stem cell are the cells of origin for MYC-driven aggressive Group 3 MBs (Kawauchi et al. 2012; Pei et al. 2012). As MYC amplification is highly enriched in Group 3 MBs, Pei et al have shown that stable expression of MYC through viral transduction in $CD133^+$ neural stem cells and MATH 1-positive CGNPs derived from postnatal mouse cerebellum induced cell proliferation when injected into immunodeficient mice (Pei et al. 2012). However, these tumors resolved as a result of MYC-induced cellular apoptosis. A combined suppression of P53 via dominant negative p53 viral infection restrained MYC-induced apoptosis and these mice developed tumors recapitulating the pathological and molecular features of human Group 3 MBs (Pei et al. 2012). Kawauchi et al have observed that enforced expression of MYC but not MYCN in atonal homologue 1 (ATOH1)-positive and ATOH1-negative CGNPs from the EGL in a P53 null background induced tumor formation with a gene expression pattern resembling that seen in embryonic stem cells (Kawauchi et al. 2012). This suggests that mature GNPs underwent dedifferentiation into a stem cell phenotype following MYC overexpression. Also, treatment with the Smo inhibitor cyclopamine and a semisynthetic cyclopamine analog, HhAntag691, had no effect on tumor cell proliferation inferring that MYC driven tumors are independent of SHH signaling (Kawauchi et al. 2012). Although these mouse models provide a valuable tool in accelerating our understanding of MYC-driven Group 3 MBs, they do not represent the metastatic counterpart of the disease, which is the main challenge in Group 3 MB treatment.

Another frequently amplified and overexpressed oncogene in Group 3 MBs is *OTX2*. OTX2 plays a major role in patterning of developing brain (Matsuo et al. 1995) and in cell fate specification (Nishida et al. 2003; Acampora, Di Giovannantonio, and Simeone 2013). OTX2 also regulates the proliferative capacity of progenitor cells in the ventral mesencephalon in a dose dependent manner (Omodei et al. 2008). However, in Group 3 MB cells, OTX2 seems to directly regulate cell cycle genes (Bunt et al. 2012) and promote tumor growth (Adamson et al. 2010). While the particular cellular context where the dysregulation of OTX2 results in tumor development is not clear, ectopic overexpression of Otx2 in mouse hindbrain results in accumulation of proliferative cells in the cerebellar white matter and dorsal brainstem of postnatal mice (Wortham et al. 2012). These cell clusters are thought to arise from neuronal progenitors of the rhombic lip and by inward migration of CGNPs of EGL. However, OTX2 dysregulation was not sufficient for full transformation of these cells (Wortham et al. 2012) suggesting the involvement of other factors in conjunction with OTX2 drive tumor initiation and progression. To date, there is no mouse model available for OTX2-driven Group 3 MBs. In addition, the underlying mechanisms and interacting partners of OTX2 involved in driving Group 3 MB tumorigenesis remain elusive.

#### 1.2.3.5 Treatment options

Frequent metastasis makes treatment of Group 3 MBs challenging under standard care options. Preclinical studies using mouse models for the identification of specific drugs targeting MYC-driven aggressive MBs are underway. A recent study by Morfouace et al, has identified two US Food and Drug Administration (FDA)-approved compounds, pemetrexed and gemcitabine for targeting Group 3 MBs (Morfouace et al. 2014). Both *in vitro* and *in vivo*, these

compounds preferentially inhibit proliferation of Group 3 MB tumors exhibiting amplifications and/or overexpression of *MYC*. The combination of both drugs showed even better results by increasing the survival in mice exhibiting MYC overexpressing cortical implants of mouse or human Group 3 MB cells (Morfouace et al. 2014). Bromodomain and extraterminal domain protein family (BET) members localize to promoter and enhancer regions and function as co-activator to transcription factors. BET inhibitors are another therapeutic drug class that interferes with the transcriptional activity of MYC and is thereby a promising candidate for treatment of Group 3 MBs (Bandopadhayay et al. 2014). MYC-driven MBs are also dependent on PI3K/mTOR signaling. Targeting PI3K/mTOR pathway using BEZ-120 (antagonist of PI3K) and BEZ-235 (antagonist of both PI3K and mTOR) leads to inhibition of tumor cell growth both *in vitro* and *in vivo* (Pei et al. 2012).

Similar to most SHH MB mouse models, MYC-driven models are generated on a P53 null background, which is a true representation for tumors exhibiting loss of one allele of TP53 (Pfister et al. 2009; Northcott et al. 2011). However, some large cell anaplastic MBs express high levels of P53 protein, indicating the presence of dysfunctional P53 protein and the P53 pathway (Eberhart et al. 2005; de Bont et al. 2008). Immunopositivity for P53 is related to poor prognosis (Woodburn et al. 2001; Ray et al. 2004; Tabori et al. 2010). This suggests that dysregulation of the P53 pathway can occur as a result of mutations in the *P53* gene and/or the presence of dysfunctional protein. *P53* mutations are associated with radiotherapy and chemotherapy failure. In a study cohort by Tabori et al, the authors observed that P53-mutated MBs showed 5-year survival of 0%, even in average-risk patients. Seventy five percent of average-risk patients had tumor recurrence as a result of P53 mutations (Tabori et al. 2010). Philipova et al have demonstrated that differential forms of P53 have been identified in MB primary tumors, cell

lines and xenograft models. The *P53* gene encodes nine different isoforms and these isoforms may have an impact on the tumor suppressor activity of P53 (Philipova et al. 2011).

So far, there are no specific treatments available for OTX2 positive Group 3 MBs. There is one report in the literature by Bai et al, 2010 suggesting the use of retinoic acid for targeting OTX2 positive MB cells. Retinoic acid reduces OTX2 expression by binding to the promoter region of OTX2 with subsequent induction of neuronal differentiation (Bai et al. 2010). However, tumor cells become resistant to retinoic acid treatment at first-time use (Freemantle, Spinella, and Dmitrovsky 2003). In fact, different MB cell lines show variable responses to retinoic acid treatment. For example, the Med-3 cell-line is sensitive to retinoic acid exposure but UW228-2 and UW228-3 are retinoic acid resistant cells (Fu et al. 2012). Moreover, retinoic acid treatment either induces apoptotic cell death or growth arrest of MB cells (Gumireddy et al. 2003; Chang et al. 2007). To date, our understanding of the signaling pathways associated with pathogenesis of Group 3 tumors is very poor, making it difficult to identify novel therapeutic targets.

### 1.2.4 Group 4

Group 4 MBs are the largest group with an incidence rate of 34%. Two out of five cases are diagnosed with Group 4 tumors and among all patients, 35-40% cases present with metastatic disease at the time of diagnosis (Kool et al. 2012; Northcott et al. 2012).

#### 1.2.4.1 Demographic distribution

Group 4 tumors have considerable gender bias and have a much higher incidence rate in males compared to females (3:1). These tumors can occur at any age but are very rare in infants;

however, the gender bias is similar across all age groups (Kool et al. 2012; Taylor et al. 2012; Northcott et al. 2012). The prevalence of this subgroup is higher in children (40-45%) compared to adults (25%); however, children exhibit an intermediate prognosis relative to adults (Remke et al. 2011; Kool et al. 2012).

#### 1.2.4.2 Histology

Both classic and large cell anaplastic histological features can be seen in Group 4 tumors. However, the frequency of large cell anaplastic histology is lower in Group 4 cases relative to Group 3 tumors (Northcott et al. 2012). Average risk Group 4 MBs do not carry metastatic disease and have a better 5-year overall survival (80%). Patients with metastatic disease are considered high-risk, exhibit inferior prognosis and a 60% overall 5-year survival rate (Northcott et al. 2012; Shih et al. 2014).

#### 1.2.4.3 Genetic and molecular alterations

Mutations that are associated with Group 4 MBs are not well studied. *MYCN* and cyclin dependent kinase 6 (*CDK6*) are the commonly amplified genes in this subgroup (Northcott et al. 2012). Genes that are commonly mutated in both Group 3 and Group 4 include *OTX2*, KDM family members, *CHD7* mutations, Growth factor independent (*GFI1*/*GFIB*) activation and *KMT2D* and *KMT2C* mutations (Northcott et al. 2012; Jones et al. 2012; Pugh et al. 2012; Robinson et al. 2012). Among the KDM family members, *KDM6A* mutations are the most common event in Group 4 tumors. KDM6A functions as a demethylase enzyme and regulates the methylation status of lysine-27 of the inactive histone mark, H3K27. H3K27 remains in a trimethylated state (H3K27me3) in stem cells and mutation in *KDM6A* prevents demethylation

of H3K27me3. These cells might be restricted to a stem cell like state (Robinson et al. 2012). Similar to Group 3 tumors, the majority (80% cases) of Group 4 tumors exhibit isochromosome 17q. Loss of one copy of the X chromosome in females with Group 4 tumors has also been reported, which indicates the presence of one or more tumor suppressor genes on the X chromosome (Northcott et al. 2012). Northcott et al, have identified a tandem duplication of chromosome 5q23.2 in 25% of Group 4 MB cases, which may contain signature genes for the identification of this subgroup (Northcott et al. 2012).

#### 1.2.4.4 Neural stem cells as cells of origin for Group 4 MB

The cell of origin for Group 4 MBs remains elusive. Recently, Lin et al have identified the differentially expressed enhancer and super-enhancer regulatory elements in MB (Lin et al. 2016). Screening of 28 fresh-frozen, treatment-naïve tissue samples and three cultured cell lines has revealed master transcriptional regulators for MB subgroups that are responsible for subgroup-specific divergence. For example the enhancer activity and expression of LIM-homeodomain transcription factor is highly discriminatory in Group 4 MB, designated as a master regulator of the Group 4 transcriptional program (Lin et al. 2016). Based on LIMX1A activity and specific expression patterns, the immature deep cerebellar nuclei residing in the nuclear transitory zone or even earlier progenitors of the upper rhombic lip are considered as putative cells of origin for Group 4 MBs (Lin et al. 2016).

#### 1.2.4.5 Treatment options

There is little information on the cells of origin as well as the underlying molecular mechanisms contributing to the development of Group 4 tumors. In addition, a lack of a

preclinical mouse models mimicking human Group 4 MBs has made it difficult to identify new therapies for this subgroup. Patients with average-risk disease perform well with the standard treatment regimens; however, the high-risk group experience poor outcomes (DeSouza et al. 2014). Common molecular profiles between Group 3 and Group 4 MBs suggests that similar drugs may function effectively in both subgroups (DeSouza et al. 2014). For example, the amplification and overexpression of OTX2 has been detected in both Group 3 and Group 4 MBs, thus, targeting OTX2 may provide a common approach to treat these aggressive subgroups.

Genomic analysis has shown that the OTX2 gene is highly amplified with a copy number increase from 8 to over 50 that is unique to MB (Michiels et al. 1999; Yokota et al. 2004; Boon, Eberhart, and Riggins 2005; Di et al. 2005). In addition, OTX2 mRNA levels are found to be high in almost 70% of MB cases and are associated with anaplastic histopathological features (Di et al. 2005). While OTX2 is very important in normal brain development, it is not expressed in adult brain except for minimal expression in the choroid plexus, retina and pineal gland (Acampora et al. 1995). OTX2 plays a major role in brain patterning, cell fate specification and retinal development and these roles are now described in detail as follows.

### 1.3 Orthodenticle homeobox2

OTX2 is a homeodomain transcription factor which belongs to a highly conserved bicoid-like transcription factor family (Simeone, Puelles, and Acampora 2002). The *OTX2* gene is located on chromosome 14q22.3 and contains 5 exons. The first two exons are non-coding. The OTX2 gene encodes 5 transcript variants comprising a homeodomain (HD) and a transactivation domain (TD). The transcript variants 1 (NM_021728.3) and 5 (NM_001270525.1) encode protein isoform-a. The other variants 2 (NM_172337), 3 (NM_001270523 and 4

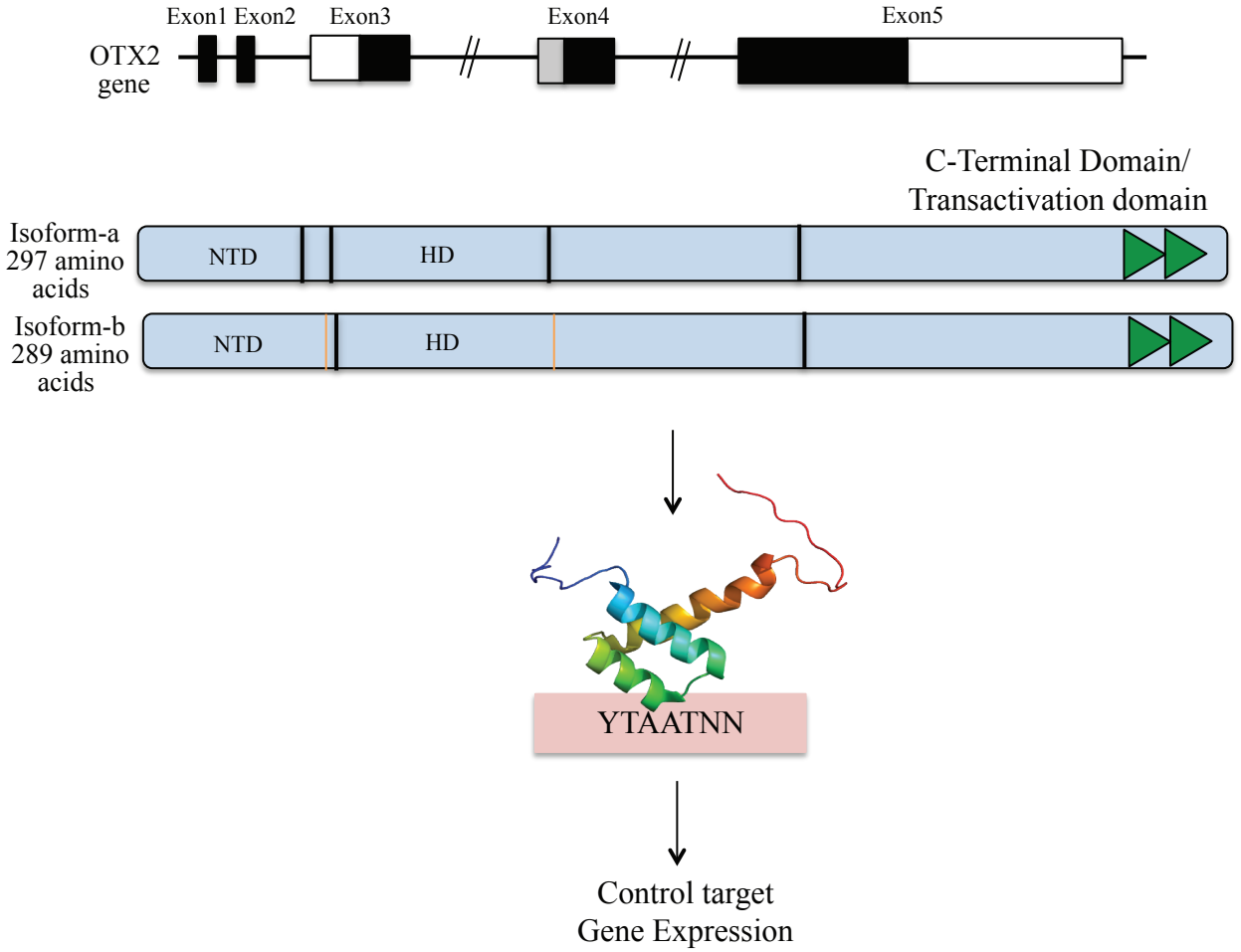


**Figure 1.5: OTX2 gene and protein:** The OTX2 gene consists of 5 exons. The OTX2 gene generates 5 different variants, which encode two functionally redundant isoforms: isoform-a and isoform-b, comprising 297 and 289 amino acids, respectively. The OTX2 transcription factor binds to a conserved YTAATNN motif present within the target gene sequence and controls the expression of its target genes (OTX2 gene structure is adapted from (Dateki et al. 2010) and protein structure is adapted from https://en.wikipedia.org/wiki/Orthodenticle_homeobox_2).

(NM_001270524) translate into isoform-b and both isoforms are functionally redundant (Dateki et al. 2010). The OTX2 protein regulates the transcription of target genes by binding to a conserved YTAATNN motif (Kimura-Yoshida et al. 2005; Chatelain et al. 2006) (Figure 1.5). Another alternative spliced variant of OTX2, which is a non-coding RNA, has been shown to be expressed in embryonic stem cells (Liu et al. 2013). This variant is tightly regulated in embryonic stem cells and then gradually decreases during differentiation (Liu et al. 2013).

Otx2 play crucial roles in the development and patterning of the brain, cerebellum, pineal gland and eye (Acampora et al. 1995; Matsuo et al. 1995; Ang et al. 1996; Simeone 1998; Beby and Lamonerie 2013). Otx2 is also involved in neuronal and retinal cell fate specifications (Puelles et al. 2004; Simeone et al. 2011; Housset et al. 2013).

### 1.3.1 OTX2 in brain development

Several studies have independently defined the role of Otx2 during early embryogenesis and head formation in Drosophila and mice (Kimura et al. 1997; Perea-Gomez et al. 2001; Acampora et al. 1995; Hirth et al. 1995; Finkelstein and Boncinelli 1994). During embryogenesis, Otx2 is expressed in the inner cell mass of the mouse blastocyst at embryonic day E3.5 and in the visceral endoderm of the pre-gastrulation embryo at the E5.5 (Kimura et al. 2001). Otx2 is not required for the proliferation of visceral endoderm; however, it plays an essential role in anteriorly directed morphogenetic movements by regulating the expression of other developmental genes such as left-right determination factors (*Lefty*) and mouse dickkopf-related protein 1 (*Mdkk1*) in this region (Perea-Gomez et al. 2001). These secreted proteins are the negative regulators of Nodal and Wnt signals, respectively, and are important in primitive streak formation (Perea-Gomez et al. 2001).

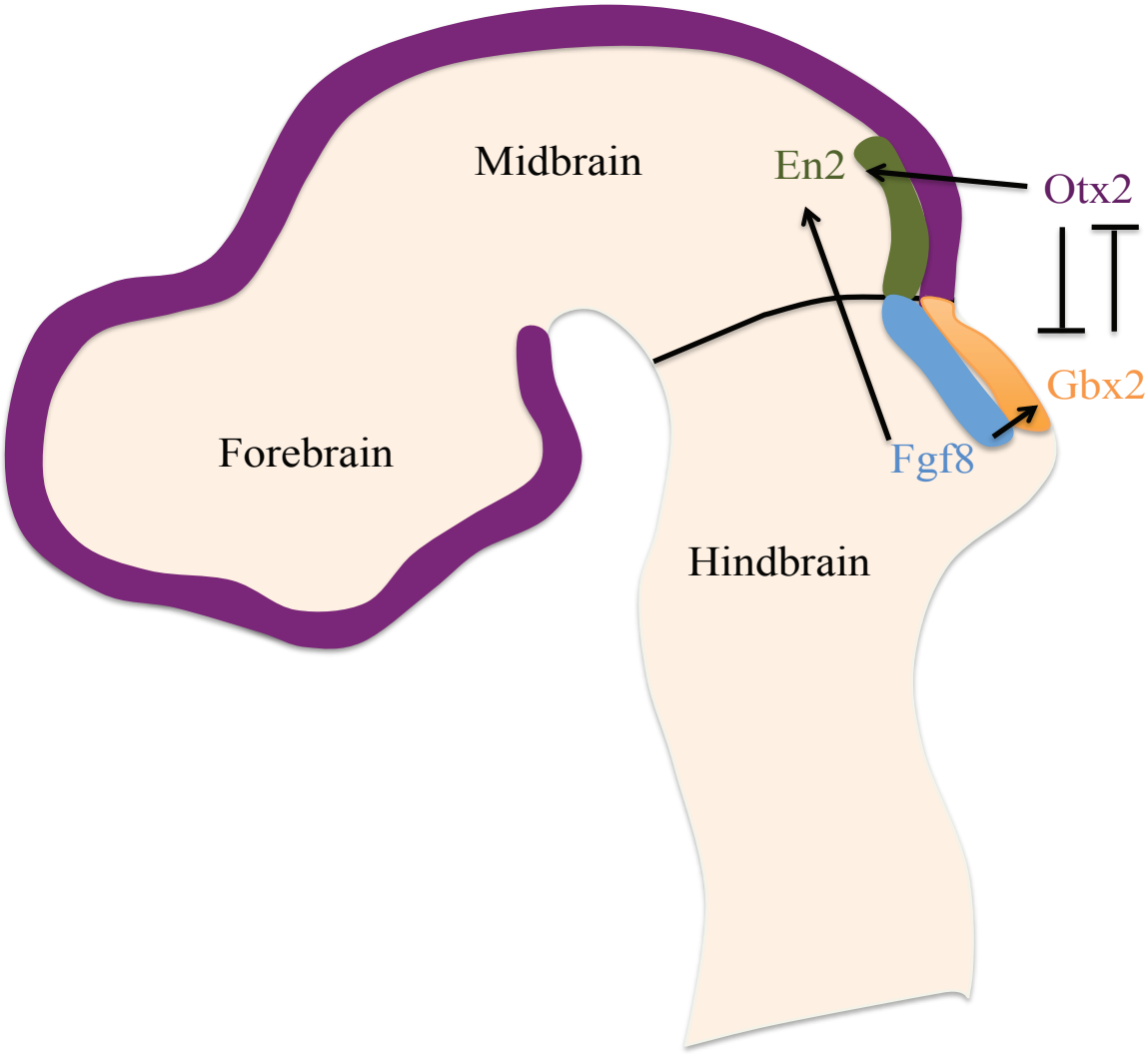


**Figure 1.6: A role for Otx2 in patterning the midbrain-hindbrain boundary:** Otx2 has an important role in patterning at the midbrain-hindbrain junction or isthmic organizer by regulating the midbrain-hindbrain markers such as En2 and Gbx2.

In pre-streak embryos, Otx2 is widely expressed in the epiblast but during gastrulation, it becomes restricted to the anterior neuroectoderm, which contains the precursor cells of the forebrain and midbrain regions of the developing brain (Tam 1989; Ang et al. 1994; Rhinn et al. 1998; Cajal et al. 2012). Severe defects in gastrulation and in formation of axial mesoderm as well as loss of anterior neural tissue have been observed in Otx2 mutant mice (Ang et al. 1996). Notably, complete loss of Otx2 ($Otx2^{-/-}$) in mice is embryonic lethal and leads to the deletion of forebrain and midbrain regions by 9.5 days post-coitum (dpc). The resultant "headless" phenotype is attributed to the defective anterior neuroectoderm specification during gastrulation (Acampora et al. 1995; Ang et al. 1996; Rhinn et al. 1998). These defects in head formation were also seen in Drosophila carrying loss of functional mutations in Drosophila orthodenticle (*otd)* (Royet and Finkelstein 1995), revealing the evolutionary conserved role of *otd* /Otx2 in head development. In contrast, the heterozygous mice ($Otx2^{+/-}$) developed craniofacial malformations such as anophthalmia/microphthalmia (absent or small eyes), short nose or agnathia/micrognathia (absent or small jaw) (Matsuo et al. 1995; Ang et al. 1996). In addition to its role in early gastrulation, Otx2 also plays a pivotal role in defining the midbrain-hindbrain junction (prospective cerebellum) or isthmic organizer by maintaining the midbrain-hindbrain marker engrailed-2 (En2) and antagonizing the expression of gastrulation brain homeobox 2 (Gbx2) (Rhinn et al. 1998; Broccoli, Boncinelli, and Wurst 1999) (Figure 1.6). Loss of function studies have demonstrated that both Otx2 and Gbx2 act antagonistically for specification of the midbrain and cerebellum, respectively, in mice (Wassarman et al. 1997; Rhinn et al. 1998; Broccoli, Boncinelli, and Wurst 1999).

### 1.3.2 OTX2 in cell fate specification

In addition to the role in normal brain patterning and formation, OTX2 also functions in the specification of certain neuronal populations within the brain. Otx2 regulates neuronal identity through its interaction with different genes/factors in neuroanatomical regions of the brain. Depending on its interacting partners, Otx2 may act as a transcriptional activator or repressor for controlling the proliferation and differentiation of various neuronal populations within the brain (Puelles et al. 2006; Omodei et al. 2008; Larder and Mellon 2009).

#### 1.3.2a Midbrain dopaminergic neurons

Otx2 is expressed in the dopaminergic progenitors of both the diencephalon and mesencephalon but preferably involved in the neurogenesis of mesencephalon/midbrain dopaminergic progenitors (mDA) (Puelles and Rubenstein 2003; Puelles et al. 2004; Prakash and Wurst 2006; Omodei et al. 2008). Overexpression and knockdown of Otx2 under the control of an En1 promoter at embryonic stage E9.0 in mouse resulted in an increase and decrease in the number of midbrain dopaminergic neurons, respectively (Ono et al. 2007; Omodei et al. 2008). These studies suggest that Otx2 is required for the identity of mDA neurons. Inactivation of Otx2 not only affected the proliferation and differentiation of mDA neurons, but also induced an imbalance in the differentiation programs of other brain regions (Vernay et al. 2005). For example, deletion of Otx2 induced an ectopic cerebellar-like structure in the ventral midbrain and also increased the number of serotonergic neurons (Puelles et al. 2004; Vernay et al. 2005). These changes are accompanied by decreased expression of LIM homeodomain transcription factor 1 alpha (*Lmx1a*) and proneural genes such as mammalian achaete scute homolog-1 (*Mash1*) and neurogenin2 (*Ngn2*) (Vernay et al. 2005; Omodei et al. 2008). These conditional

inactivation studies revealed the important functions of Otx2 in regulating the extent, identity and fate of the neuronal progenitor populations in the ventral midbrain (Puelles et al. 2004; Vernay et al. 2005; Omodei et al. 2008; Di Salvio et al. 2010a; Di Salvio et al. 2010b). However, the underlying molecular mechanisms by which Otx2 regulates the expression of genes involved in neuronal specifications are still unclear.

Wnt/β-catenin signaling is thought to be required for the maintenance of Otx2 expression in a subset of mDA progenitors (Panhuysen et al. 2004; Tang, Miyamoto, and Huang 2009). An increase in Wnt/β-catenin signaling resulted in a decreased number of Otx2 expressing mDA progenitors (Joksimovic et al. 2009). A recent study by Panman et al, also described the spatial role of Otx2 in determining the subtype of mDA neurons, particularly in the ventral tegmental area (VTA) (area located in the midbrain, at the top of the brain stem) (Panman et al. 2014). The expression pattern of transcription factors such as Otx2, sex determining region Y-box 6 (Sox6) and zinc finger protein503 (Zfp503) or Nolz1 in midbrain neural progenitors defines the subpopulations of dopaminergic neurons in different regions of the midbrain. Otx2 is expressed in neuronal progenitors of the VTA and this expression is maintained in differentiating and mature dopaminergic neurons (Chung et al. 2010; Di Salvio et al. 2010b). In neuronal progenitors of the VTA, Otx2 might functionally interact with the zinc finger protein, Nolz1, for determining the fate of VTA neurons (Panman et al. 2014). Moreover, among these dopaminergic neurons of the VTA, Otx2 specifically regulate the neurogenesis of neuronal progenitors that express calbindin and aldehyde dehydrogenase family 1 subfamily A1 gene (Ahd2) (Di Giovannantonio et al. 2013). This suggests that the differential responsiveness of mDA progenitors to Otx2 is important for establishing phenotypes of post-mitotic mDA neurons (Chung et al. 2010; Di Salvio et al. 2010a; Di Giovannantonio et al. 2013).

### 1.3.2b Glutamatergic progenitors of the thalamus

The excitatory and inhibitory networks of the CNS consist of glutamatergic and gamma-aminobutyric acid (GABAergic) neurons, respectively. Any functional impairment in these networks may cause neurological and psychiatric disorders (Bennett and Balcar 1999). Otx2 has been reported to play a crucial role in the specification of glutamatergic progenitors of the thalamus by repressing GABAeric neuron differentiation (Puelles et al. 2006). Ablation of Otx2 can induce the GABAergic differentiation program by increasing the expression of GABAergic neuron-specific markers such as the paired box genes Pax3 and Pax7 in progenitors of the thalamic region (Puelles et al. 2006).

### 1.3.2c Gonadotrophin releasing hormone neurons

Gonadotrophin releasing hormone (GnRH) neurons originate from embryonic nasal tissues (nasal placode) and then they migrate through brain into the hypothalamus. GnRH neurons are involved in regulating mammalian puberty and subsequent fertility by maintaining proper functioning of the hypothalamic-pituitary-gonadal axis. Loss of GnRH neurons, disruption of their migration, mutation in the GnRH gene or decreased GnRH expression can induce reproductive dysfunction such as congenital idiopathic hypogonadotropic hypogonadism (CIHH) (Gamble et al. 2005; Chan et al. 2009). Otx2 has been implicated in regulating GnRH gene expression through Otx2 binding sites at the proximal promoter of GnRH (Kelley et al. 2000; Larder and Mellon 2009). In GnRH neurons, binding of Otx2 at GnRH promoter increases gene activity. However, interaction of Otx2 with a member of the Groucho-related-gene family, Grg4, modulates the transcriptional activity of Otx2 from an activator to a repressor form, thereby controlling the expression of the GnRH gene (Larder and Mellon 2009). This result was

supported by the overexpression of Otx2 in GnRH neurons that increased transcriptional activity of the GnRH gene promoter (Larder and Mellon 2009). In contrast, conditional knockout of Otx2 in GnRH expressing neurons decreased the number of GnRH neurons in the ventral hypothalamus. It also lead to a delayed onset of puberty and infertility as a consequence of decreased expression of GnRH and other sex steroid hormones, suggestive of a critical requirement of Otx2 for GnRH expression and reproductive competence (Diaczok et al. 2011).

**1.3.2d Retinal cells**

During eye development in vertebrates, a pair of rudimentary structures called optic vesicles originates from each side of the forebrain. These optic vesicles interact with the surface ectoderm by invagination, followed by regionalization into a bilayered optic cup. The optic cup consists of an outer, retinal pigment epithelium (RPE) and inner, neural retina layers (Nishihara et al. 2012). These layers contain various cell types of the vertebrate eye such as the photoreceptors, retinal ganglion cells, horizontal cells, amacrine cells, bipolar and Muller glial cells (Nishihara et al. 2012). Otx2 plays an important role during this process of eye development (Cantos et al. 2000; Fossat et al. 2007). During retinal development in the mouse, Otx2 is expressed in the entire optic vesicle as early as E9 (Figure 1.7A) and then becomes restricted to the RPE (Bovolenta et al. 1997; Martinez-Morales et al. 2001; Nishihara et al. 2012). Otx2 represses the expression of neural retina markers such as fibroblast growth factor (Fgf8) and Sox2 for regionalization of RPE in the outer layer of the optic cup (Figure 1.7B). Loss of Otx2 can cause ectopic expression of Fgf8 and Sox2 and induce neural retina differentiation in this region (Nishihara et al. 2012). Otx2 is also required for the terminal

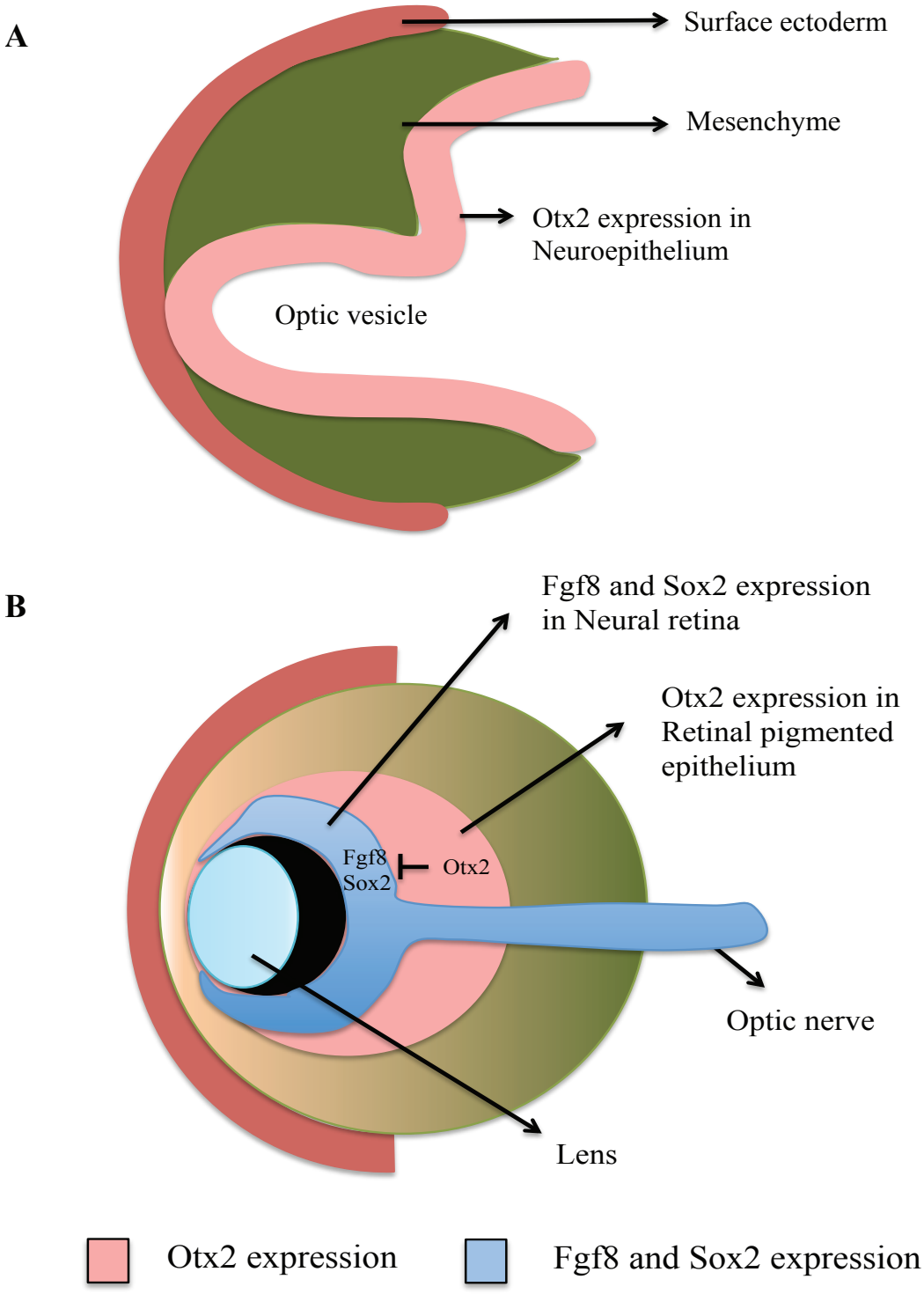


**Figure 1.7: Role of Otx2 in eye development in vertebrates:** (A) At embryonic day 9 (E9) in the mouse, Otx2 is expressed in the entire optic vesicle and (B) then becomes restricted to the retinal pigment epithelium (RPE). Otx2 is also required for the regionalization of neural retina by repressing neural retina markers such as Fgf8 and Sox2 (adapted with modification from http://discovery.lifemapsc.com/library/images/embryonic-eye-development).

differentiation and maturation of photoreceptors and bipolar cells (Nishida et al. 2003; Koike et al. 2007; Sato et al. 2007). Its expression is maintained in mature photoreceptor (rods and cones cells), bipolar cells and a subset of Mueller glial cells (Baas et al. 2000; Fossat et al. 2007; Beby et al. 2010). In the photoreceptor and bipolar cells, Otx2 is expressed throughout the life and is required for their maintenance (Fossat et al. 2007; Sugiyama et al. 2008). Mutations in human *OTX2* can cause malformation of the eye such as micropthalmia (small eye) and anophthalmia (absence of an eye) and these defects account for almost 25% of visual impairment in children (Ragge et al. 2005; Wyatt et al. 2008; Schilter et al. 2011).

As both vertebrate homeobox Otx2 and the Drosophila homologue, Otd are crucial in photoreceptor development, hypomorphic Otx2 alleles in Drosophila caused poor development of photoreceptors (Vandendries, Johnson, and Reinke 1996). Similarly, conditional deletion of Otx2 in retina induced depletion of the photoreceptors, bipolars and horizontal cells with concomitant increase in the number of other retina cell types such as amacrine cells in mice (Nishida et al. 2003; Koike et al. 2007; Sato et al. 2007). In contrast, induced expression of Otx2 increased the number of photoreceptors in rat retina and this was accompanied by loss of all other postnatal cell types (Nishida et al. 2003). Furthermore, non-neural cells can adopt a photoreceptor fate upon introduction of Otx2 (Akagi et al. 2004; Inoue et al. 2010). Analysis of conditional ablation of Otx2 in postnatal bipolar cells revealed that Otx2 is required for terminal differentiation (Koike et al. 2007). Temporal and spatial expression of Otx2 in specific populations of retinal cells seems to be controlled by multiple regulators during retinal fate specification. In fact, a retinal-specific evolutionary conserved enhancer element 2 (ECR2) recapitulates the expression and function of Otx2 in post-mitotic photoreceptors and in a subset of retinal progenitor cells. As the ECR2 element was not active in Otx2-positive bipolar cells and

RPE, a different transcriptional network might be controlling the expression of Otx2 in these cells (Emerson and Cepko 2011). This suggests a cell-type dependent regulation of expression and function of Otx2 during retinal fate specification.

### 1.3.2e Plasticity of visual cortex

Otx2 expression is retained in the adult retina for maintaining the postnatal plasticity of the visual cortex (Sugiyama et al. 2008; Spatazza et al. 2013). During early postnatal life, the neural circuits are shaped by experience. The visual input from both eyes first converge onto the individual neurons in the binocular zone of the primary visual cortex. This leads to a subsequent determination of ocular dominance of one eye following a competitive interaction (Wiesel and Hubel 1963). In some cases, the deprivation of visual input from one eye can lead to permanent loss of vision in that eye, a condition known as amblyopia or "lazy eye" affecting 2-4% of the human population (Prusky and Douglas 2003; Maurer and Hensch 2012). In the primary visual cortex, Otx2 protein starts accumulating during the onset of critical periods of plasticity and persists in the adult visual cortex (Sugiyama et al. 2008; Spatazza et al. 2013). Otx2 regulates the maturation of parvalbumin cells, which become evident at the onset of plasticity. It has been proposed by Sugiyama et al, that a cell-to-cell experience-dependent transfer of Otx2 protein might be involved in setting a physiological milieu for promoting plasticity of the neural circuit. Exogenous introduction or deprivation of Otx2 in parvalbumin cells accelerated or abolished the establishment of critical periods of plasticity, respectively. Otx2 protein is synthesized and secreted by the choroid plexus that serves as a source of Otx2 for cortical parvalbumin cells in adults (Johansson et al. 2013; Spatazza et al. 2013). Knockdown of Otx2 in the choroid plexus reduced the local content and impaired the transfer of Otx2 into distant parvalbumin cells. This

allowed the reactivation of critical periods of binocular plasticity in the visual cortex of adult mice and restored vision in adult amblyopic mice (Spatazza et al. 2013).

### 1.3.3 OTX2 in medulloblastoma

During early fetal development in humans, OTX2 is expressed in the diencephalon, mesencephalon, basal telencephalon, choroid plexus and the hippocampal regions. It is also expressed in the progenitor cells of the EGL of the developing cerebellum and pineal gland in the later stages of fetal development (de Haas et al. 2006; Larsen et al. 2010). In the postnatal cerebellum, OTX2 levels are lost as the expression is restricted to choroid plexus, pineal gland and retinal pigment epithelium in adult tissues (Fossat et al. 2006). However, high levels of OTX2 protein have been detected in Group 3 and 4 MBs but its expression is negligible in the SHH subgroup (Bunt et al. 2010). The OTX2 gene is amplified and overexpressed in 70% of MB cases (Michiels et al. 1999; Yokota et al. 2004; Boon, Eberhart, and Riggins 2005; Di et al. 2005; de Haas et al. 2006). A ten-fold average increase in the copy number of OTX2 has been identified in MB cell lines. Also, OTX2 mRNA and protein levels are higher in 75-80% of aggressive Group 3 and 4 MB tumor samples (Di et al. 2005; de Haas et al. 2006; Kool et al. 2008; Adamson et al. 2010). It has been shown that OTX2 is amplified before dissemination of tumor cells and its expression stays high in disseminated cells (Di et al. 2005).

Frequent amplification and overexpression suggests that OTX2 plays an oncogenic role in MB and is thought to be required for growth and maintenance of MB cells (Di et al. 2005; Adamson et al. 2010; Bai et al. 2012). However, studies evaluating the function of OTX2 in MB have demonstrated conflicting results. For example, OTX2 has been shown to play an oncogenic role in maintaining cell growth of Group 3 and 4 MB cell lines (Di et al. 2005; Adamson et al.

2010). Small interference RNA (siRNA)-mediated knockdown of OTX2 in Group 3 and 4 cell lines resulted in suppression of cell growth *in vitro* (Di et al. 2005). However, one study evaluating OTX2 overexpression in SHH MB lines revealed that OTX2 suppresses cell proliferation and induces cell senescence specifically *in vitro* (Bunt et al. 2010). This dichotomy is also seen in the nervous system, where OTX2 regulates proliferative and/or differentiation abilities of various cell types based on the neuroanatomical regions. For instance, Otx2 is required to maintain the proliferation and differentiation of ventral mesencephalon dopaminergic progenitor cells (Omodei et al. 2008). Loss of Otx2 results in proliferation and differentiation abnormalities of these progenitor cells and can induce their premature post-mitotic transition (Omodei et al. 2008). Conversely, Otx2 appears to inhibit proliferation in the thalamus as ablation of Otx2 enhanced the proliferative ability of thalamic progenitors, and led to the formation of hyperplastic cell masses (Puelles et al. 2006). These opposing data suggest that the effect of OTX2 on cell growth may be dependent on the cell-type and neuroanatomical region. Distinct mechanisms might be involved in the disparate context-dependent functions of this multifaceted transcription factor. However, this concept has not been directly tested in OTX2 expressing Group 3 and 4 versus SHH MB cells, which do not express OTX2. Furthermore, previous studies focused on cell proliferation/survival of MB cells and did not evaluate other cellular properties, including cell migration, and aspects of stem cell function, such as self-renewal (ability of the cells to maintain themselves for indefinite time period). This will be important as invasive growth and metastasis contribute to recurrence and poor prognosis in MB patients (Mehta 2011). Moreover, brain tumor stem cell populations have been shown to be critical for MB propagation and maintenance (Singh et al. 2003; Singh et al. 2004).

In addition, previous studies have used long-term cultured patient-derived cell lines, which exhibit numerous karyotypic abnormalities and may provide inconsistent results regarding the function of a gene. Indeed, studying the role of genes related to MB progression in well-established murine models have provided important insight, and even *Drosophila melanogaster* has recently been employed to identify novel genes associated with pediatric brain tumors such as AT/RT (Jeibmann et al. 2014). However, complementary human models are still needed to both verify and identify the functional relevance of specific genes to pediatric neural tumor progression. Moreover, primary patient samples are difficult to maintain in *in vitro* cultures and the cells often die or stop growing after 2-3 passages. Very few MB patient samples have been adapted to long-term culture conditions and thus, there is a critical need for developing alternative model systems.

## 1.4 Human embryonic stem cells and their use in regenerative medicine

Human embryonic stem cells (hESCs) were first isolated and cultured in 1998 by Thomson et al (Thomson et al. 1998). These cells were derived from the inner cell mass of the pre-implantation embryo and are known for their ability to self-renew indefinitely as well as for their potential to generate all three germ layers (ectoderm, mesoderm and endoderm) which is defined as pluripotency. Several studies have utilized hESCs for differentiation into neurons, hematopoietic cells, cardiomyocytes, pancreatic beta cells and intestinal cells (Reubinoff et al. 2001; Chadwick et al. 2003; Perrier et al. 2004; Wang et al. 2005; Gerrard, Rodgers, and Cui 2005; Roy et al. 2006; D'Amour et al. 2006; Kriks et al. 2011; Takayama et al. 2012). Recently, hESCs have also been utilized for differentiation into the renal lineage and generation of a self-organizing kidney (Takasato et al. 2014). Although hESCs hold great promise in the area of

regenerative medicine and cell replacement therapies, the associated risks of tumorigenicity hinder their usefulness in these areas (Ben-David and Benvenisty 2011). For example, human ESCs share many features with cancer cells such as indefinite self-renewal ability, high telomerase activity and genomic instability (Ben-David and Benvenisty 2011). As an alternative, researchers also utilize induced pluripotent stem cells (iPSCs) (Takahashi and Yamanaka 2006; Werbowetski-Ogilvie 2014).

## 1.5 Induced pluripotent stem cells

In 2012, Shinya Yamanaka received the Nobel Prize for the discovery of iPS cells. Generation of iPSCs have revolutionized the stem cell field as these cells are a potential source of patient-specific pluripotent stem cells (Park et al. 2008). IPS cells were generated first from mouse and then from human fibroblasts by ectopic expression of a combination of four pluripotent transcription factors such as OCT4, SOX2, KLF4 and MYC or (OCT4, SOX2, NANOG and LIN28) via retroviral transduction (Takahashi and Yamanaka 2006; Takahashi et al. 2007). These reprogrammed cells resemble embryonic stem cells in terms of morphology, gene expression profile and their ability to form the cells of all 3 germ layers (Takahashi and Yamanaka 2006; Takahashi et al. 2007; Park et al. 2008; Nakagawa et al. 2008). However, retroviral-mediated integration of genetic material posed a risk of tumorigenesis that restricts the usage of these cells in human clinical trials for cell-based therapies. Some of these issues have been resolved by utilizing non-viral methods such as recombinant proteins or chemical methods for cellular reprogramming (Zhou et al. 2009; Masuda et al. 2013).

## 1.6 Use of hESCs and iPSCs in disease modeling

Despite the drawbacks associated with both hESCs and iPS cells, "modeling disease in a dish" provides an alternative use for pluripotent cells. Several studies have demonstrated the utility of disease-specific and patient-specific iPS cells in investigating the cellular and molecular events contributing to the development of several human disorders and for screening therapeutic agents (Unternaehrer and Daley 2011). Many human early- and late-onset neurodegenerative disorders such as Alzheimer's disease, Parkinson's disease, Huntington's disease, amyotrophic lateral sclerosis and spinal muscular atrophy are characterized by memory loss and cognitive deficits as a result of chronic and progressive impairment of neuronal functions (Jung et al. 2012). However, the lack of cellular models for recapitulating disease pathogenesis *in vitro* is making it difficult for finding treatments. The recent use of patient-derived iPSCs has facilitated our understanding of disease development and/or progression. For example, the pathogenesis of Alzheimer's disease has been studied using disease-specific iPSCs-derived neurons (Yagi et al. 2011). In the last decade, substantial progress has also been made in modeling other neurodegenerative diseases as well as heart diseases such as arrhythmogenic right ventricular cardiomyopathy, other genetic arrhythmias and human cancers utilizing disease-specific iPS cells (Sanchez-Danes et al. 2012; Jung et al. 2012; Kim et al. 2013; Moretti et al. 2013; Chen et al. 2014).

Similarly, hESCs have been utilized for modeling various human genetic disorders. One of the most common neurodegenerative genetic disorders known as Huntington disease (HD) affects muscle coordination and also induces cognitive impairment; however, lack of an *in vitro* model for HD has made it difficult to understand the root causes of this disease (Niclis et al. 2009). Niclis et al. have isolated two HD hESCs lines, S1-186 and S1-187, from embryos

identified by preimplantation genetic diagnosis for investigating the relevance of associated genetic mutations to the development of HD (Niclis et al. 2009; Niclis et al. 2013). Additional hESC lines have been generated by introducing chromosomal aneuploidies for modelling widely recognized genetic disorders such as Patau syndrome (trisomy of chromosome 13), Down syndrome (trisomy of chromosome 21), Triple X syndrome (trisomy of chromosome X) and Turner syndrome (monosomy of X) (Biancotti et al. 2010). These cell lines represent an alternative source for understanding the impact of these chromosomal abnormalities on development of particular tissues/organs (Biancotti et al. 2010).

The use of hESCs is not limited to studying early- or later-onset genetic disorders. These cells have also been employed for investigating several human cancers. Both hESCs and cancer stem cells utilize similar pathways for acquisition of pluripotency and tumorigenesis, respectively. The pluripotency of hESCs is governed by a set of transcription factors such as OCT4, NANOG, SOX2 and MYC and these genes and/or their targets are also frequently upregulated in poorly differentiated human cancers such as high grade ER-negative breast cancers, bladder carcinoma, glioblastoma and MB ((Clark 2007; Ben-Porath et al. 2008; Bass et al. 2009; Kim et al. 2010; Po et al. 2010; Zbinden et al. 2010; Taylor et al. 2012). For example, the somatic cell reprogramming factor, MYC, is known for its oncogenic role in brain tumors such as MB, gliomas and primitive neuroectodermal tumors (Herms et al. 2000; Grotzer et al. 2001; Roussel and Robinson 2013; Annibali et al. 2014). NANOG, a pluripotent factor, has been implicated in maintaining the stem cell like features in the malignant brain tumor, glioblastoma (Niu et al. 2011; Higgins et al. 2013). Similarly, other pluripotent factors such as SOX2 and OCT4 are critical for maintaining proliferation of glioma cells and studies have suggested that

therapies be specifically designed to target these genes (Schmitz et al. 2007; Gangemi et al. 2009; Du et al. 2009; Werbowetski-Ogilvie 2014).

In addition to these pluripotent genes, the P53 gene that regulates the signaling pathway important for both maintaining hESCs pluripotency and for enhancing the efficiency of somatic cell reprogramming is also involved in tumorigenesis (Krizhanovsky and Lowe 2009). P53 is the most commonly mutated tumor suppressor gene in human cancers and its inactivation can accelerate tumor growth in mouse models (Mizuno et al. 2010) as described earlier. In fact, the inactivation of P53 can induce an ES-cell-like transcriptional program in breast and lung cancers further underscoring the relationship between pluripotency and malignancy (Song, Hollstein, and Xu 2007; Mizuno et al. 2010). P53 knockout hESCs provide a cellular resource for studying human cancer that are not recapitulated by p53-/- mouse models due to interspecies differences (Donehower et al. 1992; Jacks et al. 1994; Song, Hollstein, and Xu 2007). In particular, *P53* mutations mostly induce carcinomas and are linked with poor prognosis in human cancers; however, in mice, lack of *P53* results in the development of sarcomas and lymphomas (Donehower et al. 1992; Jacks et al. 1994). This could be partly defined by the differential roles of the mutant form of the P53 protein versus complete loss of normal P53 protein during tumorigenesis (Doyle et al. 2010). It has been shown that mutant form of P53 manipulate its tumor suppressive functions by acquiring new oncogenic roles (Doyle et al. 2010; Hanel et al. 2013; Muller and Vousden 2014; Lu et al. 2013).

## 1.7 Human ESCs and childhood cancers

The most common childhood cancers such as leukemia, central nervous system tumors and lymphomas manifest early during development. It has become increasingly difficult to

recapitulate the early events of disease progression using well-established cell lines. While murine models have been useful for adding insights into the tumor biology, not all murine models faithfully represent the human counterpart of disease. For example, infant pro-B acute lymphoblastic leukemia (ALL) arises prenatally as a result of fusion of mixed-lineage leukemia (MLL-AF4) genes (Bueno et al. 2012). ALL has a very brief latency and dismal prognosis in infants but this is not recapitulated in murine models of ALL (Chen et al. 2006; Metzler et al. 2006; Krivtsov et al. 2008). To understand the role of MLL fusion in ALL development, Bueno and colleagues utilized hESCs derived hemogenic precursors and demonstrated that MLL-AF4 expression is not sufficient to induce neoplastic transformation both *in vitro* and *in vivo* (Bueno et al. 2012). Another example where mouse models could not faithfully recapitulate the human developmental process is the investigation of the role of the transcription factor, stem cell leukemia/T-cell acute lymphocytic leukemia 1 (SCL/TAL1) transcription factor in human hematopoiesis (Real et al. 2012). In mouse models lacking the *SCL/TAL1* gene, a master regulator of early hematopoiesis, animals die early during embryogenesis due to complete absence of hematopoiesis (Real et al. 2012). To overcome this issue, researchers utilized hESCs for understanding the role of SCL using a stepwise hematopoietic developmental process (Real et al, 2012).

In the case of medulloblastoma, most of the currently available mouse models represent the SHH MB subgroup (Goodrich et al. 1997; Taylor et al. 2002; Hallahan et al. 2004; Oliver et al. 2005; Hatton et al. 2008). Recently, MYC-driven mouse models have been developed for understanding the role of the *MYC* gene in tumorigenesis of Group 3 and 4 MBs (Pei et al. 2012; Kawauchi et al. 2012; Swartling 2012). These mouse models have been developed on a P53 null background, which do not always recapitulate their human MB counterparts. In addition, there

are no mouse models available for understanding the role of OTX2 in Group 3 and 4 tumors. Moreover, the complete loss of OTX2 is embryonic lethal and its overexpression is not sufficient to induce cellular transformation and initiate tumorigenesis (Wortham et al. 2012). This makes it difficult to understand the functional relevance of this multifunctional transcription factor in MB progression. In order to deal with this issue, relevant hESCs-derived cellular models are needed for investigating cellular and molecular events contributing to MB progression.

### 1.8 Features of normal and transformed hESCs

Routine evaluation of normal hESCs for the acquisition of abnormal karyotypes is mandatory (Baker et al. 2007). However, normal hESCs can also acquire abnormal cellular features during long-term culture such as enhanced cell proliferation, self-renewal ability and aberrant differentiation potential with or without major chromosomal changes and these cells are known as transformed hESCs (trans-hESCs). Werbowetski-Ogilvie et al. studied the features of both normal and trans-hESCs variant and found that trans-hESCs exhibit enhanced cell proliferation, self-renewal ability *in vitro* and greater tumorigenic potential *in vivo* relative to their normal counterparts (Werbowetski-Ogilvie et al. 2009). These trans-hESCs also gain the ability to grow independent of growth factors such as basic fibroblast growth factor (bFGF), which is typically required for maintaining normal hESC pluripotency (Werbowetski-Ogilvie et al. 2009). Normal hESCs display heterogeneous morphology consisting of tightly packed colony cells with high nuclear-to-cytoplasmic ratio surrounded by more differentiated fibroblast-like cells. However, trans-hESCs exhibit more homogenous morphology and lose their fibroblast feeder layer (Werbowetski-Ogilvie et al. 2009).

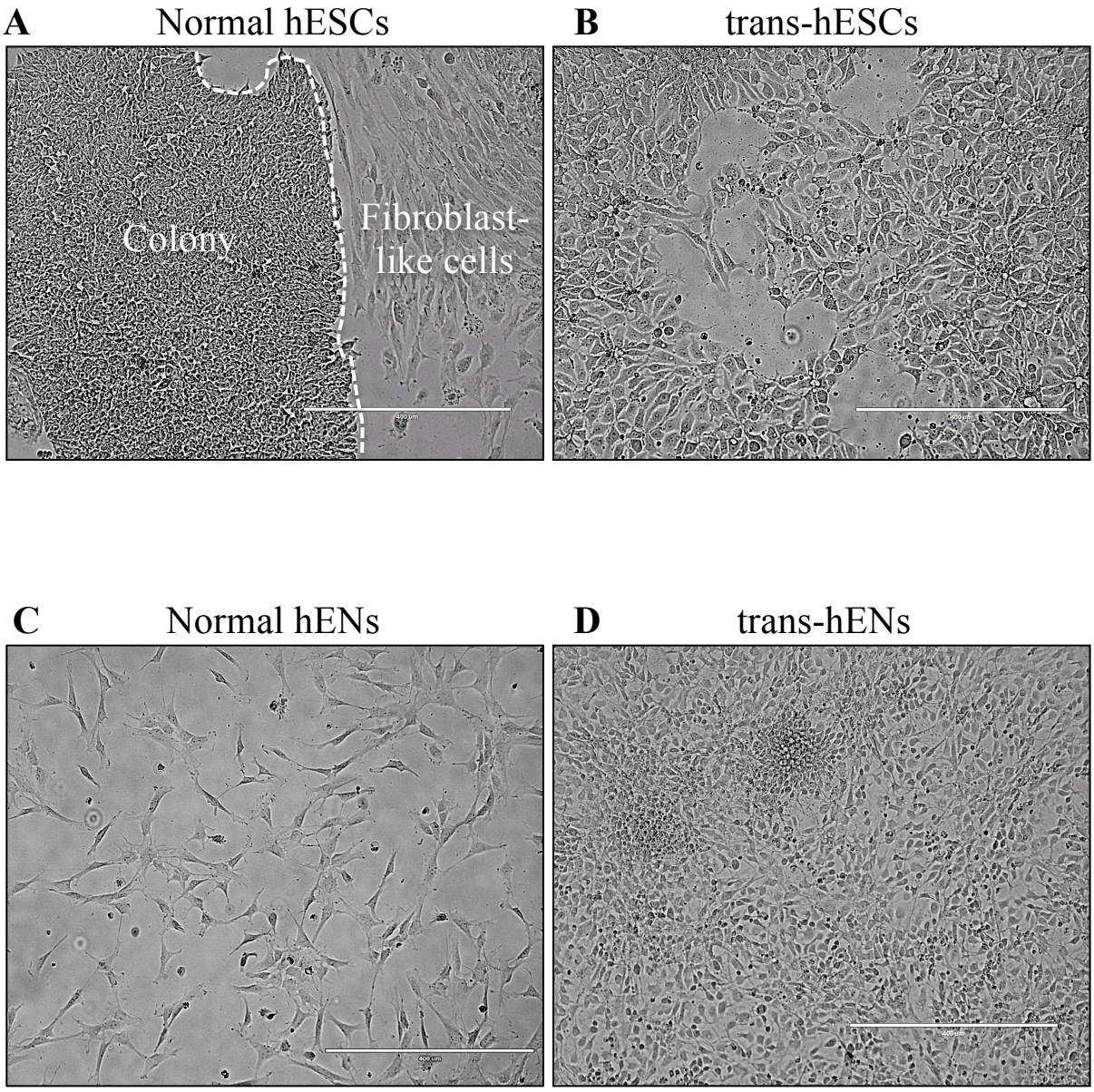


**Figure 1.8: Comparative model system of neural precursors derived from normal and transformed hESCs.** A) Normal human embryonic stem cells are highly heterogeneous cultures consisting of tightly packed colony cells with a high nuclear to cytoplasmic ratio surrounded by more differentiated fibroblast-like cells. These normal hESCs undergo cellular transformation during long-term culture and acquire neoplastic features such as elevated self-renewal and proliferation capacity as well as aberrant differentiation potential. These cells are called transformed hESCs (B). (C-D) Upon differentiation into neural precursors, the transformed human embryonic neural precursors (trans-hENs) derived from trans-hESCs retain their neoplastic features *in vitro*.

Apart from the differences in cellular features, trans-hESCs also exhibit very high endogenous expression of pluripotent markers such as stage specific embryonic antigen 3 (SSEA3), LIN28A, OCT4, NANOG and SOX2 (Werbowetski-Ogilvie et al. 2009; Ji et al. 2009). These trans-hESCs exhibit cellular and molecular profiles that closely resemble poorly differentiated cancer cells. Therefore, both normal and trans-hESCs provide an alternative and comparative system for studying various aspects of childhood cancers and for identifying novel therapies. Recently, Dingwall and colleagues utilized the transformed hESC lines to model radiation resistance of human cancer stem cells (Dingwall et al. 2015). They found that trans-hESCs are resistant to radiation treatment relative to their normal counterparts and showed decreased levels of apoptosis and altered cell cycle arrest (Dingwall et al. 2015). More recently, a study has shown the potential of hESC-derived oligodendrocytes to repair radiation-induced damage to the brain following brain cancer treatment (Piao et al. 2015). Intracranial transplantation of hESC-derived oligodendrocyte progenitors into the forebrain and cerebellum were able to recover both structural and functional insults incurred following radiation treatment (Piao et al. 2015).

### 1.9 Normal and transformed neural precursors derived from hESCs for modeling MB

As MB is thought to arise from neural stem cells or more differentiated progenitors, the neural derivatives from normal and trans-hESCs could serve as a surrogate to long-term cultured cell lines and insufficient number of patient samples. The features of neural derivatives from normal and trans-hESCs are well studied by the Werbowetski-Ogilvie laboratory (Figure 1.8) (Werbowetski-Ogilvie et al. 2012). Following differentiation of trans-hESCs into neural precursors herein called transformed human embryonic neural precursors (trans-hENs), they

retain their high self-renewal and proliferation ability compared to normal hENs (Figure 1.8). Interestingly, trans-hENs resemble human Group 3 and 4 MBs *in vivo* (Werbowetski-Ogilvie et al. 2012). Global gene expression analysis revealed differential expression of 1346 transcripts in trans-hENs vs. hENs including upregulation of both a pluripotency and a MB transcription program that exhibited similarities to Groups 3 and 4 MBs. These trans-hENs also have >10 fold high endogenous expression of OTX2 (Werbowetski-Ogilvie et al. 2012). These properties make neural precursors derived from both normal and trans-hESCs a complementary system for studying the functional relevance of genes such as OTX2 to MB progression.

# 2.0 Hypothesis and Objectives

### 2.0.1 Hypothesis

Given that OTX2 is frequently amplified and overexpressed in Group 3 and 4 MBs but rarely expressed in SHH subgroup, we hypothesize that OTX2 has a variant-dependent tumor inhibitory or oncogenic role in MB. We also hypothesize that neural derivatives from normal and trans-hESCs will provide a comparative cellular system for investigating the role of OTX2 in regulating cellular and molecular events contributing to MB progression.

**2.0.2 Objectives:** To test this hypothesis, we set four main objectives:

**Objective 1**

To evaluate the role of OTX2 overexpression in normal hENs and Daoy (representing the SHH subgroup) MB cells using lentiviral transduction *in vitro* and *in vivo*. This objective will determine the role of OTX2 in regulating cellular functions such self-renewal, cell migration and cell survival in both normal neural precursors and the SHH MB subgroup *in vitro*. The effect of

OTX2 overexpression on tumorigenic potential of the SHH MB cell line, Daoy, will also be determined *in vivo*.

**Objective 2**

To understand the molecular mechanism regulated by OTX2 in controlling cellular functions of normal hENs and Daoy MB cells. This objective will focus on investigating the interaction of OTX2 with other genes or factors involved in regulating the cellular functions in hENs and Daoy cells utilizing various molecular techniques.

**Objective 3**

To evaluate the role of OTX2 knockdown on the neoplastic features of trans-hENs and representative Group 3 and Group 4 MB cells *in vitro* and *in vivo*. This part of the study will determine the effect of OTX2 knockdown on neoplastic features such as elevated self-renewal and proliferation of trans-hENs and Group 3 and 4 MB cells *in vitro.* The effect on tumorigenic potential following OTX2 knockdown will be determined *in vivo*.

**Objective 4**

To investigate the molecular mechanisms by which OTX2 regulate the neoplastic properties of trans-hENs and Group 3 and 4 MB cells. In this objective, we will investigate the molecular mechanism(s) associated with knockdown of OTX2 in trans-hENs as well as Group 3 and 4 MB cells in the context of stem cell function or self-renewal.

# CHAPTER 2: MATERIALS AND METHODS

## 2.1 Cell culture

### 2.1.1 Human embryonic stem cells culture

Both normal hESCs (H9) and trans-hESC (v1) (Werbowetski-Ogilvie et al. 2009) were maintained on Matrigel (BD Biosciences, Mississauga, ON, Canada) in mTESR™1 with 5X supplement (Stem Cell Technologies, Vancouver, BC, Canada). Confluent cultures were dissociated for 5 min in collagenase IV (Gibco, Invitrogen, Burlington, ON, Canada) and passaged 1:4 (trans-hESCs) or 1:2 (hESCs).

### 2.1.2 Neural precursor derivation from normal and transformed hESCs

Neural precursors from normal hESCs (hENs) and their transformed derivatives (trans-hENs) (Figure 1.8) were cultured as previously described (Werbowetski-Ogilvie et al. 2012). Briefly, hESCs and trans-hESCs were dissociated in collagenase IV (Gibco) and re-plated as aggregates onto poly-L-Ornithine/laminin-coated plates (BD Biosciences) in neural precursor media, Dulbecco's modified eagle medium (DMEM)/F12, supplemented with 1% N2 (Gibco), 1% B27 (Gibco), 20 ng/ml epidermal growth factor (EGF) (BD Biosciences), and 20 ng/ml basic fibroblast growth factor (bFGF) (BD Biosciences)). After 4 days (trans-hESCs) and 6 days (hESCs) (passage 0 or start of differentiation), cultures were dissociated into single cells with Accutase (Gibco) and plated back onto laminin-coated plates in neural media for additional passages.

### 2.1.3 Maintenance of MB brain tumor cell lines

Daoy human SHH MB cells (a TP53 mutated cell line), D283 and D341 cells were purchased from the American Type Culture Collection (ATCC, Rockville, MD, USA). The Daoy MB cell line is derived from a desmoplastic MB (Jacobsen, Jenkyn, and Papadimitriou 1985), has been shown to exhibit global activation of SHH-pathway genes (Dahmane et al. 2001; Leung et al. 2004; Wang et al. 2012) and is statistically classified as SHH subgroup based on hierarchical clustering and principal component analysis (PCA) with patient samples (Triscott et al. 2013). D283 (Friedman et al. 1985; Snuderl et al. 2013) represent Group 4 MB. Cells were cultured in Eagle's Minimum Essential Media (EMEM) (ATCC) containing 10% fetal bovine serum (FBS) (Fisher Scientific, Ottawa, ON, Canada). D425 (He et al. 1991) and D341 (Friedman et al. 1988) represents Group 3 MB and were cultured in stem cell enriched conditions. D425 cell line was provided by Dr. Issai Vanan, University of Manitoba, Winnipeg, Manitoba. D425 cells were grown in StemPro media (Knockout-DMEM/F12 (Gibco), Stem pro neural supplement (Gibco REF A10508-01), 10μg EGF (Invitrogen), 10μg bFGF (Invitrogen) and L-glutamine (HyClone Cat# SH30034) in suspension culture. Confluent cultures were dissociated in Accutase (Gibco) and passed 1:15. For neural precursor differentiation, Daoy, D283, D425 and D341 cells were dissociated for 5 min in Accutase (Gibco) and re-plated in ultralow attachment 6-well plates (Corning, Tewksbury, MA, USA) in neural media. Cells were passed every 5 days with media changes every 3 days.

## 2.2 Lentiviral transduction and selection of stable cell lines

### 2.2.1 Overexpression of OTX2 in Daoy and hENs

OTX2 was stably overexpressed in Daoy and/or hENs using purchased Precision Lentiviral open reading frame (LentiORFs) (Open Biosystems, Thermo Scientific) consisting of pLOC dual expression constructs with TurboGreen fluorescent protein (GFP) as a marker to track transduction efficiency and Blasticidin S resistance for stable clone selection (Figure 2.1A). LentiORF red fluorescent protein (RFP)-expressing viral particles (from the same backbone pLOC construct) were used as a control (Figure 2.1B). On day 0, 5 $X10^4$ cells were plated in 24-well format, and incubated overnight. On day 1, medium was removed and virus was added using a multiplicity of infection (MOI) of 0.3. Medium was replaced after overnight incubation. Transduced Daoy cells were treated with Blasticidin (Mediatech, Corning) for stable clone selection (Figure 2.2A). For hENs, GFP+'s (OTX2+ hENs) and RFP+'s (RFP+ control hENs), cells were dissociated with Accutase and resuspended in sorting buffer (PBS containing 0.5% FBS) for fluorescent activated cell sorting (FACS) on a MoFlo™XDP (Beckman Coulter, Inc., Mississauga, ON, Canada) (Figure 2.2B). Sorted GFP+'s hENs and RFP+ control hENs were re-plated and expanded. OTX2 overexpression was verified by quantitative real-time polymerase chain reaction (qRT-PCR) and Western blot.

### 2.2.2 Overexpression of SOX2 in OTX2+ Daoy and hENs

For SOX2 overexpression, OTX2+ hEN, OTX2+ Daoy and control cultures were expanded to obtain sufficient cell quantities and then SOX2 was stably overexpressed SOX2 using ORF complementary deoxy-ribonucleic acid (cDNA) lentiviral particles (GeneCopoeia) consisting of the pReceiver-Lv105 expression vector with a Puromycin resistance gene. Negative Control

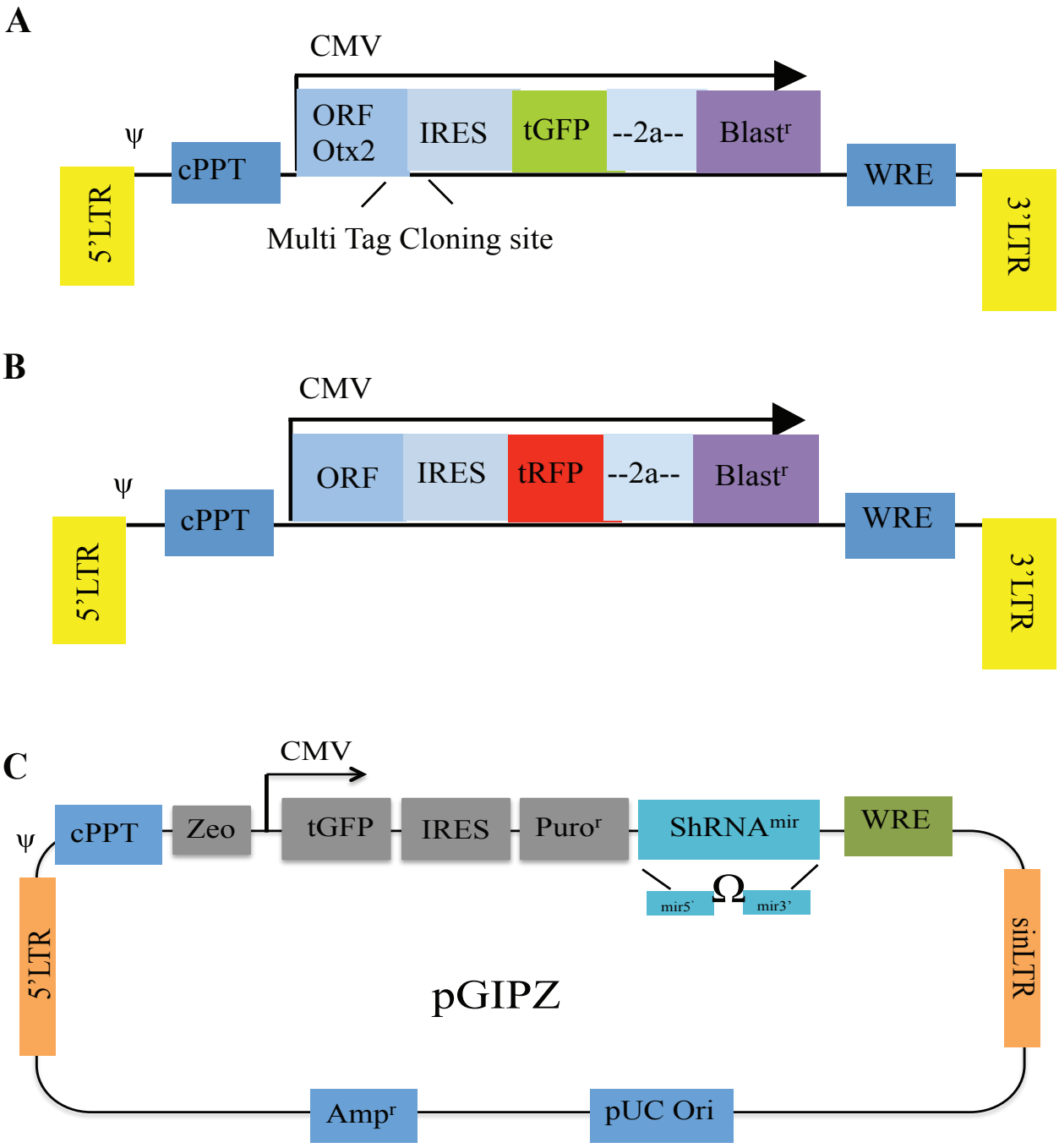


**Figure 2.1: Lentiviral constructs for stable overexpression and knockdown of OTX2:** (A) Lentiviral vector (Open Biosystems, Thermo Scientific) for overexpression of OTX2 in Daoy and normal human neural precursors (hENs) consisting of pLOC dual expression constructs with TurboGreen fluorescent protein (GFP) as a marker to track transduction efficiency and Blasticidin S resistance for stable clone selection. (B) LentiORF red fluorescent protein (RFP)-expressing control viral particles (from the same backbone pLOC construct). (C) short hairpinRNAmir (shRNAmir) constructs (Open Biosystems) consisting of a dual expression system with TurboGFP as a transduction marker.

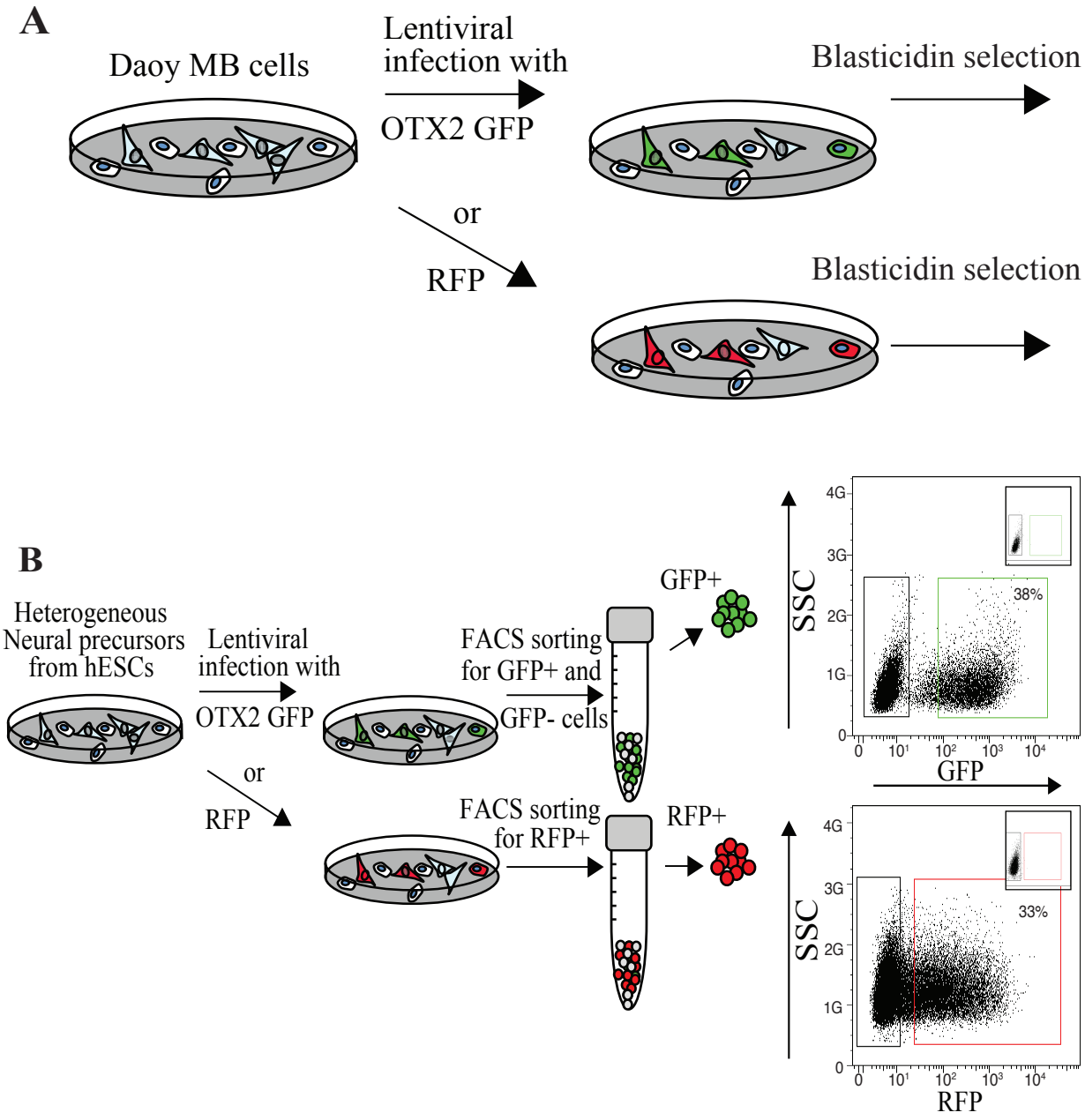


**Figure 2.2: Selection of stable OTX2 overexpressing Daoy and hENs:** (A) OTX2 overexpressing GFP+ and RFP+ control Daoy cells were selected using blasticidin. (B) As hENs are sensitive to antibiotic treatment, OTX2+ hENs and control hENs were sorted using fluorescent activated cell sorting (FACS) on a MoFlo™XDP (Beckman Coulter, Inc., Mississauga, ON, Canada) based on GFP and RFP expression.

Lentifect™ Lentiviral Particles were used as controls. SOX2 expression was evaluated by Western blot. Stably transduced Daoy and hEN cells were subjected to self-renewal, cell migration, proliferation, and survival assays using methods previously described (Werbowetski-Ogilvie et al. 2012; Morrison et al. 2013).

### 2.2.3 Stable knockdown of OTX2 in trans-hENs and D283 cells

OTX2 was stably knocked down in trans-hENs and D283 cells using 2 short hairpinRNAmir (shRNAmir) constructs (Open Biosystems) consisting of a dual expression system with Turbo-GFP as a transduction marker (Figure 2.1C). A non-silencing (scramble) shRNA sequence was used as a negative control. GFP+ cells were FACS sorted from transduced cultures 96 hours after infection, and OTX2 knockdown was determined by Western blot for shRNA sequences #1 and #2. Following stable selection, trans-hEN OTX2 KD and D283 OTX2 KD and their respective controls were subjected to cumulative cell count, viability and sphere formation assays.

### 2.2.4 Knockdown of OTX2 in trans-hENs and MB cell lines, D283, D425 and D341 using siRNA

OTX2 levels were knocked down in trans-hEN, D283, D425 and D341 cells using Silencer select siRNAs (Life Technologies, Burlington, ON, Canada). A non-silencing (scrambled) siRNA and Glyceraldehyde 3-phosphate dehydrogenase (GAPDH) siRNA were used as a negative and positive control, respectively. Three independent siRNAs targeting OTX2 (s9931, s9932 and s9933) (Table 2.1) were evaluated and all sequences were used at a final concentration of 30 nM. Knockdown of OTX2 was assessed by Western Blot.

**Table 2.1:** siRNA sequences used for knockdown of OTX2.

| siRNA | siRNA sense sequence | siRNA antisense sequence |
|---|---|---|
| OTX2 siRNA s9931 | GGCUUCAGGUUAUAGUCAATT | UUGACUAUAACCUGAAGCCTG |
| OTX2 siRNA s9932 | ACUGAUUGCUUGGAUUAUATT | UAUAAUCCAAGCAAUCAGUGG |
| OTX2 siRNA s9933 | CCAGGGAUAUGGAGCUUCATT | UGAAGCUCCAUAUCCCUGGGT |

## 2.3 *In vitro* cell functional assays

### 2.3.1 Neurosphere/tumorsphere assay for self-renewal

Following overexpression and knockdown of OTX2, the self-renewal capacity of cells was determined using a neurosphere/tumorsphere assay. Briefly, self-renewal was assessed by the ability of cells to be passaged in neurosphere/tumorsphere culture at clonal density (5-10 cells/μl) for at least 2 passages. The cells were plated in a 24-well low attachment plate at a clonal density of 10 cells/μl and kept undisturbed in the incubator for 5 days. After 5 days the number of primary spheres was counted in each well under a Zeiss Primo Vert microscope (Carl Zeiss Canada Ltd., Toronto ON, Canada). These primary spheres were dissociated in Accutase for 15 minutes and again plated at same clonal density in a new plate for secondary and tertiary sphere formation and counting (Figure 2.3A).

### 2.3.2. Proliferation assay

To assess proliferation, equal numbers of transduced cells ($4X10^4$ cells/well) were plated in neural proliferation medium and the total number of cells was calculated after 4 days in culture using an automated cell counter (TC20™ Automated Cell Counter, BIO-RAD). Trypan blue staining was used to assess cell viability.

### 2.3.3 Cell migration assay

Aliquots of $2.5x10^4$ cells were prepared as hanging drops in 20 μl media. Hanging drops were incubated for up to 4 days to form aggregates and then transferred to collagen type I gels (BD Biosciences) prepared as previously described (Werbowetski-Ogilvie et al. 2006). Following collagen gelation at 37 °C, embedded aggregates were then overlaid with media in

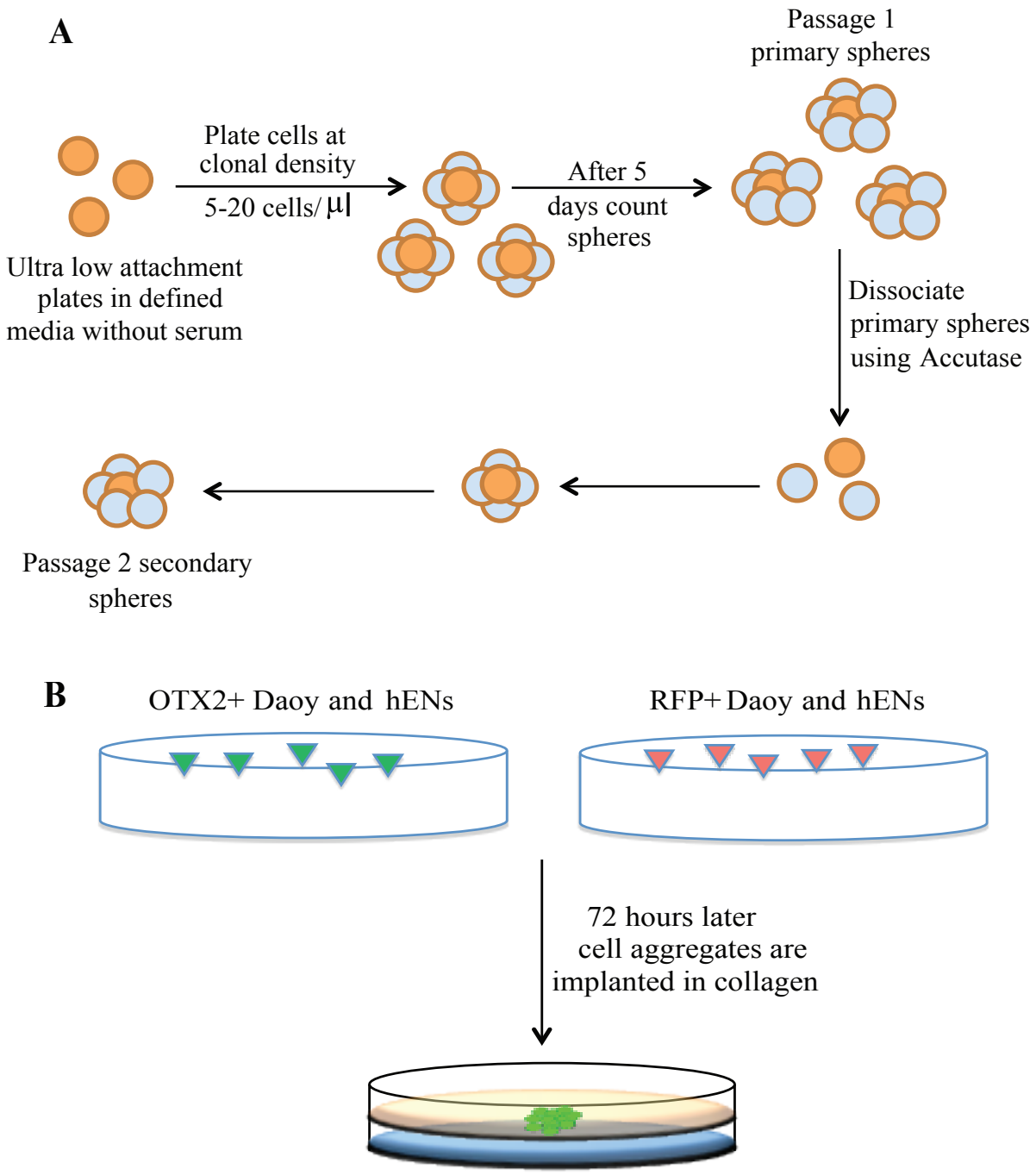


**Figure 2.3: Schematics of *in vitro* self-renewal and cell migration assays:**

(A) Neurosphere/tumorsphere assay for measuring self-renewal capacity *in vitro*. Cells were plated at clonal density of 5-20 cells/µl for primary sphere formation. After 5 days, primary spheres are counted and dissociated for subsequent passage to secondary and tertiary sphere formation. (B) For cell migration assays, hanging drops of 25,000cells/20µl are prepared and after 72 hours the aggregates are implanted in a 3D collagen matrix for evaluating cell migration ability.

which the cells are propagated. Aggregate measurements were taken at Day 0 and migration was measured at 72 hours (Day 3) using a Zeiss Primo Vert microscope (Carl Zeiss Canada Ltd., Toronto ON, Canada) with an ocular micrometer (Figure 2.3B).

### 2.4 Annexin V staining

To assess the effect on cell survival following OTX2 overexpression and knockdown, Annexin V staining method was employed as previously described (Morrison et al. 2013; Ali et al. 2015) using a phycoerythrin (PE) Annexin V Apoptosis Detection Kit (BD Biosciences) according to the manufacturer's guidelines. Annexin V is a 35-36 kDa Ca2+ dependent phospholipid-binding protein that binds to the plasma membrane component, phosphatidylserine (PS). In apoptotic cells, PS translocates from the inner to the outer side of the plasma membrane and can be stained with Annexin V (Annexin V Apoptosis Detection Kit, BD Biosciences). Cells were dissociated and a single cell suspension was prepared and stained with Annexin V-Allophycocyanin (APC) and 7-amino actinomycin D (7AAD). For each sample, 1.0 X $10^5$ cells were resuspended in 100µl of 1 X binding buffer and transferred into a 5ml culture tube. Cells were then stained with PE Annexin V and 7-AAD by incubating for 15 min at room temperature (RT) in dark. An additional 400µl of 1X binding buffer was added into each tube and flow cytometry was performed on a Gallios™ flow cytometer (Beckman Coulter). The results were analyzed using Kaluza software (Beckman Coulter).

### 2.5 Cell cycle analysis

For cell cycle analysis, cells were exposed to 10 µM bromodeoxyuridine (BrdU) for either 1 hour (adherent cultures) or 5 hours (tumorsphere/neurosphere cultures) prior to

harvesting as previously described. This allows the incorporation of BrdU into the newly synthesized DNA strands of actively proliferating cell. Cells were stained using a BD Pharmingen BrdU Flow Kit (BD Biosciences) according to the manufacturer's guidelines. Briefly, cells were dissociated to obtain single cell suspensions of 2.0 X $10^5$ cells/sample and fixed with 100µl BD Cytofix/Cytoperm buffer for 15-30 mins at RT. Cells were then washed with 1ml of 1X BD perm wash buffer and incubated with 100µl BD Cytoperm permeabilization buffer Plus for 10 mins on ice. Cells were washed with 1ml of 1X BD perm wash buffer and were re-fixed with 100µl of BD Cytofix/Cytoperm buffer for 5 mins at RT followed by washing 1ml of 1X BD perm wash buffer. Cells were then treated with 100µl of diluted DNase (diluted to 300µg/ml in (Dulbecco's phosphate-buffered saline) DPBS to obtain 30µg/$10^6$ cells) for 1 hour at 37°C and washed with 1ml of 1X BD perm wash buffer. Cells were incubated with diluted anti-BrdU antibody (1:50 dilution in 1X BD wash buffer) for 20 mins at RT and were counterstained with 7AAD for DNA content. Flow cytometry was performed on a MoFlo™ XDP (Beckman Coulter, Inc., Mississauga, ON, Canada) cell sorter and cell cycle phases in all the samples were resolved into G0/G1, S and G2/M phases (Figure). The results were analyzed using FlowJo software (Tree Star Inc., Ashland, OR).

**2.6 Intracranial transplants**

The University of Manitoba Animal Care Committee approved all procedures and protocols. Dissociated tumorspheres from OTX2+ Daoy and Daoy, as well as trans-hEN OTX2 KD, D283 OTX2 KD and their respective scramble controls were intracranially injected into nonobese diabetic/severe combined immunodeficiency (NOD SCID) mice as previously described (Singh et al. 2004; Werbowetski-Ogilvie et al. 2012; Kaur et al. 2015; Liang et al.

2015). Briefly, 5-7 week mice were weighed and administrated an anesthetic cocktail of Ketamine and Xylazine (50mg/kg of animal weight) followed with 4% isoflurane administration until there is an absence of pedal reflex. The head of the immobilized animal was fixed in a stereotactic frame and the gas anesthesia was maintained during the surgery. After securing the animal in the stereotactic frame, a vertical midline incision was made to open the skin and scalp layers and a 3.5 mm deep hole was drilled into the right frontal lobe of the brain. Using a 30 cubic centimetre (cc) needle, 10µl of cells were injected in the right frontal lobe with technical replicates consisting of $2.5X10^5$ (Daoy and D283) or $5X10^5$ (trans-hEN) cells. Following transplantation, mice were placed in a fresh cage until they regained consciousness and were observed until the animals reached humane endpoint (defined by a medical endpoint of 20% weight loss or time endpoint of 20 weeks). After 45 (D283 and trans-hEN) or 60 days (Daoy) (based on signs of tumor formation including appearance of a domed head and up to 20% weight loss), animals were perfused with formalin (VWR International, Mississauga ON, Canada) and the brains were extracted, placed in 10% formalin for 2-7 days, embedded in paraffin and then sectioned (5 µm thickness). Sections were de-waxed in xylene, rehydrated through a graded series of alcohol concentrations and stained with hematoxylin and eosin. Slides were mounted and imaged using an EVOS xl core microscope (AMG, Seattle, WA, USA).

### 2.7 Chromatin immunoprecipitation

ChIP was performed as previously described (Rao et al. 2015; Kaur et al. 2015). OTX2+ Daoy and OTX2+ hENs along with respective control cells (N=3 for each) were cross-linked using 1% formaldehyde for 10 mins and quenched by 0.125M glycine for 5 mins. Cell pellets were resuspended in 500 µL of sonication buffer (50 mM 4-(2-hydroxyethyl)-1-

piperazineethanesulfonic acid (HEPES), pH 7.9, 140 mM sodium chloride (NaCl), 1 mM ethylenediaminetetraacetic acid (EDTA), 1% (w/v) Triton X-100, 0.1% (v/v) sodium deoxycholate, 1% (w/v) sodium dodecyl sulphate (SDS) and protease inhibitors) and sonicated (17 cycles with 30 seconds ON/OFF) using a bioruptor to obtain fragments approximately 400 base pairs in length. DNA shearing was confirmed by running the samples on 1% agarose gel. Following sonication, 100 µL of chromatin was diluted by adding 900 µL dilution buffer (0.01% SDS, 1.1% Triton X-100, 1.2mM EDTA, 16.7mM Tris-HCl, pH 8.1, 167mM NaCl) containing protease inhibitors. Chromatin was precleared by incubating with protein G-Agarose /salmon sperm DNA for 1hour at 4°C with rotation. Samples were then centrifuged at 3000-5000 x g for 1 min and supernatants were collected in a fresh microfuge tube. 10 µL (1%) of supernatant was saved as an input at 4°C.

The supernatant containing precleared chromatin was fractioned for anti-trimethyl H3K4, anti-trimethyl H3K27, and anti-OTX2 antibodies and incubated with antibodies overnight at 4°C with rotation. Anti-RNA polymerase II and anti-rabbit IgG were used as positive and negative controls, respectively. The DNA-antigen-antibody complex was then coupled to protein G-Agarose by incubating for 1 hour at 4°C in IP buffer. Unbound chromatin was washed with low salt immune complex wash buffer A (20 mM Tris-HCl, pH 8.1, 150 mM NaCl, 2mM EDTA, 1% (w/v) Triton X-100, 0.1% (v/v) sodium deoxycholate), high salt immune complex wash buffer B (20 mM Tris-HCl, pH 8.1, 500 mM NaCl, 2mM EDTA, 1% (w/v) Triton X-100, 0.1% (v/v) sodium deoxycholate), LiCl immune complex wash buffer (10 mM Tris pH 8.1, 1mM EDTA, 250mM lithium chloride (LiCl), 1% IGEPAL-CA630, 1% deoxycholic acid) and Tris EDTA (TE) buffer (10mM Tris-HCl, 1mM EDTA pH 8.0). The bound fraction was eluted in 200 µL of elution buffer (10 µL 20% SDS, 20 µL 1M sodium bicarbonate ($NaHCO_3$) and 1.785 m sterile

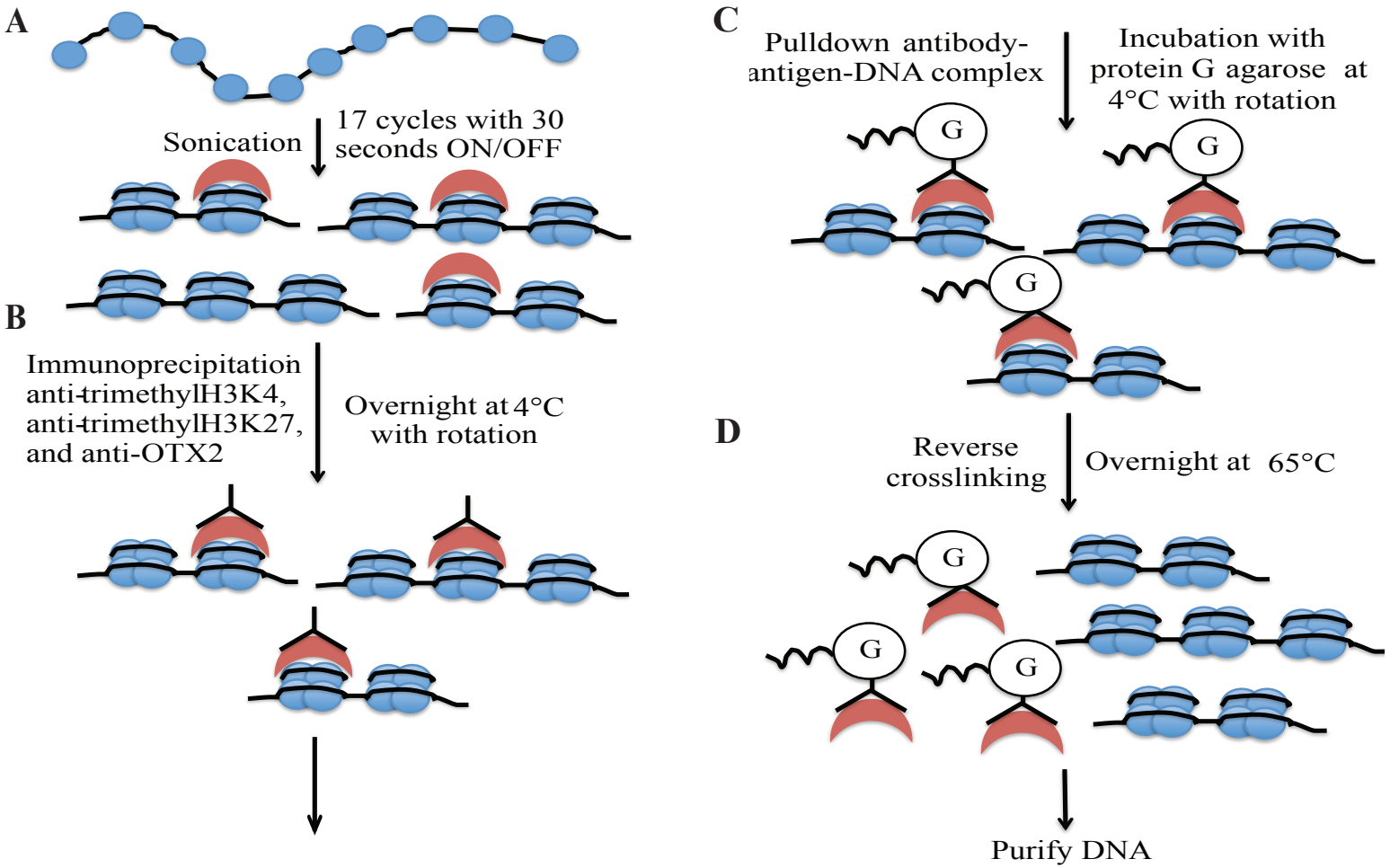


**Figure 2.4: Schematic of chromatin immunoprecipitation (ChIP) assay:** (A) Sonication (17 cycles with 30 seconds ON/OFF) of fixed samples using a bioruptor to obtain fragments approximately 400 base pairs in length. Immunoprecipitation of fractionated samples using anti-trimethyl H3K4, anti-trimethyl H3K27, and anti-OTX2 antibodies by overnight incubation at 4°C. (C) Pulldown antibody-DNA complex using protein G Agarose by incubating for 1 hour at 4°C. (D) Reverse crosslinking to obtain immunoprecipitated DNA followed by qPCR using specific primer sets based on promoter or 5' sequences.

**Table 2.2:** qPCR primers used for ChIP-qPCR.

| Gene | Forward Sequence (for ChIP-qPCR) | Reverse Sequence (for ChIP-qPCR) |
|---|---|---|
| *LIN28A* | 5'-TGT GTG TGT GTG TGT GTG T -3' | 5'-GGA ATT TGA GAT CCT GCA CTT TG -3' |
| *NANOG* | 5'-GGA CAT AGT AGG TGC TCA GTA AAT -3' | 5'-CCG GGC TAA GAA AGA AGA GAG -3' |
| *OCT4* | 5'-AGC CCC ACT AAA CAA AGC AC-3' | 5'-GCA ATC CCC TCA AAG ACT GA-3' |
| *SOX2* | 5'-GGA CTG AGA GAA AGA AGA GGA GAG-3' | 5'-CGC CGC CGA TGA TTG TTA TTA-3' |

distilled water) and reverse crosslinked with 5M NaCl (0.2M final) overnight at 65°C and then incubated with 1µl of RNaseA (1mg/ml) for 30 mins at 37°C. Samples were treated with 0.5 M EDTA, 1M Tris-HCl and 1µl proteinase K (20 µg/µL) for 2 hour at 45°C. DNA was extracted by the phenol:chloroform method and then suspended in 50µl of elution buffer (Figure 2.4). Immunoprecipitated (IPed) DNA was subjected to qPCR using specific primer sets based on promoter or 5' sequences (Table 2.2) for each gene interrogated using the Ensembl Genome Browser (*SOX2*: ENST00000325404, NM_003106; *NANOG*: ENST00000229307, NM_024865; *OCT4*: ENST00000513407, NM_001285986; *LIN28A*: ENST00000326279, NM_024674) and % material IPed was analyzed using the following formulas: 1. DNA Input = $2^{40\text{-Input Ct}}$ *1000. 2. Percent material IPed or % Recovery from IP = $2^{40\text{- IP Ct}}$ / DNA Input * 100.

### 2.8 Chromatin immunoprecipitation-sequencing (ChIP-seq)

To determine the interacting partners of OTX2 in D283 cells (Group 4 MB cell line) grown in stem cell enriched conditions, we performed ChIP-seq in collaboration with StemCore Laboratories (Ottawa Hospital Research Institute, Ottawa, Canada). The cells were fixed, sonicated and immunoprecipitated using similar protocols described above in section 2.7. The immunoprecipitated DNA sample was subjected to ChIP-seq and data were generated on a NextSeq 2500 and mapped to the GRCh38 human genome model using bowtie2 v2.2.4. OTX2 binding peaks were determined within -5kb and +2kb of the transcriptional start site (TSS) using MACS2 v2.1.0.20140616.

**A**

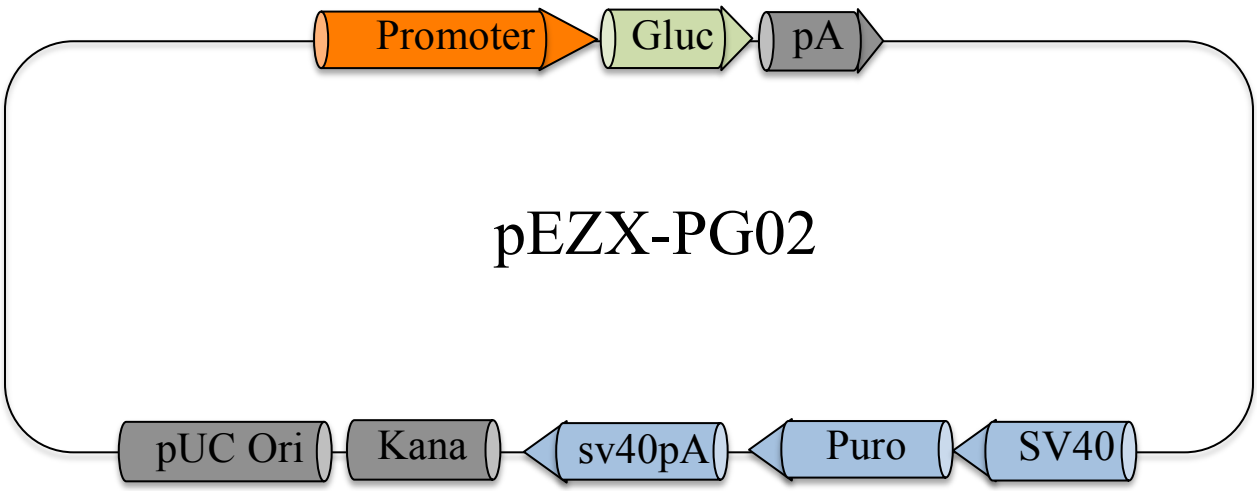


**B**

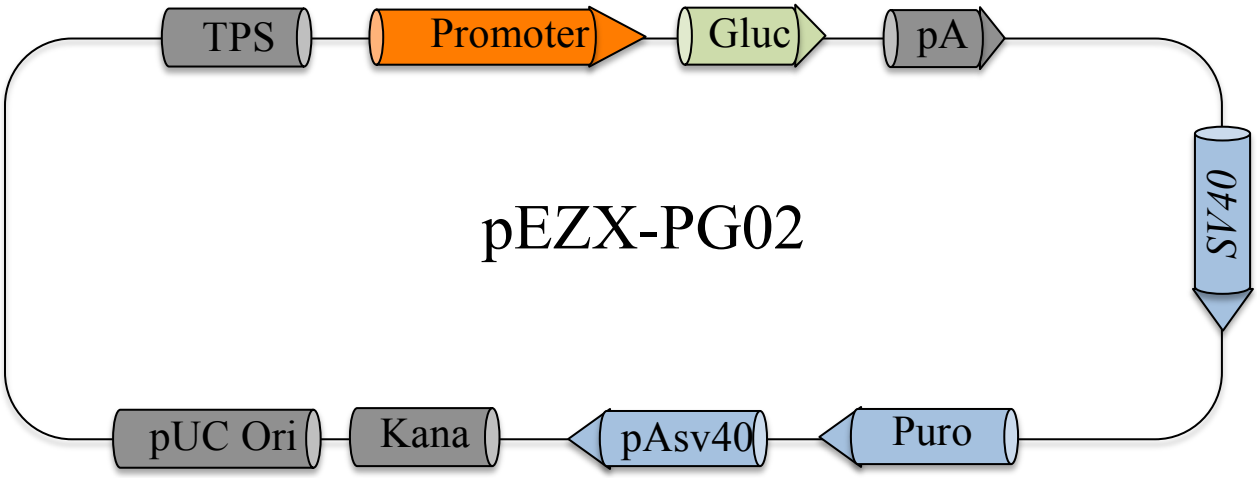


**Figure 2.5: SOX2 Promoter reporter clone used for luciferase assay:** (A) HPRM15202-PG02- SOX2 prmoter reporter clone, (B) contruct for (GAPDH)-PG02-positive and negative-PG02 control clones (Images adapted from Gene Copoeia).

## 2.9 Luciferase Assay

OTX2+ Daoy, OTX2+ hENs and their respective control cells were subjected to luciferase reporter assays using the Secrete-Pair™ Gaussia Luciferase Assay kit (SPGA-G100, Gene Copoeia) as per the manufacturer's guidelines. Briefly, OTX2+ Daoy and OTX2+ hENs along with RFP control cells ($5.0x10^4$) were transfected with a SOX2 promoter reporter clone (HPRM15202-PG02 from Gene Copoeia). Cells were also transfected with the positive GAPDH-PG02 and negative-PG02 control clones (Gene Copoeia) (Figure 2.5A-B). Culture media was collected 72 hours after transfection and luciferase activity was measured in 10µl of media on a LMAX luminometer (Molecular Devices) with 100µl of luciferase assay substrate (Gene Copoeia). Negative control values were subtracted from all data points to eliminate background signal. Data was normalized to the negative-PG02 control and presented as fold change in relative luciferase activity.

## 2.10 Western Blot

Total protein was isolated from hENs, trans-hENs, Daoy, D283, D425 and D341 MB cell lines using the All-in-One Purification Kit (Norgen Biotek, Thorold, ON, Canada) according to the manufacturer's instructions. 10ug protein samples were run on a 12% Tris-glycine gel, and subsequently transferred onto a 0.45um nitrocellulose membrane (Bio-Rad Laboratories Ltd, Mississauga, ON, Canada). OTX2 and SOX2 blots were treated with SuperSignal Western Blot Enhancer (Thermo Scientific) and then incubated in 2% skim milk overnight. Blots were incubated in primary rabbit anti-OTX2 (1:500) (Abcam, ab21990) or rabbit anti-SOX2 antibody (1:500) (Cell Signaling Technologies, #3579) for 2 hours at RT. β-actin (Sigma) was used as a loading control. Additional antibodies such as β-III tubulin/TUJ1 (1:1000), L1CAM (1:500),

Cyclin D2 (1:500) and CDK6 (1:500) were used. Blots were treated with secondary goat-anti-rabbit or anti-mouse antibodies at desired concentrations (Bio-Rad Laboratories Ltd) for 1 hour at RT. Super Signal West Pico Chemiluminescent substrate (Thermo Scientific) was used for detection.

### 2.11 Immunocytochemical staining

Immunocytochemical staining was performed on fixed tumorspheres to determine β-III tubulin/TUJ1 expression following OTX2 knockdown in D283 and D425 cells grown in sphere conditions. The tumorspheres were collected six days after OTX2 knockdown using siRNAs and fixed with 10% formalin for 2-3 hours. After washing with PBS, the tumorspheres were incubated first in 15% and then in 30% freshly made ice cold sucrose for 2-3 hours at 4°C. Without washing, the tumorspheres were transferred into a cryomold (10mm x 10mm x 5mm) (VWR Cat# 25608-922) and the an adequate amount of OCT (clear frozen section compound for optimum cutting temperature) was added (VWR cat# 95057-838). Cryomolds filled with tumorspheres and OCT were placed on dry ice for 10-15 mins and cut into 10µm sections on slides. Slides were stored at -80°C for further staining. Before staining, the slides were kept at RT for 20 mins and then washed with Tris-buffered saline (TBS 1X) for 10 mins to rehydrate the tumorspheres. Spheres were then permeabilized and blocked with 1% blocking solution (TBS 1X, 1% bovine serum albumin (BSA) (Fisher Cat# SH3057401), second animal serum (lamb serum) (Gibco Cat# 978886) and 0.1% Triton X-100). Tumorsphere sections were incubated in 200µl of diluted (1:100) anti-mouse β-III tubulin primary antibody (R&D Cat# MAB1195) for 1.5 hours at RT. The sections were washed with 1XTBS three times for 5 mins each. Goat anti-mouse Alexa Fluor 488 (Thermo fisher Cat# A-11001) secondary antibody was used and slides

were incubated for 1.5 hours followed by 3X washing with 1XTBS for 5 mins each. Slides were air-dried and a drop of DAPI (ProLong Gold Antifade Mountant with DAPI) (Life Technologies Cat# P36941) was added to each slide. After placing coverslips, the slides were transferred at 4°C overnight and images were taken using EVOS fl core microscope (AMG, Seattle, WA, USA).

### 2.12 TaqMan expression assays

MicroRNA (miRNA) was extracted using the miRVana™ isolation kit following the manufacturer instructions (Life Technologies). qRT-PCR validation of selected miRNAs was performed using TaqMan primer/probes for let-7i, let-7d, and let-7c, the MicroRNA Reverse Transcription Kit and the TaqMan® Universal Master Mix II, with UNG and performed on a Mx3000P® (Stratagene) QPCR system. Results were normalized to the U6 small nuclear RNA (snRNA) endogenous control using the delta Ct method.

### 2.13 Gene expression profiling

Extracted RNA from OTX2+ hEN and hEN neurospheres (N=3 biological replicates) were subjected to GeneChip 3' oligonucleotide microarray hybridization and processing performed by the London Regional Genomics Centre (Robarts Research Institute, London, Ontario, Canada) according to the manufacturer's protocols (Affymetrix). Ten micrograms of cRNA was labelled and hybridized to Affymetrix Human Gene 2.0 ST chips. Expression signals were scanned on an Affymetrix GeneChip Scanner and data extraction was performed using Affymetrix Genechip® Command Console® (AGCC) Software. Data normalization and analysis were performed using Partek software. Hierarchical clustering using Pearson correlation

coefficients was performed on the normalized data. Differentially expressed genes were analyzed using Ingenuity Pathway Analysis (IPA) (Redwood City, CA, USA). Transcripts differentially expressed at least 1.5-fold (up- or down-regulated) and with a $p<0.05$ were considered significant.

RNA samples from $OTX2^{KD}$ D283 (N=3 biological replicates with sequence #1) and control D283 tumorspheres or stem cell enriched populations were also analysed for global gene expression changes in collaboration with StemCore Laboratories (Ottawa Hospital Research Institute). Affymetrix HuGene 2.0 microarrays RMA expression values provided by StemCore were annotated using the HuGene-2 0-st-v1.na35.hg19.transcript.csv transcript cluster annotations, assigning each transcript cluster identifier to the first provided gene symbol in the annotation. Fold change and significance for transcript cluster identifiers between conditions was determined using the R limma package. Quality assessment was performed using the arrayQualityMetrics R package based on the CEL files. Microarray expression and fold change data were integrated with ChIP-seq peaks by peak counts within -5kb to +2kb of the gene TSS for each gene of interest.

### 2.14 Quantitative real time polymerase chain reaction (qRT-PCR)

OTX2 overexpressing Daoy and hEN cell populations were subjected to qPCR analysis of *OTX2, LIN8A, NANOG, SOX2*, *OCT4*, matrix metalloproteinase-1 (*MMP1),* Tissue inhibitor of metalloproteinases (*TIMP4*)*,* Contactin (*CNTN1*)*,* uncoordinated (*UNC5C*)*,* FBJ murine osteosarcoma virus oncogene homolog (*FOS*)*, FOSB,* and Insulin growth factor-1 (*IGF1*) transcript levels. Similarly, OTX2 knockdown D283, D425 and D341 cells were subjected to qPCR for analysing transcript levels of genes related to the eph/ephrin signaling including

*EPHA2, EPHA3, EPHA5, EPHB2, EFNA3* and *EFNB2* as well as neuronal differentiation genes such as β-III tubulin/*TUJ1,* microtubule associated proteins (*MAP2*) and *MAP6,* L1 cell adhesion molecule (*L1CAM*), Growth associated protein 43 (GAP43) and Janus kinase and microtubule interacting protein (*JAKMIP2*). Total RNA was extracted using the Norgen All in one kit (Norgen Biotek Corp. Ontario, Canada) according to the manufacturer's guidelines. First strand cDNA was synthesized using the Superscript® III First Strand Synthesis System (Invitrogen). The following PCR conditions were used: 50°C for 2 min, 95°C for 2 min, and 40 cycles of 95 ˚C for 15 s, 60°C for 30 s. Quantitative PCR was conducted using GoTaq® qPCR Master Mix (Fisher Scientific) and performed on a Mx3000P® (Stratagene) QPCR system. All values were normalized to GAPDH. Specific primer sequences for each gene are listed in the Table 2.3.

### 2.15 *In silico* analysis of patient sample transcript levels of axon guidance genes

*In silico* analysis was performed to compare our D283 $OTX2^{KD}$ global gene expression data with the MB patient data for each subgroup published by Northcott et al. (Northcott et al. 2011). We cross-referenced our global gene expression data to the Northcott data and analyzed differential expression of axon guidance genes associated with Group 3 and 4 MBs relative to other subgroups. Furthermore, the association of OTX2 and axon guidance genes was also evaluated in patients exhibiting high or low levels of OTX2 in collaboration with Dr. Michael Taylor (SickKids).

### 2.16 Statistical analysis

All tests were performed using Prism 5 software (GraphPad Software, LaJolla, CA, USA). Descriptive statistics were used to determine significant differences including mean and standard error of the mean along with one-way analysis of variance (ANOVA's), independent sample two-tailed t-tests, and Tukey's test for multiple comparisons. P values less than 0.05 were considered significant. For patient data analysis, Pearson correlation coefficient was used for determining the relation between OTX2 and axon guidance genes in different MB subtypes. As many patient samples had high OTX2 expression but no evidence of amplification, the $90^{th}$ percentile of OTX2 expression was used as the threshold for overexpression rather than the amplification status. The expression of axon guidance genes was compared in patients with OTX2 overexpression to those with normal expression using a two-sided Wilcox-sum test.

**Table 2.3:** List of primers used for qPCR.

| Gene | Forward Sequence | Reverse Sequence |
|---|---|---|
| *LIN28A* | 5'-GAG CCA AGC CAC TAC ATT CTG-3' | 5'-ATC CCA AAA GTG GGT ATG AGG-3' |
| *NANOG* | 5'-CGA AGA ATA GCA ATG GTG TGA CG-3' | 5'-TTC CAA GGC AGC CTC CAA GTC-3' |
| *OCT4* | 5'-CTG AAG CAG AAG AGG ATC AC-3' | 5'-GAC CAC ATC CTT CTC GAG CC-3' |
| *OTX2* | 5'-GAG GTG GCA CTG AAA ATC AAC-3 | 5'-TCT TCT TTT TGG CAG GTC TCA-3' |
| *SOX2* | 5'-CAG CTC GCA GAC CTA CAT GA-3' | 5'-GGG AGG AAG AGG TAA CCA CAG-3' |
| *MMP1* | 5'-CCT AGT CTA TTC ATA GCT AAT CAA GAG GAT GT-3' | 5'-AGT GGA GGA AAG CTG TGC ATA C-3' |
| *TIMP4* | 5'-GCT AGT GGA TCC CTG CAG CTG CGC CCC GGC G-3' | 5'-CGG CTT CTA GAA GGG CTG AAC GAT GTC AAC-3' |
| *CNTN1* | 5'-GAT GGT CAG AAG CAC TGA AGC-3' | 5'-TCA CAG AGA AGC ACC ATT CCT-3' |
| *UNC5C* | 5'-GCA AAT TGC TGG CTA AAT ATC AGG AA-3' | 5'-GCT CCA CTG TGT TCA GGC TAA ATC TT-3' |
| *FOS* | 5'-CTG GCG TTG TGA AGA CCA TGA-3' | 5'-CCC TTC GGA TTC TCC TTT TCT C-3' |
| *FOSB* | 5'-ACC CCA CGG ACT ACT CTC CTA-3' | 5'-CTG AGG CAA AAT GGG TTG TTA-3' |
| *EPHA2* | 5'-GACCTTCAAGTGTGTGGGAAA-3' | 5'-ATTTGGGACATTTGGGAGAAC-3' |
| *EPHA3* | 5'-GGAAGAGATCAGTGGTGTGGA-3' | 5'-TTTTGACTGTGGTCCATGACA-3' |
| *EPHA5* | 5'-ACAAAGGAAGCCAAATCACCT-3 | 5'-GGTAGAAACCCAAAGGCAGAC-3' |
| *EPHB2* | 5'-GACTCCACTACAGAGACTGCT-3' | 5'-TCTCATCGTAGCCACTCACCT-3' |
| *EFNA3* | 5'-CCTTCTCTCTGGGCTACGAGT-3' | 5'-AGACGAACACCTTCATCCTCA-3' |
| *EFNB2* | 5'- GTTCGACAACAAGTCCCTTTG-3' | 5'-CTGAAGCAATCCCTGCAAATA-3' |
| *TUJ1* | 5'-GGCCTTTGGACATCTCTTCA-3' | 5'-TCGCAGTTTTCACACTCCTTC-3' |
| *MAP2* | 5'-ATTCTGGCAGCAGTTCTCAAA-3' | 5'-TGCTTCCTCGGTTAGAGACAA-3' |
| *MAP6* | 5'-TCTAAAGAGGCCAAGGCTTTC-3' | 5'-TTCACCAAAGATGGGAGAACA-3' |
| *L1CAM* | 5'-AAATGGCTGTGAAGACCAATG-3' | 5'-GATGAAGCAGAGGATGAGCAG-3' |
| *GAP43* | 5'-TAGCAGGGAAGTCCAGAGACA-3' | 5'-GTGGAGATTTGCCCAGTATCA-3' |
| *JAKMIP2* | 5'-GCCTCCCCATGTAAAAGAAAG-3' | 5'-GGGGGAAAGGGTCTTATTTTC-3' |

# CHAPTER 3: RESULTS

## CHAPTER 3.1: Inhibitory functions of OTX2 in normal neural precursors and SHH MB cells

### 3.1.1 Rationale

OTX2 is amplified and overexpressed in 70% of MB cases (Di et al. 2005) and previous studies have evaluated the role of OTX2 by knocking it down in Group 3 and 4 MB tumor cell lines grown as adherent cultures in serum (Di et al. 2005; Adamson et al. 2010). Only one study has evaluated the effect of OTX2 on cell growth in SHH MB cells, and results were limited to 96 hours following overexpression (Bunt et al. 2010). The long-term effects of OTX2 overexpression have not been evaluated. Moreover, the role of OTX2 in regulating other cellular properties such as "self-renewal" or stem cell function and cell migration has not been investigated. Previous studies focused on utilizing long-term cultured cell lines that exhibit numerous karyotypic abnormalities and this can make it difficult to evaluate the role of a multi-faceted gene. Therefore, using hESCs derived hENs in parallel with established MB cell lines may enable one to better delineate the functional role of OTX2 in tumor progression.

#### 3.1.1.1 Effect of OTX2 overexpression on cellular functions such as proliferation, self-renewal and cell migration of hENs and Daoy MB cells

##### 3.1.1.1a Endogenous expression of OTX2 in hENs and MB cell lines

Our previous studies revealed increased OTX2 transcript levels in trans-hENs relative to hENs (Werbowetski-Ogilvie et al. 2012). In addition, OTX2 expression is increased in Group 3 and 4 MB cell lines (i.e. D425, D341 and D283 respectively) and is negligible/absent in representative SHH MB variant lines such as Daoy (Bunt et al. 2010). To confirm differential expression between these sets of cell lines, we evaluated OTX2 levels by Western blot (Figure 3.1.1A-B). OTX2 was not detected in hENs that have been cultured in neural precursor media for 7 days; however, levels were still high in trans-hENs (Figure 3.1.1A). Similarly, OTX2 was not

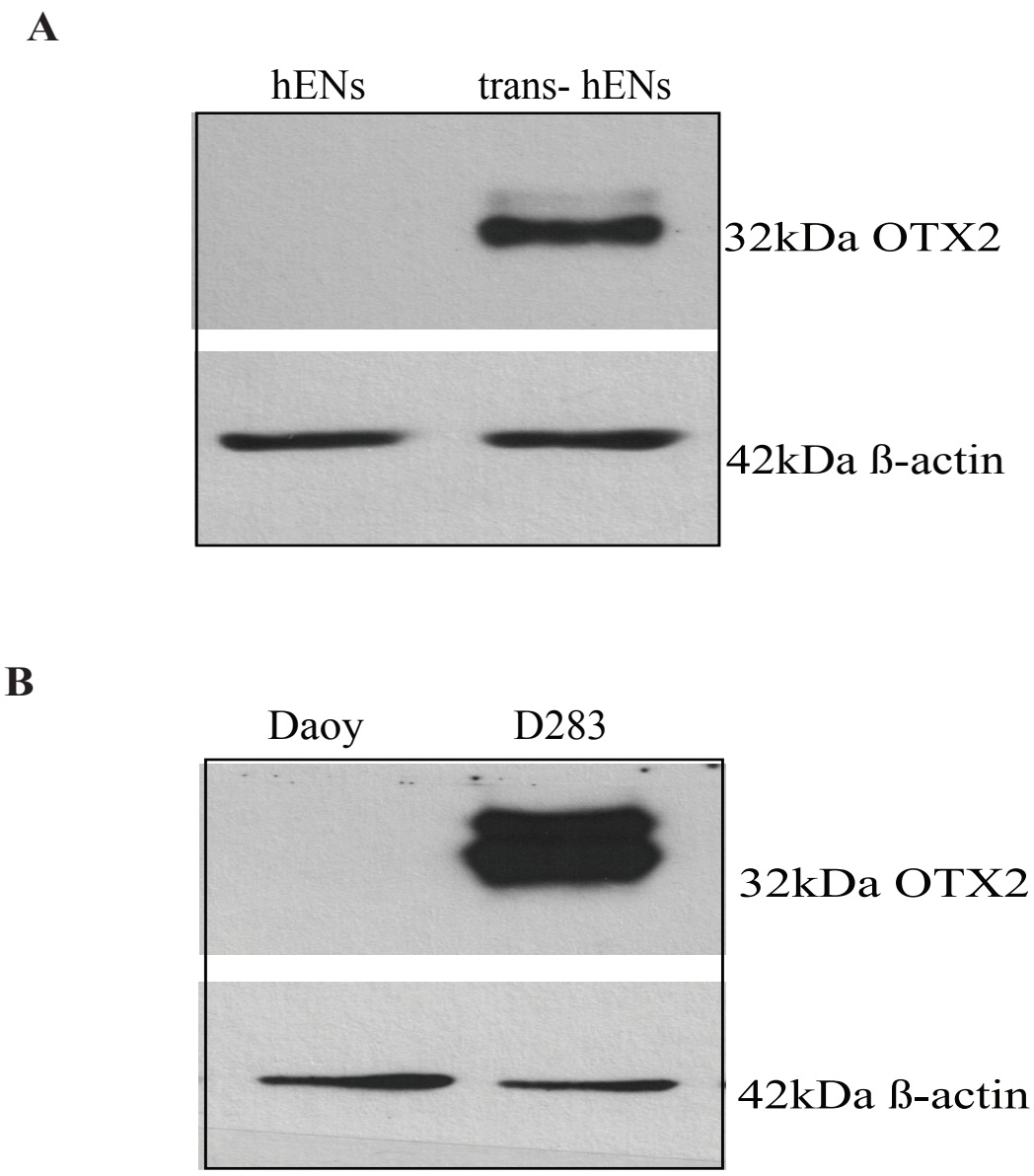


**Figure 3.1.1: Endogenous expression of OTX2 in cell lines used.** (A-B). Endogenous protein levels of OTX2 in hEN vs. trans-hEN cultured in neural precursor conditions for 7 days (A) and Daoy (SHH MB variant) vs. D283 (Group 4 MB variant) (B). β-actin serves as a loading control.

detected in Daoy cells; however, protein levels were high in D283 (Figure 3.1.1B). These paired cell lines were therefore utilized for all parallel gain and loss of function studies. Of note, two OTX2 bands were detected by Western Blot and the upper band may represent the phosphorylated form (Adamson et al. 2010; Bunt et al. 2012).

#### 3.1.1.1b Stable overexpression of OTX2 in Daoy cells and hENs

For stable OTX2 overexpression, we employed LentiORFs consisting of dual expression constructs with TurboGFP as a marker to track transduction efficiency in Daoy and hENs (Figure 2.1A). LentiORF RFP-expressing viral particles (consisting of the same backbone construct) were utilized as a control for each cell line (Figure 2.1B). Following selection of GFP+ and RFP+ cells (Figure 3.1.2A-B), OTX2 over-expression was verified by both qPCR and Western blot in OTX2+ Daoy and hEN (Figure 3.1.2C-F). For both cell lines, OTX2 expression was negligible for RFP+ and untransduced cells (Figure 3.1.2E-F). Therefore, we shall herein refer to Daoy-RFP+ and hEN-RFP+ as Daoy and hEN respectively.

### 3.1.1.2 OTX2 overexpression suppressed cellular functions *in vitro* and tumor growth *in vivo*:

#### 3.1.1.2a OTX2 overexpression decreases cell growth in both Daoy and hENs

We first compared cumulative cell growth and viability in OTX2+ cells vs. controls (Figure 3.1.3A-F). Compared with Daoy cells, OTX2+ Daoy exhibit a significant decrease in cell number over 4 days (Figure 3.1.3A, B). This was not entirely attributed to cell death, as OTX2+ cells displayed only a 20% decrease in total live cells by Trypan blue staining and no significant change by Annexin V staining (Figure 3.1.3C; Figure 3.1.4A-B). Similar results were obtained

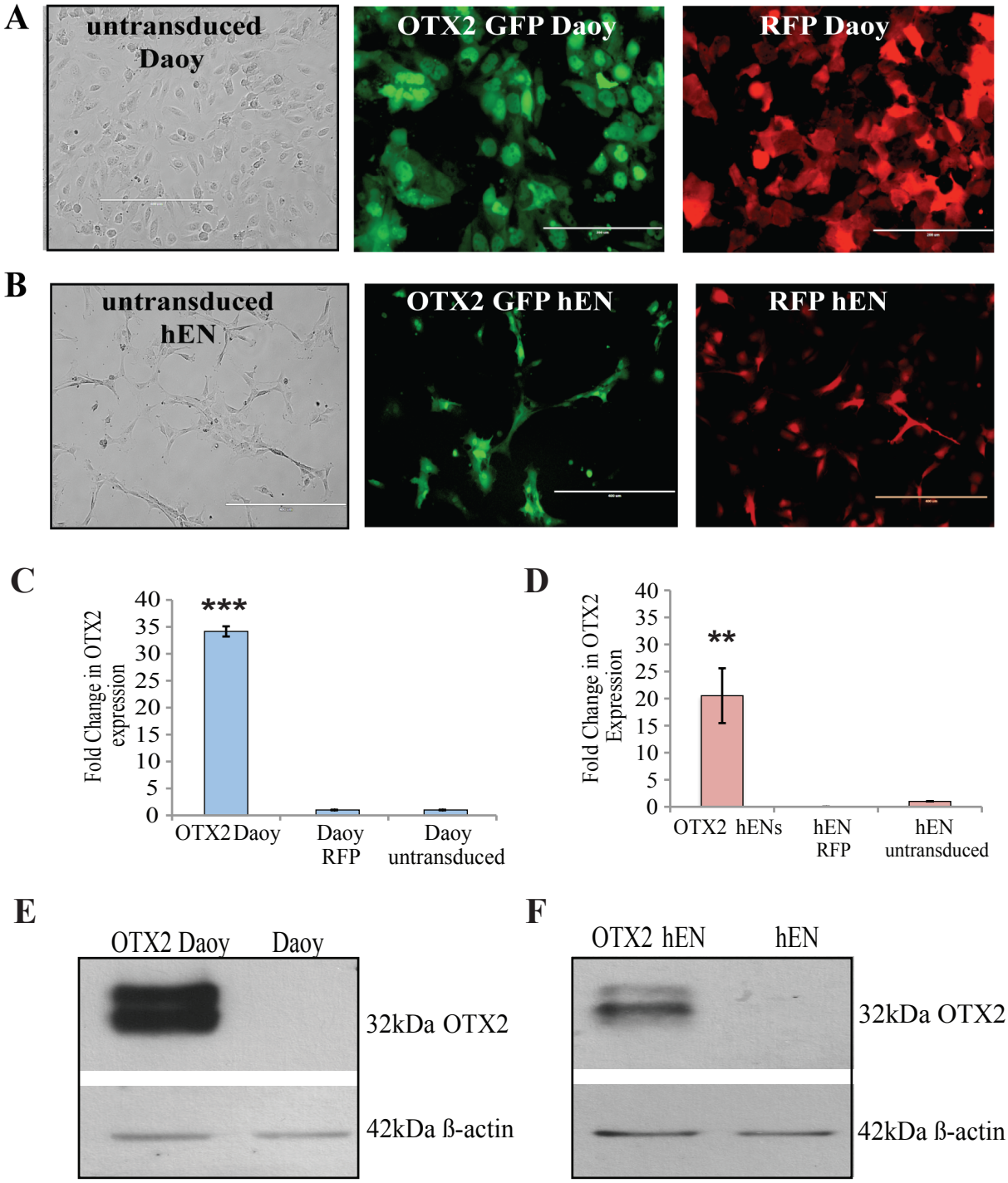


**Figure 3.1.2: Validation of stable overexpression of OTX2 in Daoy and hENs:** Stable OTX2 overexpressing Daoy (A) and hENs (B) with their respective RFP and untransduced controls. Validation of stable OTX2 overexpression in Daoy (C, E) and hEN (D, F) by qPCR (C-D) and Western Blot (E-F). β-actin serves as a loading control. Error Bars: s.e.m. P<0.01**, P<0.001***.

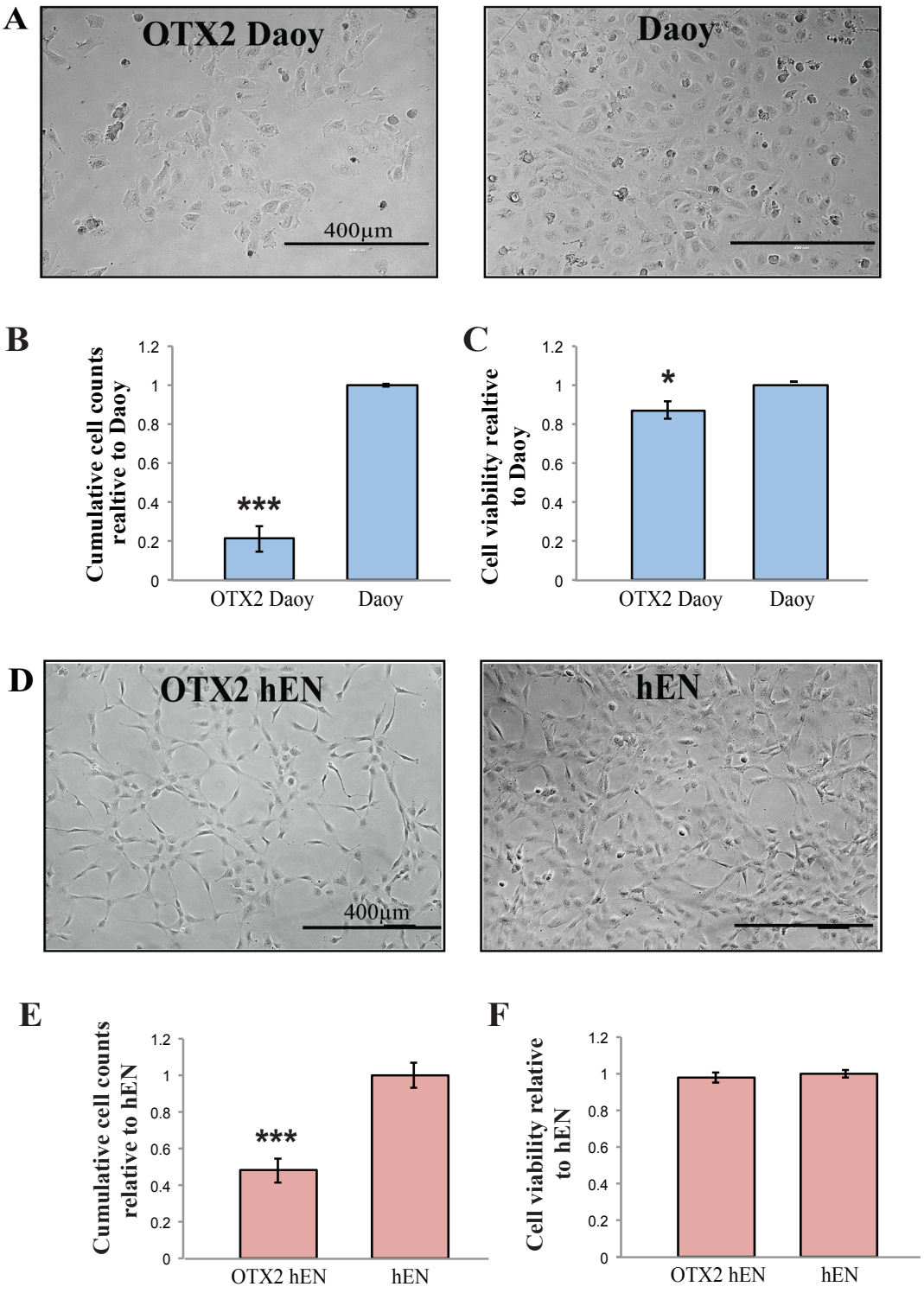


**Figure 3.1.3: OTX2 overexpression decreases cell growth in Daoy MB cells and hENs:** Overexpression of OTX2 reduces cell number in both Daoy (A-C) and hEN (D-F) cells. In both cell lines, OTX2 overexpression significantly decreases total cell number (A-B, D-E), with only a small change in cell viability (C, F). Scale bar: 400 µm. Error Bars: s.e.m. $P<0.05$*, $P<0.001$***. For all experiments, N=3 biological replicates or independent infections and n=4 technical replicates within each biological replicate.

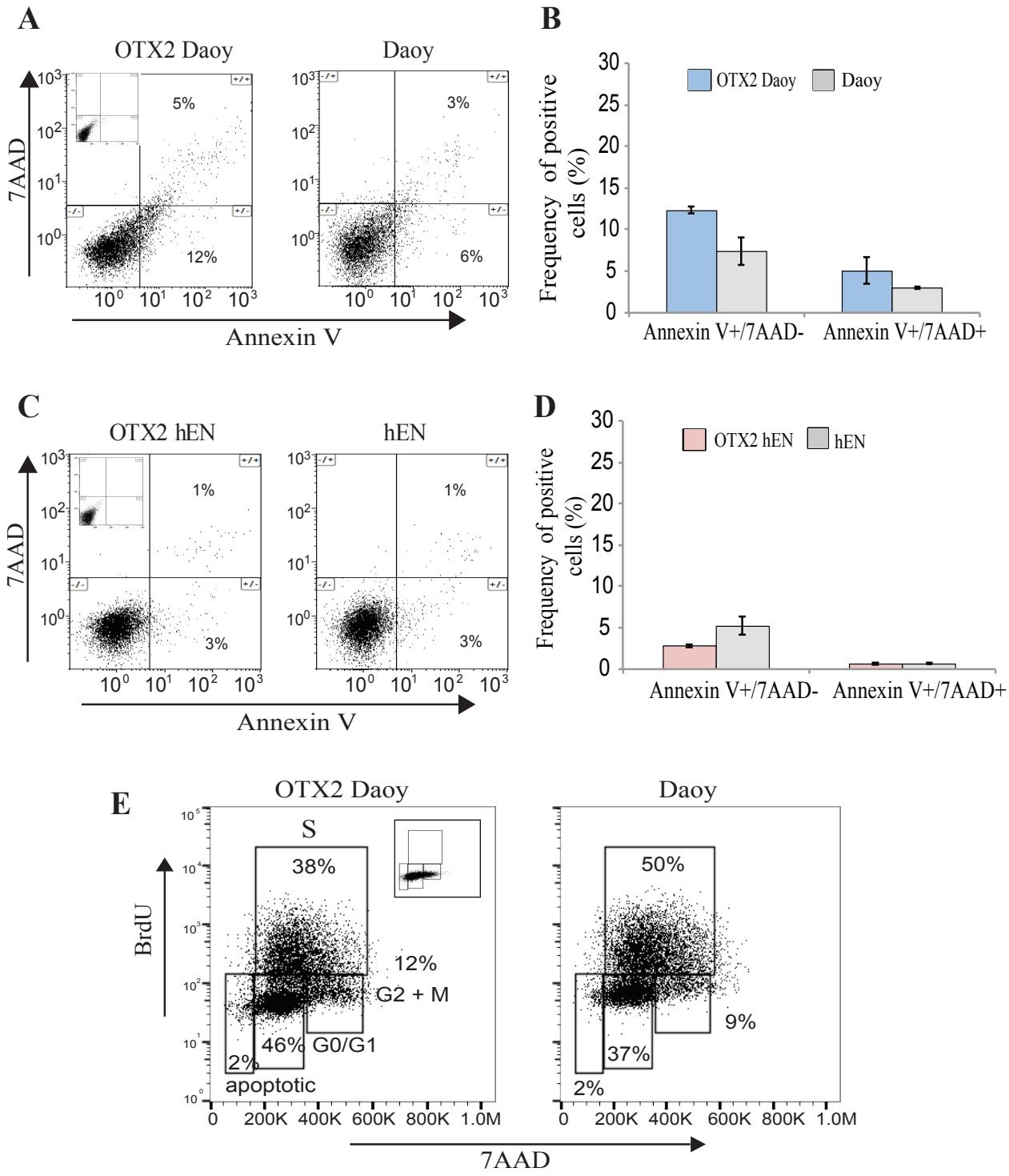


**Figure 3.1.4: Overexpression of OTX2 in Daoy and hEN does not affect viability in adherent cultures.** (A-D) Representative flow plots and quantification of Annexin V staining in Daoy (A-B) and hEN (C-D) cells in control and OTX2-overexpressing cultures. For both cell lines, no significant changes in dying (Annexin V+/7AAD-) and dead (Annexin V+/7AAD+) cells were observed. Error Bars: s.e.m. (E). Representative dot plots of BrdU incorporation and DNA content (7AAD) from Daoy adherent cultures following OTX2 overexpression. Inset: 7AAD only control.

for hENs, as overexpression of OTX2 resulted in a 60% decline in total cell number (Figure 3.1.3D, E) without significantly affecting cell viability (Figure 3.1.3F, Figure 3.1.4C-D). BrdU staining supported our findings and demonstrated a decrease of cells in S phase and an increase in G0/G1 following OTX2 overexpression (Figure 3.1.4E). We did not observe a change in the frequency of apoptotic cells (Figure 3.1.4E). These results confirm previous findings obtained for Daoy MB cells (Bunt et al. 2010) but more importantly demonstrate that overexpression of OTX2 in hENs also recapitulates the inhibitory effect on cell growth.

**3.1.1.2b Overexpression of OTX2 in Daoy and hENs decreases self-renewal and survival.**

We next evaluated the effect of OTX2 overexpression on self-renewal capacity using neurosphere assays *in vitro*. OTX2+ and control cells were subjected to neurospheres/tumorsphere assays and the number of spheres assessed over subsequent passage (Figure 3.1.5 and 3.1.6). Compared with Daoy, OTX2+ Daoy displayed a significantly decreased capacity for self-renewal (Figure 3.1.5A-B). However, we also observed a significant drop in cell viability with each passage by Trypan Blue and Annexin V staining (Figure 3.1.5C, 3.1.7A-D). This was supported by BrdU staining that demonstrated a concomitant decrease in S phase and increase in apoptotic cells following OTX2 overexpression (Figure 3.1.9). Similar results were obtained for hENs, as OTX2+ hENs displayed a lower capacity for self-renewal (Figure 3.1.6A-B) and a significant drop in cell viability (Figure 3.1.6C, 3.1.8A-D). These results demonstrate that OTX2 plays a novel role in regulating stem cell properties of both SHH MB cells and hENs and that cell survival contributes to these adverse effects in stem cell-enriched conditions.

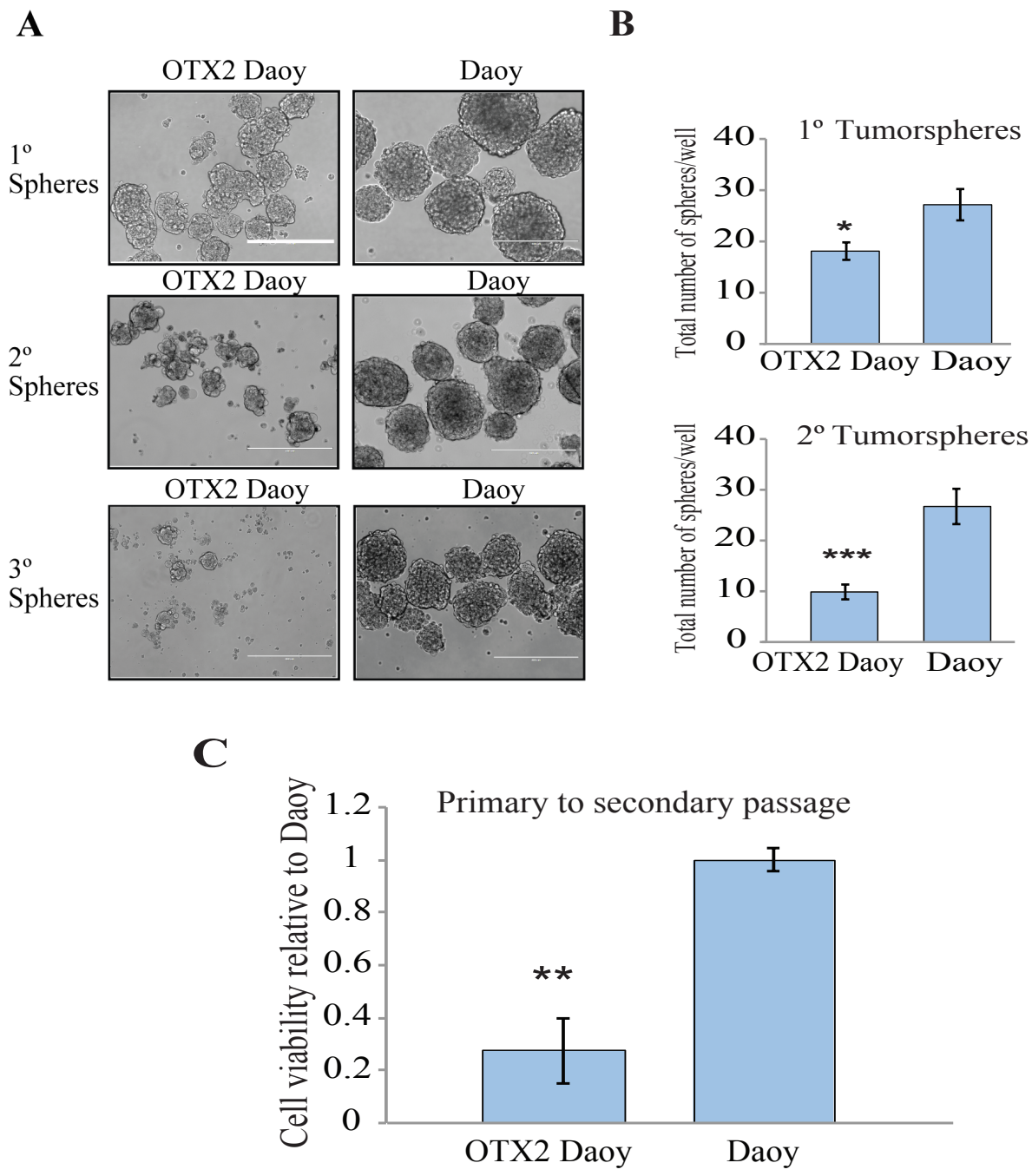


**Figure 3.1.5: OTX2 overexpression decreases self-renewal and viability in Daoy MB cells.** (A) Representative images of tumorspheres over subsequent passage following OTX2 overexpression in Daoy cells. (B) OTX2 overexpression decreases self-renewal capacity in Daoy tumorspheres. OTX2 overexpression decreases cell viability in OTX2 Daoy (C) spheres between passages as measured by Trypan Blue staining. Error Bars: s.e.m. P<0.05*, P<0.01**, P<0.001***. Scale bars: 400 μm. For all experiments, N=3 biological replicates or independent infections and n=4 technical replicates within each biological replicate.

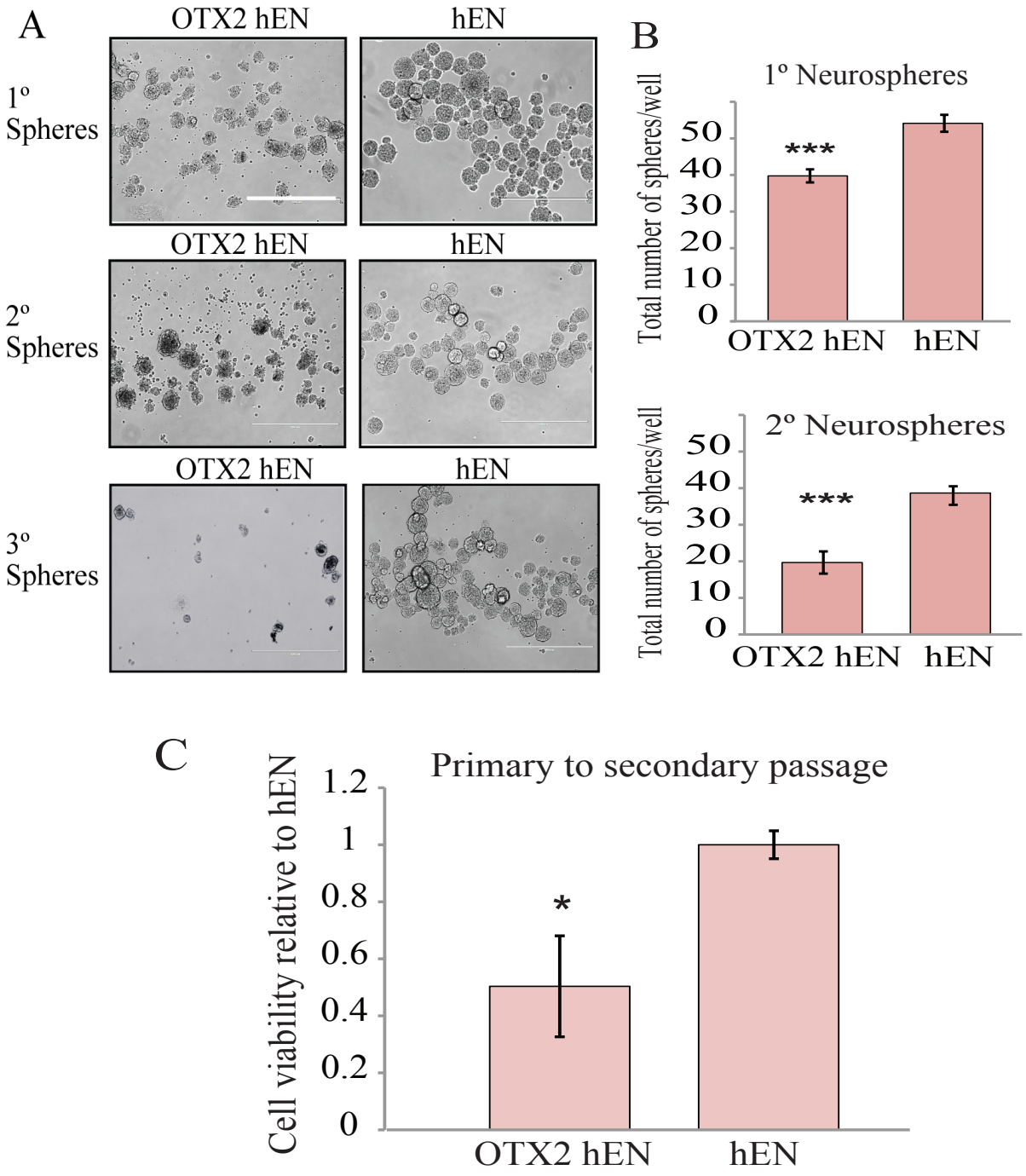


**Figure 3.1.6: OTX2 overexpression decreases self-renewal and viability in hENs.** (A) Representative images of neurospheres over subsequent passage following OTX2 overexpression in hENs. (B) OTX2 overexpression decreases self-renewal capacity in hENs neurospheres. OTX2 overexpression decreases cell viability in OTX2 hENs (C) neurospheres between passages as measured by Trypan Blue staining. Error Bars: s.e.m. P<0.05*, P<0.01**, P<0.001***. Scale bars: 400 μm. For all experiments, N=3 biological replicates or independent infections and n=4 technical replicates within each biological replicate.

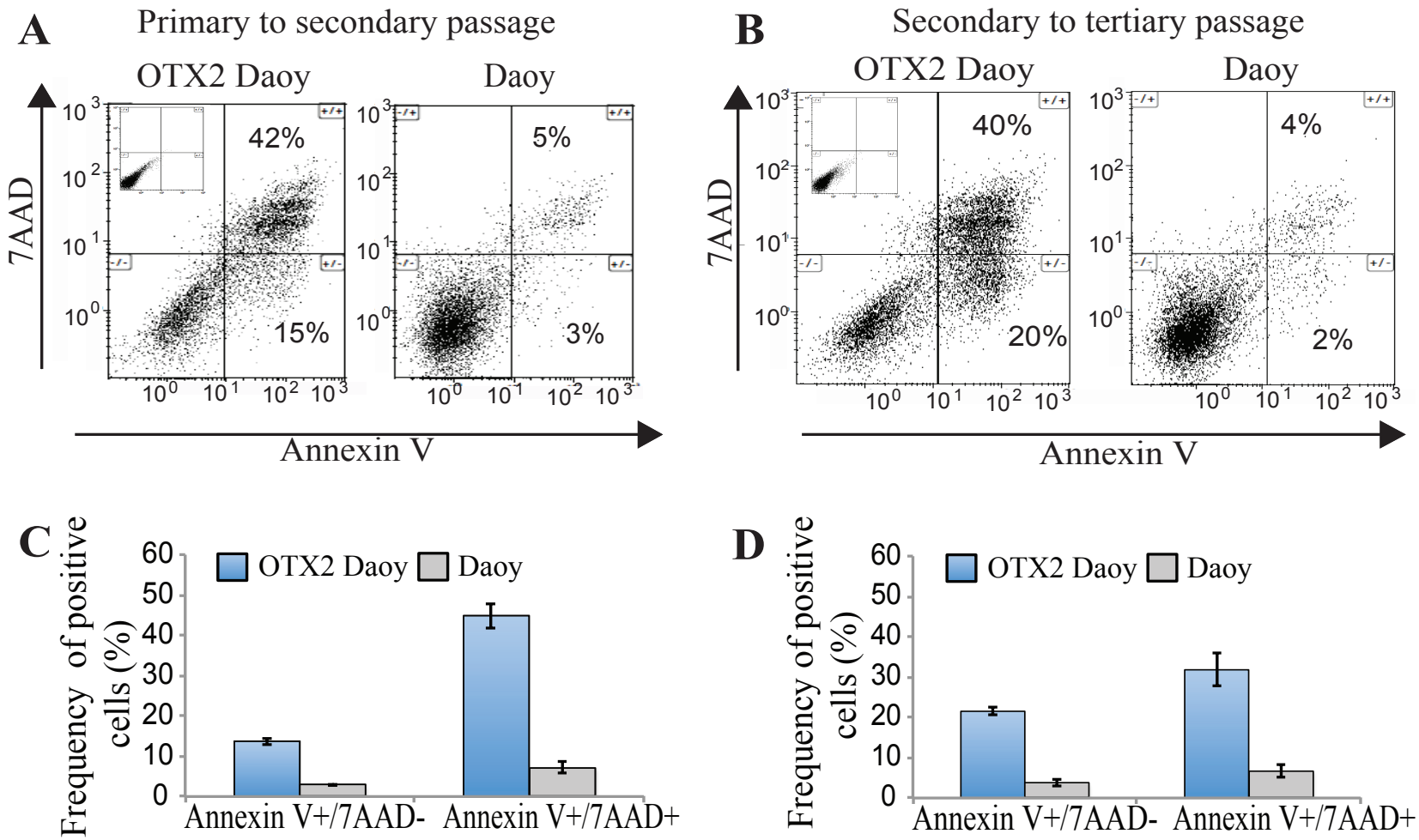


**Figure 3.1.7: Overexpression of OTX2 in Daoy tumorspheres results in decreased cell survival.** Annexin V staining demonstrates significant decreases in cell viability in both OTX2 Daoy (A-D) spheres relative to controls over subsequent passage. Increases in both dying (Annexin V+/7AAD-) and dead (Annexin V+/7AAD+) cells were evident. For all paired comparisons of dead/dying cells, P<0.001***. Error Bars: s.e.m.

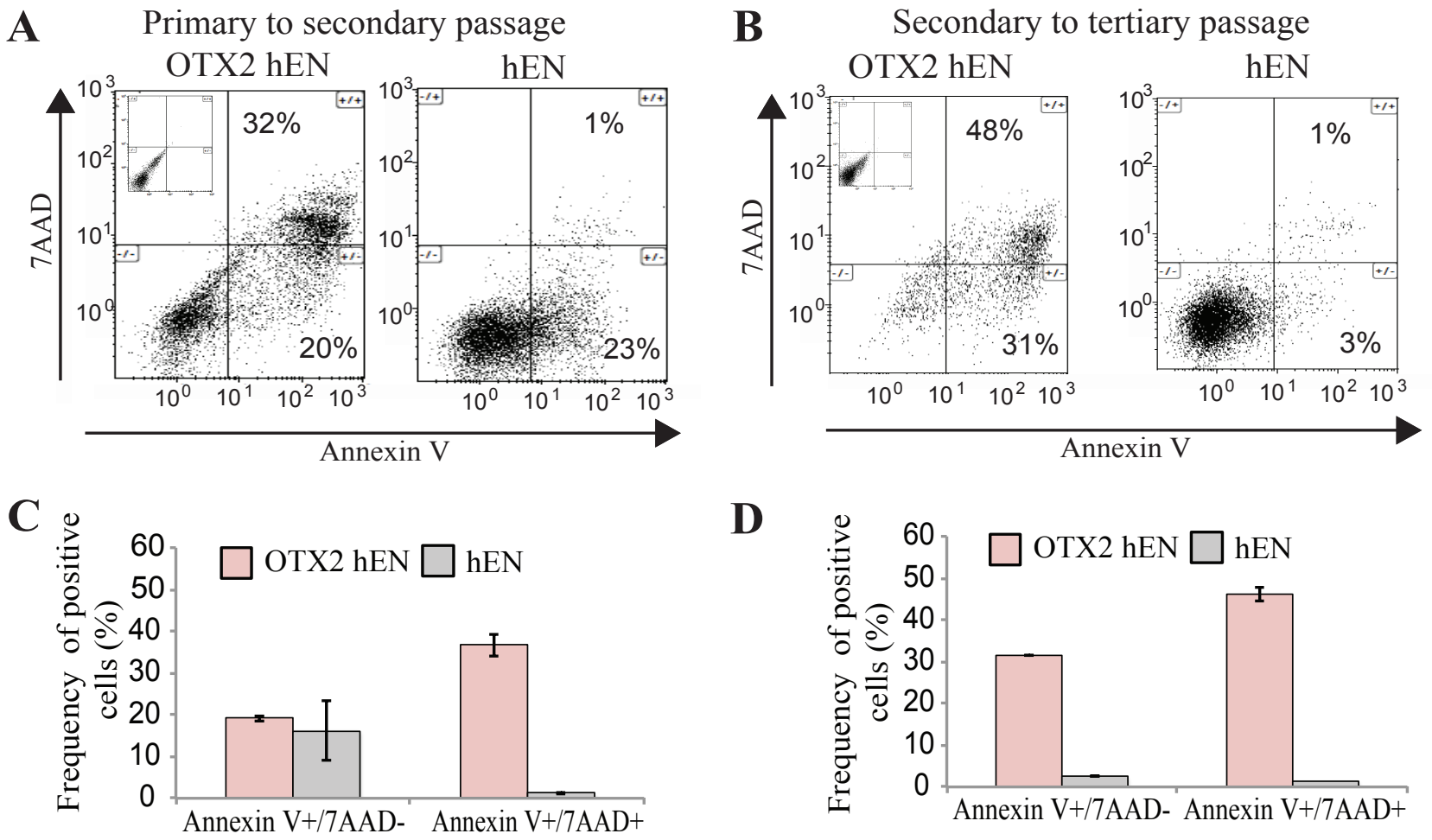


**Figure 3.1.8: Overexpression of OTX2 in hEN neurospheres results in decreased cell survival.** Annexin V staining demonstrates significant decreases in cell viability in both OTX2 hEN (A-D) spheres relative to controls over subsequent passage. Increases in both dying (Annexin V+/7AAD-) and dead (Annexin V+/7AAD+) cells were evident. For all paired comparisons of dead/dying cells, P<0.001***, except for dying cells in p1 hEN spheres which were not significantly different. Error Bars: s.e.m.

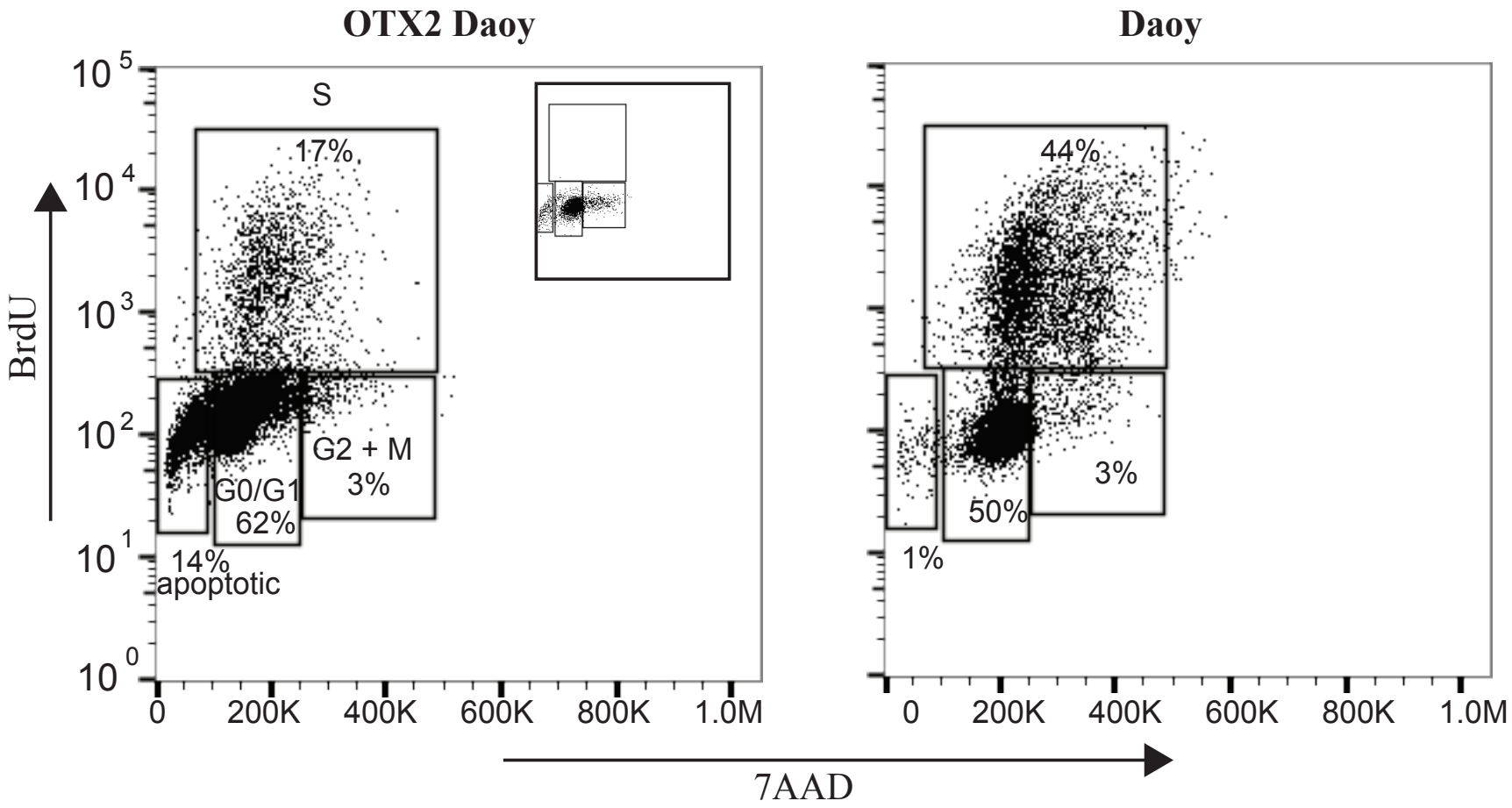


**Figure 3.1.9: BrdU staining revealed changes in the phases of cell cycle following OTX2 overexpression in Daoy tumorspheres:** Overexpression of OTX2 decreases the frequency of cells in S phase and increases the frequency of G0/G1 and apoptotic cells in sphere culture. Representative dot plots of BrdU incorporation and DNA content (7AAD) from Daoy tumorspheres following OTX2 overexpression. Inset: 7AAD only control.

### 3.1.1.2c OTX2 overexpression also decreases cell migration in both Daoy and hENs

To evaluate cell migration, we prepared hanging drops from OTX2+ and control cells from both cell lines and evaluated cell motility in collagen gels. Compared with respective controls, both OTX2+ Daoy and OTX2+ hENs exhibit a significant decline in cell migration (Figure 3.1.10A-D) over 72 hours. Taken together, these results indicate that OTX2 overexpression results in a general repressive effect on all cellular properties examined *in vitro* for both SHH MB cells and hENs.

### 3.1.1.2d OTX2 overexpression decreases tumor growth *in vivo*

Although Bunt et al. (Bunt et al. 2010) previously evaluated the effect of OTX2 overexpression on SHH MB cell line growth *in vitro* they did not determine the effect on tumor growth *in vivo*. To compare the tumorigenic potential of OTX2+ Daoy and Daoy *in vivo*, 2.5 X $10^5$ cells for each line were injected into the right frontal lobe of NOD SCID mice and examined for tumor formation. As hENs are normal cells, not amenable to tumor formation (Werbowetski-Ogilvie et al. 2012) and all cellular properties were reduced following OTX2 overexpression, we did not inject hENs and OTX2+ hENs into NOD SCID mice. All mice developed tumors in the striatum. Compared with Daoy, mice injected with OTX2+ Daoy cells displayed smaller tumors (Figure 3.1.11A-B) but were histologically similar to controls. Tumors were well circumscribed and consisted of large pleomorphic cells with small nodules also visible along the lateral and third ventricles (Figure 3.1.11A-B). These results support our *in vitro* findings and demonstrate that OTX2 overexpression also suppresses Daoy MB tumor growth *in vivo*.

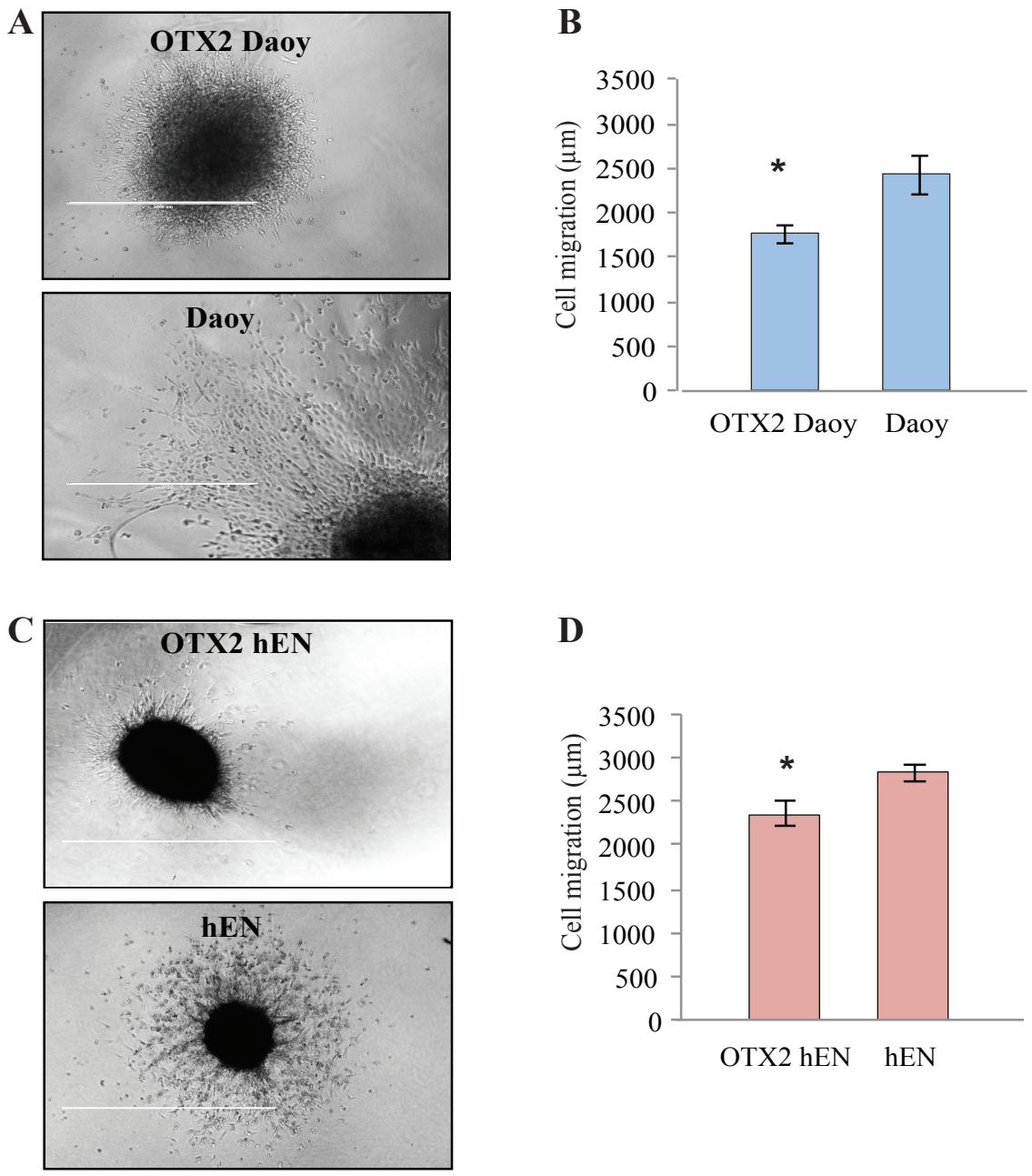


**Figure 3.1.10: OTX2 overexpression decreases cell migration *in vitro*.** OTX2 overexpression decreases migration in collagen gels for both Daoy (A-B) and hENs (C-D). Error Bars: s.e.m. P<0.05*. Representative images of Daoy (A) and hEN (C) aggregates in collagen over 3 days following OTX2 overexpression. Scale bar: 1000 µm. For all experiments, N=3 biological replicates or independent infections and n=4 technical replicates within each biological replicate.
.

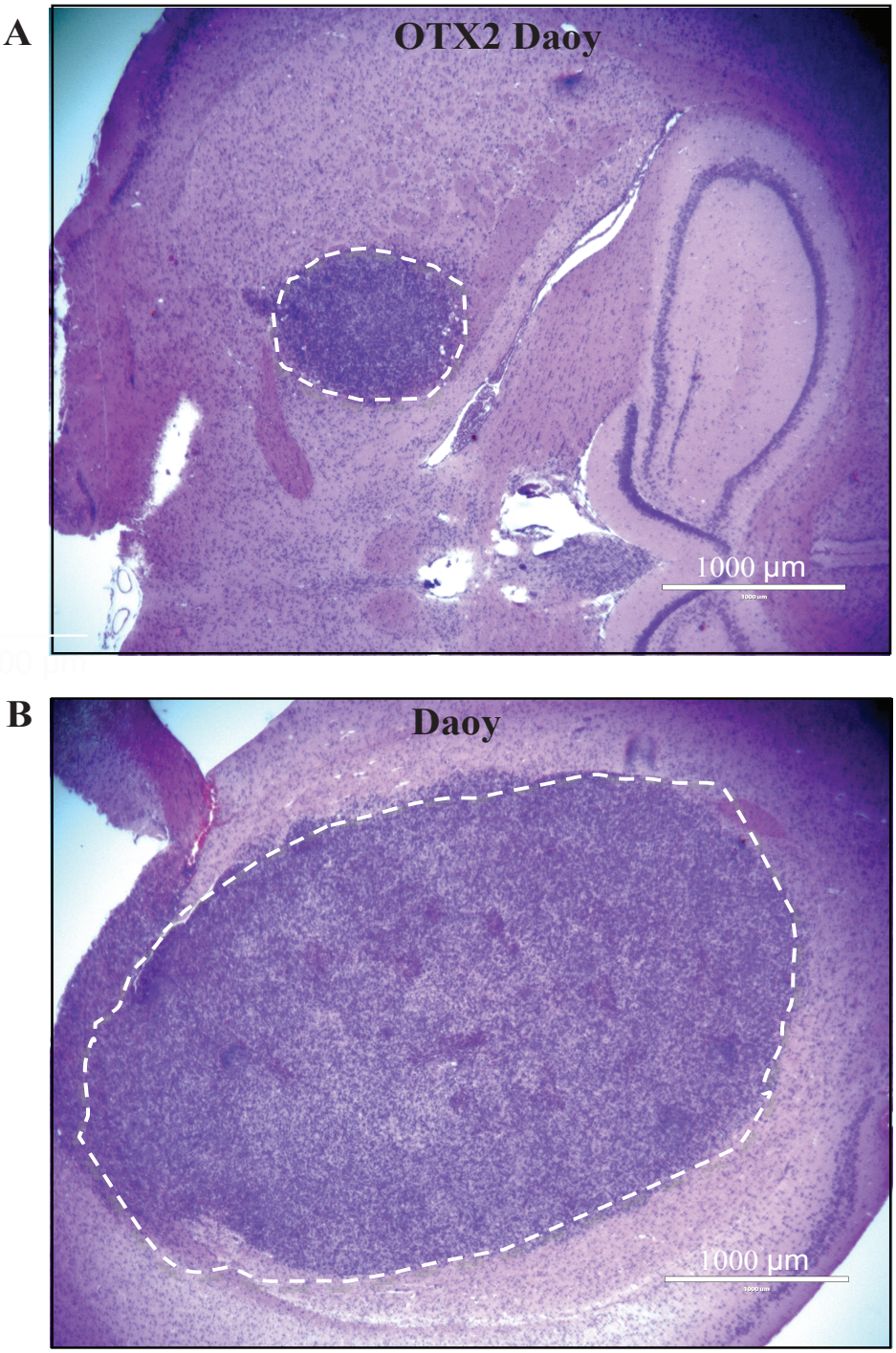


**Figure 3.1.11: OTX2 overexpression reduced growth of Daoy MB cells *in vivo*.** Tumor growth of OTX2+ Daoy (A) relative to Daoy cells (B) in NOD SCID mice (N=5 for OTX2+ Daoy and N=3 for Daoy). All mice developed solid tumors in the striatum and were histologically similar in both OTX2+ Daoy and control groups. All solid tumors were well circumscribed with some additional small nodules along the lateral and third ventricles. Histological analysis revealed the presence of large pleomorphic cells within the tumor masses. Scale bar: 1000 µm.

### 3.1.2 Global gene expression analysis of OTX2+ hENs vs hENs

#### 3.1.2.1a Global gene expression analysis reveals downregulation of transcripts associated with cell proliferation, migration and pluripotency following OTX2 overexpression.

We next wanted to investigate the molecular mechanisms that contribute to the overall inhibitory effects of OTX2 on cell properties in both Daoy and hEN cells. We conducted global gene expression analysis comparing the molecular profiles specifically in OTX2+ hENs relative to hENs. Affymetrix analysis revealed that a total of 319 transcripts were significantly and differentially expressed in OTX2+ hENs vs. hENs (Table 3.1.1 and 3.1.2). Of these 319 transcripts, 238, or 75% were downregulated. Interacting transcripts associated with cell proliferation and motility represented the top dysregulated networks (Figure 3.1.12 and 3.1.13). Based on the known function and directional changes of the differentially expressed cell proliferation and cell motility transcripts, these properties were predicted to be decreased in OTX2+ hENs (Tables 3.1.1-3.1.2), providing further support for our cell function studies. From the cell proliferation and motility transcript lists, we validated decreased expression of *FOS, FOSB, IGF1, MMP1, TIMP4, CNTN1* and *UNC5C* by qPCR in OTX2 + hEN and OTX2+ Daoy cells (Figure 3.1.14). However, we did not observe a difference in neuregulin (*NRG1*) expression between OTX2+ hEN and OTX2+ Daoy cells relative to their respective controls (data not shown). Interestingly, within the top dysregulated networks, transcripts associated with hESC function and pluripotency, including *SOX2, OCT4, NANOG* and *LIN28A*, were also significantly downregulated in OTX2+ hENs (Figure 3.1.12, Figure 3.1.15A). This was accompanied by concomitant significant increases in major *LIN28A* target miRNAs such as *let-7i, let-7d* and *let-7c* (Figure 3.1.15B). Downregulation of hESC transcripts was confirmed by qPCR for both OTX2+ hEN and OTX2+ Daoy relative to controls (Figure 3.1.15C-D). These results suggest

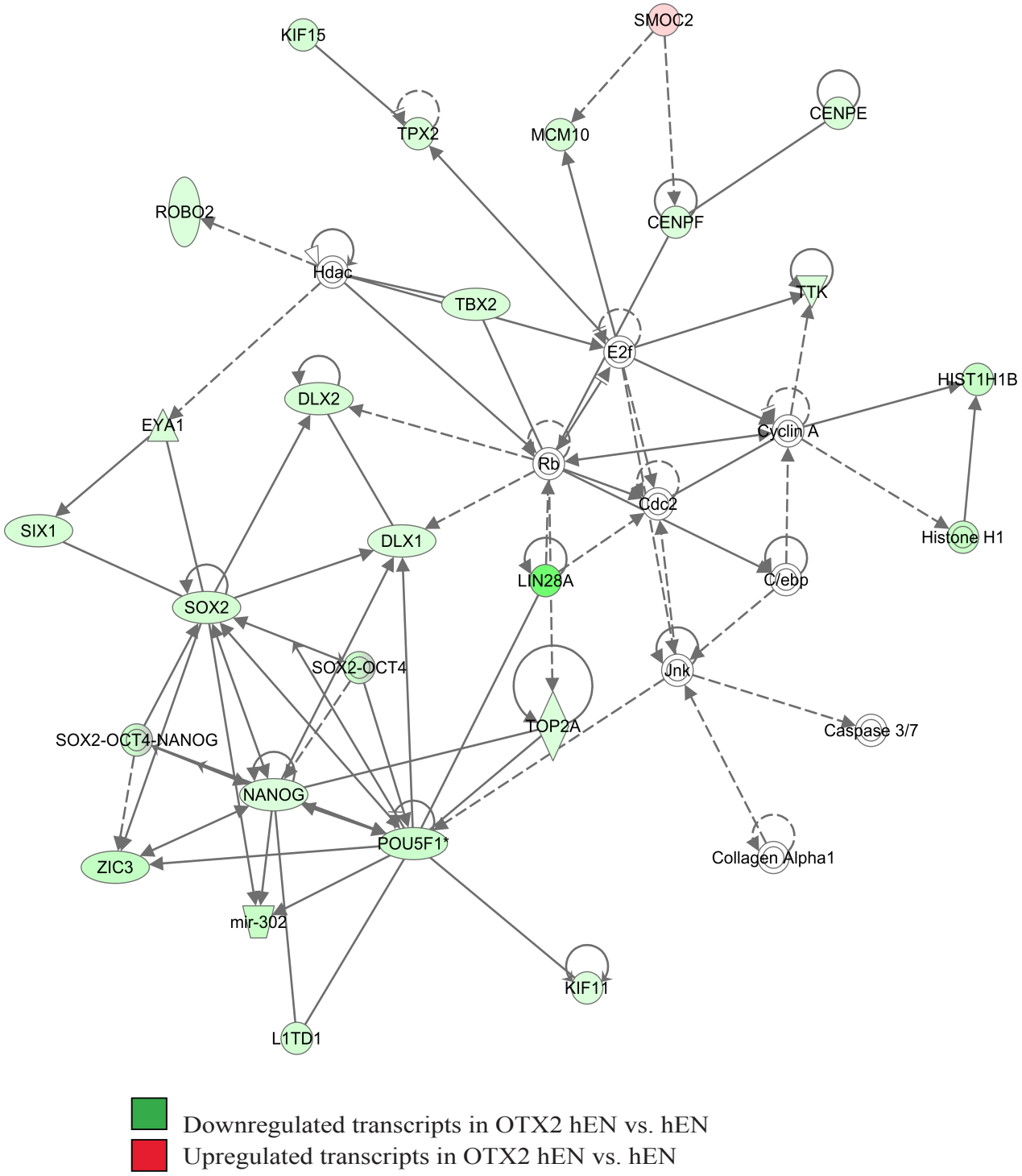


**Figure 3.1.12: Global gene expression analysis revealed dysregulation of a transcriptome network associated with cell proliferation.** Top dysregulated cellular network consisting of transcripts associated with cell proliferation. Shaded green areas denote transcripts that are significantly downregulated and red areas denote significantly upregulated transcripts in OTX2 hENs vs. hENs. Note that the vast majority of transcripts are downregulated in OTX2 hENs. N=3 biological replicates or independent infections.

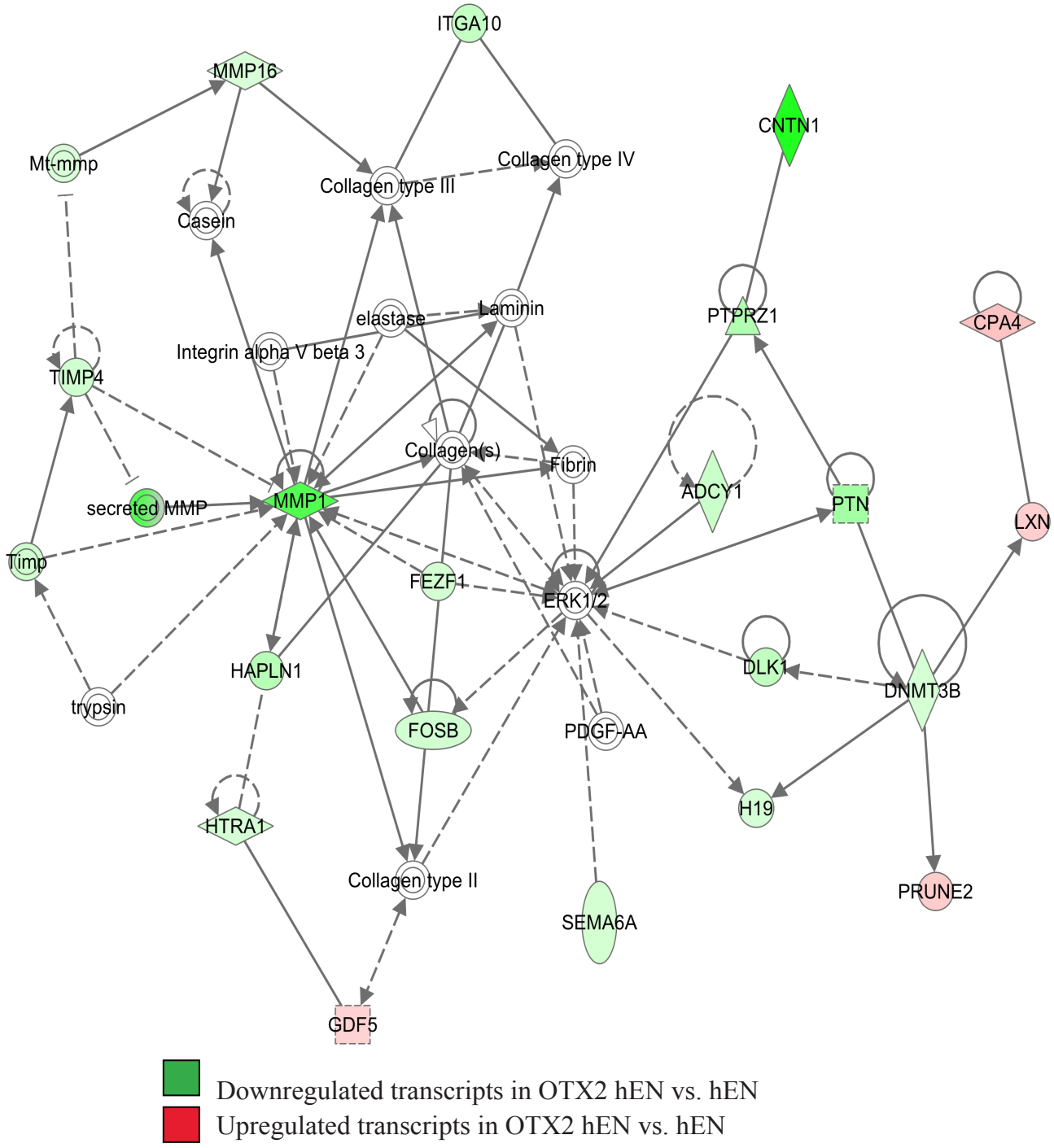


**Figure 3.1.13: Global gene expression also showed dysregulation of transcripts related to cell motility.** Shaded green areas denote transcripts that are significantly downregulated and red areas denote significantly upregulated transcripts in OTX2 hENs vs. hENs. N=3 biological replicates or independent infections.

**Table 3.1.1: Predicted activation states of differentially expressed cell proliferation transcripts in OTX2 hEN vs. hEN cells**

| Genes in dataset | Prediction (based on expression direction) | Fold Change | Findings |
|---|---|---|---|
| CSMD3 | Affected | -3.954 | Affects (1) |
| KIF15 | Affected | -1.794 | Affects (1) |
| LXN | Affected | 1.737 | Affects (1) |
| CLDN6 | Affected | -1.862 | Affects (2) |
| EFEMP1 | Affected | 2.833 | Affects (2) |
| GDF5 | Affected | 1.564 | Affects (2) |
| IL32 | Affected | 1.538 | Affects (2) |
| SCG2 | Affected | -1.586 | Affects (2) |
| TNMD | Affected | -1.672 | Affects (2) |
| DLK1 | Affected | -2.598 | Affects (3) |
| DNMT3B | Affected | -1.782 | Affects (7) |
| ADAMTS5 | Increased | -1.654 | Decreases (1) |
| ADCY1 | Increased | -2.215 | Decreases (1) |
| CYP2S1 | Increased | -1.899 | Decreases (1) |
| GNAO1 | Increased | -2.445 | Decreases (1) |
| HTRA1 | Increased | -1.743 | Decreases (1) |
| LECT1 | Increased | -1.620 | Decreases (1) |
| LIN28A | Increased | -5.995 | Decreases (1) |
| MAGI2 | Decreased | 1.583 | Decreases (1) |
| PODN | Decreased | 2.238 | Decreases (1) |
| RXFP2 | Increased | -1.502 | Decreases (1) |
| SMPD1 | Decreased | 1.565 | Decreases (1) |
| STC1 | Increased | -2.977 | Decreases (1) |
| TIMP4 | Increased | -1.954 | Decreases (2) |
| UNC5C | Increased | -2.897 | Decreases (2) |
| CNTN1 | Increased | -9.469 | Decreases (3) |
| H19 | Increased | -1.658 | Decreases (4) |
| PTPRZ1 | Increased | -3.232 | Decreases (4) |
| IGFBP3 | Increased | -1.822 | Decreases (42) |
| SNAI2 | Increased | -1.606 | Decreases (6) |
| TEK | Increased | -1.660 | Decreases (6) |
| RRAD | Decreased | 1.512 | Decreases (7) |
| CD34 | Decreased | -2.379 | Increases (1) |
| CENPF | Decreased | -1.519 | Increases (1) |
| COL6A3 | Decreased | -2.190 | Increases (1) |
| DLX2 | Decreased | -1.709 | Increases (1) |
| EPGN | Decreased | -2.505 | Increases (1) |
| KIF11 | Decreased | -1.513 | Increases (1) |
| MCM10 | Decreased | -1.738 | Increases (1) |
| NRCAM | Decreased | -1.697 | Increases (1) |
| PYGM | Decreased | -1.624 | Increases (1) |

| | | | |
|---|---|---|---|
| TTK | Decreased | -1.552 | Increases (1) |
| FEZF1 | Decreased | -1.831 | Increases (10) |
| NANOG | Decreased | -1.551 | Increases (12) |
| SIX1 | Decreased | -1.727 | Increases (13) |
| SOX2 | Decreased | -1.840 | Increases (14) |
| HTR2B | Increased | 3.014 | Increases (16) |
| MMP9 | Decreased | -1.919 | Increases (19) |
| PTN | Decreased | -3.822 | Increases (19) |
| ALOX5AP | Decreased | -1.515 | Increases (2) |
| AVPR1A | Decreased | -3.280 | Increases (2) |
| EYA1 | Decreased | -1.652 | Increases (2) |
| FOSB | Decreased | -1.927 | Increases (2) |
| NPY1R | Decreased | -2.083 | Increases (2) |
| SEMA6A | Decreased | -1.859 | Increases (2) |
| TACR1 | Decreased | -1.727 | Increases (2) |
| TOP2A | Decreased | -1.542 | Increases (2) |
| ZIC2 | Decreased | -1.612 | Increases (2) |
| FOS | Decreased | -2.373 | Increases (22) |
| TAC1 | Decreased | -2.636 | Increases (24) |
| mir-221 | Decreased | -1.801 | Increases (26) |
| IL6 | Increased | 1.571 | Increases (268) |
| MMP1 | Decreased | -7.394 | Increases (3) |
| TBX2 | Decreased | -1.598 | Increases (3) |
| IGF1 | Decreased | -2.292 | Increases (389) |
| ANGPT1 | Decreased | -2.080 | Increases (4) |
| FABP4 | Increased | 2.893 | Increases (4) |
| PAX9 | Decreased | -1.699 | Increases (4) |
| TNFAIP6 | Decreased | -1.965 | Increases (4) |
| PIM1 | Increased | 2.018 | Increases (43) |
| SPP1 | Decreased | -3.416 | Increases (45) |
| MYBL1 | Decreased | -1.828 | Increases (5) |
| TPX2 | Decreased | -1.573 | Increases (5) |
| BCL2 | Decreased | -2.124 | Increases (53) |
| DLGAP5 | Decreased | -1.586 | Increases (6) |
| LIN28B | Decreased | -1.837 | Increases (6) |
| TGM2 | Decreased | -3.726 | Increases (6) |
| POU5F1 | Decreased | -2.169 | Increases (7) |
| AGTR1 | Decreased | -3.103 | Increases (8) |
| A2M | Decreased | -1.593 | Increases (9) |
| C3 | Increased | 1.756 | Increases (9) |

**** 48 of 81 genes have expression direction consistent with decreases in cell proliferation**

**Table 3.1.2: Predicted activation states of differentially expressed cell migration transcripts in OTX2 hEN vs. hEN cells**

| Genes in dataset | Prediction (based on expression direction) | Fold Change | Findings |
|---|---|---|---|
| CD34 | Affected | -2.379 | Affects (1) |
| FAP | Affected | -1.506 | Affects (1) |
| HTR2B | Affected | 3.014 | Affects (1) |
| ROBO2 | Affected | -1.547 | Affects (1) |
| SIX1 | Affected | -1.727 | Affects (1) |
| UNC5C | Affected | -2.897 | Affects (1) |
| FEZF1 | Affected | -1.831 | Affects (2) |
| SEMA6A | Affected | -1.859 | Affects (2) |
| IGFBP3 | Affected | -1.822 | Affects (4) |
| A2M | Increased | -1.593 | Decreases (1) |
| CYP2S1 | Increased | -1.899 | Decreases (1) |
| GDF5 | Decreased | 1.564 | Decreases (1) |
| IL32 | Decreased | 1.538 | Decreases (1) |
| MAGI2 | Decreased | 1.583 | Decreases (1) |
| PODN | Decreased | 2.238 | Decreases (1) |
| POU5F1 | Increased | -2.169 | Decreases (1) |
| PTPRZ1 | Increased | -3.232 | Decreases (10) |
| ACAN | Increased | -1.832 | Decreases (2) |
| SMPD1 | Decreased | 1.565 | Decreases (2) |
| mir-221 | Increased | -1.801 | Decreases (3) |
| STC1 | Increased | -2.977 | Decreases (4) |
| CNTN1 | Decreased | -9.469 | Increases (1) |
| PIM1 | Increased | 2.018 | Increases (1) |
| PLCL1 | Decreased | -1.759 | Increases (1) |
| SCG2 | Decreased | -1.586 | Increases (10) |
| ANGPT1 | Decreased | -2.080 | Increases (13) |
| SNAI2 | Decreased | -1.606 | Increases (16) |
| TAC1 | Decreased | -2.636 | Increases (16) |
| GNAO1 | Decreased | -2.445 | Increases (2) |
| LIN28B | Decreased | -1.837 | Increases (2) |
| C3 | Increased | 1.756 | Increases (23) |
| TGM2 | Decreased | -3.726 | Increases (26) |
| ALOX5AP | Decreased | -1.515 | Increases (3) |
| BCL2 | Decreased | -2.124 | Increases (3) |
| DLX1 | Decreased | -1.526 | Increases (3) |
| FABP4 | Increased | 2.893 | Increases (3) |
| IL6 | Increased | 1.571 | Increases (37) |
| MMP9 | Decreased | -1.919 | Increases (37) |
| PTN | Decreased | -3.822 | Increases (39) |
| DLX2 | Decreased | -1.709 | Increases (4) |

| | | | |
|---|---|---|---|
| TACR1 | Decreased | -1.727 | Increases (4) |
| MMP1 | Decreased | -7.394 | Increases (5) |
| IGF1 | Decreased | -2.292 | Increases (73) |
| SPP1 | Decreased | -3.416 | Increases (79) |
| TEK | Decreased | -1.660 | Increases (8) |

**** 25 of 45 genes have expression direction consistent with decreases in cell migration.**

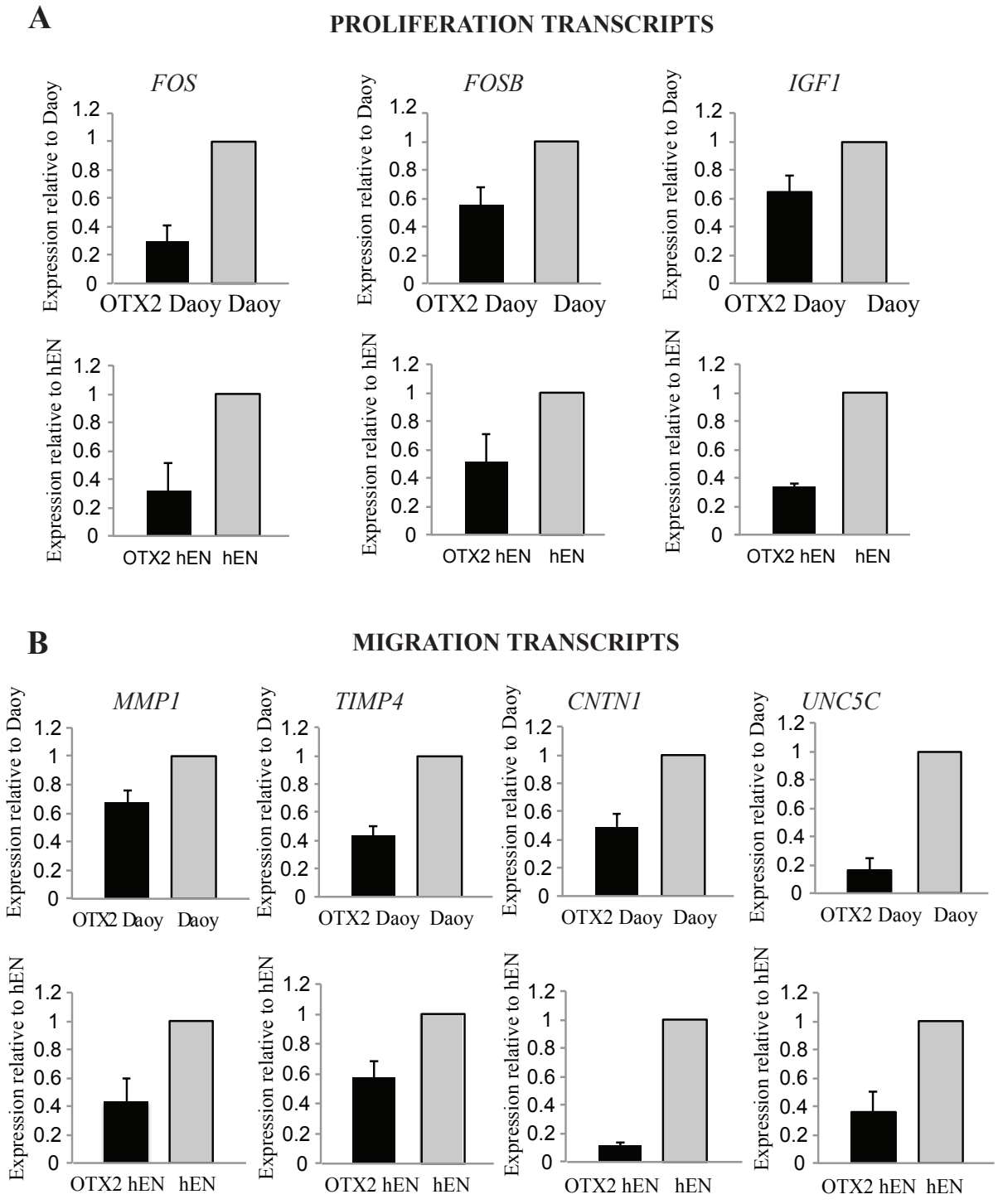


**Figure 3.1.14: OTX2 overexpression decreases levels of both proliferation and migration transcripts.** (A) Validation of proliferation transcript downregulation in Daoy (upper) and hENs (lower) following OTX2 overexpression by qPCR. Error Bars: s.e.m. N=3 independent biological replicates. (B) Validation of migration transcript downregulation in Daoy (upper) and hENs (lower) following OTX2 overexpression by qPCR. Error Bars: s.e.m. N=3 independent biological replicates.

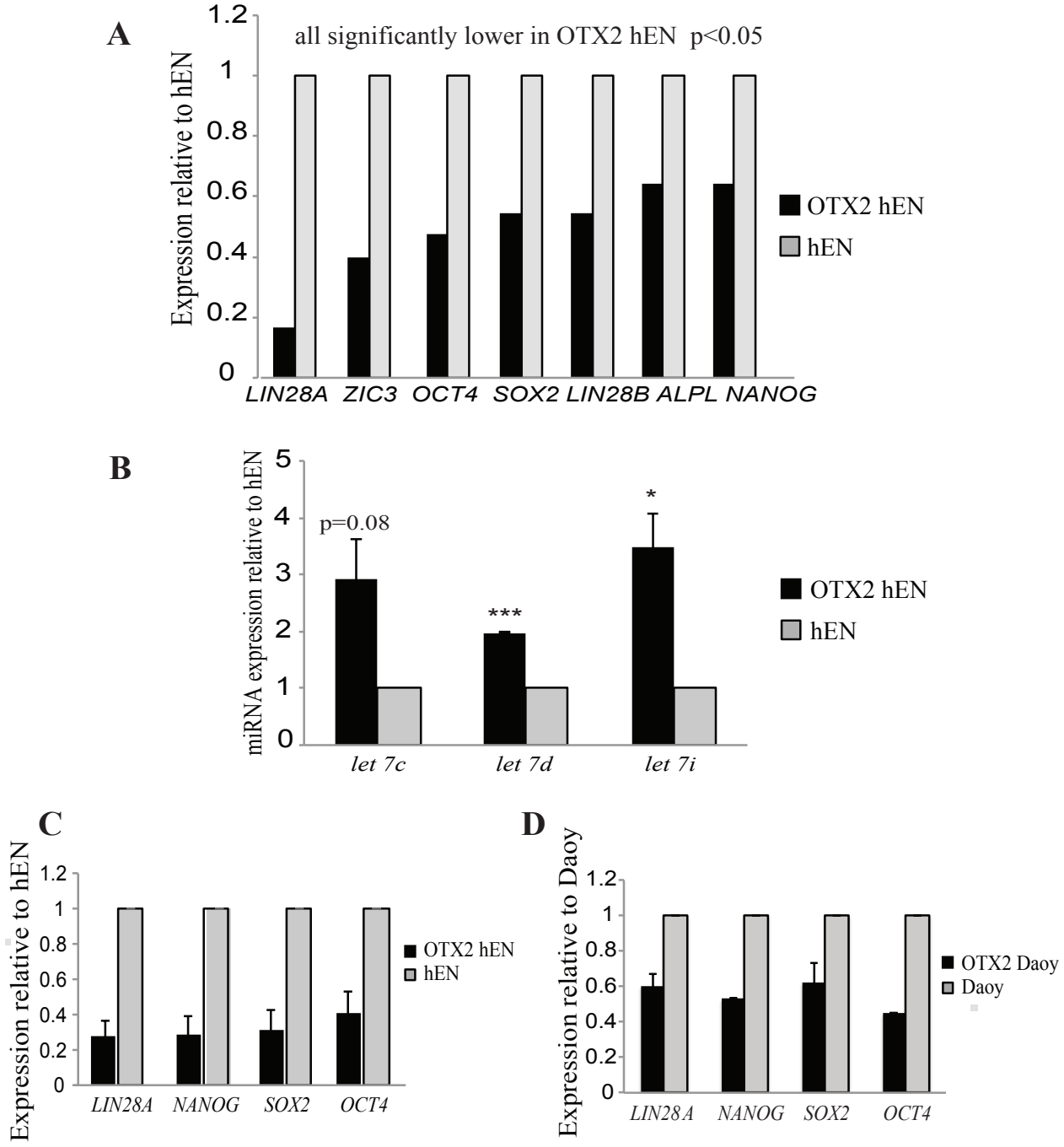


**Figure 3.1.15: OTX2 overexpression significantly decreases levels of hESC genes**. (A) Results from global gene expression analysis demonstrating overall downregulation of hESC pluripotency genes in OTX2-overexpressing hENs. Graph represents N=3 biological replicate pairs of OTX2 hEN and hENs. All transcripts are significantly different. P<0.05*. (B) Upregulation of representative miRNA targets of LIN28A following OTX2 overexpression in hENs. N=3 independent biological replicates and n=3 technical replicates within each biological replicate. (C-D) Validation of hESC transcript downregulation in hENs (C) and Daoy (D) following OTX2 overexpression by qPCR. Error Bars: s.e.m. P<0.05*, P<0.01**, P<0.001***.

that OTX2 control stem cells function in hENs and Daoy cells by regulating expression of *SOX2, OCT4, NANOG* and *LIN28A* genes. To further study the mechanism of OTX2-mediated regulation of stem cell genes, we employed chromatin immunoprecipitation assays.

**3.1.2.1b Chromatin immunoprecipitation and promoter reporter assay revealed a novel interaction between OTX2 and pluripotent stem cell genes.**

To test whether OTX2 associates with specific DNA binding sites present within the promoter region of candidate hESC genes (*OCT4, SOX2, NANOG, LIN28A*), we performed ChIP-qPCR assays specifically in OTX2+ Daoy and OTX2+ hENs along with respective control cells. OTX2 does not localize to the promoter regions of *OCT4, NANOG* and *LIN28A* (Figure 3.1.16A-C, 3.1.17A-C); however, we observed an increase in OTX2 recruitment on the *SOX2* loci in OTX2+ Daoy and hENs relative to Daoy and hEN controls (Figure 3.1.16D and 3.1.17D). To evaluate the functional significance of this interaction, luciferase reporter gene assays were performed. Co-transfection of OTX2+ Daoy and OTX2+ hEN cells with a SOX2 promoter reporter construct resulted in decreased luciferase expression relative to Daoy and hEN controls (Figure 3.1.18A-B).

In support of our expression profile studies, H3K4me3 activating histone modifications were downregulated on *OCT4, NANOG,* and *LIN28A* promoter loci in OTX2+ Daoy and OTX2+ hENs compared to control cells (Figure 3.1.16A-C and 3.1.17A-C). We observed a 30% reduction in H3K4me3 marks on the *SOX2* promoter in OTX2 overexpressing cells (Figure 3.1.16D and 3.1.17D). We did not see any changes in H3K27 repressive histone modifications.

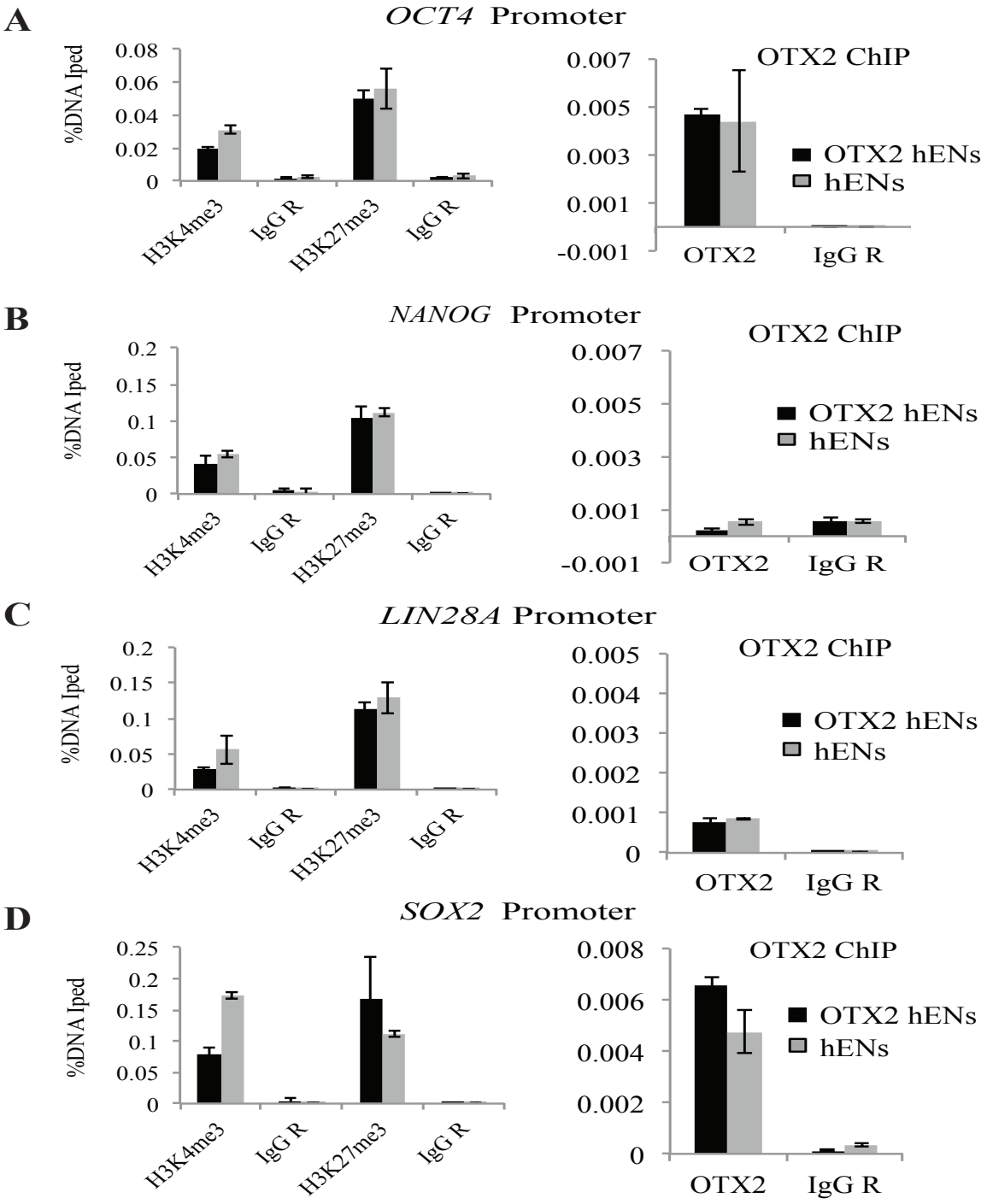


**Figure 3.1.16: Chromatin immunoprecipitation revealed a novel interaction between OTX2 and *SOX2* in hENs.** Comparative ChIP-qPCR analysis for OTX2 binding and histone modifications (H3K4me3 and H3K27me3) on the *OCT4, NANOG, LIN28A* and *SOX2* promoters in OTX2+ hENs vs. hENs. Error bars: s.d. ChIP assay showed a downregulation of active histone mark, H3K4me3 on *OCT4, NANOG, LIN28A* and *SOX2* promoter (A-D). An increase in the recruitment of OTX2 was observed only at the SOX2 promoter (D) but not at the promoter region of other stem cell genes (A-C).

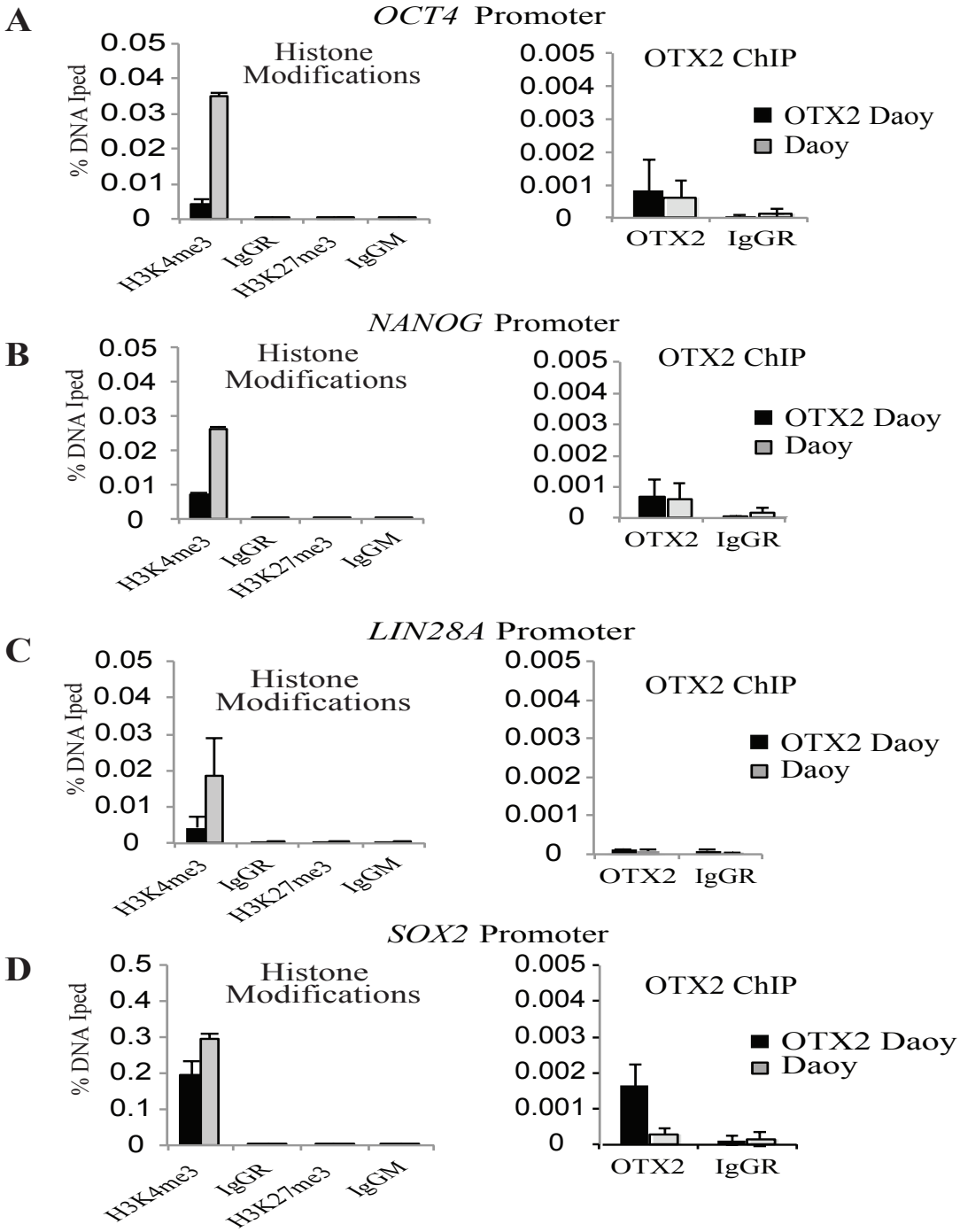


**Figure 3.1.17: Chromatin immunoprecipitation revealed a novel interaction between OTX2 and *SOX2* in Daoy MB cells.** Comparative ChIP-qPCR analysis for OTX2 binding and histone modifications (H3K4me3 and H3K27me3) on the *OCT4, NANOG, LIN28A* and *SOX2* promoters in OTX2+ Daoy vs. Daoy cells. Error bars: s.d. ChIP assay showed a downregulation of active histone mark, H3K4me3 on *OCT4, NANOG, LIN28A* and *SOX2* promoter (A-D). An increase in the recruitment of OTX2 was observed only at the SOX2 promoter (D).

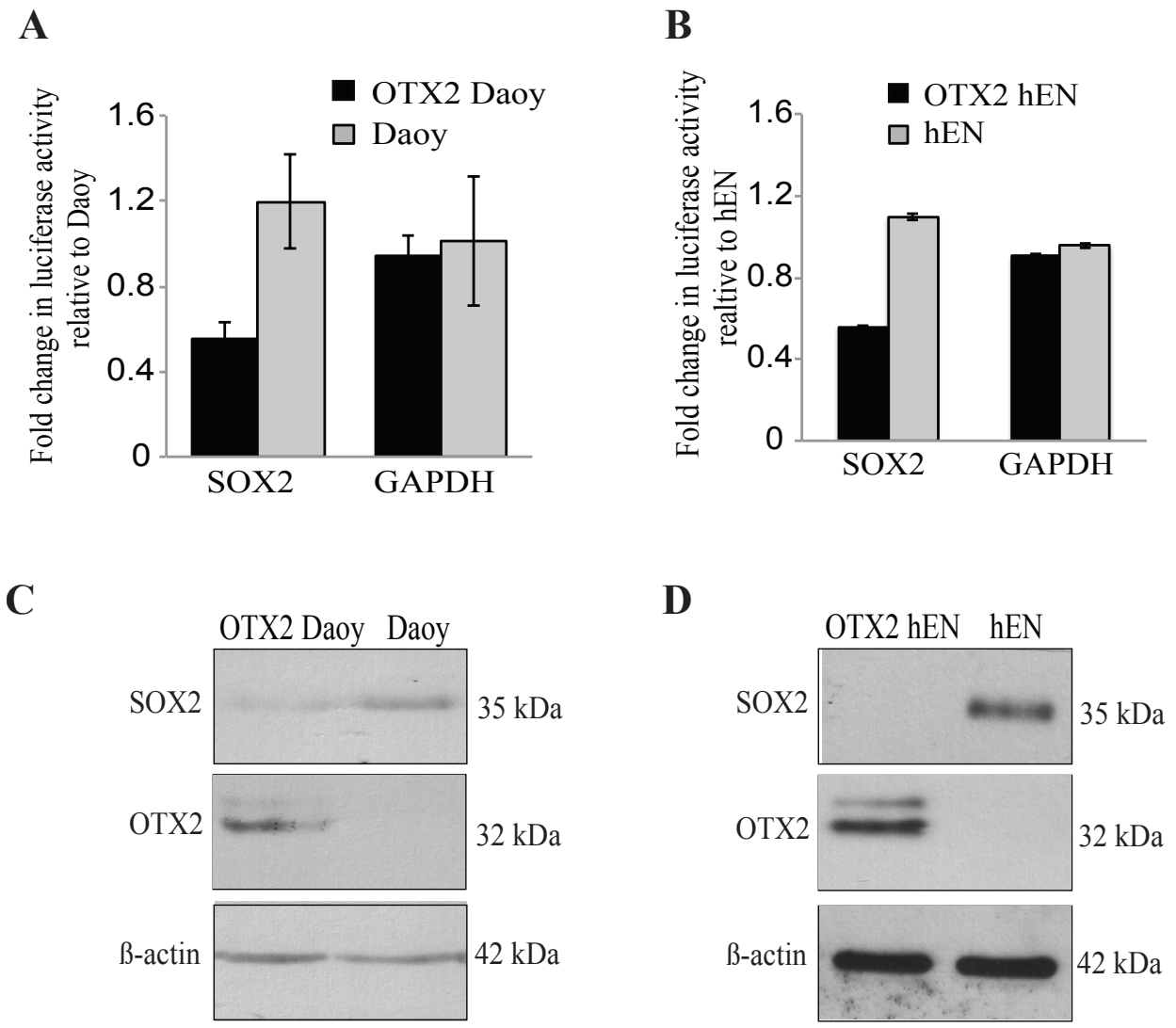


**Figure 3.1.18: OTX2 may directly/indirectly decrease SOX2 expression in hENs and Daoy cells.** A decrease in luciferase activity was observed in OTX2+ Daoy (A) and OTX2+ hEN (B) following transfection of a SOX2 promoter reporter construct. Error Bars: s.e.m. Luciferase activity was normalized relative to the control in each cell line. Western blots depicting decreased levels of SOX2 in Daoy SHH MB (C) and hEN (D) cells following OTX2 overexpression. β-actin serves as a loading control.

We also observed a decrease in SOX2 protein levels following OTX2 overexpression in Daoy and hENs (Figure 3.1.18C-D). Collectively, these data support our cellular studies and reveal novel functional interactions between OTX2 and SOX2 in human cells.

### 3.1.3 Rescue of cell functional deficits by overexpressing SOX2 in OTX2+ Daoy and hENs

#### 3.1.3.1 Rationale

Danno et al, have shown a physical interaction between Otx2 and Sox2 proteins during ocular development in Xenopus (Danno et al. 2008). Otx2 also plays a role in specification of retinal pigment epithelium by repressing neural retina markers such as Sox2 and Fgf8 (Nishihara et al. 2012). SOX2+ tumor propagating cells have recently been shown to drive cell growth specifically in SHH MB mouse tumors (Ahlfeld et al. 2013; Vanner et al. 2014). Given the downregulation of SOX2 following OTX2 overexpression in our model systems, we wanted to determine whether introduction of exogenous SOX2 could rescue the cell deficits in OTX2+ SHH MB and hENs.

#### 3.1.3.2 Stable overexpression of SOX2 in OTX2+ Daoy and hENs

We stably overexpressed SOX2 in OTX2+ Daoy, OTX2+ hEN and their respective controls (that subsequently lose SOX2 expression following extended culture) using pReceiver-Lv105 lentiviral particles containing puromycin as a selection marker (Figure 3.1.19A). We selected the stable SOX2 overexpressing OTX2+ Daoy and hENs using puromycin and validated the expression of SOX2 in double positive OTX2+/SOX2+ cells by Western blot (Figure 3.1.19B-C). We also evaluated the expression of OTX2 in double positive OTX2+/SOX2+ and single positive OTX2+/SOX2- Daoy and hENs (Figure 3.1.19B-C).

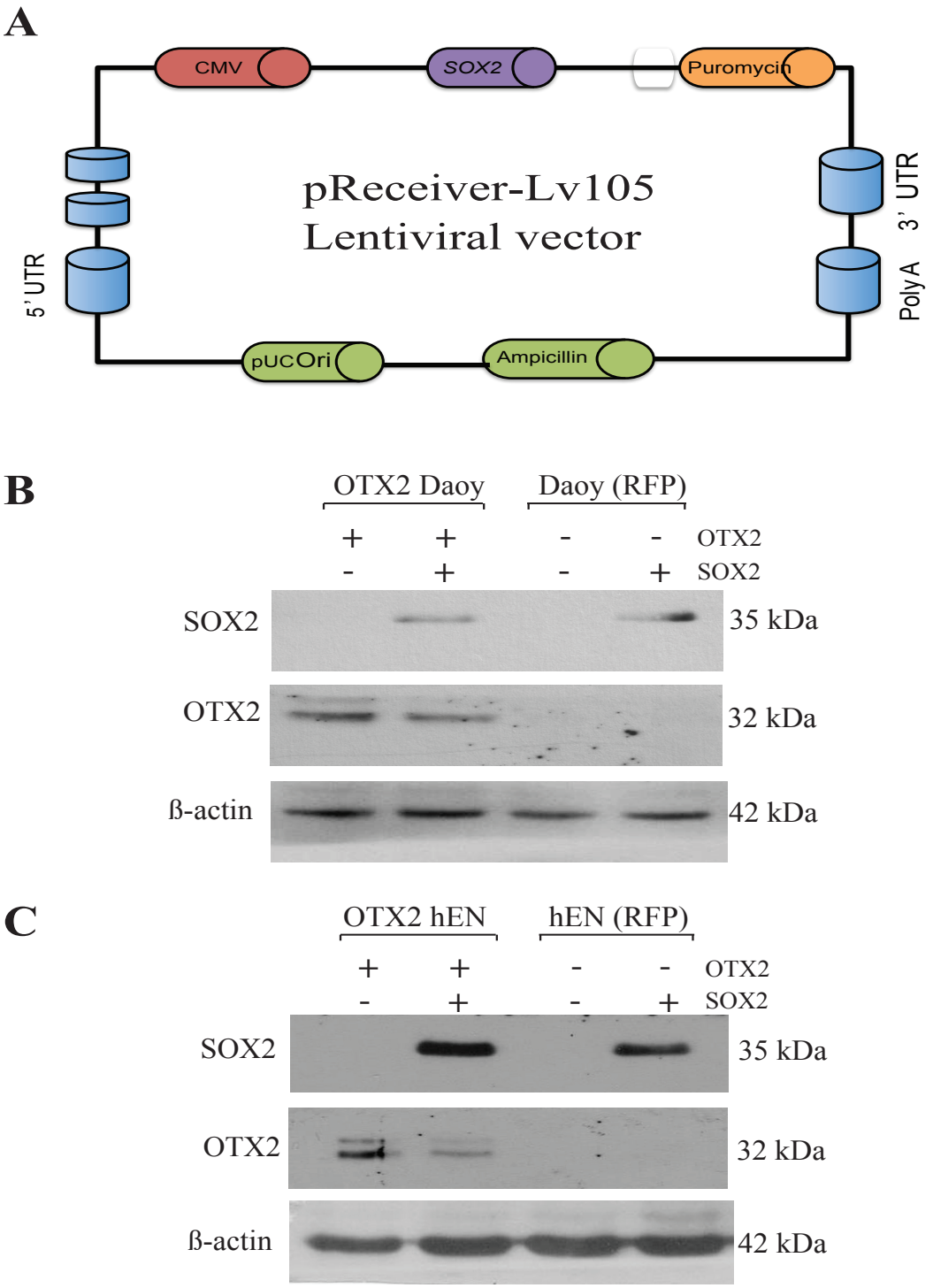


**Figure 3.1.19: Stable overexpression of SOX2 in OTX2 + Daoy and hENs.** (A) pReceiver-Lv-105 vector construct used for stable overexpression of SOX2 in Daoy SHH MB cells and hENs in the presence/absence of OTX2 overexpression. (B-C) Western blots depicting overexpression of SOX2 in Daoy SHH MB (B) and hEN (C) cells in the presence/absence of OTX2 overexpression.

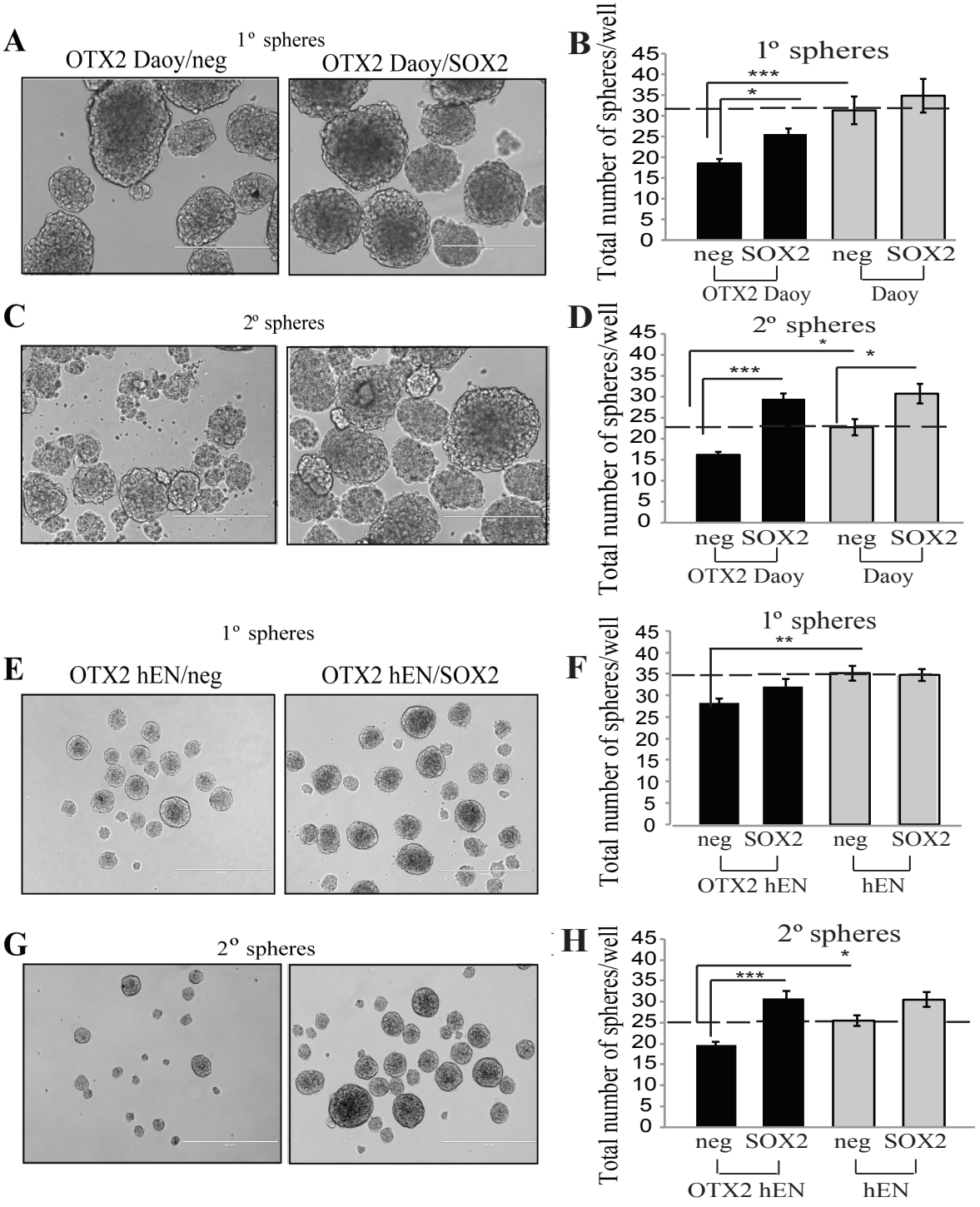


**Figure 3.1.20: Overexpression of SOX2 in OTX2+ Daoy and hENs rescues self-renewal.** SOX2 overexpression in OTX2+ cells results in a significant recovery in self-renewal for both Daoy (A-D) and hEN (E-H). (A, C) Representative images of spheres over subsequent passage following SOX2 overexpression in OTX2+ Daoy. (E,G) Representative images of spheres over subsequent passage following SOX2 overexpression in OTX2+ hENs. N=3 biological replicates and n=4 technical replicates within each biological replicate. Scale bar: 400 μm.

#### 3.1.3.3 SOX2 overexpression rescued the self-renewal and migration abilities of both OTX2+ Daoy and hENs

Interestingly, following SOX2 overexpression, we observed a decrease in OTX2 levels for both OTX2+ Daoy and OTX2+ hEN suggesting that SOX2 could be suppressing OTX2 (Figure 3.1.19B-C). In terms of cell function, we did not observe significant changes in cell growth (data not shown); however, we did observe a significant rescue of self-renewal (Figure 3.1.20A-H) and migration (Figure 3.1.21A-D) for both cell lines following SOX2 overexpression. Given the role of SOX2+ cells in driving SHH MB progression (Ahlfeld et al. 2013; Vanner et al. 2014), we also expected to see effects from SOX2 overexpression alone independent of an OTX2 phenotypic rescue. No significant changes in primary spheres or migration were detected; however, we observed a small, but significant increase in control Daoy secondary spheres following SOX2 overexpression. Together, these results demonstrate that SOX2 is sufficient to rescue the inhibitory effects of OTX2 on hEN and SHH MB cell self-renewal and migration. The downregulation of OTX2 following SOX2 overexpression suggests that these 2 transcription factors may participate in a negative feedback loop that regulates cell properties in our model systems.

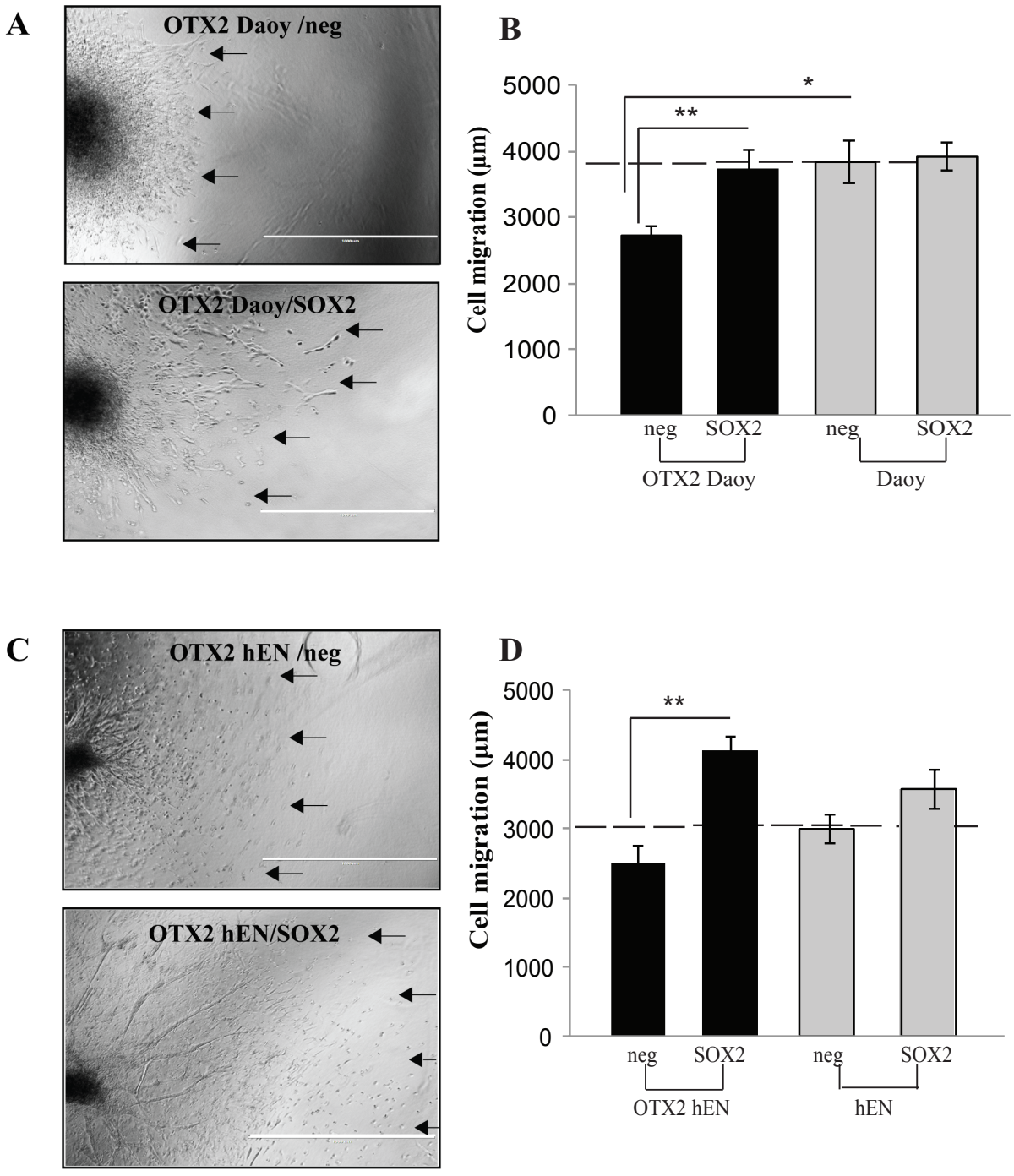


**Figure 3.1.21: SOX2 overexpression also rescues cell migration ability of OTX2+Daoy and hENs.** SOX2 overexpression in OTX2+ cells rescues cell migration deficits in both Daoy (A-B) and hEN (C-D). Error bars: s.e.m. P<0.05*, P<0.01**, P<0.001***. (A, C) Representative images of OTX2+ Daoy (A) and OTX2+ hEN (C) aggregates in collagen over 3 days following SOX2 overexpression. Arrows denote migration front for representative aggregates. N=3 biological replicates and n=3 technical replicates within each biological replicate. Scale bar: 1000 µm.

# CHAPTER 3.2: Oncogenic role of OTX2 in transformed-hENs and Group 3 and 4 MB cells

### 3.2.1 The oncogenic role of OTX2 on tumorigenic properties of trans-hENs as well as Group 3 and 4 MB cells.

#### 3.2.1.1 OTX2 knockdown decreases cell growth in trans-hENs as well as Groups 3 and 4 MB cells *in vitro*.

While OTX2 has been shown to induce cell senescence in SHH MB *in vitro* (Bunt et al. 2010), studies involving Group 3 and Group 4 MB variants have demonstrated an oncogenic role for OTX2 in regulating cell growth (Di et al. 2005; Adamson et al. 2010). To determine whether we could also model this oncogenic role using neural derivatives from hESCs and whether OTX2 also plays a role in other cell properties, using siRNAs, we knocked down OTX2 in the Group 3 and 4 MB cell lines, D283, D425 and D341 as well as in trans-hENs, that resemble Group 3 and 4 MB *in vivo* (Werbowetski-Ogilvie et al. 2012). We first evaluated the transfection efficiency of D283, D425, D341 and trans-hENs using a Block-iT™ Red Fluorescent control and demonstrated near 100% transfection of cell lines after 24 hours (Figure 3.2.1A-B, D-E and Figure 3.2.2A-B, D-E). Three siRNAs targeting OTX2 were tested, and all 3 generated a significant knockdown at the protein level relative to scramble siRNA by Western Blot (Figure 3.2.1C, F and Figure 3.2.2C, F). Following OTX2 knockdown, D283, D425 MB cells and trans-hENs exhibited a significant decrease in cell growth (Figure 3.2.3A-B, 3.2.4A-B and 3.2.5A-B). We did not observe change in the cell viability of D283 and trans-hENs; however, an insignificant decrease in the viability of D425 cells was determined by trypan blue staining (Figure 3.2.3C, 3.2.4C and 3.2.5C).

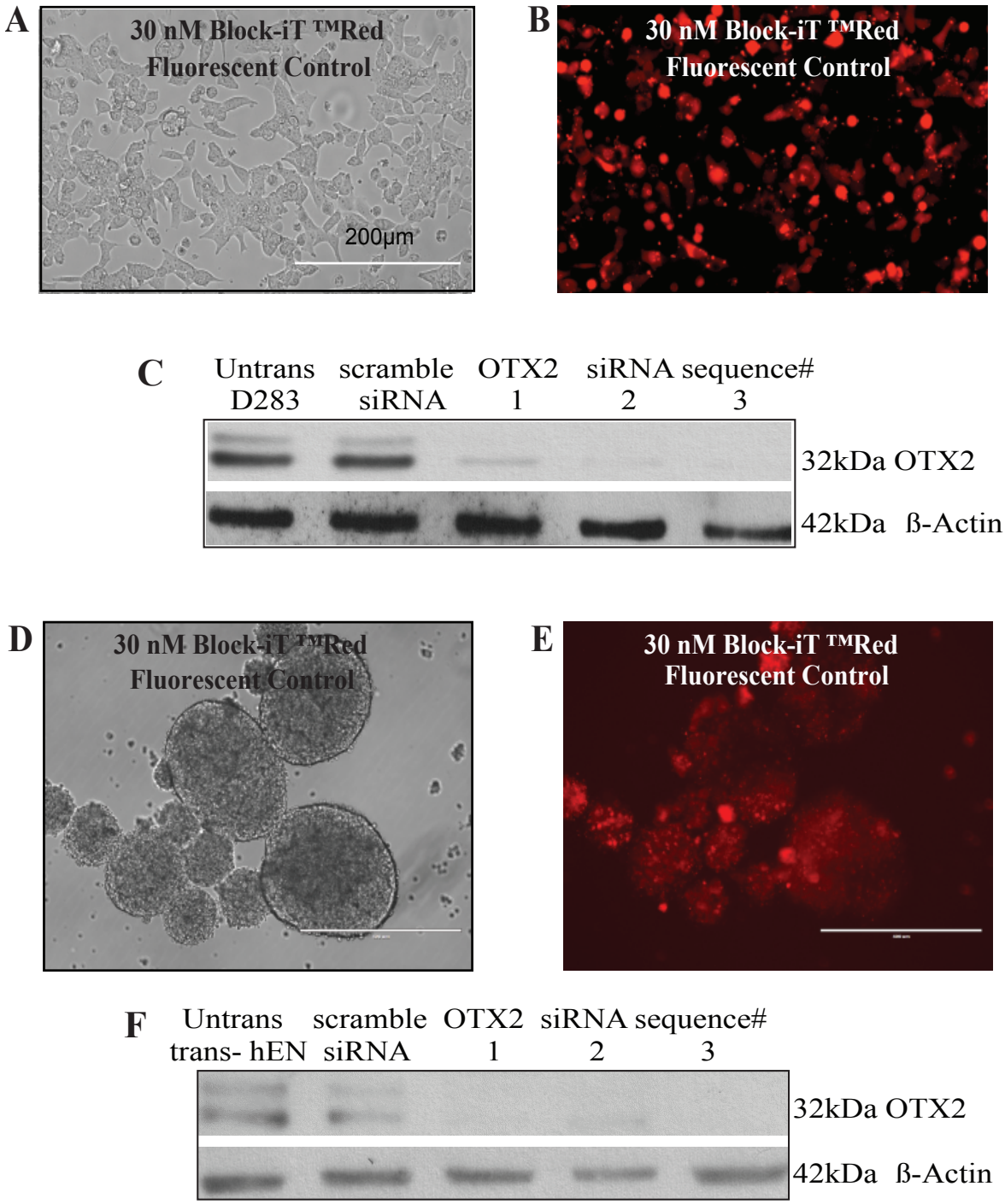


**Figure 3.2.1: Knockdown of OTX2 in trans-hENs and D283 cells:** Representative brightfield (A, D) and fluorescent (B, E) images of adherent D283 cells and trans-hENs neurospheres cells following transfection with a Block IT™ Red Fluorescent control to determine transduction efficiency. (A-B) Scale bar: 200 µm. (D-E) Scale bar: 400 µm. Western blot depicting significant knockdown of OTX2 in (C) D283 and (F) trans-hENs cells following transfection using 3 siRNAs sequences relative to scrambled (2nd lane) and untransduced (1st lane) controls.

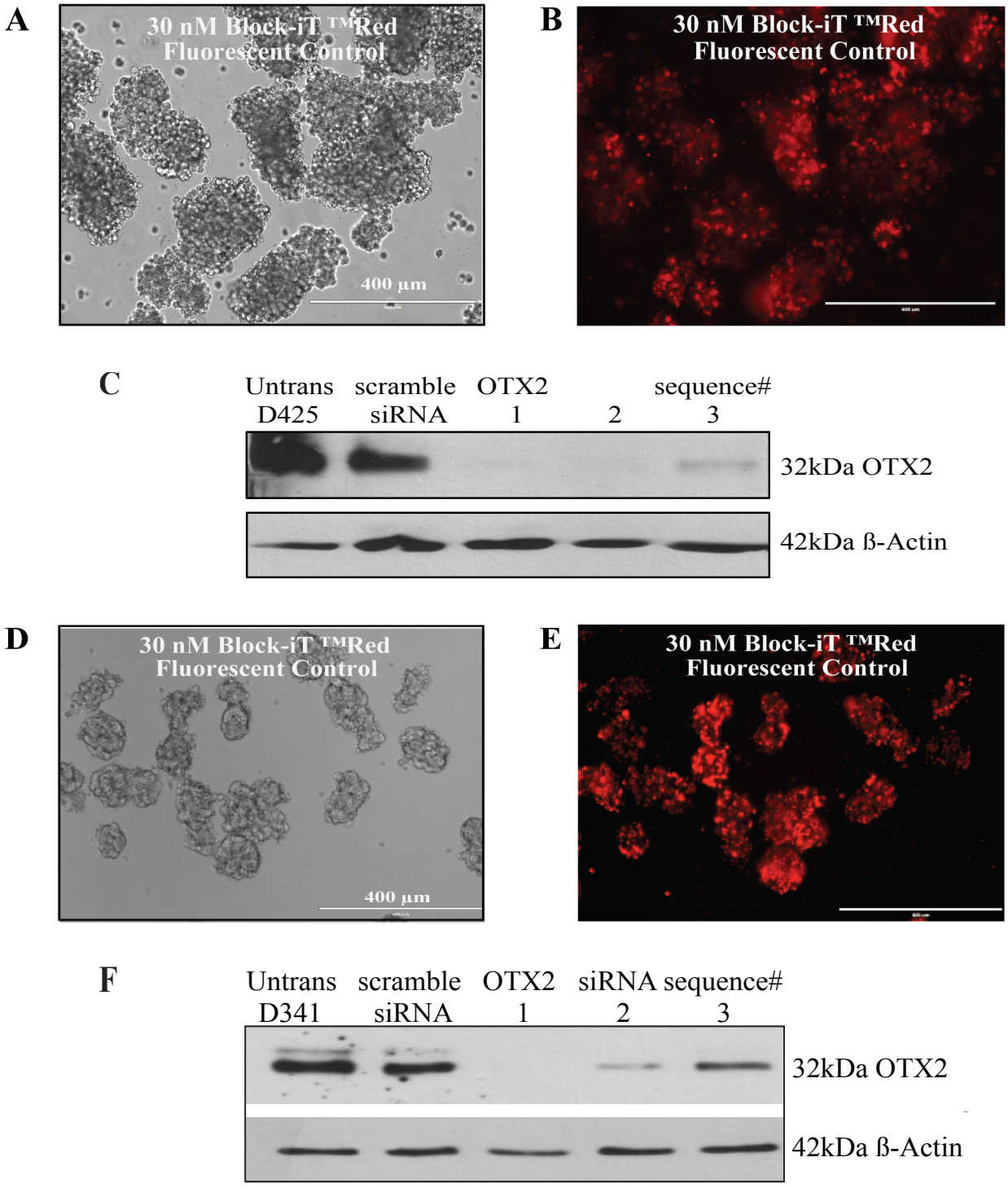


**Figure 3.2.2: Knockdown of OTX2 in D425 and D341 Group 3 MB cells:** Representative brightfield (A, D) and fluorescent (B, E) images of D425 and D341 tumorspheres cells following transfection with a Block IT™ Red Fluorescent control to determine transduction efficiency. (A-B and D-E) Scale bar: 400 µm. Western blot showed significant knockdown of OTX2 in (C) D425 and (F) D341 cells following transfection using 3 siRNAs sequences relative to scrambled (2nd lane) and untransduced (1st lane) controls.

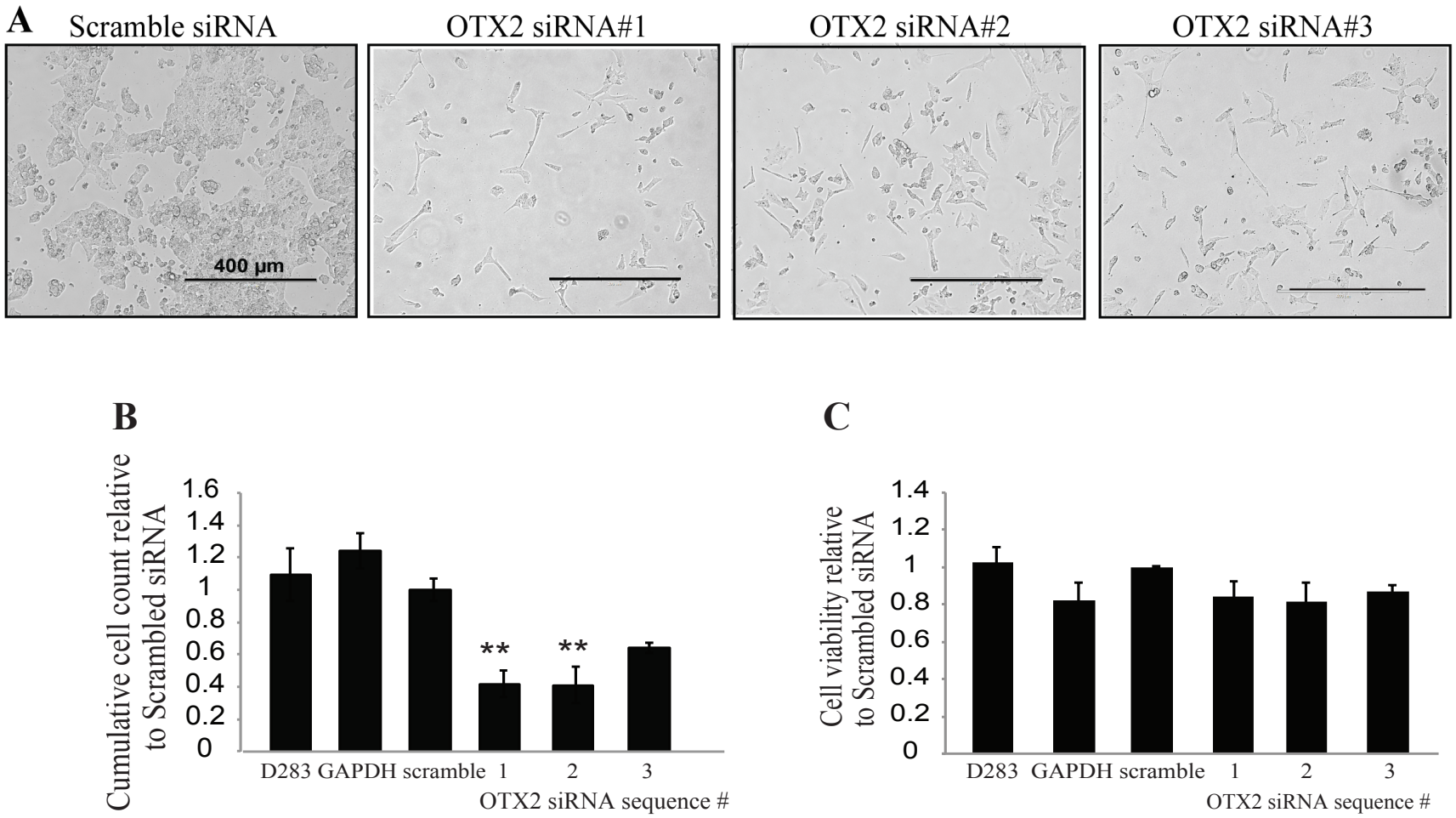


**Figure 3.2.3: OTX2 knockdown significantly inhibits cell proliferation in D283 Group 4 cells.** (A) Representative images of D283 MB cells in adherent culture following 4 days knockdown of OTX2. Scale bar: 400 µm. (B) Quantification of total cell number in D283 cells following knockdown of OTX2 over 4 days. Error bars: s.e.m. P<0.01**. For all experiments, N=3 biological replicates or independent transfections and n=4 technical replicates within each biological replicate.

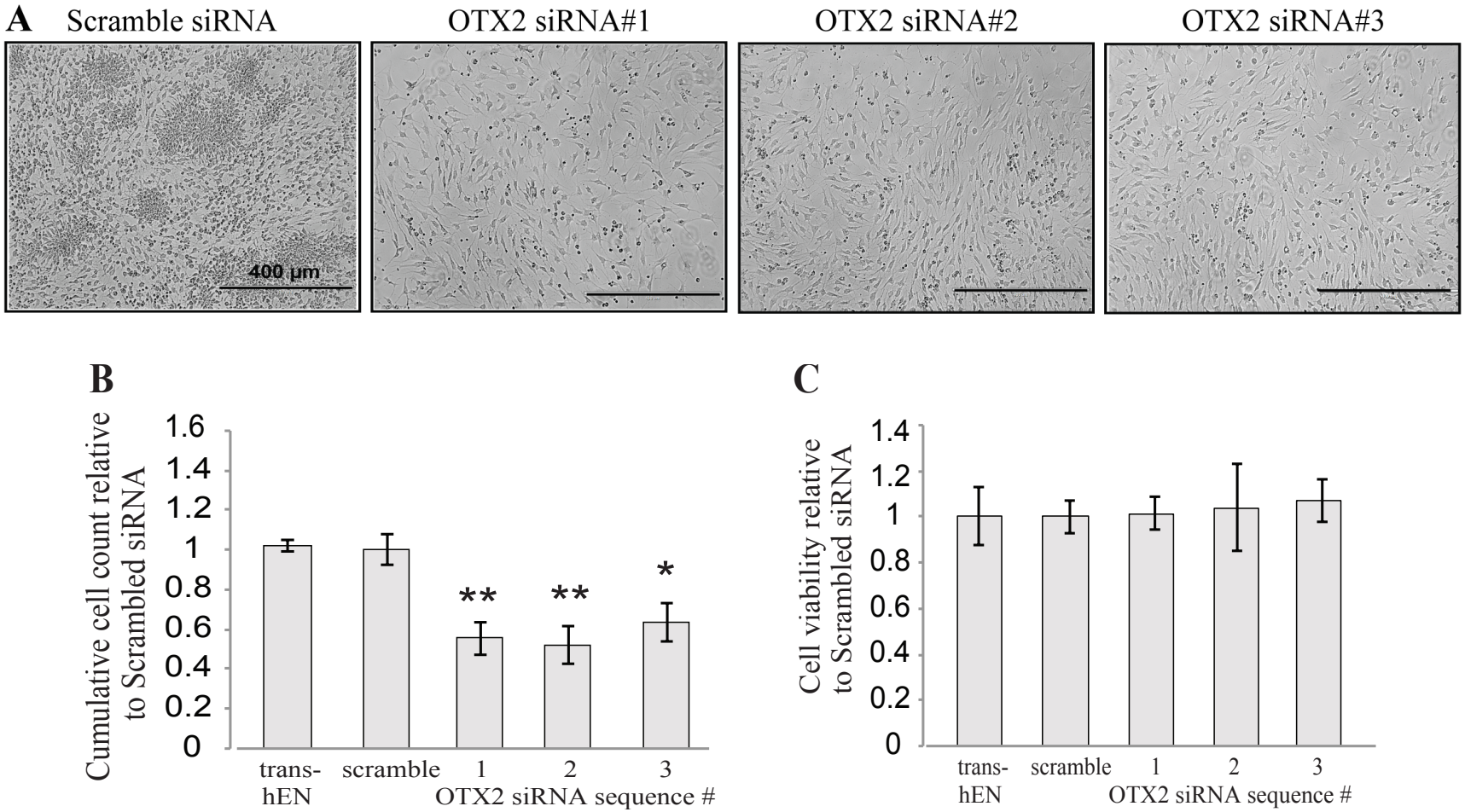


**Figure 3.2.4: OTX2 knockdown significantly inhibits cell proliferation in trans-hENs**. (A) Representative images of trans-hENs in adherent culture following 4 days knockdown of OTX2. Scale bar: 400 µm. (B) Quantification of total cell number in trans-hENs following knockdown of OTX2 over 4 days. Error bars: s.e.m. $P<0.05$*, $P<0.01$**. For all experiments, N=3 biological replicates or independent transfections and n=4 technical replicates within each biological replicate.

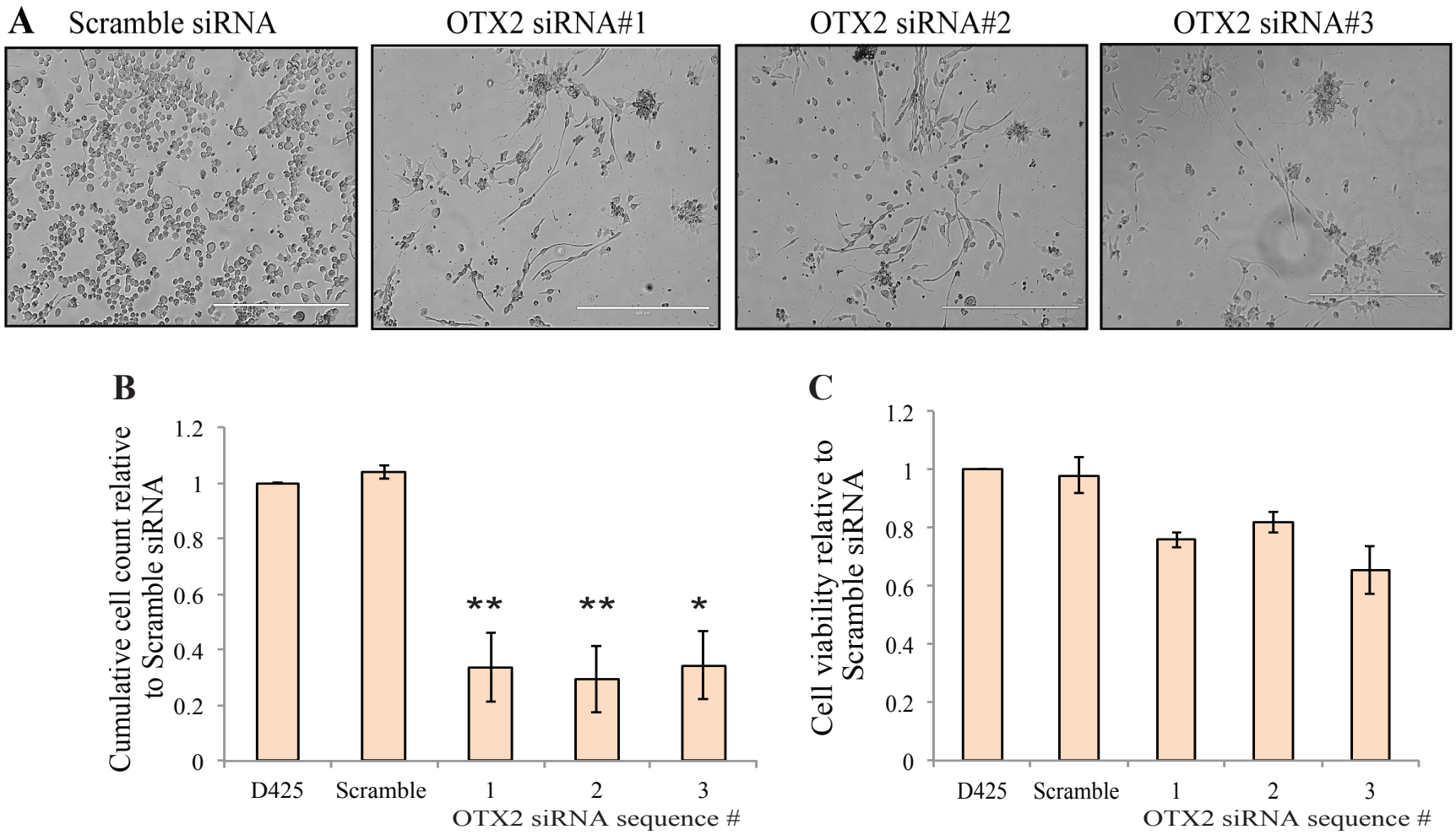


**Figure 3.2.5: OTX2 knockdown significantly inhibits cell proliferation in D425 Group 3 MB cells.** (A) Representative images of D425 in adherent culture following 4 days knockdown of OTX2. Scale bar: 400 μm. (B) Quantification of total cell number in D425 cells following knockdown of OTX2 over 4 days. Error bars: s.e.m. P<0.05*, P<0.01**. For all experiments, N=2 biological replicates or independent transfections and n=4 technical replicates within each biological replicate.

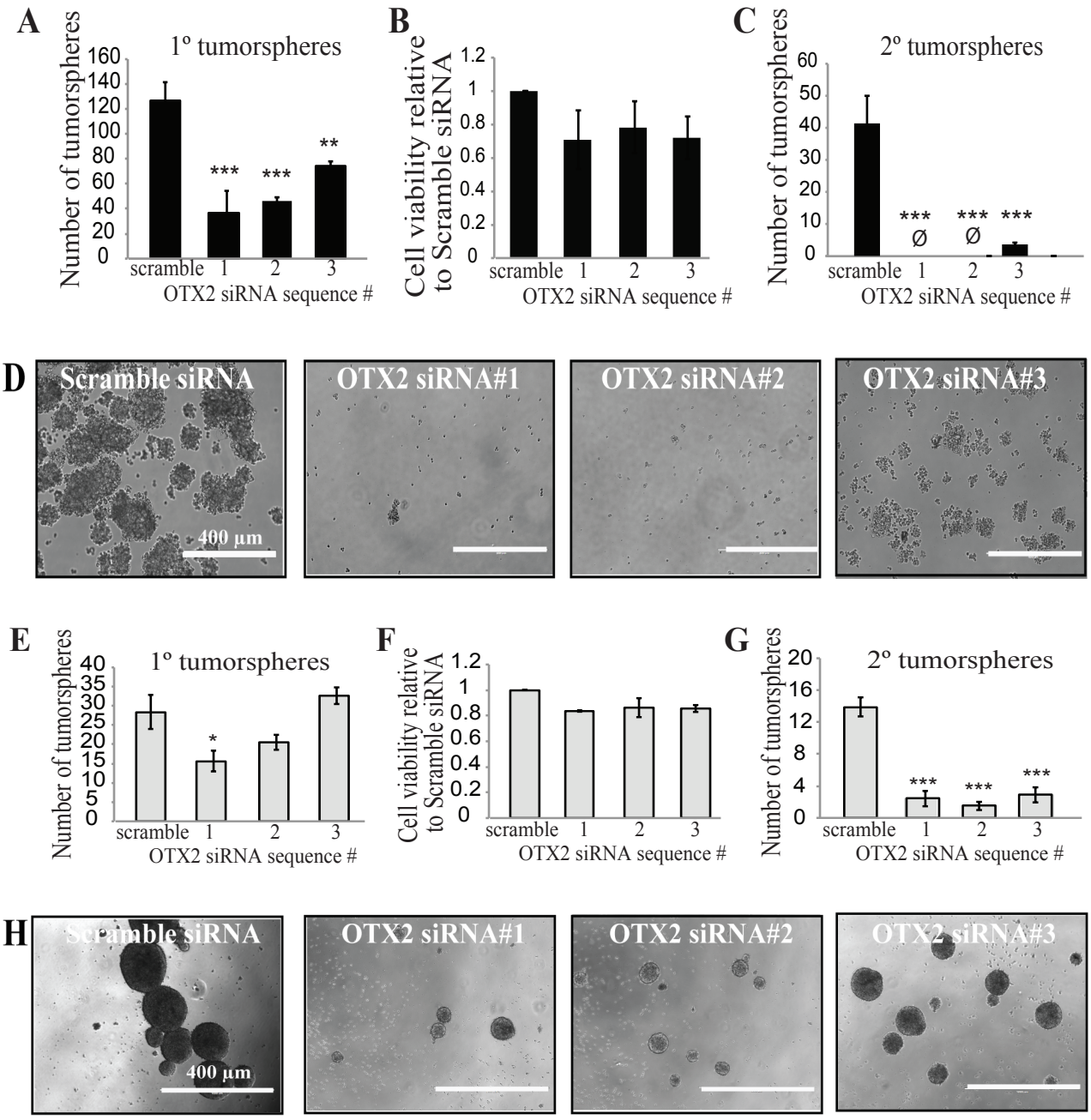


**Figure 3.2.6. OTX2 knockdown significantly inhibits self-renewal in D283, Group 4 MB cells, and trans-hENs.** Self-renewal capacity following OTX2 knockdown in D283 (A-D) and trans-hENs (E-H). In D283, self-renewal capacity was almost completely inhibited following passage to secondary spheres (A-B), and this was evident in representative brightfield images of secondary spheres in (D). (E-G) Significant decreases in neurosphere-forming capacity were also evident in trans-hENs (E-F) following OTX2 knockdown and similar to D283, self-renewal capacity was significantly inhibited (H). For both cell lines, cell viability was not significantly decreased (B, F). Error bars: s.e.m. $P<0.05$*, $P<0.01$**, $P<0.001$***. For all experiments, N=3 biological replicates or independent transfections and n=4 technical replicates within each biological replicate.

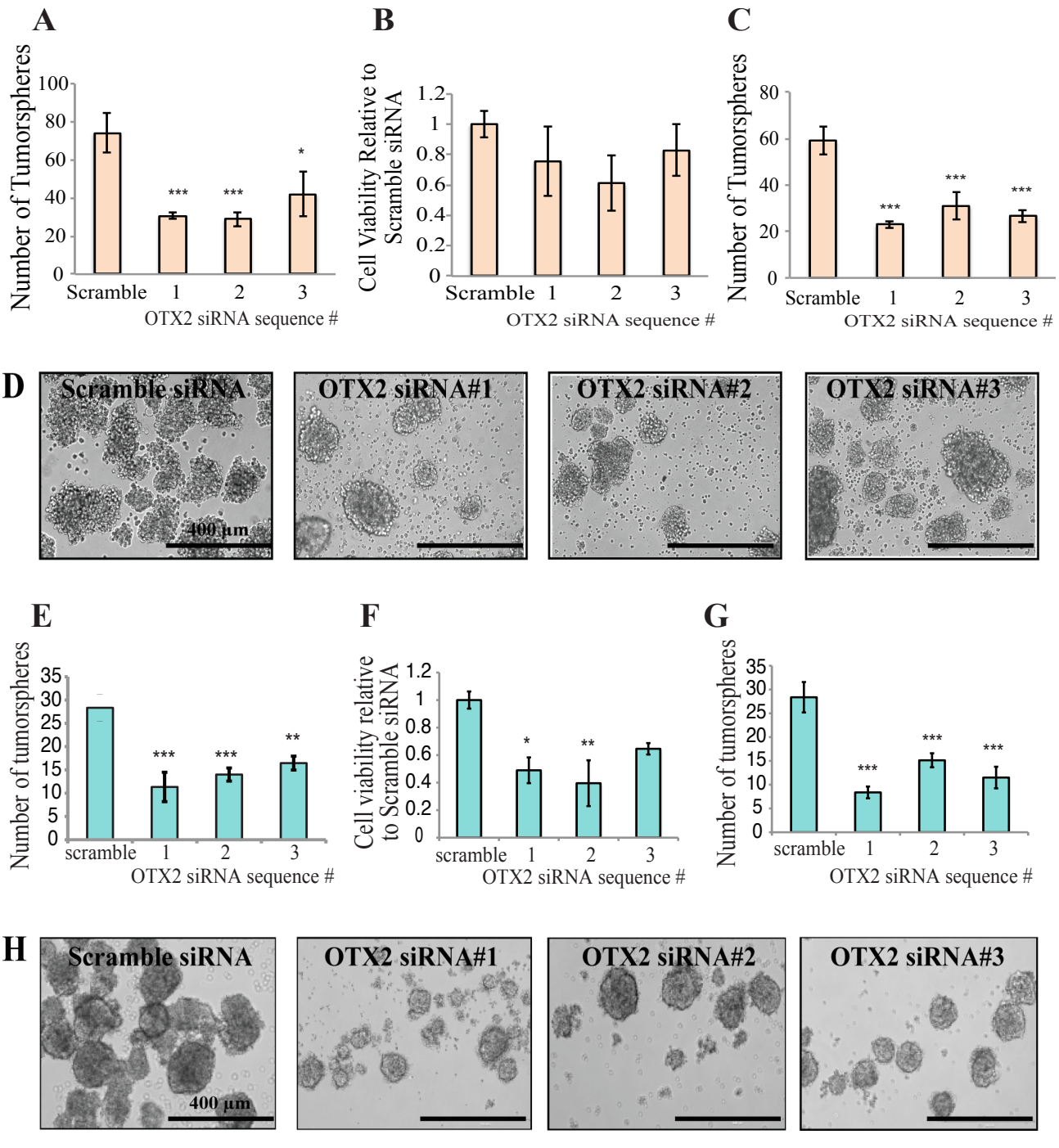


**Figure 3.2.7 Knockdown of OTX2 decreases self-renewal capacity in D425 and D341, Group 3 MB cells.** Representative images of D425 (D) and D341 (H) MB cells in sphere culture or stem cell enriched conditions following 6 days knockdown of OTX2. Scale bar: 400 µm. Tumorsphere formation and self-renewal capacity were significantly inhibited following OTX2 knockdown in D425 (A,C) and D341 cells (E,G). The cell viability was not changed in D425 cells but was significantly decreased in D341 cells. Error bars: s.e.m. $P<0.05$*, $P<0.01$**, $P<0.001$***. For all experiments, N=3 biological replicates or independent transfections and n=4 technical replicates within each biological replicate.

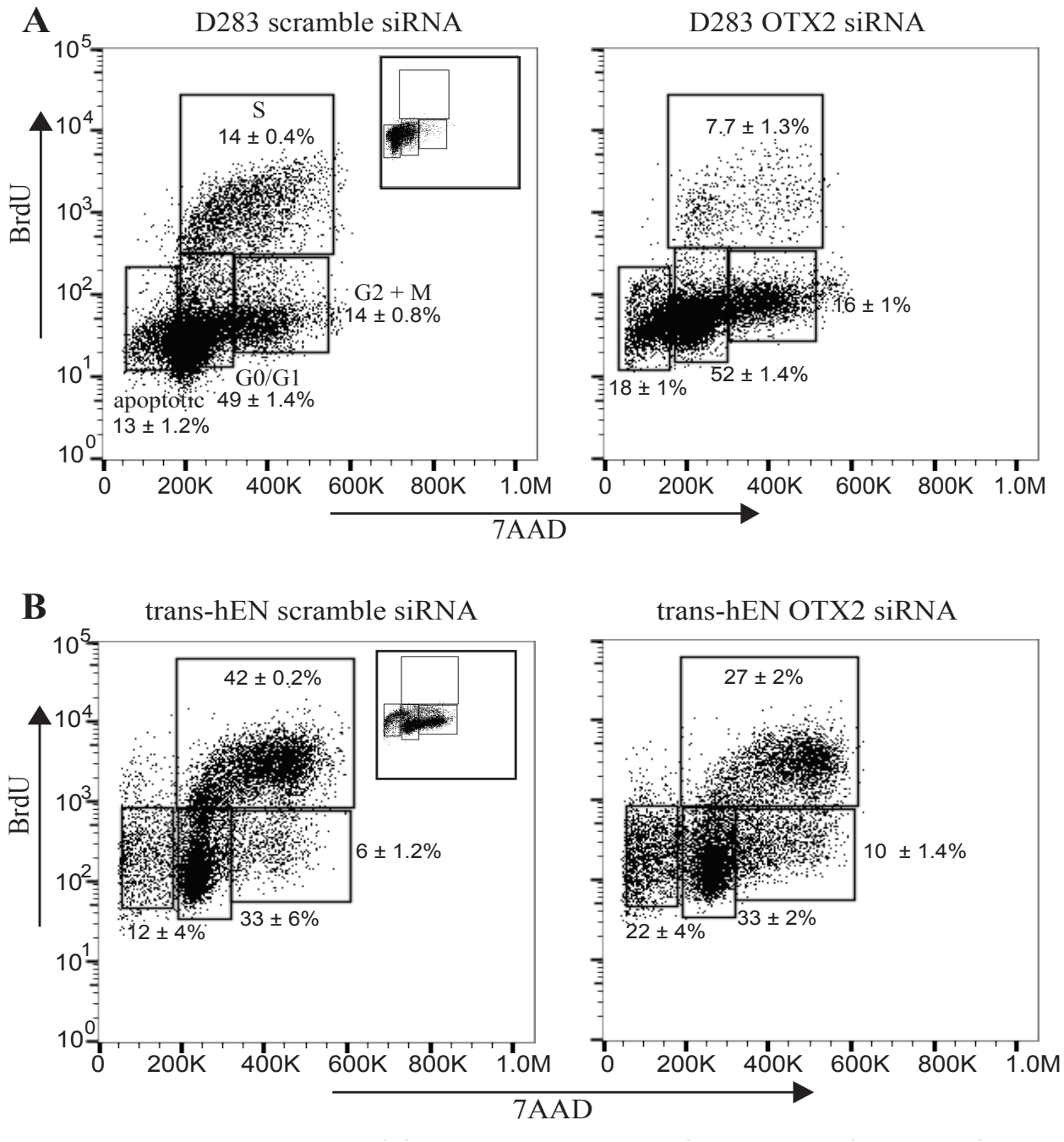


**Figure 3.2.8: Knockdown of OTX2 decreases the frequency of cells in S phase and increases the frequency of apoptotic cells.** (A) Representative dot plots of BrdU incorporation and DNA content (7AAD) in D283 tumorspheres following OTX2 knockdown. Inset: 7AAD only control. For clarity, results from the 3 siRNA sequences were pooled and presented as the mean ± s.e.m. N=2 independent biological replicates for each sequence. (B) Representative dot plots of BrdU incorporation and DNA content (7AAD) in trans-hEN neurospheres following OTX2 knockdown. Inset: 7AAD only control. For clarity, results from the 3 siRNA sequences were pooled and presented as the mean ± s.e.m. N=2 independent biological replicates for each sequence.

### 3.2.1.2 OTX2 decreases self-renewal in trans-hENs as well as Groups 3 and 4 MB cells *in vitro*.

Knockdown of OTX2 significantly impaired self-renewal capacity of D283, (Figure 3.2.6A-D), D425 (Figure 3.2.7A-D) and trans-hENs (Figure 3.2.6E-H) over subsequent passages. Knockdown of OTX2 also resulted in a decrease in cell viability; however, the results were not significant (Figure 3.2.6B, F and 3.2.7B). BrdU staining and analysis supported these findings in sphere culture and demonstrated a decrease in S phase and a concomitant increase in apoptotic cells in D283 and trans-hENs (Figure 3.2.8A-B). We also knocked down OTX2 in D341 (Group 3) MB cells that are exclusively grown in suspension culture or sphere conditions (Figure 3.2.7E-G). Similar to D283, D425 and trans-hENs, reduction of OTX2 resulted in a significant decline in self-renewal capacity (Figure 3.2.7E-G); however, for D341, Group 3 MB cell line, a significant decrease in cell viability was observed (Figure 3.2.7F).

### 3.2.1.3 OTX2 knockdown decreases *in vivo* tumor growth of trans-hENs and Group 4 MB tumorsphere cells

To examine the tumorigenic potential of trans-hENs and D283 MB cells following OTX2 knockdown *in vivo*, we stably knocked down OTX2 in trans-hENs and D283 MB cells using shRNAmir constructs. Following stable selection and validation by Western blot (Figure 3.2.9A), we confirmed the inhibitory effect of OTX2 knockdown on cumulative cell count and sphere formation seen with the shRNA sequences for both cell lines (Figure 3.2.9B-G).

Following validations *in vitro*, 5.0 X $10^5$ (trans-hEN OTX2 KD and trans-hEN scramble) and 2.5 X $10^5$ (D283 OTX2 KD and D283 scramble) cells from tumorspheres were injected into the right frontal lobe (N=5 for each condition and cell line) of NOD SCID mice and examined

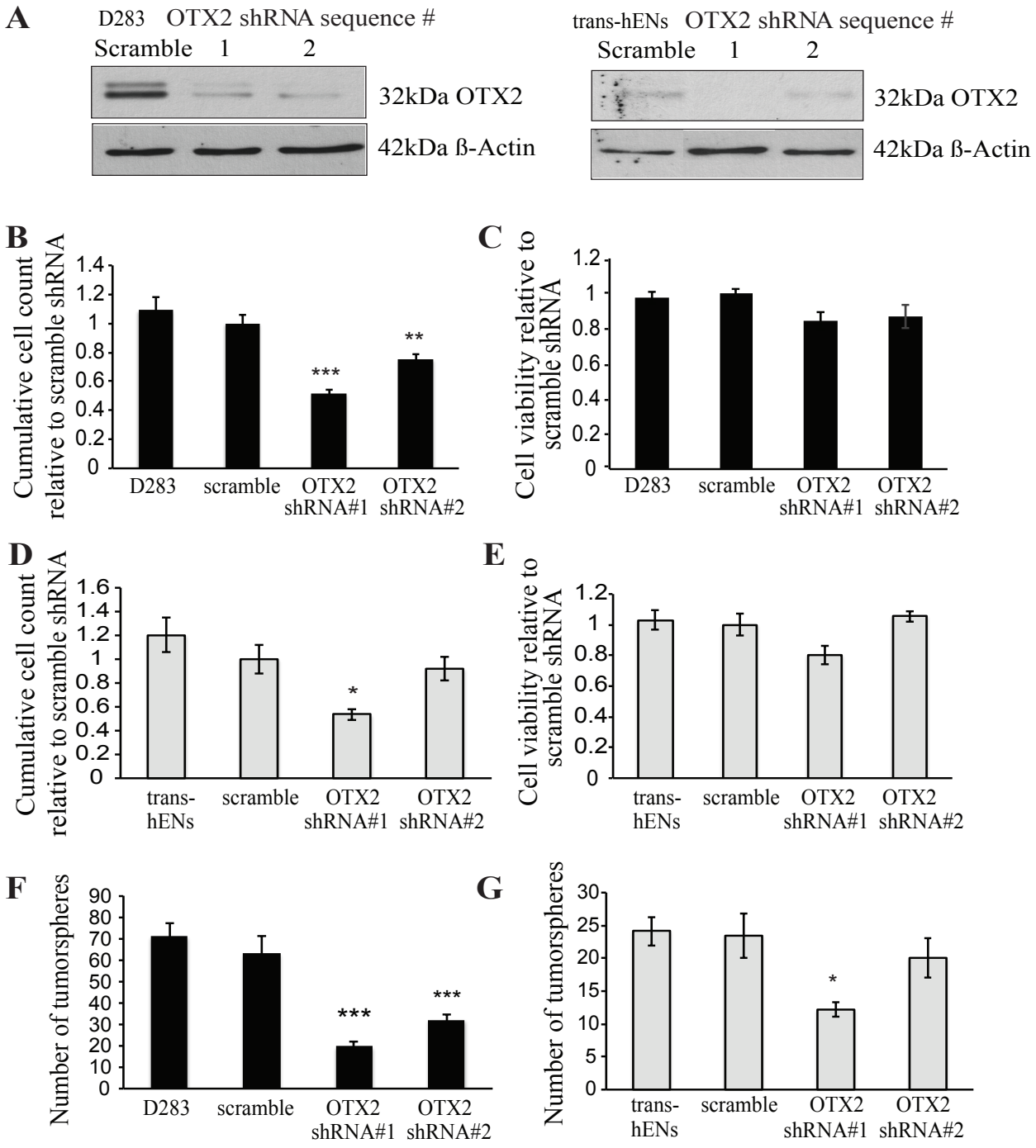


**Figure 3.2.9: Stable knockdown of OTX2 shows similar decrease in cumulative cell counts and sphere forming ability of both D283 and trans-hENs *in vitro*.** (A) Western Blot of OTX2 knockdown in 2 independent shRNA sequences relative to scramble shRNA. β-actin serves as a loading control. (B-E) Quantification of total cell number (B,D) and cell viability (C,E) in D283 (B-C) and trans-hENs (D-E) following knockdown of OTX2 over 4 days. (F-G) Sphere formation following OTX2 knockdown in D283 (F) and trans-hENs (G). Error bars: s.e.m. P<0.05*, P<0.01**, P<0.001***.

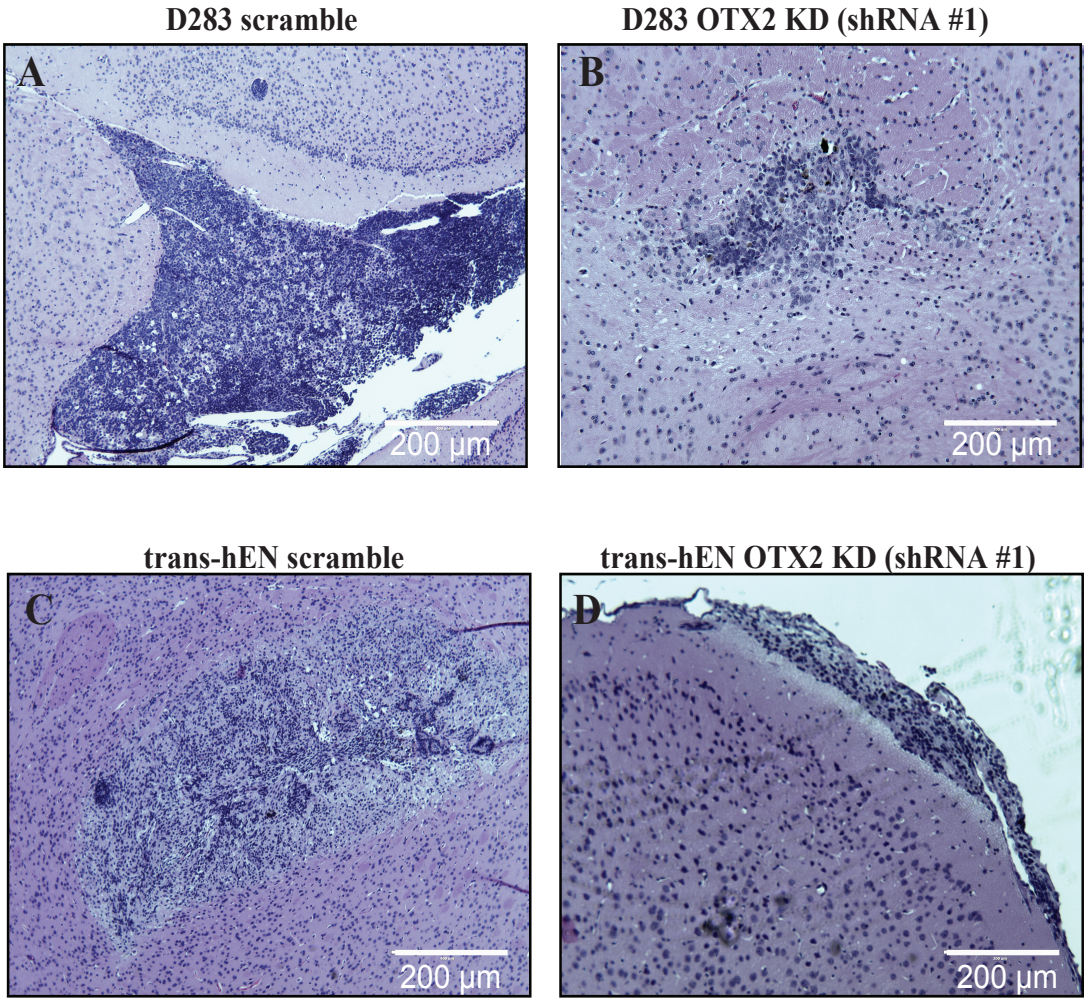


**Figure 3.2.10: Knockdown of OTX2 decreases tumor growth *in vivo*** (A-D) Tumorigenic capacity of D283 OTX2 KD (A-B) and trans-hEN OTX2 KD (C-D) relative to respective scramble control cells in NOD SCID mice. For D283 cells, tumors were densely packed, consisting of numerous mitoses in both the dorsal and ventral subarachnoid compartments. Tumors also frequently invaded the fourth ventricle (A, B). Mice injected with trans-hENs OTX2 KD and scramble cells developed densely packed neural tumors in both the striatum and thalamus. These tumors consisted of many neural rosettes with rare mitoses. N=5 mice were used for each condition and cell line. Scale bar: 200 µm.

for tumor formation after 45 days. For both cell lines, knockdown of OTX2 resulted in smaller, but histologically similar, tumors compared with respective controls (Figure 3.2.10A-D). For D283, tumors were densely packed, consisting of numerous mitoses in both the dorsal and ventral subarachnoid compartments, and this was accompanied by frequent diffuse invasion into the fourth ventricle. Similar differences in size were seen for trans-hEN cells with densely packed neural tumors evident in both the striatum and thalamus consisting of many neural rosettes and rare mitoses (Figure 3.2.10A-D). These results support our *in vitro* findings and demonstrate that OTX2 knockdown suppresses trans-hEN and D283 tumor growth *in vivo*.

While OTX2 has previously been shown to regulate cell growth *in vitro* (Di et al. 2005; Adamson et al. 2010), our results demonstrate that OTX2 is important for regulating the balance between self-renewal and differentiation of trans-hENs and aggressive Group 3 and 4 MB cells *in vitro*. We further explored the molecular mechanisms contributing to the oncogenic role of OTX2 in Group 3 and 4 MB cells.

#### 3.2.1.4 Knockdown of OTX2 increases neuronal differentiation but does not induce changes in expression of hESCs genes.

OTX2 knockdown revealed differentiated cell morphology of D283, D425 and trans-hENs in adherent cultures (Figure 3.2.3A-D, 3.2.4A-D, 3.2.5A-D). In support of these findings, immunocytochemical staining of D283 and D425 tumorspheres for the neuronal marker β-III tubulin revealed a significant increase in differentiation following OTX2 knockdown (3.2.11A-F). However, in contrast to the results obtained following OTX2 overexpression, we did not observe any consistent or significant changes in expression of human pluripotent stem cells genes such *SOX2, OCT4, LIN28A* and *NANOG*. Evaluation of hESCs genes by qPCR following

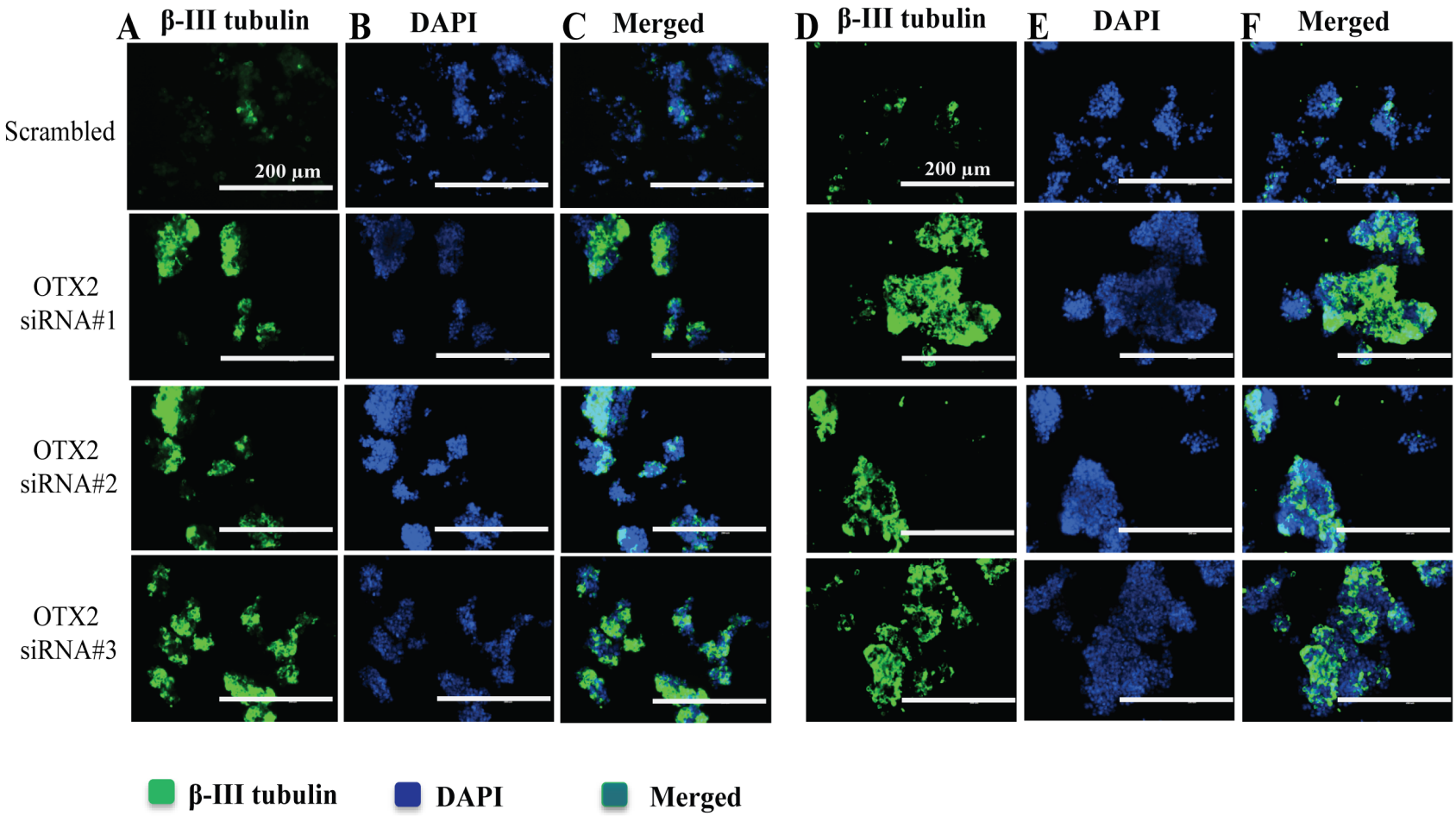


**Figure 3.2.11: Knockdown of OTX2 induced the expression of the neuronal marker β-III tubulin.** Representative images of fixed (A-C) D283 and (D-F) D425 MB tumorspheres following 4 days knockdown of OTX2. Scale bar: 200 µm. Fixed tumorspheres were stained for β-III tubulin (A, D) and nuclear stain DAPI (B, E). An increase in β-III tubulin staining was observed following OTX2 knockdown in both D283 (C) and D425 cells (F).

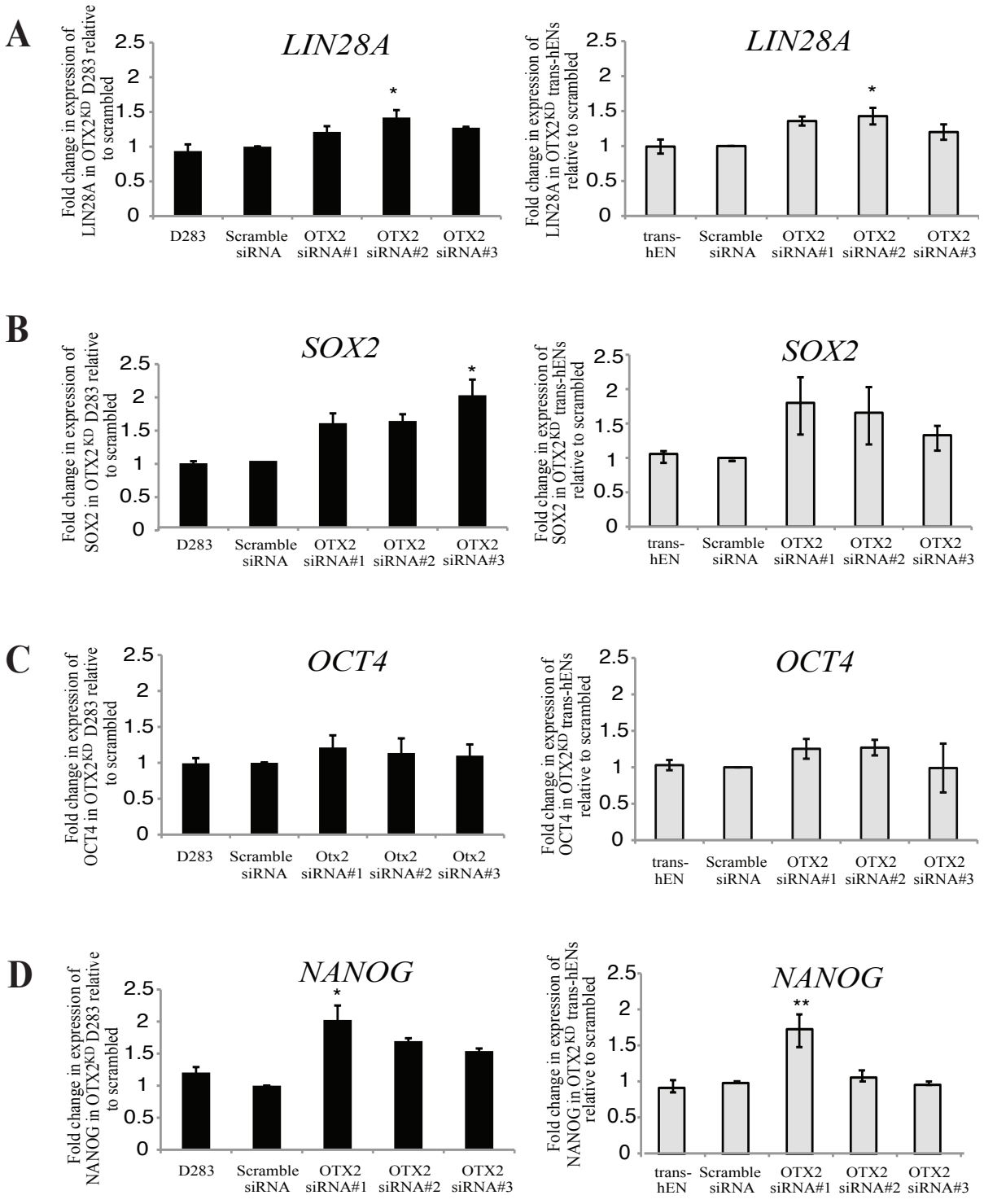


**FIGURE 3.2.12: OTX2 knockdown results in only modest changes in hESC gene expression levels in D283 and trans-hENs.** (A-D) hESC pluripotency factor transcript levels in D283 (black bars) and trans- hEN (grey bars) following OTX2 knockdown by qPCR. Error Bars: s.e.m. $P<0.05$*. N=3 biological replicates for each cell line and n=3 technical replicates within each biological replicate.

OTX2 knockdown revealed significant upregulation of *LIN28A* and *NANOG* only for one siRNA sequence in D283 and trans-hENs (Figure 3.2.12A-D).

### 3.2.2 Global gene expression analysis of stem cell enriched D283 OTX2$^{KD}$ tumorspheres relative to control D283 tumorspheres.

#### 3.2.2.1 Global gene expression analysis revealed novel associations between OTX2 and axon guidance genes.

In our OTX2 overexpression studies, we identified a novel link between OTX2 and stem cell genes. This relationship plays an important role in regulating cellular properties, especially self-renewal and migration, in both normal hENs and Daoy MB cells. However, the oncogenic role of OTX2 in Group 3 and 4 MB cells is independent of hESC genes. As OTX2 knockdown abolished the self-renewal capacity of trans-hENs and the D283, D425 and D341 MB cell lines, we wanted to investigate the downstream signaling pathways associated with the oncogenic role of OTX2 in stem cell enriched conditions. We performed global gene expression analysis comparing the molecular profiles of OTX2$^{KD}$ D283 and control D283 tumorspheres or stem cell enriched populations (N=3 biological samples). Comparative global gene expression analysis of OTX2$^{KD}$ D283 relative to control D283 tumorspheres revealed significant and differential expression ($P<0.05$ and ±2 fold) of 3614 genes. Transcripts associated with nervous system development and function represented the top dysregulated network in OTX2$^{KD}$ D283 relative to D283 control tumorspheres. Among this list of neurodevelopmental genes, transcripts related to axon guidance pathways including Eph receptors and ephrin ligands (eph/ephrins), semaphorin, slit, and netrin were the most differentially expressed following OTX2 knockdown (Table 3.2.1). These axon guidance gene families have been found to play prominent role in tumor cell

**Table 3.2.1: List of differentially expressed axon guidance genes in $OTX2^{KD}$ D283 cells relative to control D283 cells.**

| Symbol | Entrez Gene Name | Fold change | Type(s) | Entrez Gene ID for Human |
|---|---|---|---|---|
| ABLIM3 | actin binding LIM protein family, member 3 | 0.358488812 | Other | 22885 |
| ADAM11 | ADAM metallopeptidase domain 11 | 4.629960868 | Peptidase | 4185 |
| ADAM23 | ADAM metallopeptidase domain 23 | 2.298989696 | Peptidase | 8745 |
| ADAMTS7 | ADAM metallopeptidase with thrombospondin type 1 motif, 7 | 2.484576564 | Peptidase | 11173 |
| ARPC1B | actin related protein 2/3 complex, subunit 1B, 41kDa | 0.467163673 | Other | 10095 |
| BMP1 | bone morphogenetic protein 1 | 2.38998241 | Peptidase | 649 |
| BMP2 | bone morphogenetic protein 2 | 0.166200889 | growth factor | 650 |
| BMP7 | bone morphogenetic protein 7 | 0.414659773 | growth factor | 655 |
| C9orf3 | chromosome 9 open reading frame 3 | 0.428390977 | Peptidase | 84909 |
| CXCR4 | chemokine (C-X-C motif) receptor 4 | 0.35013908 | G-protein coupled receptor | 7852 |
| DCC | DCC netrin 1 receptor | 19.91798777 | transmembrane receptor | 1630 |
| DOCK1 | dedicator of cytokinesis 1 | 0.464902471 | Other | 1793 |
| DPYSL2 | dihydropyrimidinase-like 2 | 2.284692494 | Enzyme | 1808 |
| DPYSL5 | dihydropyrimidinase-like 5 | 2.223758315 | Enzyme | 56896 |
| EFNA3 | ephrin-A3 | 3.294364069 | Kinase | 1944 |
| EFNA4 | ephrin-A4 | 0.178624267 | Kinase | 1945 |
| EFNB2 | ephrin-B2 | 8.456144324 | Other | 1948 |
| EPHA2 | EPH receptor A2 | 0.18595172 | Kinase | 1969 |
| EPHA3 | EPH receptor A3 | 35.97692556 | Kinase | 2042 |
| EPHA4 | EPH receptor A4 | 2.713208655 | Kinase | 2043 |
| EPHA5 | EPH receptor A5 | 29.79503423 | Kinase | 2044 |
| EPHB2 | EPH receptor B2 | 2.72829567 | Kinase | 2048 |
| EPHB4 | EPH receptor B4 | 0.273763118 | Kinase | 2050 |
| ERBB2 | erb-b2 receptor tyrosine kinase 2 | 0.438910899 | Kinase | 2064 |
| FYN | FYN proto-oncogene, Src family tyrosine kinase | 3.280691645 | Kinase | 2534 |

| | | | | |
|---|---|---|---|---|
| FZD1 | frizzled class receptor 1 | 0.411510173 | G-protein coupled receptor | 8321 |
| FZD5 | frizzled class receptor 5 | 0.456599125 | G-protein coupled receptor | 7855 |
| FZD7 | frizzled class receptor 7 | 0.08207007 | G-protein coupled receptor | 8324 |
| GLI3 | GLI family zinc finger 3 | 0.243163737 | transcription regulator | 2737 |
| GNAO1 | guanine nucleotide binding protein (G protein), alpha activating activity polypeptide O | 5.747760706 | Enzyme | 2775 |
| GNB3 | guanine nucleotide binding protein (G protein), beta polypeptide 3 | 0.257206677 | Enzyme | 2784 |
| GNB4 | guanine nucleotide binding protein (G protein), beta polypeptide 4 | 0.294226684 | Enzyme | 59345 |
| GNB5 | guanine nucleotide binding protein (G protein), beta 5 | 2.131693472 | Enzyme | 10681 |
| GNG2 | guanine nucleotide binding protein (G protein), gamma 2 | 3.020945171 | Enzyme | 54331 |
| GNG3 | guanine nucleotide binding protein (G protein), gamma 3 | 6.143241079 | Enzyme | 2785 |
| GNG5 | guanine nucleotide binding protein (G protein), gamma 5 | 0.40584479 | Other | 2787 |
| GNG11 | guanine nucleotide binding protein (G protein), gamma 11 | 0.367801686 | Enzyme | 2791 |
| GNG12 | guanine nucleotide binding protein (G protein), gamma 12 | 0.300200857 | Enzyme | 55970 |
| IGF1 | insulin-like growth factor 1 (somatomedin C) | 0.467163673 | growth factor | 3479 |
| ITGA4 | integrin, alpha 4 (antigen CD49D, alpha 4 subunit of VLA-4 receptor) | 2.25792881 | transmembrane receptor | 3676 |
| KALRN | kalirin, RhoGEF kinase | 4.806544198 | Kinase | 8997 |
| KLC1 | kinesin light chain 1 | 2.164449289 | Other | 3831 |
| L1CAM | L1 cell adhesion molecule | 5.105315075 | Other | 3897 |
| LINGO1 | leucine rich repeat and Ig domain containing 1 | 2.153972752 | Other | 84894 |
| LRRC4C | leucine rich repeat containing 4C | 3.69609029 | Other | 57689 |
| MICAL1 | microtubule associated monooxygenase, calponin and LIM domain containing 1 | 2.425025638 | Enzyme | 64780 |
| MYL4 | myosin, light chain 4, alkali; atrial, embryonic | 0.357000995 | Other | 4635 |

| | | | | |
|---|---|---|---|---|
| NGF | nerve growth factor (beta polypeptide) | 0.220064753 | growth factor | 4803 |
| NRP1 | neuropilin 1 | 4.525257851 | transmembrane receptor | 8829 |
| NRP2 | neuropilin 2 | 5.392670927 | Kinase | 8828 |
| NTF3 | neurotrophin 3 | 0.321078952 | growth factor | 4908 |
| NTRK3 | neurotrophic tyrosine kinase, receptor, type 3 | 3.721798631 | Kinase | 4916 |
| PAK3 | p21 protein (Cdc42/Rac)-activated kinase 3 | 5.540437872 | Kinase | 5063 |
| PAK7 | p21 protein (Cdc42/Rac)-activated kinase 7 | 4.688089135 | Kinase | 57144 |
| PAPPA2 | pappalysin 2 | 0.147624083 | Peptidase | 60676 |
| PLCB4 | phospholipase C, beta 4 | 9.428315262 | Enzyme | 5332 |
| PLCD3 | phospholipase C, delta 3 | 0.392292049 | Enzyme | 113026 |
| PLCD4 | phospholipase C, delta 4 | 3.267075964 | Enzyme | 84812 |
| PLCE1 | phospholipase C, epsilon 1 | 0.341036959 | Enzyme | 51196 |
| PLCG1 | phospholipase C, gamma 1 | 2.403272099 | Enzyme | 5335 |
| PLCL1 | phospholipase C-like 1 | 4.500233939 | Enzyme | 5334 |
| PLXNA2 | plexin A2 | 3.43664302 | transmembrane receptor | 5362 |
| PLXNA3 | plexin A3 | 3.431882122 | transmembrane receptor | 55558 |
| PLXND1 | plexin D1 | 2.284692494 | transmembrane receptor | 23129 |
| PPP3CA | protein phosphatase 3, catalytic subunit, alpha isozyme | 2.488023307 | Phosphatase | 5530 |
| PRKAR2B | protein kinase, cAMP-dependent, regulatory, type II, beta | 2.486299338 | Kinase | 5577 |
| PRKCE | protein kinase C, epsilon | 3.396384986 | Kinase | 5581 |
| PRKD3 | protein kinase D3 | 0.459456442 | Kinase | 23683 |
| PTCH2 | patched 2 | 3.164549205 | transmembrane receptor | 8643 |
| ROBO2 | roundabout guidance receptor 2 | 2.406606052 | transmembrane receptor | 6092 |
| RRAS | related RAS viral (r-ras) oncogene homolog | 0.323985241 | Enzyme | 6237 |
| RTN4 | reticulon 4 | 2.057653416 | Other | 57142 |
| SDC2 | syndecan 2 | 0.492433221 | Other | 6383 |
| SEMA4D | sema domain, immunoglobulin domain (Ig), transmembrane domain (TM) and short cytoplasmic domain, (semaphorin) 4D | 3.45575275 | transmembrane receptor | 10507 |

| | | | | |
|---|---|---|---|---|
| SEMA6A | sema domain, transmembrane domain (TM), and cytoplasmic domain, (semaphorin) 6A | 5.544279543 | transmembrane receptor | 57556 |
| SEMA6C | sema domain, transmembrane domain (TM), and cytoplasmic domain, (semaphorin) 6C | 2.8108374 | Other | 10500 |
| SHC1 | SHC (Src homology 2 domain containing) transforming protein 1 | 0.486327474 | Kinase | 6464 |
| SLIT1 | slit guidance ligand 1 | 13.04115732 | Other | 6585 |
| SLIT2 | slit guidance ligand 2 | 3.365917929 | Other | 9353 |
| SMO | smoothened, frizzled class receptor | 0.422786144 | G-protein coupled receptor | 6608 |
| SOS2 | son of sevenless homolog 2 (Drosophila) | 2.033549347 | Other | 6655 |
| SRGAP2 | SLIT-ROBO Rho GTPase activating protein 2 | 2.106722072 | Other | 23380 |
| TUBB6 | tubulin, beta 6 class V | 0.284204243 | Other | 84617 |
| TUBB2A | tubulin, beta 2A class IIa | 2.358713185 | Other | 7280 |
| TUBB2B | tubulin, beta 2B class IIb | 2.00416321 | Other | 347733 |
| TUBB4A | tubulin, beta 4A class Iva | 2.124318373 | Other | 10382 |
| UNC5A | unc-5 netrin receptor A | 3.647732662 | transmembrane receptor | 90249 |
| UNC5B | unc-5 netrin receptor B | 2.599078125 | transmembrane receptor | 219699 |
| UNC5D | unc-5 netrin receptor D | 8.094825608 | Other | 137970 |
| WNT7B | wingless-type MMTV integration site family, member 7B | 3.035638506 | Other | 7477 |

*** A total of 236 genes were differentially expressed in D283 OTX2$^{KD}$ relative to control D283 cells and among them 78 genes were upregulated.**

proliferation, survival, anchorage dependence, angiogenesis and migration (Kerjan et al. 2005; Sikkema et al. 2012). For the first time, we have identified an association between OTX2 and axon guidance genes in MB stem cell populations.

Eph/ephrin signaling plays important roles in developmental processes such as neural development, axon guidance, cell proliferation and angiogenesis (Sikkema et al. 2012). eph/ephrin signaling can be bidirectional depending on receptor-ligand or receptor-receptor clustering in a particular cellular context (Lisabeth, Falivelli, and Pasquale 2013). Members of the eph receptor family including EphA2, EphB2 and EphB4, have been found to be upregulated in MB cells and contribute to tumor cell invasion (Sikkema et al. 2012; Bhatia et al. 2015). We have shown that downregulation of OTX2 in D283 stem cell populations significantly affected expression of several members of the eph/ephrin pathway. Among the EPH receptors, *EPHA3* (+35.98 fold) *EPHA5* (+29.80 fold) and *EPHB2* (+2.73 fold) are the most upregulated, however; *EPHA2* (-0.19 fold) is downregulated. The upregulation of EPH receptors such as *EPHA3, EPHA5* and *EPHB2* was validated by qPCR (Figure 3.2.13-3.2.15B-D). However, *EPHA2* showed the opposite trend by qPCR (Figure 3.2.13-3.3.15A). The cognate ligands of ephrin signaling such as *EFNA3* (+3.29) and *EFNB2* (+8.46 fold) were also differentially expressed in OTX2 knockdown D283 cells relative to controls and were validated by qPCR (Figure 3.2.13-3.2.15E-F).

Following OTX2 knockdown in D283 cells, we also observed differential expression of genes associated with other axon guidance pathways such as Semaphorin signaling i.e. Sema 6A (+5.54 fold), Sema 4D (+3.46) and *L1CAM* (+5.11 fold), Slit signaling (*SLIT1* (+13.04 fold) and *SLIT2* (+3.37 fold) and *ROBO2* (+2.40)) and netrin signaling (deleted in colorectal cancer (*DCC*) (+19.92 fold) and *UNC5D* (+8.10 fold)). Sema6A is involved in controlling the tangential

migration of postmitotic CGNPs in the deep EGL (Kerjan et al. 2005). The secreted proteins, Slit1 and Slit2, act as repulsive cues for regulating the guidance of axon projections, cell proliferation and dendritic patterning (Brose et al. 1999; Borrell et al. 2012; Gibson et al. 2014). Both Semaphorin and Slit molecules as well as their cognate receptors are dysregulated in MB cells and are linked to more invasive phenotypes (Werbowetski-Ogilvie et al. 2006; Northcott et al. 2011). Introduction of recombinant Slit2 protein can reduce MB tumor cell invasion (Werbowetski-Ogilvie et al. 2006). Similarly, molecules associated with netrin signaling such as netrin-1 are linked to more invasive MB phenotypes (Akino et al. 2014). However, the molecular interaction between OTX2 and these cell motility genes needs to be elucidated in detail.

In addition to genes associated with axon guidance pathways, we also observed differential expression of additional neuronal differentiation genes (63 out of 236) including microtubule-associated proteins, *JAKMIP2* (+29.18 fold), *MAP2* (+17.27 fold), *MAP6* (+12.91 fold), *CNTN*3 (+7.95 fold), *CNTN4* (+5.17 fold), neural cell adhesion molecule (*NCAM*)2 (+13.83 fold) and neuronal differentiation (*NEUROD*)4 (+4.41 fold), which were all upregulated following OTX2 knockdown (Table 3.2.2). We validated the expression levels of β-III tubulin or *TUJ1*, *MAP2, MAP6, L1CAM, GAP43* and *JAKMIP2* in D283, D425 and D341 cells by qPCR (Figure 3.2.16-3.2.18A-F). We have also shown an increase in protein levels of β-III tubulin and L1CAM in D283 and D425 cells following OTX2 knockdown (Figure 3.2.19). These findings demonstrate that OTX2 knockdown might be promoting neuronal differentiation of MB stem/progenitor cell populations.

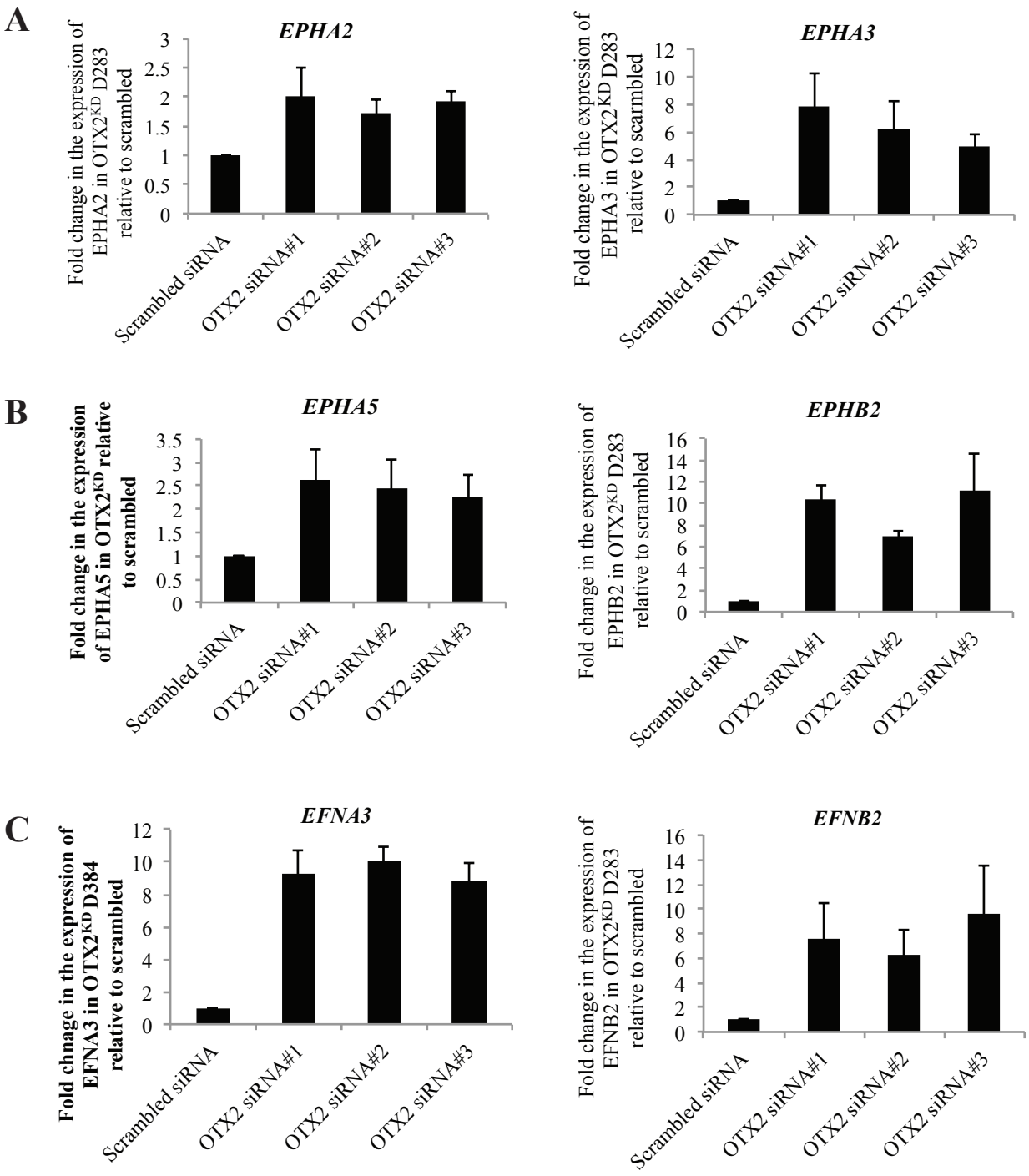


**Figure 3.2.13: OTX2 knockdown results in an increase in the expression of genes related to eph/ephrin signaling in D283 cells.** (A-C) The genes related to eph/ephrin signaling were differentially expressed following OTX2 knockdown in D283 cells. Differential expression was validated by qPCR. N=3 biological replicates and n=3 technical replicates within each biological replicate.

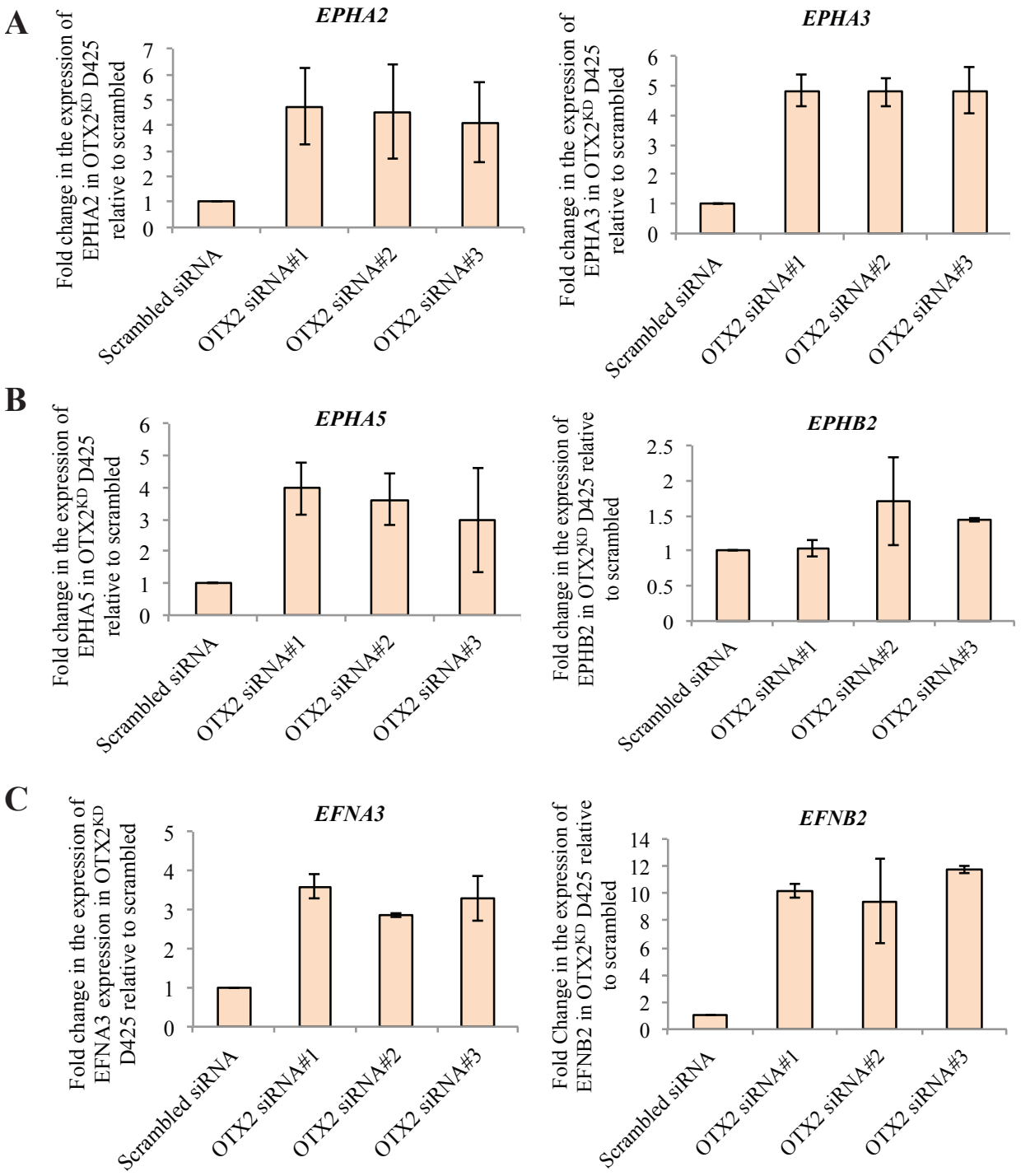


**Figure 3.2.14: OTX2 knockdown results in an increase in the expression of genes related to eph/ephrin signaling in D425 cells.** (A-C) The genes related to eph/ephrin signaling were differentially expressed following OTX2 knockdown in D425 cells. Differential expression was validated by qPCR. N=2 biological replicates and n=3 technical replicates within each biological replicate.

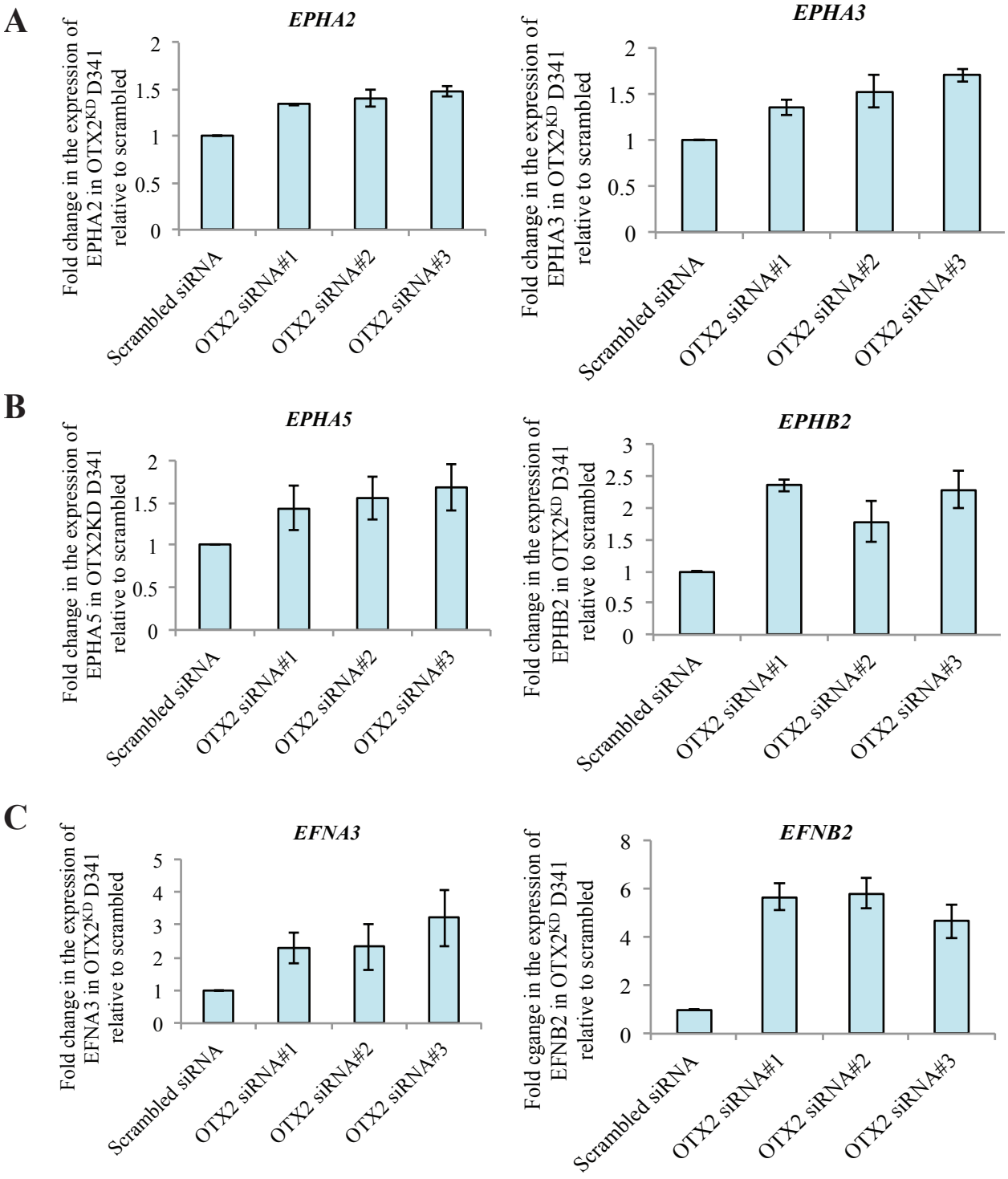


**Figure 3.2.15: OTX2 knockdown results in an increase in the expression of genes related to eph/ephrin signaling in D341 cells.** (A-C) The genes related to eph/ephrin signaling were differentially expressed following OTX2 knockdown in D341 cells. Differential expression was validated by qPCR. N=2 biological replicates and n=3 technical replicates within each biological replicate.

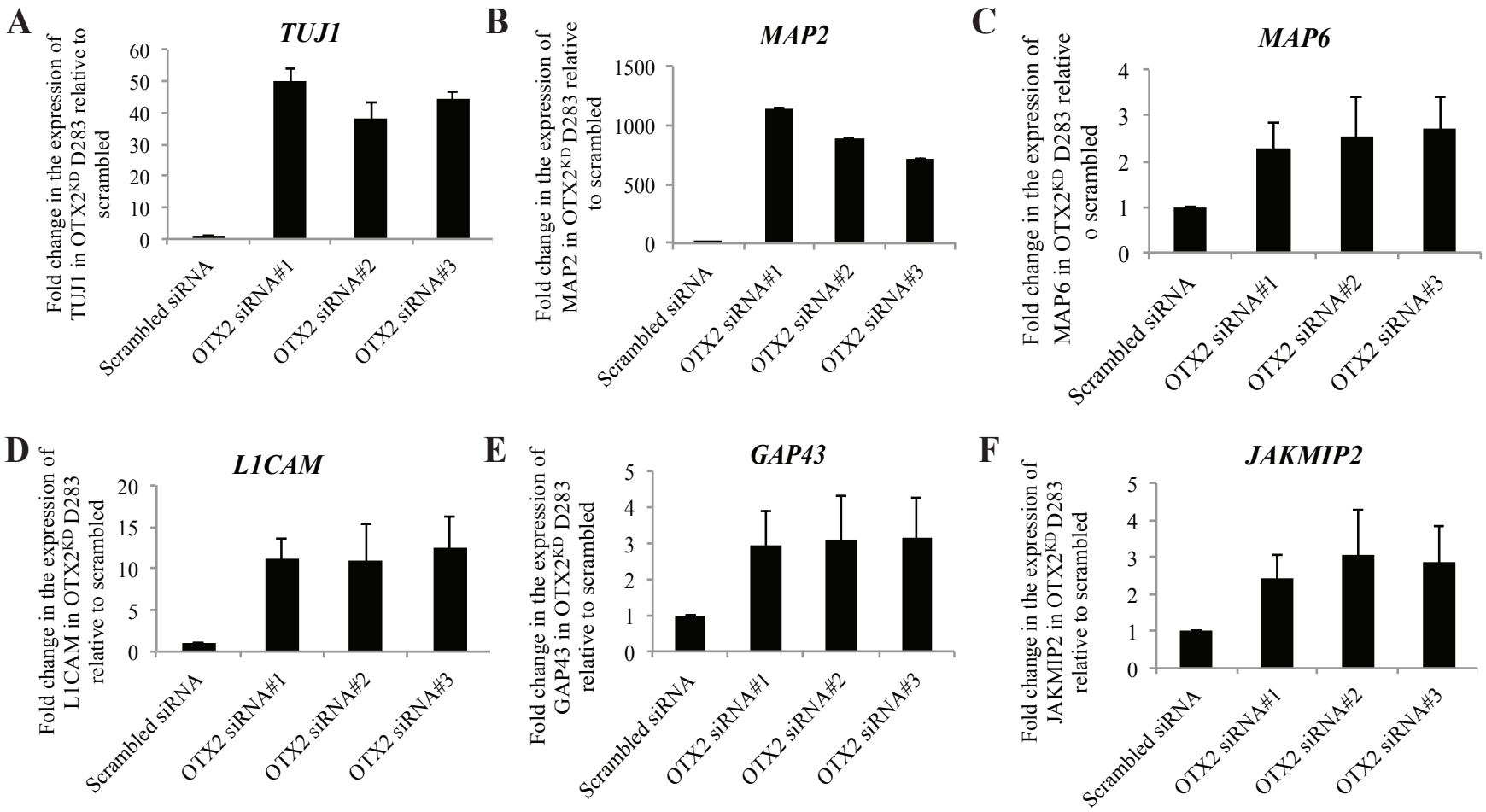


**Figure 3.2.16: OTX2 knockdown results in differential expression of genes related to neuronal differentiation in D283 cells.** (A-F). OTX2 knockdown in D283 cells induced neuronal differentiation and increased the expression of neuronal transcripts such as *TUJ1, MAP2, MAP6, L1CAM, GAP43* and *JAKMIP2*. N=3 biological replicates and n=3 technical replicates within each biological replicate.

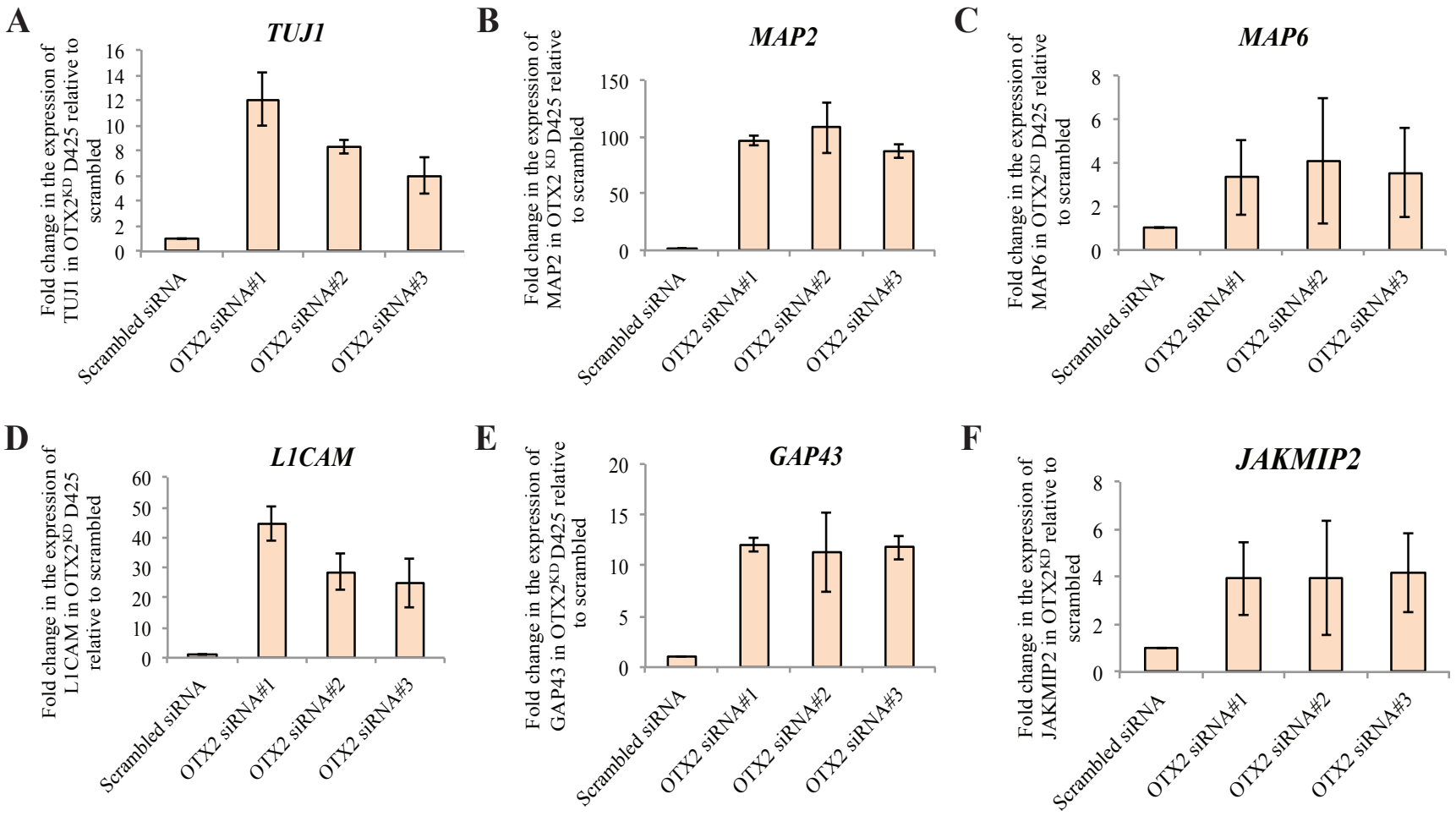


**Figure 3.2.17: OTX2 knockdown results in differential expression of genes related to neuronal differentiation in D425 cells.** (A-F). OTX2 knockdown in D425 cells induced neuronal differentiation and increased the expression of neuronal transcripts such as *TUJ1, MAP2, MAP6, L1CAM, GAP43* and *JAKMIP2*. N=2 biological replicates and n=3 technical replicates within each biological replicate.

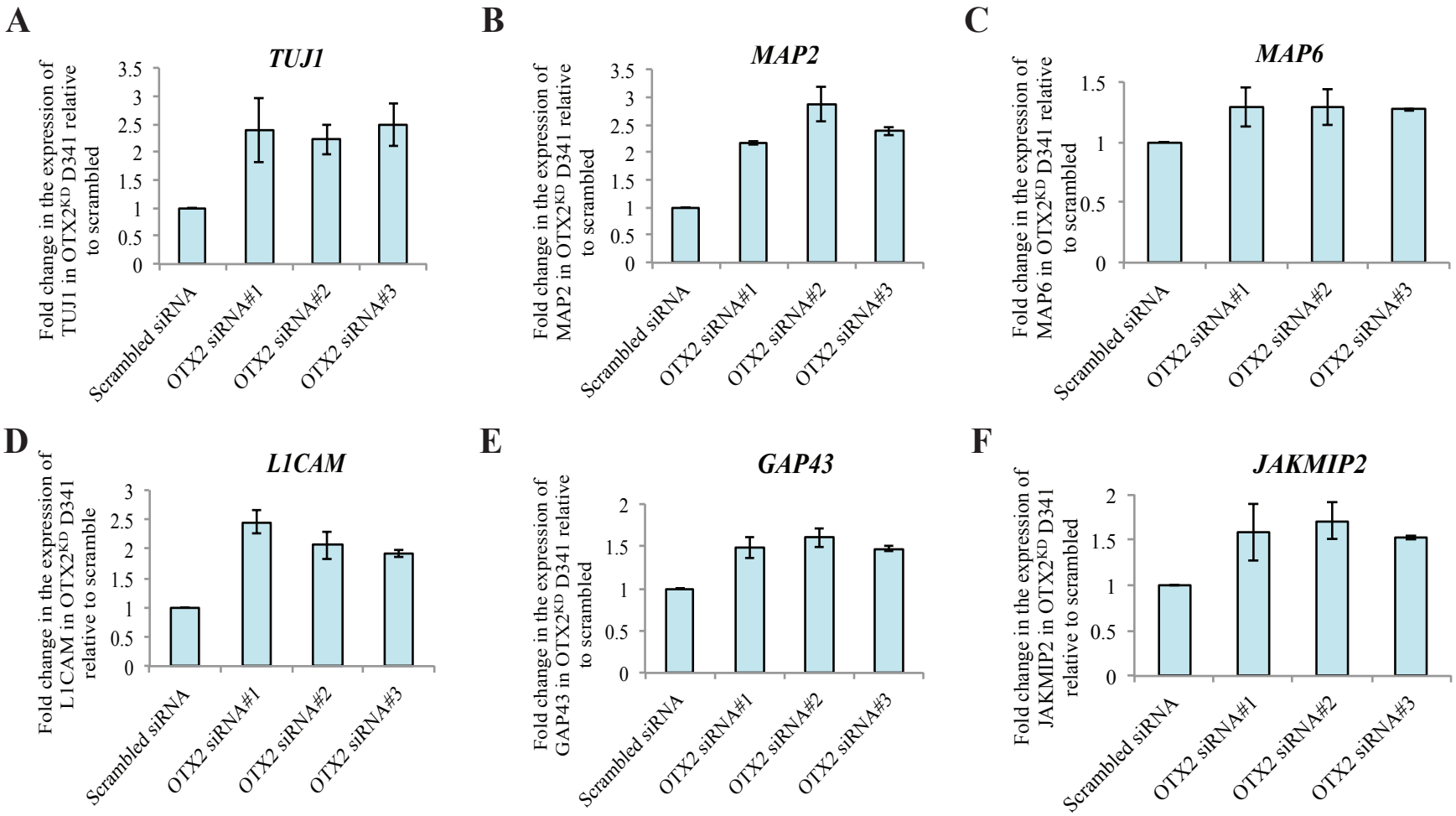


**Figure 3.2.18: OTX2 knockdown results in differential expression of genes related to neuronal differentiation in D341 cells.** (A-F). OTX2 knockdown in D341 cells induced neuronal differentiation and increased the expression of neuronal transcripts such as *TUJ1, MAP2, MAP6, L1CAM, GAP43* and *JAKMIP2*. N=2 biological replicates and n=3 technical replicates within each biological replicate.

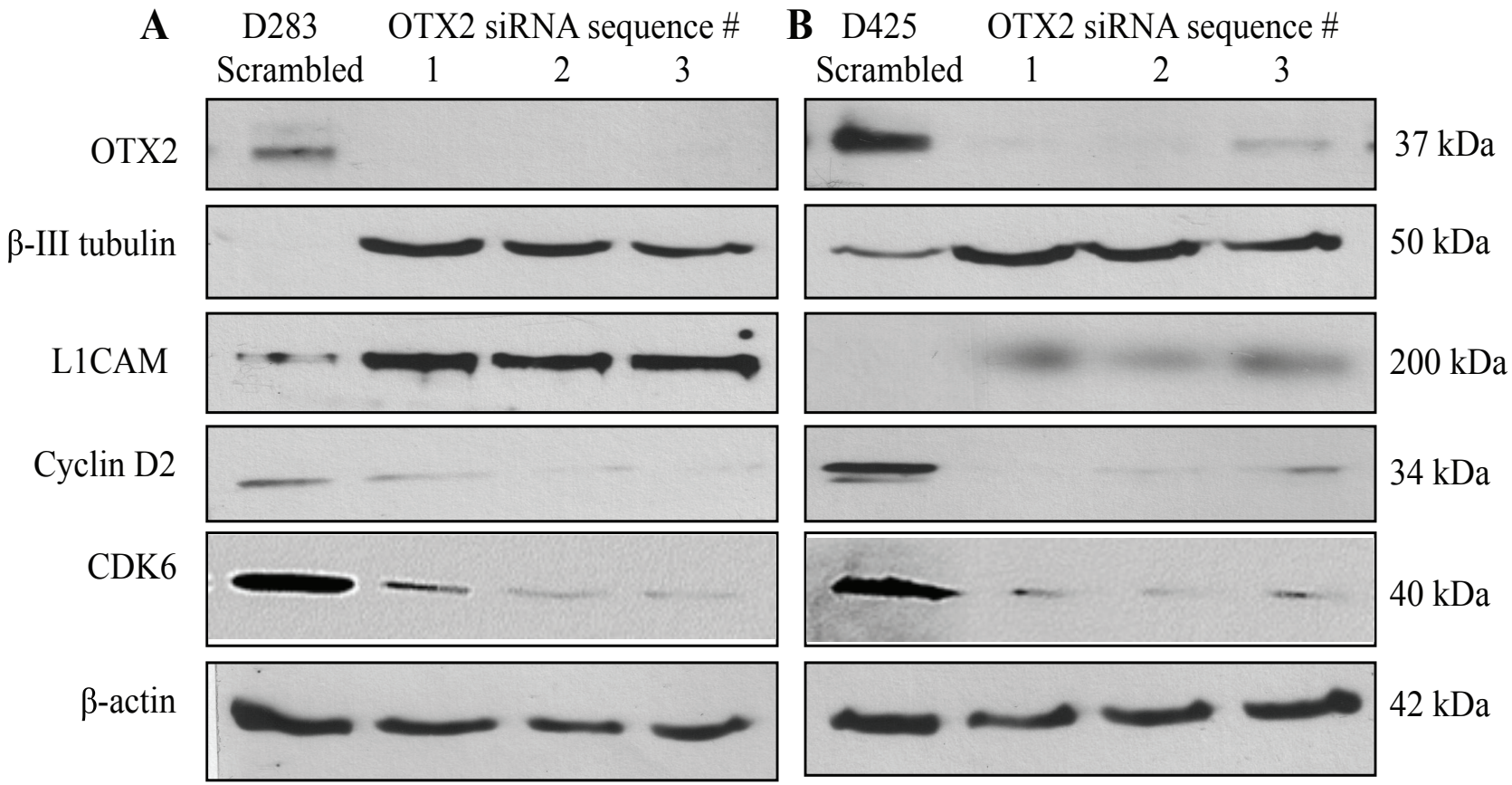


**Figure 3.2.19: OTX2 knockdown results in an increase in protein levels of genes related to neuronal differentiation and a decrease in protein levels of cell cycle genes in D283 and D425 cells.** OTX2 knockdown increased the protein levels of β-III tubulin and L1CAM but decreased the level of cell cycle genes, cyclin D2 and CDK6 in both D283 (A) and D425 (B) cells as determined by Western Blot. β-actin was used as loading control.

**Table 3.2.2: Differential expression of cell cycle genes in $OTX2^{KD}$ D283 cells relative to control D283 cells.**

| ID | Genes in dataset | Prediction (based on expression direction) | Fold change | Findings |
|---|---|---|---|---|
| 17045198 | ANLN | Affected | 0.230206424 | Affects (1) |
| 16762573 | ASUN | Affected | 0.440740079 | Affects (1) |
| 16791909 | BAZ1A | Affected | 0.349654021 | Affects (1) |
| 16710436 | BCCIP | Affected | 0.499307333 | Affects (1) |
| 16775324 | BORA | Affected | 0.308640652 | Affects (1) |
| 16840284 | C1QBP | Affected | 0.37035995 | Affects (1) |
| 16799598 | CASC5 | Affected | 0.184028358 | Affects (1) |
| 16737200 | CD59 | Affected | 2.211461307 | Affects (1) |
| 16833159 | CDK5R1 | Affected | 2.756810306 | Affects (1) |
| 16877956 | CENPA | Affected | 0.26425451 | Affects (1) |
| 16985614 | CENPH | Affected | 0.232290169 | Affects (1) |
| 17105401 | CENPI | Affected | 0.301243079 | Affects (1) |
| 16671503 | CKS1B | Affected | 0.311218559 | Affects (1) |
| 17086634 | CKS2 | Affected | 0.314907495 | Affects (1) |
| 16779546 | DIAPH3 | Affected | 0.136786713 | Affects (1) |
| 16793225 | DLGAP5 | Affected | 0.113833729 | Affects (1) |
| 16714998 | DNA2 | Affected | 0.356012549 | Affects (1) |
| 16677201 | DTL | Affected | 0.150204506 | Affects (1) |
| 16910501 | DTYMK | Affected | 0.416965522 | Affects (1) |
| 16847771 | ERN1 | Affected | 0.468460723 | Affects (1) |
| 17067332 | ESCO2 | Affected | 0.158439065 | Affects (1) |
| 17093595 | FANCG | Affected | 0.371645746 | Affects (1) |
| 16841137 | GAS7 | Affected | 0.185436867 | Affects (1) |
| 17079210 | GEM | Affected | 0.268501118 | Affects (1) |
| 16701748 | GTPBP4 | Affected | 0.489370825 | Affects (1) |
| 16931384 | GTSE1 | Affected | 0.225000482 | Affects (1) |
| 16887635 | HAT1 | Affected | 0.426022048 | Affects (1) |
| 16968765 | HERC5 | Affected | 0.167589074 | Affects (1) |
| 17047504 | HSPB1 | Affected | 0.407253782 | Affects (1) |
| 16817254 | IL4R | Affected | 0.471719125 | Affects (1) |
| 16938271 | KAT2B | Affected | 0.379981214 | Affects (1) |
| 16810543 | KIAA0101 | Affected | 0.299369676 | Affects (1) |
| 16939960 | KIF15 | Affected | 0.1986086 | Affects (1) |
| 16736891 | KIF18A | Affected | 0.222673225 | Affects (1) |
| 16845794 | KIF18B | Affected | 0.221288441 | Affects (1) |
| 16991460 | KIF4B | Affected | 0.424253951 | Affects (1) |
| 16758336 | KNTC1 | Affected | 0.283220971 | Affects (1) |
| 17075221 | LZTS1 | Affected | 2.350552657 | Affects (1) |
| 16765325 | MAP3K12 | Affected | 4.115306832 | Affects (1) |

| | | | | |
|---|---|---|---|---|
| 16945101 | MCM2 | Affected | 0.230685623 | Affects (1) |
| 17114334 | mir-503 | Affected | 0.362738052 | Affects (1) |
| 16924966 | MIS18A | Affected | 0.471719125 | Affects (1) |
| 17092767 | MLLT3 | Affected | 2.029325093 | Affects (1) |
| 17021845 | MMS22L | Affected | 0.296478625 | Affects (1) |
| 16685769 | MYCL | Affected | 0.430474594 | Affects (1) |
| 16664118 | NASP | Affected | 0.482299092 | Affects (1) |
| 16691668 | NOTCH2 | Affected | 0.273383864 | Affects (1) |
| 16869769 | NOTCH3 | Affected | 0.301870148 | Affects (1) |
| 17001256 | PPP2R2B | Affected | 4.23393758 | Affects (1) |
| 16836492 | PRR11 | Affected | 0.229092161 | Affects (1) |
| 16843374 | RAD51D | Affected | 2.105262309 | Affects (1) |
| 16916901 | RASSF2 | Affected | 3.815838202 | Affects (1) |
| 16782222 | REM2 | Affected | 2.270484204 | Affects (1) |
| 16967091 | REST | Affected | 0.123535706 | Affects (1) |
| 16721126 | RRM1 | Affected | 0.371645746 | Affects (1) |
| 17079037 | RUNX1T1 | Affected | 3.82378127 | Affects (1) |
| 16667760 | S1PR1 | Affected | 0.340564509 | Affects (1) |
| 16951485 | SGOL1 | Affected | 0.141806936 | Affects (1) |
| 16852312 | SKA1 | Affected | 0.185694115 | Affects (1) |
| 16777278 | SKA3 | Affected | 0.147317426 | Affects (1) |
| 16842673 | SPAG5 | Affected | 0.210807778 | Affects (1) |
| 16964000 | TACC3 | Affected | 0.216284173 | Affects (1) |
| 16709333 | TCF7L2 | Affected | 0.221595425 | Affects (1) |
| 17010552 | TTK | Affected | 0.156366135 | Affects (1) |
| 17101815 | TXLNG | Affected | 0.492092011 | Affects (1) |
| 16772172 | UBC | Affected | 2.869899069 | Affects (1) |
| 16665447 | USP1 | Affected | 0.458819941 | Affects (1) |
| 17064679 | XRCC2 | Affected | 0.295043586 | Affects (1) |
| 16714504 | ZWINT | Affected | 0.227509706 | Affects (1) |
| 16733104 | CHEK1 | Affected | 0.193579757 | Affects (11) |
| 16863922 | BAX | Affected | 0.441963766 | Affects (2) |
| 16804902 | BLM | Affected | 0.152301283 | Affects (2) |
| 16834056 | CDC6 | Affected | 0.11727765 | Affects (2) |
| 16771067 | CIT | Affected | 0.377356492 | Affects (2) |
| 16818842 | CYLD | Affected | 2.373473595 | Affects (2) |
| 16778067 | DCLK1 | Affected | 4 | Affects (2) |
| 16751709 | ESPL1 | Affected | 0.220828763 | Affects (2) |
| 16829369 | FANCA | Affected | 0.335178148 | Affects (2) |
| 16800108 | HAUS2 | Affected | 0.490389502 | Affects (2) |
| 16790592 | HAUS4 | Affected | 0.413798408 | Affects (2) |
| 17092688 | HAUS6 | Affected | 0.459456442 | Affects (2) |
| 16817647 | KIF22 | Affected | 0.474013483 | Affects (2) |

| | | | | |
|---|---|---|---|---|
| 17104484 | KIF4A | Affected | 0.255076165 | Affects (2) |
| 17084904 | MELK | Affected | 0.125173407 | Affects (2) |
| 16879883 | MSH2 | Affected | 0.422493192 | Affects (2) |
| 16698159 | MYOG | Affected | 0.262611136 | Affects (2) |
| 16708552 | NOLC1 | Affected | 0.412081042 | Affects (2) |
| 16903897 | NR4A2 | Affected | 3.906834116 | Affects (2) |
| 16970563 | PLK4 | Affected | 0.191312096 | Affects (2) |
| 16661589 | RCC1 | Affected | 0.392292049 | Affects (2) |
| 16815905 | RMI2 | Affected | 0.421323415 | Affects (2) |
| 16904780 | SPC25 | Affected | 0.15976242 | Affects (2) |
| 16850625 | TGIF1 | Affected | 0.378929142 | Affects (2) |
| 16912379 | TPX2 | Affected | 0.153893052 | Affects (2) |
| 16744501 | ZW10 | Affected | 0.443498153 | Affects (2) |
| 16771680 | CLIP1 | Affected | 2.082043195 | Affects (3) |
| 16892446 | INPP5D | Affected | 0.466516496 | Affects (3) |
| 16731858 | KMT2A | Affected | 2.005552872 | Affects (3) |
| 17069063 | LYN | Affected | 0.185436867 | Affects (3) |
| 16790556 | PRMT5 | Affected | 0.453445164 | Affects (3) |
| 16903863 | RPRM | Affected | 0.341746863 | Affects (3) |
| 16951644 | TOP2B | Affected | 2.046274939 | Affects (3) |
| 16719025 | FGFR2 | Affected | 0.248445273 | Affects (4) |
| 16870131 | HAUS8 | Affected | 0.382624192 | Affects (4) |
| 16698984 | NEK2 | Affected | 0.186468003 | Affects (4) |
| 17024394 | PLAGL1 | Affected | 0.390934822 | Affects (4) |
| 16817017 | PLK1 | Affected | 0.231647015 | Affects (45) |
| 16775014 | CKAP2 | Affected | 0.309712174 | Affects (5) |
| 16850517 | NDC80 | Affected | 0.115663054 | Affects (5) |
| 16978568 | CENPE | Affected | 0.181872585 | Affects (6) |
| 16707468 | KIF11 | Affected | 0.152301283 | Affects (6) |
| 16703478 | MASTL | Affected | 0.196690611 | Affects (6) |
| 16737056 | PAX6 | Affected | 3.031433133 | Affects (7) |
| 16664569 | CDKN2C | Affected | 0.488692883 | Affects (8) |
| 16658192 | TP73 | Affected | 5.045509635 | Affects (9) |
| 17093186 | B4GALT1 | Increased | 0.399702915 | Decreases (1) |
| 16789926 | CCNB1IP1 | Increased | 0.44596426 | Decreases (1) |
| 16857192 | CHAF1A | Increased | 0.265171935 | Decreases (1) |
| 17002846 | DUSP1 | Decreased | 2.020902893 | Decreases (1) |
| 16707695 | HELLS | Increased | 0.243838865 | Decreases (1) |
| 16843376 | NLE1 | Increased | 0.498270131 | Decreases (1) |
| 16818600 | ORC6 | Increased | 0.234068062 | Decreases (1) |
| 16839412 | PITPNA | Increased | 0.47237352 | Decreases (1) |
| 16797051 | PPP1R13B | Decreased | 2.365262 | Decreases (1) |
| 16690067 | SASS6 | Increased | 0.471392268 | Decreases (1) |

| | | | | |
|---|---|---|---|---|
| 16914791 | SNAI1 | Increased | 0.409518349 | Decreases (1) |
| 16686796 | STIL | Increased | 0.240481864 | Decreases (1) |
| 16843658 | TBC1D3H (includes others) | Decreased | 2.054802879 | Decreases (1) |
| 16849556 | TIMP2 | Decreased | 2.948538435 | Decreases (1) |
| 16730503 | YAP1 | Increased | 0.184028358 | Decreases (1) |
| 16957636 | ZBTB20 | Decreased | 2.283109414 | Decreases (1) |
| 16722526 | MYOD1 | Increased | 0.172898829 | Decreases (11) |
| 16663514 | CDC20 | Increased | 0.178376813 | Decreases (13) |
| 16855673 | BCL2 | Decreased | 2.63170905 | Decreases (15) |
| 16969051 | BMPR1B | Increased | 0.401090583 | Decreases (2) |
| 16987468 | CAST | Increased | 0.41065535 | Decreases (2) |
| 16667037 | CDC7 | Increased | 0.363493129 | Decreases (2) |
| 16681304 | ERRFI1 | Decreased | 2.080600533 | Decreases (2) |
| 16937505 | FANCD2 | Increased | 0.174342958 | Decreases (2) |
| 16812942 | NTRK3 | Decreased | 3.721798631 | Decreases (2) |
| 16673154 | NUF2 | Increased | 0.235206527 | Decreases (2) |
| 16767911 | PAWR | Increased | 0.372677597 | Decreases (2) |
| 16753533 | RASSF3 | Increased | 0.311002913 | Decreases (2) |
| 16851397 | RBBP8 | Increased | 0.381829374 | Decreases (2) |
| 16938562 | TGFBR2 | Increased | 0.227509706 | Decreases (2) |
| 16906620 | TMEFF2 | Decreased | 4.404566392 | Decreases (2) |
| 16979389 | MAD2L1 | Increased | 0.163345657 | Decreases (20) |
| 16924305 | BTG3 | Increased | 0.334250124 | Decreases (3) |
| 16933502 | CHEK2 | Increased | 0.407818747 | Decreases (3) |
| 16707149 | FAS | Increased | 0.440129507 | Decreases (3) |
| 17005396 | GMNN | Increased | 0.248962438 | Decreases (3) |
| 16663958 | KIF2C | Increased | 0.195874297 | Decreases (3) |
| 17038792 | KIFC1 | Increased | 0.309712174 | Decreases (3) |
| 16906131 | NEUROD1 | Decreased | 2.193143177 | Decreases (3) |
| 17022691 | FYN | Decreased | 3.280691645 | Decreases (4) |
| 16938407 | RARB | Increased | 0.269060031 | Decreases (4) |
| 17024980 | FBXO5 | Increased | 0.258816231 | Decreases (5) |
| 16735018 | APBB1 | Decreased | 2.112571251 | Decreases (6) |
| 16901755 | BUB1 | Increased | 0.14958112 | Decreases (6) |
| 17075731 | CLU | Increased | 0.393926943 | Decreases (6) |
| 17119348 | GNL3 | Increased | 0.469761375 | Decreases (6) |
| 16845349 | BRCA1 | Increased | 0.248273124 | Decreases (7) |
| 17117110 | CD24 | Decreased | 6.543216468 | Decreases (7) |
| 16823229 | PKMYT1 | Increased | 0.398044049 | Decreases (7) |
| 16802251 | SMAD3 | Increased | 0.44844408 | Decreases (7) |
| 16737105 | WT1 | Increased | 0.487339815 | Decreases (7) |
| 16872551 | TGFB1 | Increased | 0.279709275 | Decreases (78) |

| | | | | |
|---|---|---|---|---|
| 16790614 | AJUBA | Decreased | 0.305236628 | Increases (1) |
| 16749423 | ARNTL2 | Decreased | 0.387159514 | Increases (1) |
| 17040561 | ATAT1 | Increased | 2.323017464 | Increases (1) |
| 16694556 | C1orf61 | Increased | 4.141059695 | Increases (1) |
| 16978959 | CASP6 | Decreased | 0.480630464 | Increases (1) |
| 16868130 | CD320 | Decreased | 0.494485458 | Increases (1) |
| 16662648 | CDCA8 | Decreased | 0.231807637 | Increases (1) |
| 17024285 | CITED2 | Increased | 2.044857061 | Increases (1) |
| 17079588 | FBXO43 | Decreased | 0.429878243 | Increases (1) |
| 16963876 | FGFRL1 | Decreased | 0.477310507 | Increases (1) |
| 16725806 | INCENP | Decreased | 0.287772373 | Increases (1) |
| 16698049 | KDM5B | Increased | 2.319799309 | Increases (1) |
| 17060412 | MCM7 | Decreased | 0.482633512 | Increases (1) |
| 16702047 | NET1 | Decreased | 0.402483069 | Increases (1) |
| 16913806 | PLCG1 | Increased | 2.403272099 | Increases (1) |
| 17102230 | POLA1 | Decreased | 0.318640157 | Increases (1) |
| 17050154 | PRKAR2B | Increased | 2.486299338 | Increases (1) |
| 16896502 | PRKD3 | Decreased | 0.459456442 | Increases (1) |
| 16724593 | PTPMT1 | Decreased | 0.462973011 | Increases (1) |
| 16678518 | RHOU | Increased | 2.783692784 | Increases (1) |
| 16829580 | RPA1 | Decreased | 0.290578527 | Increases (1) |
| 17126218 | RPS15A | Increased | 2.577549261 | Increases (1) |
| 16855090 | SMAD2 | Increased | 2.177994031 | Increases (1) |
| 16735443 | ST5 | Decreased | 0.420739741 | Increases (1) |
| 17069816 | SULF1 | Decreased | 0.458819941 | Increases (1) |
| 17075426 | TNFRSF10B | Decreased | 0.218999579 | Increases (1) |
| 17126024 | TRIM25 | Decreased | 0.383686524 | Increases (1) |
| 16914315 | UBE2C | Decreased | 0.228299563 | Increases (1) |
| 16745343 | USP2 | Decreased | 0.46554741 | Increases (1) |
| 17005234 | E2F3 | Decreased | 0.204333832 | Increases (10) |
| 16683358 | E2F2 | Decreased | 0.336341802 | Increases (11) |
| 16693898 | SHC1 | Decreased | 0.486327474 | Increases (11) |
| 16984032 | SKP2 | Decreased | 0.236678408 | Increases (11) |
| 16953279 | CDC25A | Decreased | 0.109272328 | Increases (12) |
| 16691327 | NGF | Decreased | 0.220064753 | Increases (12) |
| 16705159 | CDK1 | Decreased | 0.113833729 | Increases (13) |
| 17000439 | CDC25C | Decreased | 0.204617295 | Increases (14) |
| 16833839 | ERBB2 | Decreased | 0.438910899 | Increases (14) |
| 16909165 | IRS1 | Decreased | 0.398596238 | Increases (15) |
| 16760048 | FOXM1 | Decreased | 0.185051662 | Increases (16) |
| 17067739 | NRG1 | Increased | 3.60500185 | Increases (16) |
| 16924551 | APP | Increased | 2.360348687 | Increases (17) |
| 16755958 | ASCL1 | Increased | 3.640155296 | Increases (2) |

| | | | | |
|---|---|---|---|---|
| 16774053 | CCNA1 | Decreased | 0.264437741 | Increases (2) |
| 16815090 | CCNF | Decreased | 0.498270131 | Increases (2) |
| 16685165 | CLSPN | Decreased | 0.172779026 | Increases (2) |
| 16740630 | FOSL1 | Decreased | 0.337977708 | Increases (2) |
| 17012148 | GJA1 | Decreased | 0.095127086 | Increases (2) |
| 16933760 | LIF | Decreased | 0.414659773 | Increases (2) |
| 16719515 | MKI67 | Decreased | 0.2032039 | Increases (2) |
| 16913957 | MYBL2 | Decreased | 0.144485838 | Increases (2) |
| 16916233 | MYT1 | Increased | 5.180171995 | Increases (2) |
| 16816200 | NDE1 | Decreased | 0.431071773 | Increases (2) |
| 16916958 | PCNA | Decreased | 0.255961725 | Increases (2) |
| 16822961 | PKD1 | Increased | 2.284692494 | Increases (2) |
| 17094064 | SHB | Increased | 3.012580933 | Increases (2) |
| 16951567 | THRB | Decreased | 0.453445164 | Increases (2) |
| 16850477 | TYMS | Decreased | 0.133138525 | Increases (2) |
| 16752305 | CDK2 | Decreased | 0.31273227 | Increases (20) |
| 16860418 | CCNE1 | Decreased | 0.179368692 | Increases (21) |
| 16920548 | AURKA | Decreased | 0.242154547 | Increases (22) |
| 16838359 | BIRC5 | Decreased | 0.176043028 | Increases (22) |
| 16773840 | BRCA2 | Decreased | 0.164481816 | Increases (3) |
| 16723614 | CD44 | Increased | 2.615342697 | Increases (3) |
| 16740282 | CDCA5 | Decreased | 0.399149193 | Increases (3) |
| 16784299 | CDKN3 | Decreased | 0.148136596 | Increases (3) |
| 17120506 | DBF4 | Decreased | 0.212274062 | Increases (3) |
| 16852206 | HAUS1 | Decreased | 0.391748593 | Increases (3) |
| 17123388 | HMGB1 | Decreased | 0.482299092 | Increases (3) |
| 16972129 | KLHL2 | Increased | 2.023706402 | Increases (3) |
| 16836131 | NME1 | Decreased | 0.44844408 | Increases (3) |
| 16842517 | NOS2 | Decreased | 0.177759676 | Increases (3) |
| 16747158 | NTF3 | Decreased | 0.321078952 | Increases (3) |
| 16827227 | RRAD | Decreased | 0.35379854 | Increases (3) |
| 16918445 | E2F1 | Decreased | 0.345797657 | Increases (34) |
| 17079293 | CCNE2 | Decreased | 0.176165094 | Increases (4) |
| 16677425 | CENPF | Decreased | 0.250520401 | Increases (4) |
| 16799793 | NUSAP1 | Decreased | 0.161208531 | Increases (4) |
| 16966809 | PDGFRA | Increased | 4.982949662 | Increases (4) |
| 16799426 | BUB1B | Decreased | 0.254017536 | Increases (5) |
| 16985599 | CCNB1 | Decreased | 0.15346696 | Increases (5) |
| 16912362 | ID1 | Decreased | 0.4181232 | Increases (5) |
| 16777259 | LATS2 | Decreased | 0.382624192 | Increases (5) |
| 16844312 | TOP2A | Decreased | 0.198470983 | Increases (5) |
| 16721835 | WEE1 | Decreased | 0.340800652 | Increases (5) |
| 16769250 | IGF1 | Decreased | 0.467163673 | Increases (51) |

| | | | | |
|---|---|---|---|---|
| 16970404 | FGF2 | Decreased | 0.281069731 | Increases (53) |
| 17064105 | EZH2 | Decreased | 0.437392382 | Increases (6) |
| 16878947 | LTBP1 | Decreased | 0.310356873 | Increases (6) |
| 17100036 | NOTCH1 | Decreased | 0.384751805 | Increases (6) |
| 17072669 | MYC | Decreased | 0.363997387 | Increases (61) |
| 16979515 | CCNA2 | Decreased | 0.174222155 | Increases (7) |
| 16752397 | ERBB3 | Decreased | 0.416099367 | Increases (7) |
| 16840902 | AURKB | Decreased | 0.167240944 | Increases (8) |
| 16911261 | BMP2 | Decreased | 0.166200889 | Increases (9) |
| 16920585 | BMP7 | Decreased | 0.414659773 | Increases (9) |

* A total of 263 genes were differentially expressed in D283 $OTX2^{KD}$ relative to control D283 cells and among them 91 genes were downregulated.

Conversely, genes related to cell cycle progression (91 out of 263) were downregulated (Table 3.2.2). For example, the cyclin dependent kinases (CDKs), *CDK1* (0.114 fold), *CDK2* (0.313 fold) and cell division cycle (CDC) genes such as *CDC6* (0.117 fold), *CDC20* (0.178 fold), *CDC25A* (0.109 fold) and *CDC25C* (0.205 fold), which are involved in regulating specific phases of cell cycle, were downregulated. We observed decreased protein levels of cell cycle genes such as cyclin D2 and CDK6 in D283 and D425 cells following OTX2 knockdown (Figure 3.2.19). These results correlate with our findings from BrdU staining demonstrating a decrease in the S phase of cell cycle in both D283 and trans-hENs following OTX2 knockdown in tumorsphere or stem cell-enriched populations.

#### 3.2.2.2 Chromatin immunoprecipitation-sequencing (ChIP-seq) reveals a direct or indirect regulation of axon guidance genes by OTX2

To identify which of the differentially expressed axon guidance genes are regulated by OTX2, ChIP-seq was performed on OTX2-expressing D283 Group 4 tumorspheres in partnership with StemCore Laboratories (Ottawa Hospital Research Institute, Ottawa, Ontario). A clear statistically significant association between fold change in axon guidance pathway genes, observed by global gene expression analysis, and the presence of one or more OTX2 peaks within -5kb to +2kb of the TSS (Fisher Exact Test; $P<2.2e-16$) was observed (Table 3.2.3). Eph/ephrin was the most overrepresented pathway in the top 30 followed by Semaphorin signaling. These results indicate that OTX2 may serve as a transcriptional regulator of axon guidance pathways which were mostly upregulated following inhibition of OTX2 expression in Group 3 and 4 MB tumorspheres by knockdown.

### 3.2.2.3 *In silico* analysis and screening of patient samples revealed the clinical implications of the association between OTX2 and axon guidance genes

We cross-referenced our Affymetrix and ChIP-seq data with the clinical data published by Northcott et al. (2011) and found that axon guidance genes are mostly downregulated in Group 3 and 4 MBs (Table 3.2.4 and 3.2.5). These genes are negatively correlated with the expression levels of OTX2 in Group 4 and 4 MBs. This was further supported by screening available data from 234 Group 3 and 4 MB patients in collaboration with Dr. Michael Taylor (Hospital for Sick Children, Toronto, ON) to identify which axon guidance genes are differentially expressed in tumor samples that exhibit OTX2 amplification/overexpression relative to those that do not. Thirty-nine axon guidance genes were differentially expressed and out of these 23 genes (59%) exhibited the same trends observed in our global gene expression data. Most genes were also negatively correlated with OTX2 expression and included *EPHA3, EPHA5, EPHB2, EPHB4* and *L1CAM* (Figure 3.2.20-3.2.24). Among these 23 genes, 15 genes (65%) had peak overlaps in their transcriptional start sites for OTX2 (Table 3.2.3) suggesting that they could be direct targets. These clinical data provide further support for the association between OTX2 and axon guidance genes in Group 3 and 4 MB.

**Table 3.2.3: OTX2 binding peaks and sites in the top 30 genes from ChIP-seq analysis and their relative transcript levels (Fold Change).**

| Gene Assignment | Affymetrix Fold Change | OTX2 Peaks | OTX2 Binding Sites |
|---|---|---|---|
| DCC | 19.9143847 | 1 | 1 |
| EFNB2 | 8.458995374 | 3 | 1 |
| EPHA3 | 35.96546453 | 1 | 2 |
| EPHA4 | 2.713058833 | 2 | 1 |
| EPHA5 | 29.7964111 | 1 | 1 |
| FZD1 | 0.411479558 | 2 | 2 |
| FZD5 | 0.456667281 | 3 | 4 |
| FZD7 | 0.082085886 | 1 | 1 |
| GNG11 | 0.367793953 | 2 | 3 |
| GNG12 | 0.30012554 | 3 | 2 |
| GNG3 | 6.14369672 | 2 | 0 |
| IGF1 | 0.467094383 | 3 | 4 |
| KLC1 | 2.163857258 | 3 | 1 |
| LRRC4C | 3.696844429 | 3 | 5 |
| NRP1 | 4.525936467 | 2 | 7 |
| NRP2 | 5.392071649 | 2 | 1 |
| PLCB4 | 9.425849634 | 1 | 2 |
| PLCD3 | 0.392306551 | 2 | 5 |
| PLCE1 | 0.340932018 | 2 | 2 |
| PLCL1 | 4.499103846 | 2 | 1 |
| PLXNA2 | 3.436757362 | 3 | 3 |
| RRAS | 0.324050897 | 2 | 4 |
| SEMA6A | 5.542465942 | 3 | 1 |
| SEMA6C | 2.811277756 | 2 | 4 |
| SHC1 | 0.486217368 | 3 | 4 |
| SLIT2 | 3.365945926 | 4 | 3 |
| SRGAP2 | 2.107118816 | 2 | 4 |
| UNC5B | 2.599856508 | 5 | 3 |
| UNC5D | 8.093918561 | 1 | 0 |

**Table 3.2.4: *In silico* analysis showed differential expression of transcripts in Group 3 relative to WNT and SHH MBs and their relative Fold Change.**

| Gene Assignment | Fold Change (Group 3 vs. WNT and SHH) | Affymetrix Fold Change |
|---|---|---|
| DCC | 0.3381339 | 19.9143847 |
| EPHA2 | 1.7074639 | 0.185952068 |
| FZD1 | 2.7109131 | 0.411479568 |
| FZD5 | 1.443012 | 0.45666727 |
| GAP43 | 0.3475301 | 10.44460719 |
| GNG2 | 0.4348251 | 3.021322798 |
| GNG3 | 0.2100385 | 6.14369672 |
| JAKMIP2 | 0.470199 | 29.17675091 |
| KLF12 | 0.4581686 | 4.266161762 |
| KLF7 | 0.5699869 | 2.797721449 |
| MAP6 | 0.5467956 | 12.92545651 |
| OTX2 | 4.6649713 | 0.232956857 |
| PLCB4 | 0.4991053 | 9.425849654 |
| SEMA6A | 0.2825166 | 5.542465942 |

**Table 3.2.5: *In silico* analysis showed differential expression of transcripts in Group 4 relative to WNT and SHH MBs and their relative Fold Change.**

| Gene Assignment | Fold Change (Group 4 vs. WNT and SHH) | Affymetrix Fold Change |
|---|---|---|
| EPHA4 | 0.3380606 | 2.713058827 |
| EPHA5 | 1.7405107 | 29.79641178 |
| FIGF | 1.1261531 | 0.467094383 |
| GNG3 | 0.2666926 | 6.14369672 |
| MAP2 | 0.5398727 | 17.31444213 |
| OTX2 | 4.7238524 | 0.232956857 |
| PLCL2 | 0.5365473 | 4.499103856 |
| SEMA6A | 0.354432 | 5.542465942 |
| SRGAP | 0.4779591 | 2.107118816 |

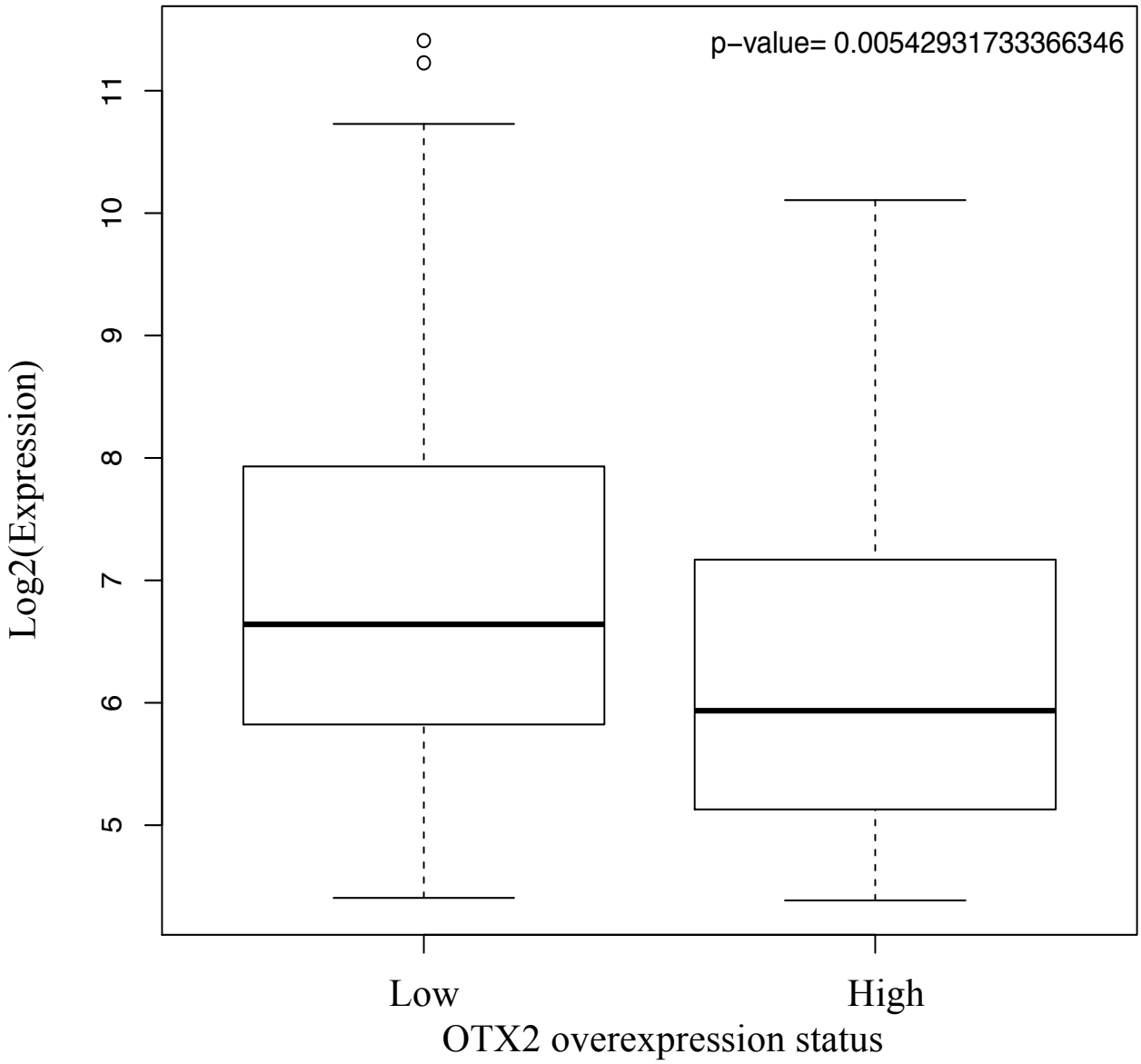


**Figure 3.2.20: Box plot showing negative correlation between OTX2 and *EPHA3* in Group 3 and 4 MB patient samples.** The X-axis represents the expression levels of OTX2 in MB subtypes. Group 3 and 4 MBs samples that exhibit high OTX2 expression were clustered together. The Y-axis represents the Log2 fold change in the expression of the gene of interest. For patients with high OTX2 expression but no evidence of amplification, the 90$^{th}$ percentile of OTX2 expression was used as the threshold for overexpression. $P<0.05$ was used for highest confidence correlation.

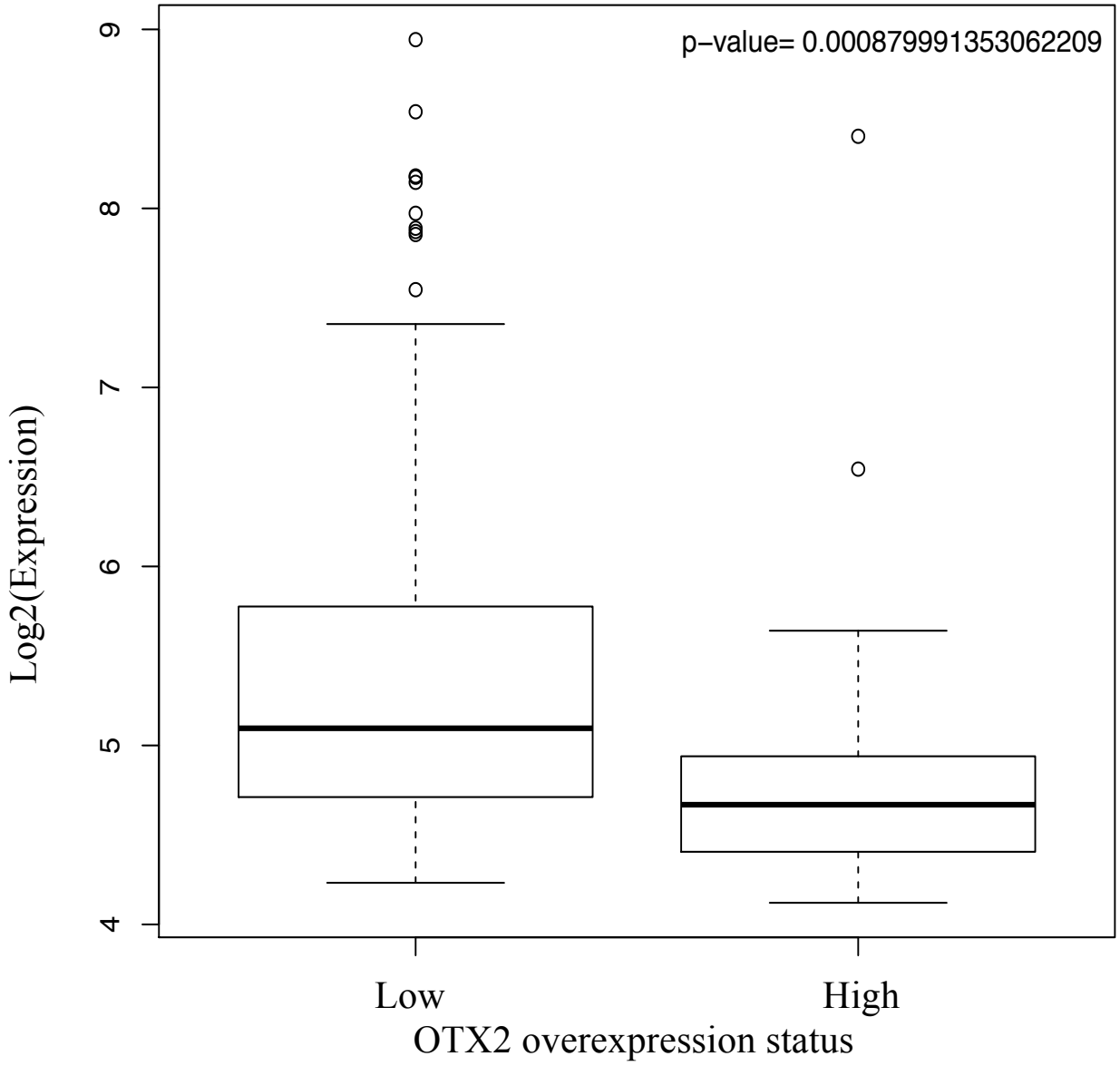


**Figure 3.2.21: Box plot showing negative correlation between OTX2 and *EPHA5* in Group 3 and 4 MB patient samples.** The X-axis represents the expression levels of OTX2 in MB subtypes. Group 3 and 4 MBs samples that exhibit high OTX2 expression were clustered together. The Y-axis represents the Log2 fold change in the expression of the gene of interest. For patients with high OTX2 expression but no evidence of amplification, the $90^{th}$ percentile of OTX2 expression was used as the threshold for overexpression. $P<0.05$ was used for highest confidence correlation.

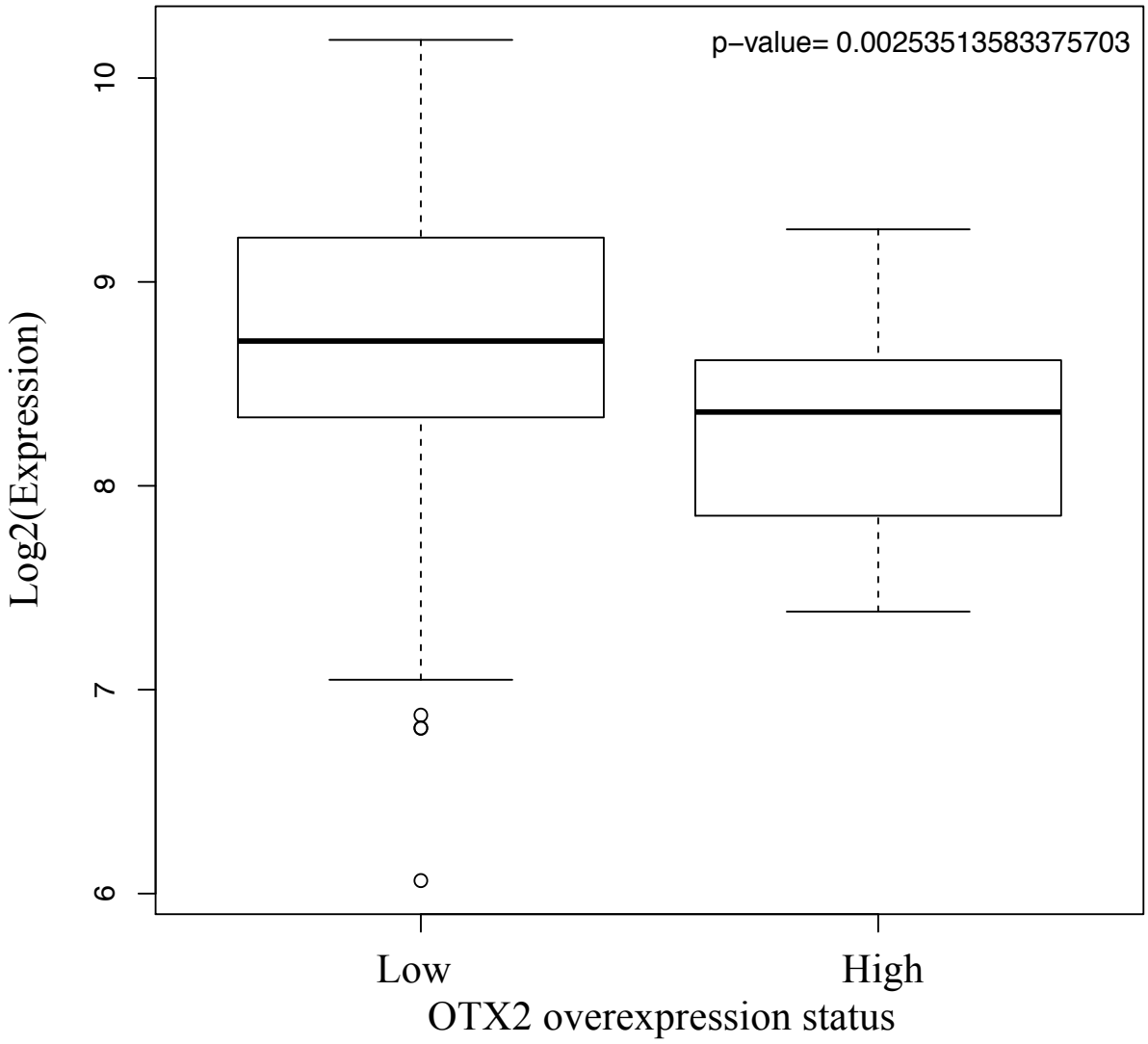


**Figure 3.2.22: Box plot showing negative correlation between OTX2 and *EPHB2* in Group 3 and 4 MB patient samples.** The X-axis represents the expression levels of OTX2 in MB subtypes. Group 3 and 4 MBs samples that exhibit high OTX2 expression were clustered together. The Y-axis represents the Log2 fold change in the expression of the gene of interest. For patients with high OTX2 expression but no evidence of amplification, the $90^{th}$ percentile of OTX2 expression was used as the threshold for overexpression. $P<0.05$ was used for highest confidence correlation.

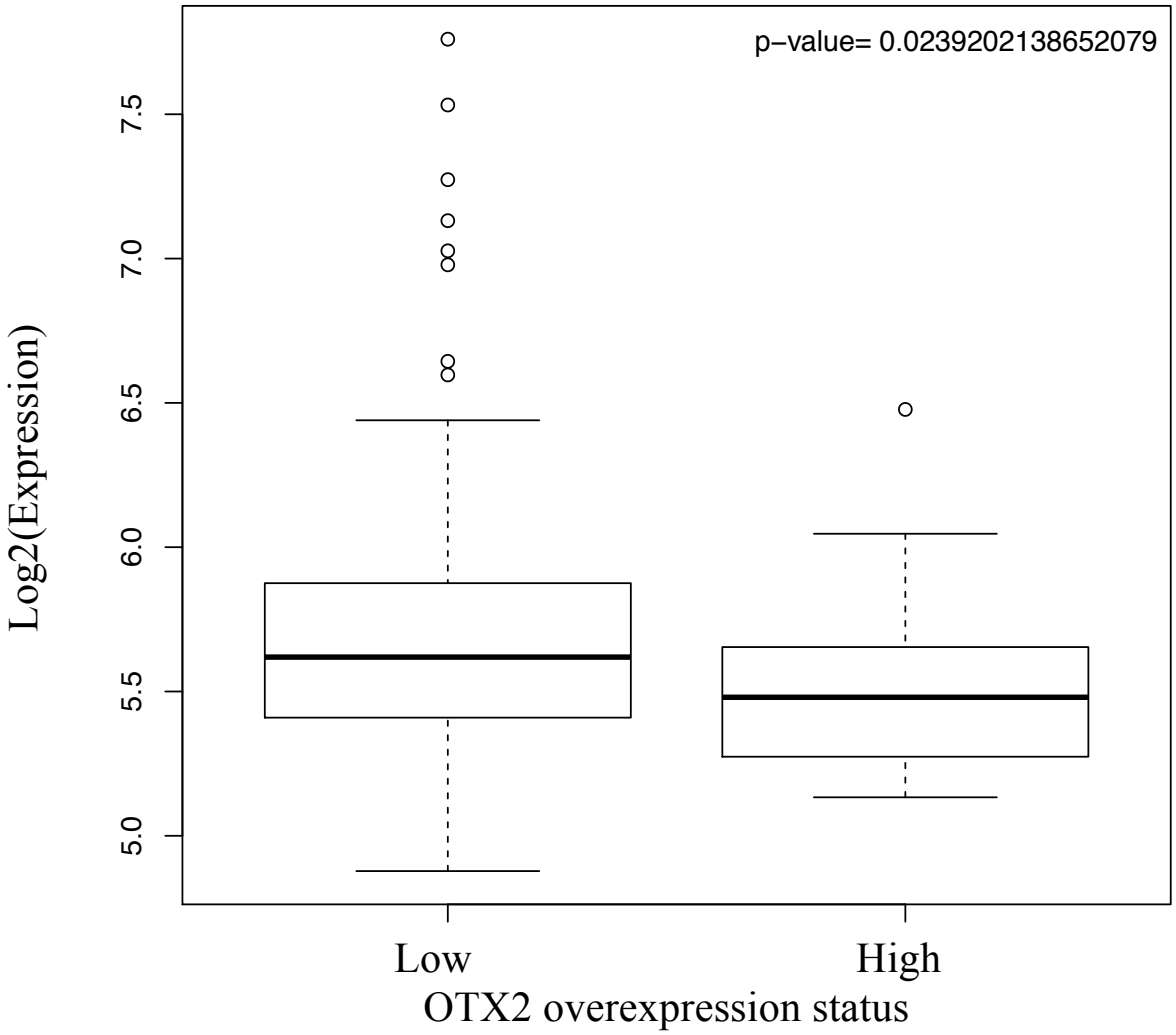


**Figure 3.2.23: Box plot showing negative correlation between OTX2 and *EPHB4* in Group 3 and 4 MB patient samples.** The X-axis represents the expression levels of OTX2 in MB subtypes. Group 3 and 4 MBs samples that exhibit high OTX2 expression were clustered together. The Y-axis represents the Log2 fold change in the expression of the gene of interest. For patients with high OTX2 expression but no evidence of amplification, the 90$^{th}$ percentile of OTX2 expression was used as the threshold for overexpression. $P<0.05$ was used for highest confidence correlation.

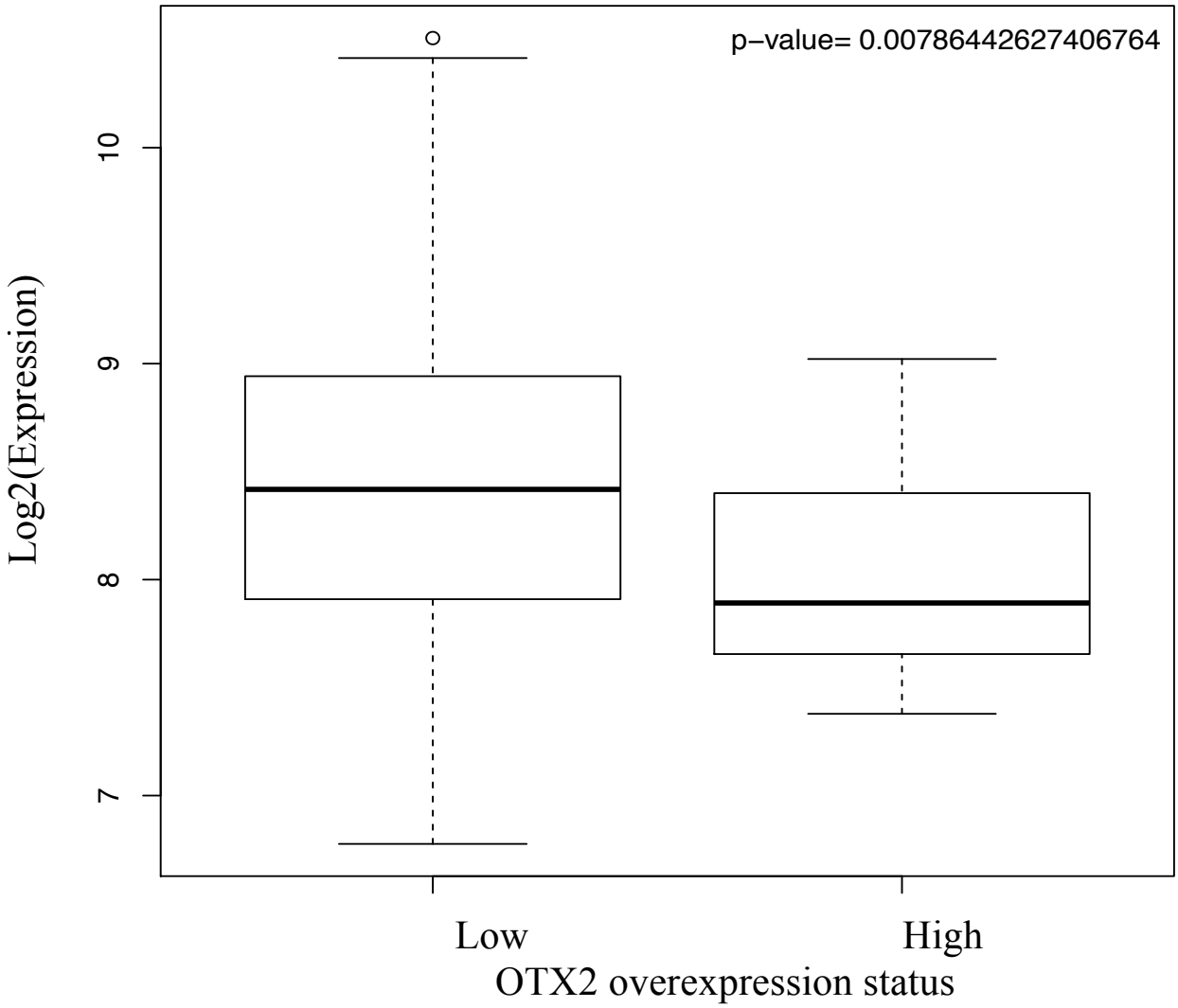


**Figure 3.2.24: Box plot showing negative correlation between OTX2 and *L1CAM* in Group 3 and 4 MB patient samples.** The X-axis represents the expression levels of OTX2 in MB subtypes. Group 3 and 4 MBs samples that exhibit high OTX2 expression were clustered together. The Y-axis represents the Log2 fold change in the expression of the gene of interest. For patients with high OTX2 expression but no evidence of amplification, the 90$^{th}$ percentile of OTX2 expression was used as the threshold for overexpression. $P<0.05$ was used for highest confidence correlation.

# CHAPTER 4: DISCUSSION

### 4.1 OTX2 is required for regulating cellular functions in normal hENs and Daoy MB cells.

OTX2 is a multifaceted transcription factor and plays a crucial role in early brain development (Acampora et al. 1995). Its role in brain patterning, in defining the midbrain-hindbrain junction and in cell fate specification is evident (Acampora et al. 1995; Matsuo et al. 1995; Ang et al. 1996; Simeone 1998; Puelles et al. 2004; Simeone et al. 2011; Beby and Lamonerie 2013; Housset et al. 2013). Despite its various functions in normal development, OTX2 is frequently amplified and overexpressed in the most aggressive Group 3 and 4 MBs (Di et al. 2005; Adamson et al. 2010; Bai et al. 2012). One study evaluating the role of OTX2 overexpression in the Daoy SHH MB cell line, revealed a decrease in cell proliferation attributed to induction of cellular senescence (Bunt et al. 2010). However, the role of OTX2 in regulating other cellular functions such as self-renewal, cell survival and cell migration was not examined. Our studies demonstrate a novel role for OTX2 in self-renewal and migration of human neural precursors and MB cells and we have identified a cell context-dependent regulation of these cellular properties.

### 4.2 The association between OTX2 and hESC genes is important for regulating cellular functions in hENs and Daoy MB cells

Using normal hENs, we discovered a novel link between OTX2 and hESC gene expression. Our working model is depicted in Figure 4.1 and we propose that OTX2 plays a central role in regulating the earliest stages of neural differentiation to ensure appropriate downregulation of pluripotent genes such as SOX2 and to prevent acquisition of tumorigenic properties in SHH MB and hENs. OTX2 and SOX2 may also participate in a negative feedback loop that provides greater control over cellular functions in these cells (Figure 4.1A-B). Indeed,

there are 3 SOX2 binding sites (TTCAAAG and TACAAAG sequences) on the OTX2 promoter (Ferrari et al. 1992; Okumura-Nakanishi et al. 2005); however, additional studies still need to be conducted to further evaluate potential interactions in our model systems.

Work by Acampora et al. (Acampora, Di Giovannantonio, and Simeone 2013) supports our model by demonstrating that OTX2 inhibits embryonic stem cell pluripotency and promotes commitment to the epiblast state specifically in mouse cells. Other studies have shown a direct interaction between OTX2 and SOX2 to control ocular development in Xenopus (Danno et al. 2008). However, to our knowledge, we are the first to demonstrate an association between OTX2 and SOX2 in regulating self-renewal and migration of human cells.

It has been recently shown that SOX2 binds to the *LIN28A* promoter and that a *SOX2-LIN28A-let-7* pathway regulates hESC-derived neural precursor proliferation and differentiation (Cimadamore et al. 2013). In hEN and SHH MB OTX2-overexpressing cells, interaction of OTX2 with SOX2 may prevent subsequent activation of *LIN28A* resulting in upregulation of *let-7* miRNAs (Figure 4.1A-B). Our ChIP studies demonstrated an association between OTX2 and SOX2; however they did not determine whether OTX2 binds directly or indirectly via other proteins to the SOX2 promoter region. Moreover, whether this association is only transcriptional (i.e. OTX2 suppresses hESC gene expression by directly repressing their promoters) or mediated by protein-protein interactions or both in our models is unknown (Figure 4.1A). Future studies will evaluate the mechanism(s) by which OTX2 and SOX2 regulate each other and how this interaction between them affects expression of *LIN28A*, downstream target *let-7* miRNAs, and other hESC genes to regulate self-renewal and other cellular properties in our models. In addition, as Daoy is a long-term cultured cell lines which has acquired additional genetic changes, low passage primary SHH MB cultures will be utilized to further explore the

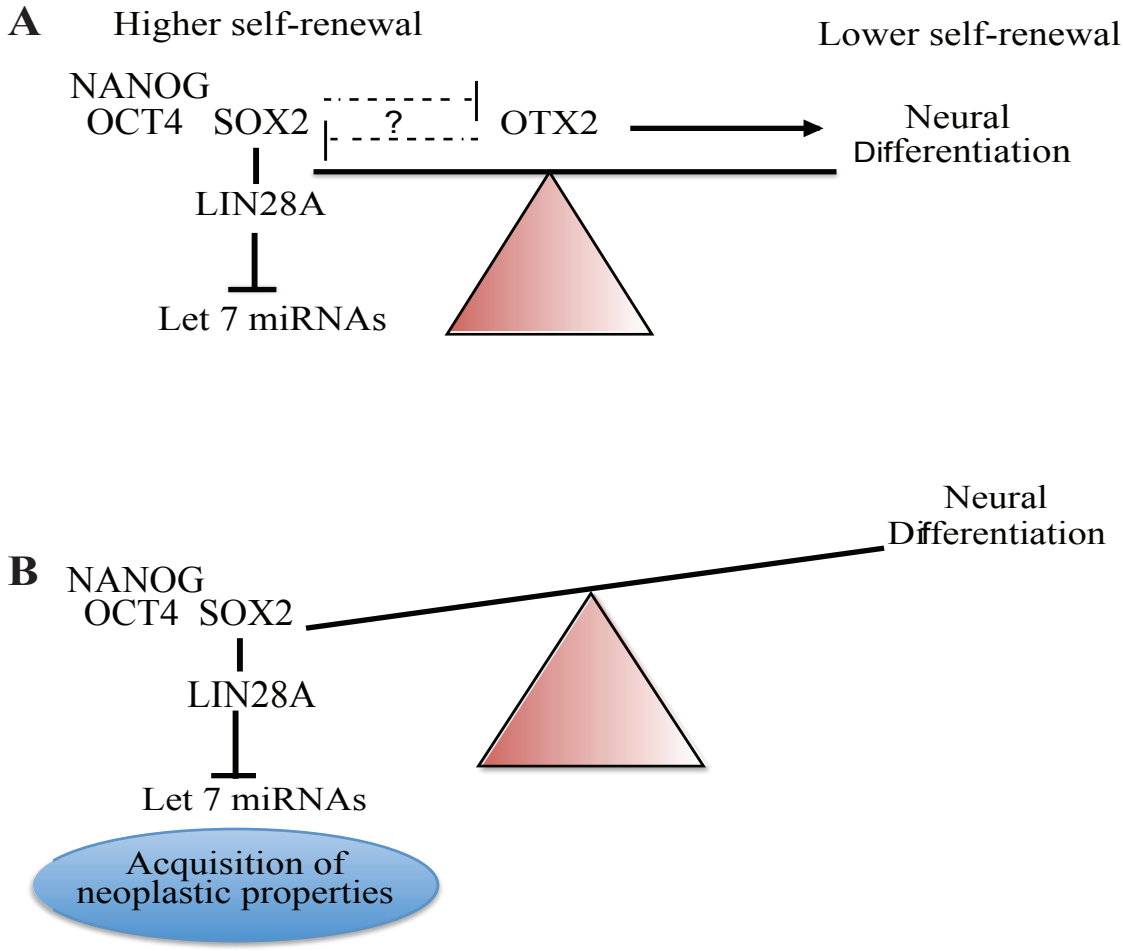


**Figure 4.1: Working model depicting the role of OTX2 in regulating the balance between self-renewal and differentiation during normal and aberrant neural development.** The relationship between OTX2 and hESC genes duing normal vs. aberrant embryonic neural development (A, B). (A) During normal human neural development, OTX2 expression is predicted to regulate the balance between self-renewal and differentiation by controlling the expression of pluripotent genes. Following OTX2 overexpression, pluripotent genes are downregulated and our study provides evidence of interaction between OTX2 and SOX2. (B) Lack of OTX2 prevents the appropriate downregulation of these stem cell genes leading to aberrant neural development and acquisition of neoplastic transformation.

mechanism behind the inhibitory role of OTX2 in the SHH subgroup. Recently, our laboratory has acquired a low passage primary SHH MB culture, UI226 (Passage <10 times in nude mice and then adapted to cell culture in Stem Pro® Neural Stem Cell Medium) and has been tested for their sphere forming ability (Liang et al. 2015).

### 4.3 Oncogenic role of OTX2 in Group 3 and 4 MB cells is independent of hESC genes.

While the inhibitory effects of OTX2 in hEN and SHH MB cells are at least, in part, regulated by pluripotent factors, the oncogenic effects of OTX2 on trans-hENs as well as Group 3 and 4 MBs are not mediated by hESC genes (Figure 3.2.12). Indeed, knockdown of OTX2 resulted in a decrease in cell growth and revealed a novel role for OTX2 in regulating self-renewal of human cells; however, this was accompanied by only modest changes in hESC gene levels that are already quite elevated in these cells. The context-dependent function of transcription factors is well documented. For example, *OCT4* and *NANOG* are required for maintaining pluripotency; however, their roles change once a hESC acquires tumorigenic features (Ji et al. 2009). Additional studies have shown that both overexpression and knockdown of OCT4 in embryonic stem cells induce differentiation, suggesting that optimal levels are required for maintaining pluripotency (Niwa, Miyazaki, and Smith 2000; Chen et al. 2007). For trans-hENs and Groups 3 and 4 MB, OTX2 interacts with other factors to maintain high self-renewal and growth, and this will require further investigation. Additionally, subcellular localization (Baas et al. 2000) and post-translational modifications including phosphorylation (Kim and Lemke 2006) may contribute to OTX2's differential roles in our model systems and represent important avenues for future study. For example, cell type-specific subcellular localization of Otx2 to either the nucleus and/or cytoplasm has been shown to contribute to cell

fate determination during retinal development in the mouse (Baas et al. 2000). Similarly, other homeodomain proteins such as Vax2 have also been shown to shuttle between the nucleus and cytoplasm during sequential stages of retinal differentiation (Kim and Lemke 2006).

**4.4 Interaction between OTX2 and axon guidance genes in Group 3 and 4 MB cells.**

By propagating D283, D425 and D341 (Group 3 and 4 MB) cells in stem cell enriched conditions, we discovered that OTX2 may act as a transcriptional regulator of axonal guidance pathway genes including those genes associated with eph/ephrin, semaphorin, Slit and netrin signaling. These axonal guidance genes are crucial for regulating various developmental processes including neuronal projections, cell proliferation and cell migration (Brose et al. 1999; Kerjan et al. 2005; Borrell et al. 2012; Sikkema et al. 2012; Bhatia et al. 2015). During cerebellar development, the CGNPs of EGL undergo a series of cell proliferation and cell migration events (ten Donkelaar et al. 2003) (Figure 1.4A-B). Axonal guidance signaling pathways such as eph/ephrin, semaphorin and Slit are shown to regulate both proliferation and directional movements of these CGNPs (Karam et al. 2000; Kerjan et al. 2005; Gibson et al. 2014). For example, it has been reported that the ephrin-A5 ligand plays an important role in CGNPs formation and migration from the EGL to the IGL by binding to its high-affinity receptors, EphA4 and EphA7 (Karam et al. 2000). Similarly, high expression of semaphorin (Sema6A) is required for the tangential movement of CGNPs into the deep external granular cell layer (Kerjan et al. 2005). In addition, previous reports have demonstrated a role for homeobox genes in regulating axonal guidance molecules during brain and retinal development (Le et al. 2007; Zhang and Eisenstat 2012). For example, the vertebrate orthologs of *Distal-less*, *Dlx1/Dlx2,* facilitate the tangential interneuron migration from basal forebrain by repressing the semaphorin

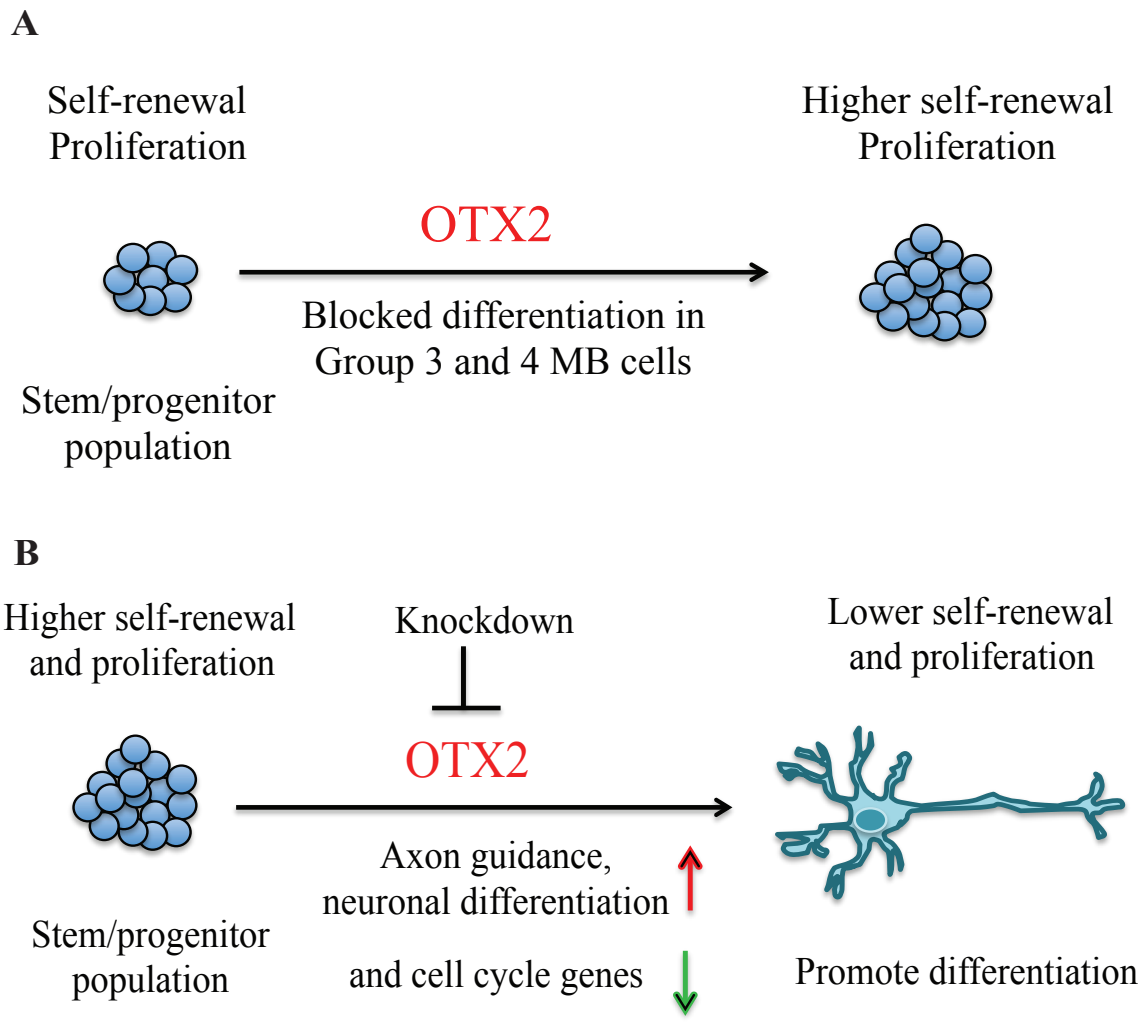


**Figure 4.2: Predicted working model depicting the oncogenic roles of OTX2 in Group 3 and Group 4 aggressive MB cells.** Global gene expression analysis and ChIP-sequencing revealed a novel association between OTX2 and axonal guidance genes. Based on these findings, we propose that OTX2 maintains highly self-renewing primitive stem/progenitor populations by inhibiting expression of genes that promote differentiation in Group 3 and 4 MB cells (A). Knockdown of OTX2 resulted in an upregulation of most of axonal guidance genes related to eph/ephrin and semaphorin signaling as well as neuronal differentiation genes (B).

receptor neuropilin-2 (Nrp2) in the developing forebrain of mice (Le et al. 2007). Similarly, the ventral anterior homeobox-containing genes, *Vax1/Vax2*, regulate the ventral retina markers Ephb2/EphB3 during retinal development (Zhang and Eisenstat 2012). These signaling pathways are found to be dysregulated in MB subgroups (Werbowetski-Ogilvie et al. 2006; Northcott et al. 2011) but their roles in progression and metastasis of Group 3 and 4 MB is poorly understood. Our study highlights, for the first time, an association between MB stem/progenitor cells and axonal guidance signaling pathways in MB extending our current knowledge that axonal guidance genes are differentially expressed between the MB subtypes. The differential expression of axonal guidance genes in OTX2 overexpressing Group 3 and 4 MB patient samples further strengthens the clinical implications of this novel association for identification of therapeutic targets. Future studies are needed to explore the role of eph/ephrin and semaphorin signaling in regulating Group 3 and 4 stem cell function and cell motility.

### 4.5 Human embryonic stem cells and their neural derivatives as a complementary model system for studying gene functions related to MB

While our work focused on medulloblastoma as proof of principle, a hESC-based model system can be utilized to study the role of pluripotency factors and other genes in a diverse range of pediatric neural malignancies. For example, *LIN28A*, a known pluripotent factor and oncogene (Viswanathan and Daley 2010), has also been found to be a prognostic and diagnostic marker for PNETs (Ma et al. 2012) and other rare embryonal brain tumors (Grange et al. 2008). In support of these findings, work in our laboratory has demonstrated that stable overexpression of LIN28A in hENs induces neoplastic features *in vitro* including enhanced proliferation, neurosphere formation and migration (unpublished data). Recently, Funato et al have utilized hESCs derived

neural precursors to model the childhood brainstem tumor, diffuse intrinsic pontine gliomas (DIPGs) (Funato et al. 2014). More than 70% of DIPGs have somatic mutations in the H3F3A gene encoding histone H3.3 and exhibit poor prognosis (Schwartzentruber et al. 2012; Wu et al. 2012; Zhang et al. 2013). Expression of the mutant form of H3.3K27M in conjunction with p53 loss and platelet-derived growth factor receptor α (PDGFRA) activation induced neoplastic transformation in neural derivatives of hESCs (Funato et al. 2014). In addition, chemical screening using these transformed neural precursors identified a compound that inhibited tumor growth *in vitro* and in mice, further strengthening the use of neural derivatives of hESCs for understanding the relevance of genetic dysregulations to disease progression and for identification of novel therapeutics targets (Funato et al. 2014).

Our study has revealed a previously unappreciated role for hESCs and their neural derivatives as cellular resources for investigating the molecular mechanisms contributing to MB progression. The use of hENs and trans-hENs circumvents the immediate need for large quantities of expanded cells from heterogeneous MB patient samples, which are very difficult to obtain. They also provide a scalable and reliable *in vitro* surrogate for putative human somatic cancer stem cell populations that can be utilized in high-throughput screening platforms (Sachlos et al. 2012) prior to moving into validation studies with patient samples. Finally, this model provides a complementary system to genetically engineered mouse models for studying and validating the function of genes of current clinical interest to the neuro-oncology community.

While our work specifically focused on the functional role of OTX2 both *in vitro* and *in vivo*, neural precursors from hESCs can be utilized for studying any gene or signaling pathway that regulates cellular processes such as growth, self-renewal and migration. The findings from

these studies will have important implications not only for neurodevelopment but also for understanding the fundamental processes contributing to pediatric brain tumor initiation and progression. Using hESCs as both a complement to and surrogate for existing cell lines and heterogeneous patient samples, the goal is to identify the next generation of targeted therapies that may apply not only to MB, but also other nervous system cancers, ultimately improving the quality of life for children who survive long-term.

## 4.6 Future Directions

In our overexpression studies, we have determined that the interaction between OTX2 and *SOX2* is important for regulating the balance between self-renewal and differentiation. Our ChIP-qPCR experiments demonstrated that OTX2 regulates SOX2 expression directly/indirectly in hENs and Daoy cells. The interaction between SOX2 and *LIN28A*-*let7* has been shown to regulate cell proliferation and differentiation of neural precursors derived from hESCs (Cimadamore et al. 2013). OTX2 may suppress SOX2 expression leading to downregulation of *LIN28A* and subsequent upregulation of *let7* miRNAs. Thus, future studies will explore the role of the OTX2-SOX2-*LIN28A*-*let7* pathway in regulating cellular properties of human neural precursors and SHH MB cells.

We have also discovered a novel association between OTX2 and axon guidance pathway genes in the most aggressive Group 3 and Group 4 MB cells. OTX2 may directly/indirectly regulate these genes as one or more OTX2 binding peaks have been identified within -5kb to +2kb of the transcriptional start sites for many axon guidance genes. As axon guidance pathways such as eph/ephrins, semaphorins and slit are found to be dysregulated in invasive Group 3 and 4 MB cells, it would be interesting to further explore how OTX2 regulates these genes using

molecular techniques such as electrophoretic mobility shift assays (EMSA) and luciferase assays. As eph/ephrin and semaphorins signaling are the most overerepresented pathways from our global gene expression, ChIP-seq and patient sample data, the functional relevance of genes associated with these pathways such as EPHA3, EPHA5, L1CAM, NRP1 and SEMA4D will be evaluated using gain or loss of function studies in Group 3 and 4 MB cells. These candidate genes are either directly or indirectly regulated by OTX2 as some of them exhibit OTX2 binding peaks within their transcriptional start sites (Table 3.2.3). All these genes are negatively correlated with OTX2 expression in Group 3 and Group 4 patient samples (Figure 3.2.20-3.2.24). The effect of these genes on stem cell function or self-renewal and cell motility will be evaluated both *in vitro* and *in vivo* in Group 3 and 4 MB cells. Finally, the association of selected genes with overall survival will be estimated in those patients exhibiting high or low levels of the gene of interest in collaboration with Dr. Michael Taylor (Hospital for Sick Children, Toronto, ON). This will enable us to determine whether axonal guidance genes serve as prognostic indicators in Group 3 and 4 MB.

Current standard treatments such as surgery, radiation and chemotherapy result in various neurological deficits in the developing nervous system of young MB patients. Although high-throughput genomic techniques have improved our understanding of the genetic and molecular diversity within MB, the functional relevance of these differentially expressed genes and genetic changes must be further evaluated. Recently, Lin et al have defined the subgroup specific MB enhancers and super-enhancers responsible for tumor divergence, inferring distinct cells of origin based on master transcriptional regulators (Lin et al. 2016). The activity and expression of master transcriptional regulators such as LIMX1A and OTX2 are tightly controlled during development but how they deviate from their normal functions and promote tumorigenesis is not fully

understood. Our study also demonstrate that OTX2 is a master regulator of the Group 3 and 4 MB transcriptional program, suggesting that OTX2 and its downstream effectors are potential therapeutic targets for these poorly characterized and highly aggressive Group 3 and 4 MBs.

# REFERENCES

# References:


Acampora, D., L. G. Di Giovannantonio, and A. Simeone. 2013. 'Otx2 is an intrinsic determinant of the embryonic stem cell state and is required for transition to a stable epiblast stem cell condition', *Development*, 140: 43-55.

Acampora, D., S. Mazan, Y. Lallemand, V. Avantaggiato, M. Maury, A. Simeone, and P. Brulet. 1995. 'Forebrain and midbrain regions are deleted in Otx2-/- mutants due to a defective anterior neuroectoderm specification during gastrulation', *Development*, 121: 3279-90.

Adamson, D. C., Q. Shi, M. Wortham, P. A. Northcott, C. Di, C. G. Duncan, J. Li, R. E. McLendon, D. D. Bigner, M. D. Taylor, and H. Yan. 2010. 'OTX2 is critical for the maintenance and progression of Shh-independent medulloblastomas', *Cancer Res*, 70: 181-91.

Ahlfeld, J., R. Favaro, P. Pagella, H. A. Kretzschmar, S. Nicolis, and U. Schuller. 2013. 'Sox2 requirement in sonic hedgehog-associated medulloblastoma', *Cancer Res*, 73: 3796-807.

Akagi, T., M. Mandai, S. Ooto, Y. Hirami, F. Osakada, R. Kageyama, N. Yoshimura, and M. Takahashi. 2004. 'Otx2 homeobox gene induces photoreceptor-specific phenotypes in cells derived from adult iris and ciliary tissue', *Invest Ophthalmol Vis Sci*, 45: 4570-5.

Akino, T., X. Han, H. Nakayama, B. McNeish, D. Zurakowski, A. Mammoto, M. Klagsbrun, and E. Smith. 2014. 'Netrin-1 promotes medulloblastoma cell invasiveness and angiogenesis, and demonstrates elevated expression in tumor tissue and urine of patients with pediatric medulloblastoma', *Cancer Res*, 74: 3716-26.

Ali, J. L., B. J. Lagasse, A. J. Minuk, A. J. Love, A. I. Moraya, L. Lam, G. Arthur, S. B. Gibson, L. C. Morrison, T. E. Werbowetski-Ogilvie, Y. Fu, and M. W. Nachtigal. 2015. 'Differential cellular responses induced by dorsomorphin and LDN-193189 in chemotherapy-sensitive and chemotherapy-resistant human epithelial ovarian cancer cells', *Int J Cancer*, 136: E455-69.

Ang, S. L., R. A. Conlon, O. Jin, and J. Rossant. 1994. 'Positive and negative signals from mesoderm regulate the expression of mouse Otx2 in ectoderm explants', *Development*, 120: 2979-89.

Ang, S. L., O. Jin, M. Rhinn, N. Daigle, L. Stevenson, and J. Rossant. 1996. 'A targeted mouse Otx2 mutation leads to severe defects in gastrulation and formation of axial mesoderm and to deletion of rostral brain', *Development*, 122: 243-52.

Annibali, D., J. R. Whitfield, E. Favuzzi, T. Jauset, E. Serrano, I. Cuartas, S. Redondo-Campos, G. Folch, A. Gonzalez-Junca, N. M. Sodir, D. Masso-Valles, M. E. Beaulieu, L. B. Swigart, M. M. Mc Gee, M. P. Somma, S. Nasi, J. Seoane, G. I. Evan, and L. Soucek. 2014. 'Myc inhibition is effective against glioma and reveals a role for Myc in proficient mitosis', *Nat Commun*, 5: 4632.

Ayrault, O., F. Zindy, J. Rehg, C. J. Sherr, and M. F. Roussel. 2009. 'Two tumor suppressors, p27Kip1 and patched-1, collaborate to prevent medulloblastoma', *Mol Cancer Res*, 7: 33-40.

Baas, D., K. M. Bumsted, J. A. Martinez, F. M. Vaccarino, K. C. Wikler, and C. J. Barnstable. 2000. 'The subcellular localization of Otx2 is cell-type specific and developmentally regulated in the mouse retina', *Brain Res Mol Brain Res*, 78: 26-37.

Baeza, N., J. Masuoka, P. Kleihues, and H. Ohgaki. 2003. 'AXIN1 mutations but not deletions in cerebellar medulloblastomas. Oncogene. ', *Oncogene*, 22: 632-6.

Bai, R., I. M. Siu, B. M. Tyler, V. Staedtke, G. L. Gallia, and G. J. Riggins. 2010. 'Evaluation of retinoic acid therapy for OTX2-positive medulloblastomas', *Neuro Oncol*, 12: 655-63.

Bai, R. Y., V. Staedtke, H. G. Lidov, C. G. Eberhart, and G. J. Riggins. 2012. 'OTX2 represses myogenic and neuronal differentiation in medulloblastoma cells', *Cancer Res*, 72: 5988-6001.

Baker, D. E., N. J. Harrison, E. Maltby, K. Smith, H. D. Moore, P. J. Shaw, P. R. Heath, H. Holden, and P. W. Andrews. 2007. 'Adaptation to culture of human embryonic stem cells and oncogenesis in vivo', *Nat Biotechnol*, 25: 207-15.

Bandopadhayay, P., G. Bergthold, B. Nguyen, S. Schubert, S. Gholamin, Y. Tang, S. Bolin, S. E. Schumacher, R. Zeid, S. Masoud, F. Yu, N. Vue, W. J. Gibson, B. R. Paolella, S. S. Mitra, S. H. Cheshier, J. Qi, K. W. Liu, R. Wechsler-Reya, W. A. Weiss, F. J. Swartling, M. W. Kieran, J. E. Bradner, R. Beroukhim, and Y. J. Cho. 2014. 'BET bromodomain inhibition of MYC-amplified medulloblastoma', *Clin Cancer Res*, 20: 912-25.

Baryawno, N., B. Sveinbjornsson, S. Eksborg, C. S. Chen, P. Kogner, and J. I. Johnsen. 2010. 'Small-molecule inhibitors of phosphatidylinositol 3-kinase/Akt signaling inhibit Wnt/beta-catenin pathway cross-talk and suppress medulloblastoma growth', *Cancer Res*, 70: 266-76.

Bass, A. J., H. Watanabe, C. H. Mermel, S. Yu, S. Perner, R. G. Verhaak, S. Y. Kim, L. Wardwell, P. Tamayo, I. Gat-Viks, A. H. Ramos, M. S. Woo, B. A. Weir, G. Getz, R. Beroukhim, M. O'Kelly, A. Dutt, O. Rozenblatt-Rosen, P. Dziunycz, J. Komisarof, L. R. Chirieac, C. J. Lafargue, V. Scheble, T. Wilbertz, C. Ma, S. Rao, H. Nakagawa, D. B. Stairs, L. Lin, T. J. Giordano, P. Wagner, J. D. Minna, A. F. Gazdar, C. Q. Zhu, M. S. Brose, I. Cecconello, U. R. Jr, S. K. Marie, O. Dahl, R. A. Shivdasani, M. S. Tsao, M. A. Rubin, K. K. Wong, A. Regev, W. C. Hahn, D. G. Beer, A. K. Rustgi, and M. Meyerson. 2009. 'SOX2 is an amplified lineage-survival oncogene in lung and esophageal squamous cell carcinomas', *Nat Genet*, 41: 1238-42.

Beauchamp, E. M., L. Ringer, G. Bulut, K. P. Sajwan, M. D. Hall, Y. C. Lee, D. Peaceman, M. Ozdemirli, O. Rodriguez, T. J. Macdonald, C. Albanese, J. A. Toretsky, and A. Uren. 2011. 'Arsenic trioxide inhibits human cancer cell growth and tumor development in mice by blocking Hedgehog/GLI pathway', *J Clin Invest*, 121: 148-60.

Beby, F., M. Housset, N. Fossat, C. Le Greneur, F. Flamant, P. Godement, and T. Lamonerie. 2010. 'Otx2 gene deletion in adult mouse retina induces rapid RPE dystrophy and slow photoreceptor degeneration', *PLoS One*, 5: e11673.

Beby, F., and T. Lamonerie. 2013. 'The homeobox gene Otx2 in development and disease', *Exp Eye Res*, 111: 9-16.

Ben-David, U., and N. Benvenisty. 2011. 'The tumorigenicity of human embryonic and induced pluripotent stem cells', *Nat Rev Cancer*, 11: 268-77.

Ben-Porath, I., M. W. Thomson, V. J. Carey, R. Ge, G. W. Bell, A. Regev, and R. A. Weinberg. 2008. 'An embryonic stem cell-like gene expression signature in poorly differentiated aggressive human tumors', *Nat Genet*, 40: 499-507.

Bennett, M. R., and V. J. Balcar. 1999. 'Forty years of amino acid transmission in the brain', *Neurochem Int*, 35: 269-80.

Berman, D. M., S. S. Karhadkar, A. R. Hallahan, J. I. Pritchard, C. G. Eberhart, D. N. Watkins, J. K. Chen, M. K. Cooper, J. Taipale, J. M. Olson, and P. A. Beachy. 2002.

'Medulloblastoma growth inhibition by hedgehog pathway blockade', *Science*, 297: 1559-61.

Bhatia, S., K. Hirsch, N. A. Baig, O. Rodriguez, O. Timofeeva, K. Kavanagh, Y. C. Lee, X. J. Wang, C. Albanese, and S. D. Karam. 2015. 'Effects of altered ephrin-A5 and EphA4/EphA7 expression on tumor growth in a medulloblastoma mouse model', *J Hematol Oncol*, 8: 105.

Biancotti, J. C., K. Narwani, N. Buehler, B. Mandefro, T. Golan-Lev, O. Yanuka, A. Clark, D. Hill, N. Benvenisty, and N. Lavon. 2010. 'Human embryonic stem cells as models for aneuploid chromosomal syndromes', *Stem Cells*, 28: 1530-40.

Boon, K., C. G. Eberhart, and G. J. Riggins. 2005. 'Genomic amplification of orthodenticle homologue 2 in medulloblastomas', *Cancer Res*, 65: 703-7.

Borrell, V., A. Cardenas, G. Ciceri, J. Galceran, N. Flames, R. Pla, S. Nobrega-Pereira, C. Garcia-Frigola, S. Peregrin, Z. Zhao, L. Ma, M. Tessier-Lavigne, and O. Marin. 2012. 'Slit/Robo signaling modulates the proliferation of central nervous system progenitors', *Neuron*, 76: 338-52.

Bovolenta, P., A. Mallamaci, P. Briata, G. Corte, and E. Boncinelli. 1997. 'Implication of OTX2 in pigment epithelium determination and neural retina differentiation', *J Neurosci*, 17: 4243-52.

Briggs, K. J., I. M. Corcoran-Schwartz, W. Zhang, T. Harcke, W. L. Devereux, S. B. Baylin, C. G. Eberhart, and D. N. Watkins. 2008. 'Cooperation between the Hic1 and Ptch1 tumor suppressors in medulloblastoma', *Genes Dev*, 22: 770-85.

Broccoli, V., E. Boncinelli, and W. Wurst. 1999. 'The caudal limit of Otx2 expression positions the isthmic organizer', *Nature*, 401: 164-8.

Brose, K., K. S. Bland, K. H. Wang, D. Arnott, W. Henzel, C. S. Goodman, M. Tessier-Lavigne, and T. Kidd. 1999. 'Slit proteins bind Robo receptors and have an evolutionarily conserved role in repulsive axon guidance', *Cell*, 96: 795-806.

Bueno, C., R. Montes, G. J. Melen, V. Ramos-Mejia, P. J. Real, V. Ayllon, L. Sanchez, G. Ligero, I. Gutierrez-Aranda, A. F. Fernandez, M. F. Fraga, I. Moreno-Gimeno, D. Burks, C. Plaza-Calonge Mdel, J. C. Rodriguez-Manzaneque, and P. Menendez. 2012. 'A human ESC model for MLL-AF4 leukemic fusion gene reveals an impaired early hematopoietic-endothelial specification', *Cell Res*, 22: 986-1002.

Bunt, J., T. G. de Haas, N. E. Hasselt, D. A. Zwijnenburg, J. Koster, R. Versteeg, and M. Kool. 2010. 'Regulation of cell cycle genes and induction of senescence by overexpression of OTX2 in medulloblastoma cell lines', *Mol Cancer Res*, 8: 1344-57.

Bunt, J., N. E. Hasselt, D. A. Zwijnenburg, M. Hamdi, J. Koster, R. Versteeg, and M. Kool. 2012. 'OTX2 directly activates cell cycle genes and inhibits differentiation in medulloblastoma cells', *Int J Cancer*, 131: E21-32.

Buonamici, S., J. Williams, M. Morrissey, A. Wang, R. Guo, A. Vattay, K. Hsiao, J. Yuan, J. Green, B. Ospina, Q. Yu, L. Ostrom, P. Fordjour, D. L. Anderson, J. E. Monahan, J. F. Kelleher, S. Peukert, S. Pan, X. Wu, S. M. Maira, C. Garcia-Echeverria, K. J. Briggs, D. N. Watkins, Y. M. Yao, C. Lengauer, M. Warmuth, W. R. Sellers, and M. Dorsch. 2010. 'Interfering with resistance to smoothened antagonists by inhibition of the PI3K pathway in medulloblastoma', *Sci Transl Med*, 2: 51ra70.

Cajal, M., K. A. Lawson, B. Hill, A. Moreau, J. Rao, A. Ross, J. Collignon, and A. Camus. 2012. 'Clonal and molecular analysis of the prospective anterior neural boundary in the mouse embryo', *Development*, 139: 423-36.

Cantos, R., L. K. Cole, D. Acampora, A. Simeone, and D. K. Wu. 2000. 'Patterning of the mammalian cochlea', *Proc Natl Acad Sci U S A*, 97: 11707-13.

Chadwick, K., L. Wang, L. Li, P. Menendez, B. Murdoch, A. Rouleau, and M. Bhatia. 2003. 'Cytokines and BMP-4 promote hematopoietic differentiation of human embryonic stem cells', *Blood*, 102: 906-15.

Chan, Y. M., A. de Guillebon, M. Lang-Muritano, L. Plummer, F. Cerrato, S. Tsiaras, A. Gaspert, H. B. Lavoie, C. H. Wu, W. F. Crowley, Jr., J. K. Amory, N. Pitteloud, and S. B. Seminara. 2009. 'GNRH1 mutations in patients with idiopathic hypogonadotropic hypogonadism', *Proc Natl Acad Sci U S A*, 106: 11703-8.

Chang, Q., Z. Chen, J. You, M. A. McNutt, T. Zhang, Z. Han, X. Zhang, E. Gong, and J. Gu. 2007. 'All-trans-retinoic acid induces cell growth arrest in a human medulloblastoma cell line', *J Neurooncol*, 84: 263-7.

Chatelain, G., N. Fossat, G. Brun, and T. Lamonerie. 2006. 'Molecular dissection reveals decreased activity and not dominant negative effect in human OTX2 mutants', *J Mol Med (Berl)*, 84: 604-15.

Chen, H. L., F. Pistollato, D. J. Hoeppner, H. T. Ni, R. D. McKay, and D. M. Panchision. 2007. 'Oxygen tension regulates survival and fate of mouse central nervous system precursors at multiple levels', *Stem Cells*, 25: 2291-301.

Chen, H., K. Qian, Z. Du, J. Cao, A. Petersen, H. Liu, L. W. th Blackbourn, C. L. Huang, A. Errigo, Y. Yin, J. Lu, M. Ayala, and S. C. Zhang. 2014. 'Modeling ALS with iPSCs reveals that mutant SOD1 misregulates neurofilament balance in motor neurons', *Cell Stem Cell*, 14: 796-809.

Chen, W., Q. Li, W. A. Hudson, A. Kumar, N. Kirchhof, and J. H. Kersey. 2006. 'A murine Mll-AF4 knock-in model results in lymphoid and myeloid deregulation and hematologic malignancy', *Blood*, 108: 669-77.

Chenn, A. 2008. 'Wnt/beta-catenin signaling in cerebral cortical development', *Organogenesis*, 4: 76-80.

Cho, Y. J., A. Tsherniak, P. Tamayo, S. Santagata, A. Ligon, H. Greulich, R. Berhoukim, V. Amani, L. Goumnerova, C. G. Eberhart, C. C. Lau, J. M. Olson, R. J. Gilbertson, A. Gajjar, O. Delattre, M. Kool, K. Ligon, M. Meyerson, J. P. Mesirov, and S. L. Pomeroy. 2011. 'Integrative genomic analysis of medulloblastoma identifies a molecular subgroup that drives poor clinical outcome', *J Clin Oncol*, 29: 1424-30.

Chung, C. Y., P. Licznerski, K. N. Alavian, A. Simeone, Z. Lin, E. Martin, J. Vance, and O. Isacson. 2010. 'The transcription factor orthodenticle homeobox 2 influences axonal projections and vulnerability of midbrain dopaminergic neurons', *Brain*, 133: 2022-31.

Cimadamore, F., A. Amador-Arjona, C. Chen, C. T. Huang, and A. V. Terskikh. 2013. 'SOX2-LIN28/let-7 pathway regulates proliferation and neurogenesis in neural precursors', *Proc Natl Acad Sci U S A*, 110: E3017-26.

Cimmino, F., M. N. Scoppettuolo, M. Carotenuto, P. De Antonellis, V. D. Dato, G. De Vita, and M. Zollo. 2012. 'Norcantharidin impairs medulloblastoma growth by inhibition of Wnt/beta-catenin signaling', *J Neurooncol*, 106: 59-70.

Clark, A. T. 2007. 'The stem cell identity of testicular cancer', *Stem Cell Rev*, 3: 49-59.

D'Amour, K. A., A. G. Bang, S. Eliazer, O. G. Kelly, A. D. Agulnick, N. G. Smart, M. A. Moorman, E. Kroon, M. K. Carpenter, and E. E. Baetge. 2006. 'Production of pancreatic hormone-expressing endocrine cells from human embryonic stem cells', *Nat Biotechnol*, 24: 1392-401.

da Silva, R., S.K.N. Marie, M. Uno, H. Matushita, A. Wakamatsu, S Rosemberg, and S.M. BOba-Shinjo. 2013. 'CTNNB1, AXIN1 and APC expression analysis of different medulloblastoma variants', *Clinics (Sao Paulo)*, 68: 167-72.

Dahmane, N., P. Sanchez, Y. Gitton, V. Palma, T. Sun, M. Beyna, H. Weiner, and A. Ruiz i Altaba. 2001. 'The Sonic Hedgehog-Gli pathway regulates dorsal brain growth and tumorigenesis', *Development*, 128: 5201-12.

Danno, H., T. Michiue, K. Hitachi, A. Yukita, S. Ishiura, and M. Asashima. 2008. 'Molecular links among the causative genes for ocular malformation: Otx2 and Sox2 coregulate Rax expression', *Proc Natl Acad Sci U S A*, 105: 5408-13.

Dateki, S., K. Kosaka, K. Hasegawa, H. Tanaka, N. Azuma, S. Yokoya, K. Muroya, M. Adachi, T. Tajima, K. Motomura, E. Kinoshita, H. Moriuchi, N. Sato, M. Fukami, and T. Ogata. 2010. 'Heterozygous orthodenticle homeobox 2 mutations are associated with variable pituitary phenotype', *J Clin Endocrinol Metab*, 95: 756-64.

de Bont, J. M., R. J. Packer, E. M. Michiels, M. L. den Boer, and R. Pieters. 2008. 'Biological background of pediatric medulloblastoma and ependymoma: a review from a translational research perspective', *Neuro Oncol*, 10: 1040-60.

de Haas, T., E. Oussoren, W. Grajkowska, M. Perek-Polnik, M. Popovic, L. Zadravec-Zaletel, M. Perera, G. Corte, O. Wirths, P. van Sluis, T. Pietsch, D. Troost, F. Baas, R. Versteeg, and M. Kool. 2006. 'OTX1 and OTX2 expression correlates with the clinicopathologic classification of medulloblastomas', *J Neuropathol Exp Neurol*, 65: 176-86.

DeSouza, R. M., B. R. Jones, S. P. Lowis, and K. M. Kurian. 2014. 'Pediatric medulloblastoma - update on molecular classification driving targeted therapies', *Front Oncol*, 4: 176.

Di, C., S. Liao, D. C. Adamson, T. J. Parrett, D. K. Broderick, Q. Shi, C. Lengauer, J. M. Cummins, V. E. Velculescu, D. W. Fults, R. E. McLendon, D. D. Bigner, and H. Yan. 2005. 'Identification of OTX2 as a medulloblastoma oncogene whose product can be targeted by all-trans retinoic acid', *Cancer Res*, 65: 919-24.

Di Giovannantonio, L. G., M. Di Salvio, D. Acampora, N. Prakash, W. Wurst, and A. Simeone. 2013. 'Otx2 selectively controls the neurogenesis of specific neuronal subtypes of the ventral tegmental area and compensates En1-dependent neuronal loss and MPTP vulnerability', *Dev Biol*, 373: 176-83.

Di Salvio, M., L. G. Di Giovannantonio, D. Acampora, R. Prosperi, D. Omodei, N. Prakash, W. Wurst, and A. Simeone. 2010a. 'Otx2 controls neuron subtype identity in ventral tegmental area and antagonizes vulnerability to MPTP', *Nat Neurosci*, 13: 1481-8.

Di Salvio, M., L. G. Di Giovannantonio, D. Omodei, D. Acampora, and A. Simeone. 2010b. 'Otx2 expression is restricted to dopaminergic neurons of the ventral tegmental area in the adult brain', *Int J Dev Biol*, 54: 939-45.

Diaczok, D., S. DiVall, I. Matsuo, F. E. Wondisford, A. M. Wolfe, and S. Radovick. 2011. 'Deletion of Otx2 in GnRH neurons results in a mouse model of hypogonadotropic hypogonadism', *Mol Endocrinol*, 25: 833-46.

Dijkgraaf, G. J., B. Alicke, L. Weinmann, T. Januario, K. West, Z. Modrusan, D. Burdick, R. Goldsmith, K. Robarge, D. Sutherlin, S. J. Scales, S. E. Gould, R. L. Yauch, and F. J. de Sauvage. 2011. 'Small molecule inhibition of GDC-0449 refractory smoothened mutants and downstream mechanisms of drug resistance', *Cancer Res*, 71: 435-44.

Dingwall, S., J. B. Lee, B. Guezguez, A. Fiebig, J. McNicol, D. Boreham, T. J. Collins, and M. Bhatia. 2015. 'Neoplastic human embryonic stem cells as a model of radiation resistance of human cancer stem cells', *Oncotarget*, 6: 22258-69.

Donehower, L. A., M. Harvey, B. L. Slagle, M. J. McArthur, C. A. Montgomery, Jr., J. S. Butel, and A. Bradley. 1992. 'Mice deficient for p53 are developmentally normal but susceptible to spontaneous tumours', *Nature*, 356: 215-21.

Doyle, B., J. P. Morton, D. W. Delaney, R. A. Ridgway, J. A. Wilkins, and O. J. Sansom. 2010. 'p53 mutation and loss have different effects on tumourigenesis in a novel mouse model of pleomorphic rhabdomyosarcoma', *J Pathol*, 222: 129-37.

Du, Z., D. Jia, S. Liu, F. Wang, G. Li, Y. Zhang, X. Cao, E. A. Ling, and A. Hao. 2009. 'Oct4 is expressed in human gliomas and promotes colony formation in glioma cells', *Glia*, 57: 724-33.

Eberhart, C.G., A. Chaudhry, R.W. Daniel, L. Khaki, K.V. Shah, and P.E. Gravitt. 2005. 'Increased p53 immunopositivity in anaplastic medulloblastoma and supratentorial PNET is not caused by JC virus.', *BMC Cancer*, 5: 441-9.

Ecke, I., F. Petry, A. Rosenberger, S. Tauber, S. Monkemeyer, I. Hess, C. Dullin, S. Kimmina, J. Pirngruber, S. A. Johnsen, A. Uhmann, F. Nitzki, L. Wojnowski, W. Schulz-Schaeffer, O. Witt, and H. Hahn. 2009. 'Antitumor effects of a combined 5-aza-2'deoxycytidine and valproic acid treatment on rhabdomyosarcoma and medulloblastoma in Ptch mutant mice', *Cancer Res*, 69: 887-95.

Ellison, D. 2002. 'Classifying the medulloblastoma: insights from morphology and molecular genetics', *Neuropathol Appl Neurobiol*, 28: 257-82.

Ellison, D. W., J. Dalton, M. Kocak, S. L. Nicholson, C. Fraga, G. Neale, A. M. Kenney, D. J. Brat, A. Perry, W. H. Yong, R. E. Taylor, S. Bailey, S. C. Clifford, and R. J. Gilbertson. 2011. 'Medulloblastoma: clinicopathological correlates of SHH, WNT, and non-SHH/WNT molecular subgroups', *Acta Neuropathol*, 121: 381-96.

Emerson, M. M., and C. L. Cepko. 2011. 'Identification of a retina-specific Otx2 enhancer element active in immature developing photoreceptors', *Dev Biol*, 360: 241-55.

Enguita-German, M., P. Schiapparelli, J. A. Rey, and J. S. Castresana. 2010. 'CD133+ cells from medulloblastoma and PNET cell lines are more resistant to cyclopamine inhibition of the sonic hedgehog signaling pathway than CD133- cells', *Tumour Biol*, 31: 381-90.

Fan, X., W. Matsui, L. Khaki, D. Stearns, J. Chun, Y. M. Li, and C. G. Eberhart. 2006. 'Notch pathway inhibition depletes stem-like cells and blocks engraftment in embryonal brain tumors', *Cancer Res*, 66: 7445-52.

Fan, X., I. Mikolaenko, I. Elhassan, X. Ni, Y. Wang, D. Ball, D. J. Brat, A. Perry, and C. G. Eberhart. 2004. 'Notch1 and notch2 have opposite effects on embryonal brain tumor growth', *Cancer Res*, 64: 7787-93.

Ferrari, S., V. R. Harley, A. Pontiggia, P. N. Goodfellow, R. Lovell-Badge, and M. E. Bianchi. 1992. 'SRY, like HMG1, recognizes sharp angles in DNA', *Embo j*, 11: 4497-506.

Finkelstein, R., and E. Boncinelli. 1994. 'From fly head to mammalian forebrain: the story of otd and Otx', *Trends Genet*, 10: 310-5.

Fossat, N., G. Chatelain, G. Brun, and T. Lamonerie. 2006. 'Temporal and spatial delineation of mouse Otx2 functions by conditional self-knockout', *EMBO Rep*, 7: 824-30.

Fossat, N., C. Le Greneur, F. Beby, S. Vincent, P. Godement, G. Chatelain, and T. Lamonerie. 2007. 'A new GFP-tagged line reveals unexpected Otx2 protein localization in retinal photoreceptors', *BMC Dev Biol*, 7: 122.

Frange, P., C. Alapetite, G. Gaboriaud, D. Bours, J. M. Zucker, M. Zerah, H. Brisse, M. Chevignard, V. Mosseri, E. Bouffet, and F. Doz. 2009. 'From childhood to adulthood:

long-term outcome of medulloblastoma patients. The Institut Curie experience (1980-2000)', *J Neurooncol*, 95: 271-9.

Freemantle, S. J., M. J. Spinella, and E. Dmitrovsky. 2003. 'Retinoids in cancer therapy and chemoprevention: promise meets resistance', *Oncogene*, 22: 7305-15.

Friedman, H. S., P. C. Burger, S. H. Bigner, J. Q. Trojanowski, G. M. Brodeur, X. M. He, C. J. Wikstrand, J. Kurtzberg, M. E. Berens, E. C. Halperin, and et al. 1988. 'Phenotypic and genotypic analysis of a human medulloblastoma cell line and transplantable xenograft (D341 Med) demonstrating amplification of c-myc', *Am J Pathol*, 130: 472-84.

Friedman, H. S., P. C. Burger, S. H. Bigner, J. Q. Trojanowski, C. J. Wikstrand, E. C. Halperin, and D. D. Bigner. 1985. 'Establishment and characterization of the human medulloblastoma cell line and transplantable xenograft D283 Med', *J Neuropathol Exp Neurol*, 44: 592-605.

Fu, Y. S., Q. Wang, J. X. Ma, X. H. Yang, M. L. Wu, K. L. Zhang, Q. Y. Kong, X. Y. Chen, Y. Sun, N. N. Chen, X. H. Shu, H. Li, and J. Liu. 2012. 'CRABP-II methylation: a critical determinant of retinoic acid resistance of medulloblastoma cells', *Mol Oncol*, 6: 48-61.

Funato, K., T. Major, P. W. Lewis, C. D. Allis, and V. Tabar. 2014. 'Use of human embryonic stem cells to model pediatric gliomas with H3.3K27M histone mutation', *Science*, 346: 1529-33.

Gajjar, A., M. Chintagumpala, D. Ashley, .S Kellie, L.E. Kun, T.E. Merchant, Woo. S., G. Wheeler, V. Ahern, M.J. Krasin, M. Fouladi, A. Broniscer, R. Krance, G.A. Hale, C.F. Stewart, R. Dauser, R.A. Sanford, C. Fuller, C. Lau, J.M. Boyett, D. Wallace, and R.J. Gilbertson. 2006. 'Risk-adapted craniospinal radiotherapy followed by high-dose chemotherapy and stem-cell rescue in children with newly diagnosed medulloblastoma (St Jude Medulloblastoma-96): long-term results from a prospective, multicentre trial.', *Lancet Oncol*, 7: 813-20.

Gajjar, A. J., and G. W. Robinson. 2014. 'Medulloblastoma-translating discoveries from the bench to the bedside', *Nat Rev Clin Oncol*, 11: 714-22.

Gajjar, A., R. J. Packer, N. K. Foreman, K. Cohen, D. Haas-Kogan, and T. E. Merchant. 2013. 'Children's Oncology Group's 2013 blueprint for research: central nervous system tumors', *Pediatr Blood Cancer*, 60: 1022-6.

Gamble, J. A., D. K. Karunadasa, J. R. Pape, M. J. Skynner, M. G. Todman, R. J. Bicknell, J. P. Allen, and A. E. Herbison. 2005. 'Disruption of ephrin signaling associates with disordered axophilic migration of the gonadotropin-releasing hormone neurons', *J Neurosci*, 25: 3142-50.

Gangemi, R. M., F. Griffero, D. Marubbi, M. Perera, M. C. Capra, P. Malatesta, G. L. Ravetti, G. L. Zona, A. Daga, and G. Corte. 2009. 'SOX2 silencing in glioblastoma tumor-initiating cells causes stop of proliferation and loss of tumorigenicity', *Stem Cells*, 27: 40-8.

Gerrard, L., L. Rodgers, and W. Cui. 2005. 'Differentiation of human embryonic stem cells to neural lineages in adherent culture by blocking bone morphogenetic protein signaling', *Stem Cells*, 23: 1234-41.

Giangaspero, F., G. Perilongo, M. P. Fondelli, M. Brisigotti, C. Carollo, R. Burnelli, P. C. Burger, and M. L. Garre. 1999. 'Medulloblastoma with extensive nodularity: a variant with favorable prognosis', *J Neurosurg*, 91: 971-7.

Giangaspero, F., S. Wellek, J. Masuoka, M. Gessi, P. Kleihues, and H. Ohgaki. 2006. 'Stratification of medulloblastoma on the basis of histopathological grading', *Acta Neuropathol*, 112: 5-12.

Gibson, D. A., S. Tymanskyj, R. C. Yuan, H. C. Leung, J. L. Lefebvre, J. R. Sanes, A. Chedotal, and L. Ma. 2014. 'Dendrite self-avoidance requires cell-autonomous slit/robo signaling in cerebellar purkinje cells', *Neuron*, 81: 1040-56.

Gibson, P., Y. Tong, G. Robinson, M. C. Thompson, D. S. Currle, C. Eden, T. A. Kranenburg, T. Hogg, H. Poppleton, J. Martin, D. Finkelstein, S. Pounds, A. Weiss, Z. Patay, M. Scoggins, R. Ogg, Y. Pei, Z. J. Yang, S. Brun, Y. Lee, F. Zindy, J. C. Lindsey, M. M. Taketo, F. A. Boop, R. A. Sanford, A. Gajjar, S. C. Clifford, M. F. Roussel, P. J. McKinnon, D. H. Gutmann, D. W. Ellison, R. Wechsler-Reya, and R. J. Gilbertson. 2010. 'Subtypes of medulloblastoma have distinct developmental origins', *Nature*, 468: 1095-9.

Gilbertson, R. J., and D. W. Ellison. 2008. 'The origins of medulloblastoma subtypes', *Annu Rev Pathol*, 3: 341-65.

Gomez-Orte, E., B. Saenz-Narciso, S. Moreno, and J. Cabello. 2013. 'Multiple functions of the noncanonical Wnt pathway', *Trends Genet*, 29: 545-53.

Goodrich, L. V., L. Milenkovic, K. M. Higgins, and M. P. Scott. 1997. 'Altered neural cell fates and medulloblastoma in mouse patched mutants', *Science*, 277: 1109-13.

Gorlin, R. J. 1995. 'Nevoid basal cell carcinoma syndrome', *Dermatol Clin*, 13: 113-25.

Grammel, D., M. Warmuth-Metz, A. O. von Bueren, M. Kool, T. Pietsch, H. A. Kretzschmar, D. H. Rowitch, S. Rutkowski, S. M. Pfister, and U. Schuller. 2012. 'Sonic hedgehog-associated medulloblastoma arising from the cochlear nuclei of the brainstem', *Acta Neuropathol*, 123: 601-14.

Grange, C., S. Lanzardo, F. Cavallo, G. Camussi, and B. Bussolati. 2008. 'Sca-1 identifies the tumor-initiating cells in mammary tumors of BALB-neuT transgenic mice', *Neoplasia*, 10: 1433-43.

Griffin, C. A., A. L. Hawkins, R. J. Packer, L. B. Rorke, and B. S. Emanuel. 1988. 'Chromosome abnormalities in pediatric brain tumors', *Cancer Res*, 48: 175-80.

Grotzer, M. A., M. D. Hogarty, A. J. Janss, X. Liu, H. Zhao, A. Eggert, L. N. Sutton, L. B. Rorke, G. M. Brodeur, and P. C. Phillips. 2001. 'MYC messenger RNA expression predicts survival outcome in childhood primitive neuroectodermal tumor/medulloblastoma', *Clin Cancer Res*, 7: 2425-33.

Gumireddy, K., L. N. Sutton, P. C. Phillips, and C. D. Reddy. 2003. 'All-trans-retinoic acid-induced apoptosis in human medulloblastoma: activation of caspase-3/poly(ADP-ribose) polymerase 1 pathway', *Clin Cancer Res*, 9: 4052-9.

Haberler, C., I. Slavc, T. Czech, E. Gelpi, H. Heinzl, H. Budka, C. Urban, M. Scarpatetti, G. Ebetsberger-Dachs, C. Schindler, N. Jones, A. Klein-Franke, H. Maier, B. Jauk, A. Kiefer, and J. A. Hainfellner. 2006. 'Histopathological prognostic factors in medulloblastoma: high expression of survivin is related to unfavourable outcome', *Eur J Cancer*, 42: 2996-3003.

Hahn, H., C. Wicking, P. G. Zaphiropoulous, M. R. Gailani, S. Shanley, A. Chidambaram, I. Vorechovsky, E. Holmberg, A. B. Unden, S. Gillies, K. Negus, I. Smyth, C. Pressman, D. J. Leffell, B. Gerrard, A. M. Goldstein, M. Dean, R. Toftgard, G. Chenevix-Trench, B. Wainwright, and A. E. Bale. 1996. 'Mutations of the human homolog of Drosophila patched in the nevoid basal cell carcinoma syndrome', *Cell*, 85: 841-51.

Hall, A. C., F. R. Lucas, and P. C. Salinas. 2000. 'Axonal remodeling and synaptic differentiation in the cerebellum is regulated by WNT-7a signaling.', *Cell*, 100: 525-35.

Hallahan, A. R., J. I. Pritchard, S. Hansen, M. Benson, J. Stoeck, B. A. Hatton, T. L. Russell, R. G. Ellenbogen, I. D. Bernstein, P. A. Beachy, and J. M. Olson. 2004. 'The SmoA1 mouse model reveals that notch signaling is critical for the growth and survival of sonic hedgehog-induced medulloblastomas', *Cancer Res*, 64: 7794-800.

Hambardzumyan, D., O. J. Becher, M. K. Rosenblum, P. P. Pandolfi, K. Manova-Todorova, and E. C. Holland. 2008. 'PI3K pathway regulates survival of cancer stem cells residing in the perivascular niche following radiation in medulloblastoma in vivo', *Genes Dev*, 22: 436-48.

Han, Y. G., H. J. Kim, A. A. Dlugosz, D. W. Ellison, R. J. Gilbertson, and A. Alvarez-Buylla. 2009. 'Dual and opposing roles of primary cilia in medulloblastoma development', *Nat Med*, 15: 1062-5.

Hanel, W., N. Marchenko, S. Xu, S. X. Yu, W. Weng, and U. Moll. 2013. 'Two hot spot mutant p53 mouse models display differential gain of function in tumorigenesis', *Cell Death Differ*, 20: 898-909.

Hartmann, W., B. Digon-Sontgerath, A. Koch, A. Waha, E. Endl, I. Dani, D. Denkhaus, C. G. Goodyer, N. Sorensen, O. D. Wiestler, and T. Pietsch. 2006. 'Phosphatidylinositol 3'-kinase/AKT signaling is activated in medulloblastoma cell proliferation and is associated with reduced expression of PTEN', *Clin Cancer Res*, 12: 3019-27.

Hassounah, N. B., T. A. Bunch, and K. M. McDermott. 2012. 'Molecular pathways: the role of primary cilia in cancer progression and therapeutics with a focus on Hedgehog signaling', *Clin Cancer Res*, 18: 2429-35.

Hatton, B. A., E. H. Villavicencio, J. Pritchard, M. LeBlanc, S. Hansen, M. Ulrich, S. Ditzler, B. Pullar, M. R. Stroud, and J. M. Olson. 2010. 'Notch signaling is not essential in sonic hedgehog-activated medulloblastoma', *Oncogene*, 29: 3865-72.

Hatton, B. A., E. H. Villavicencio, K. D. Tsuchiya, J. I. Pritchard, S. Ditzler, B. Pullar, S. Hansen, S. E. Knoblaugh, D. Lee, C. G. Eberhart, A. R. Hallahan, and J. M. Olson. 2008. 'The Smo/Smo model: hedgehog-induced medulloblastoma with 90% incidence and leptomeningeal spread', *Cancer Res*, 68: 1768-76.

He, T.C., A.B. Sparks, C. Rago, H. Hermeking, L. Zawel, L.T. da Costa, P.J. Morin, B. Vogelstein, and Kinzler K.W. 1998. 'Identification of c-MYC as a target of the APC pathway', *Science*, 281: 1509-12.

He, X. M., C. J. Wikstrand, H. S. Friedman, S. H. Bigner, S. Pleasure, J. Q. Trojanowski, and D. D. Bigner. 1991. 'Differentiation characteristics of newly established medulloblastoma cell lines (D384 Med, D425 Med, and D458 Med) and their transplantable xenografts', *Lab Invest*, 64: 833-43.

Herms, J., I. Neidt, B. Luscher, A. Sommer, P. Schurmann, T. Schroder, M. Bergmann, B. Wilken, S. Probst-Cousin, P. Hernaiz-Driever, J. Behnke, F. Hanefeld, T. Pietsch, and H. A. Kretzschmar. 2000. 'C-MYC expression in medulloblastoma and its prognostic value', *Int J Cancer*, 89: 395-402.

Higgins, D. M., R. Wang, B. Milligan, M. Schroeder, B. Carlson, J. Pokorny, S. H. Cheshier, F. B. Meyer, I. L. Weissman, J. N. Sarkaria, and J. R. Henley. 2013. 'Brain tumor stem cell multipotency correlates with nanog expression and extent of passaging in human glioblastoma xenografts', *Oncotarget*, 4: 792-801.

Hirth, F., S. Therianos, T. Loop, W. J. Gehring, H. Reichert, and K. Furukubo-Tokunaga. 1995. 'Developmental defects in brain segmentation caused by mutations of the homeobox genes orthodenticle and empty spiracles in Drosophila', *Neuron*, 15: 769-78.

Housset, M., A. Samuel, M. Ettaiche, A. Bemelmans, F. Beby, N. Billon, and T. Lamonerie. 2013. 'Loss of Otx2 in the adult retina disrupts retinal pigment epithelium function, causing photoreceptor degeneration', *J Neurosci*, 33: 9890-904.

Huang, H., B. M. Mahler-Araujo, A. Sankila, L. Chimelli, Y. Yonekawa, P. Kleihues, and H. Ohgaki. 2000. 'APC mutations in sporadic medulloblastomas', *Am J Pathol*, 156: 433-7.

Humke, E. W., K. V. Dorn, L. Milenkovic, M. P. Scott, and R. Rohatgi. 2010. 'The output of Hedgehog signaling is controlled by the dynamic association between Suppressor of Fused and the Gli proteins', *Genes Dev*, 24: 670-82.

Ikeya, M., S. M. Lee, J. E. Johnson, A. P. McMahon, and S. Takada. 1997. 'Wnt signalling required for expansion of neural crest and CNS progenitors', *Nature*, 389: 966-70.

Inda, M. M., J. Mercapide, J. Munoz, P. Coullin, G. Danglot, T. Tunon, J. M. Martinez-Penuela, J. M. Rivera, J. J. Burgos, A. Bernheim, and J. S. Castresana. 2004. 'PTEN and DMBT1 homozygous deletion and expression in medulloblastomas and supratentorial primitive neuroectodermal tumors', *Oncol Rep*, 12: 1341-7.

Inoue, T., B. L. Coles, K. Dorval, R. Bremner, Y. Bessho, R. Kageyama, S. Hino, M. Matsuoka, C. M. Craft, R. R. McInnes, F. Tremblay, G. T. Prusky, and D. van der Kooy. 2010. 'Maximizing functional photoreceptor differentiation from adult human retinal stem cells', *Stem Cells*, 28: 489-500.

Jacks, T., L. Remington, B. O. Williams, E. M. Schmitt, S. Halachmi, R. T. Bronson, and R. A. Weinberg. 1994. 'Tumor spectrum analysis in p53-mutant mice', *Curr Biol*, 4: 1-7.

Jacobsen, P. F., D. J. Jenkyn, and J. M. Papadimitriou. 1985. 'Establishment of a human medulloblastoma cell line and its heterotransplantation into nude mice', *J Neuropathol Exp Neurol*, 44: 472-85.

Jeibmann, A., K. Eikmeier, A. Linge, M. Kool, B. Koos, J. Schulz, S. Albrecht, K. Bartelheim, M. C. Fruhwald, S. M. Pfister, W. Paulus, and M. Hasselblatt. 2014. 'Identification of genes involved in the biology of atypical teratoid/rhabdoid tumours using Drosophila melanogaster', *Nat Commun*, 5: 4005.

Ji, J., T. E. Werbowetski-Ogilvie, B. Zhong, S. H. Hong, and M. Bhatia. 2009. 'Pluripotent transcription factors possess distinct roles in normal versus transformed human stem cells', *PLoS One*, 4: e8065.

Johansson, P. A., M. Irmler, D. Acampora, J. Beckers, A. Simeone, and M. Gotz. 2013. 'The transcription factor Otx2 regulates choroid plexus development and function', *Development*, 140: 1055-66.

Joksimovic, M., B. A. Yun, R. Kittappa, A. M. Anderegg, W. W. Chang, M. M. Taketo, R. D. McKay, and R. B. Awatramani. 2009. 'Wnt antagonism of Shh facilitates midbrain floor plate neurogenesis', *Nat Neurosci*, 12: 125-31.

Jones, D. T., N. Jager, M. Kool, T. Zichner, B. Hutter, M. Sultan, Y. J. Cho, T. J. Pugh, V. Hovestadt, A. M. Stutz, T. Rausch, H. J. Warnatz, M. Ryzhova, S. Bender, D. Sturm, S. Pleier, H. Cin, E. Pfaff, L. Sieber, A. Wittmann, M. Remke, H. Witt, S. Hutter, T. Tzaridis, J. Weischenfeldt, B. Raeder, M. Avci, V. Amstislavskiy, M. Zapatka, U. D. Weber, Q. Wang, B. Lasitschka, C. C. Bartholomae, M. Schmidt, C. von Kalle, V. Ast, C. Lawerenz, J. Eils, R. Kabbe, V. Benes, P. van Sluis, J. Koster, R. Volckmann, D. Shih, M. J. Betts, R. B. Russell, S. Coco, G. P. Tonini, U. Schuller, V. Hans, N. Graf, Y. J. Kim, C. Monoranu, W. Roggendorf, A. Unterberg, C. Herold-Mende, T. Milde, A. E. Kulozik, A. von Deimling, O. Witt, E. Maass, J. Rossler, M. Ebinger, M. U. Schuhmann, M. C. Fruhwald, M. Hasselblatt, N. Jabado, S. Rutkowski, A. O. von Bueren, D.

Williamson, S. C. Clifford, M. G. McCabe, V. P. Collins, S. Wolf, S. Wiemann, H. Lehrach, B. Brors, W. Scheurlen, J. Felsberg, G. Reifenberger, P. A. Northcott, M. D. Taylor, M. Meyerson, S. L. Pomeroy, M. L. Yaspo, J. O. Korbel, A. Korshunov, R. Eils, S. M. Pfister, and P. Lichter. 2012. 'Dissecting the genomic complexity underlying medulloblastoma', *Nature*, 488: 100-5.

Jung, Y. W., E. Hysolli, K. Y. Kim, Y. Tanaka, and I. H. Park. 2012. 'Human induced pluripotent stem cells and neurodegenerative disease: prospects for novel therapies', *Curr Opin Neurol*, 25: 125-30.

Karam, S. D., R. C. Burrows, C. Logan, S. Koblar, E. B. Pasquale, and M. Bothwell. 2000. 'Eph receptors and ephrins in the developing chick cerebellum: relationship to sagittal patterning and granule cell migration', *J Neurosci*, 20: 6488-500.

Kaur, R., C. Aiken, L. C. Morrison, R. Rao, M. R. Del Bigio, S. Rampalli, and T. Werbowetski-Ogilvie. 2015. 'OTX2 exhibits cell-context-dependent effects on cellular and molecular properties of human embryonic neural precursors and medulloblastoma cells', *Dis Model Mech*, 8: 1295-309.

Kawauchi, D., G. Robinson, T. Uziel, P. Gibson, J. Rehg, C. Gao, D. Finkelstein, C. Qu, S. Pounds, D. W. Ellison, R. J. Gilbertson, and M. F. Roussel. 2012. 'A mouse model of the most aggressive subgroup of human medulloblastoma', *Cancer Cell*, 21: 168-80.

Kelley, C. G., G. Lavorgna, M. E. Clark, E. Boncinelli, and P. L. Mellon. 2000. 'The Otx2 homeoprotein regulates expression from the gonadotropin-releasing hormone proximal promoter', *Mol Endocrinol*, 14: 1246-56.

Kenney, A. M., M. D. Cole, and D. H. Rowitch. 2003. 'Nmyc upregulation by sonic hedgehog signaling promotes proliferation in developing cerebellar granule neuron precursors', *Development*, 130: 15-28.

Kerjan, G., J. Dolan, C. Haumaitre, S. Schneider-Maunoury, H. Fujisawa, K. J. Mitchell, and A. Chedotal. 2005. 'The transmembrane semaphorin Sema6A controls cerebellar granule cell migration', *Nat Neurosci*, 8: 1516-24.

Kim, J., J. P. Hoffman, R. K. Alpaugh, A. D. Rhim, M. Reichert, B. Z. Stanger, E. E. Furth, A. R. Sepulveda, C. X. Yuan, K. J. Won, G. Donahue, J. Sands, A. A. Gumbs, and K. S. Zaret. 2013. 'An iPSC line from human pancreatic ductal adenocarcinoma undergoes early to invasive stages of pancreatic cancer progression', *Cell Rep*, 3: 2088-99.

Kim, J. W., and G. Lemke. 2006. 'Hedgehog-regulated localization of Vax2 controls eye development', *Genes Dev*, 20: 2833-47.

Kim, J., A. J. Woo, J. Chu, J. W. Snow, Y. Fujiwara, C. G. Kim, A. B. Cantor, and S. H. Orkin. 2010. 'A Myc network accounts for similarities between embryonic stem and cancer cell transcription programs', *Cell*, 143: 313-24.

Kimura, C., M. M. Shen, N. Takeda, S. Aizawa, and I. Matsuo. 2001. 'Complementary functions of Otx2 and Cripto in initial patterning of mouse epiblast', *Dev Biol*, 235: 12-32.

Kimura, C., N. Takeda, M. Suzuki, M. Oshimura, S. Aizawa, and I. Matsuo. 1997. 'Cis-acting elements conserved between mouse and pufferfish Otx2 genes govern the expression in mesencephalic neural crest cells', *Development*, 124: 3929-41.

Kimura, H., J. M. Ng, and T. Curran. 2008. 'Transient inhibition of the Hedgehog pathway in young mice causes permanent defects in bone structure', *Cancer Cell*, 13: 249-60.

Kimura-Yoshida, C., H. Nakano, D. Okamura, K. Nakao, S. Yonemura, J. A. Belo, S. Aizawa, Y. Matsui, and I. Matsuo. 2005. 'Canonical Wnt signaling and its antagonist regulate

anterior-posterior axis polarization by guiding cell migration in mouse visceral endoderm', *Dev Cell*, 9: 639-50.

Koch, A., A. Hrychyk, W. Hartmann, A. Waha, T. Mikeska, A. Waha, U. Schuller, N. Sorensen, F. Berthold, C. G. Goodyer, O. D. Wiestler, W. Birchmeier, J. Behrens, and T. Pietsch. 2007. 'Mutations of the Wnt antagonist AXIN2 (Conductin) result in TCF-dependent transcription in medulloblastomas', *Int J Cancer*, 121: 284-91.

Koike, C., A. Nishida, S. Ueno, H. Saito, R. Sanuki, S. Sato, A. Furukawa, S. Aizawa, I. Matsuo, N. Suzuki, M. Kondo, and T. Furukawa. 2007. 'Functional roles of Otx2 transcription factor in postnatal mouse retinal development', *Mol Cell Biol*, 27: 8318-29.

Kool, M., A. Korshunov, M. Remke, D. T. Jones, M. Schlanstein, P. A. Northcott, Y. J. Cho, J. Koster, A. Schouten-van Meeteren, D. van Vuurden, S. C. Clifford, T. Pietsch, A. O. von Bueren, S. Rutkowski, M. McCabe, V. P. Collins, M. L. Backlund, C. Haberler, F. Bourdeaut, O. Delattre, F. Doz, D. W. Ellison, R. J. Gilbertson, S. L. Pomeroy, M. D. Taylor, P. Lichter, and S. M. Pfister. 2012. 'Molecular subgroups of medulloblastoma: an international meta-analysis of transcriptome, genetic aberrations, and clinical data of WNT, SHH, Group 3, and Group 4 medulloblastomas', *Acta Neuropathol*, 123: 473-84.

Kool, M., J. Koster, J. Bunt, N. E. Hasselt, A. Lakeman, P. van Sluis, D. Troost, N. S. Meeteren, H. N. Caron, J. Cloos, A. Mrsic, B. Ylstra, W. Grajkowska, W. Hartmann, T. Pietsch, D. Ellison, S. C. Clifford, and R. Versteeg. 2008. 'Integrated genomics identifies five medulloblastoma subtypes with distinct genetic profiles, pathway signatures and clinicopathological features', *PLoS One*, 3: e3088.

Kriks, S., J. W. Shim, J. Piao, Y. M. Ganat, D. R. Wakeman, Z. Xie, L. Carrillo-Reid, G. Auyeung, C. Antonacci, A. Buch, L. Yang, M. F. Beal, D. J. Surmeier, J. H. Kordower, V. Tabar, and L. Studer. 2011. 'Dopamine neurons derived from human ES cells efficiently engraft in animal models of Parkinson's disease', *Nature*, 480: 547-51.

Krivtsov, A. V., Z. Feng, M. E. Lemieux, J. Faber, S. Vempati, A. U. Sinha, X. Xia, J. Jesneck, A. P. Bracken, L. B. Silverman, J. L. Kutok, A. L. Kung, and S. A. Armstrong. 2008. 'H3K79 methylation profiles define murine and human MLL-AF4 leukemias', *Cancer Cell*, 14: 355-68.

Krizhanovsky, V., and S. W. Lowe. 2009. 'Stem cells: The promises and perils of p53', *Nature*, 460: 1085-6.

Larder, R., and P. L. Mellon. 2009. 'Otx2 induction of the gonadotropin-releasing hormone promoter is modulated by direct interactions with Grg co-repressors', *J Biol Chem*, 284: 16966-78.

Larsen, K. B., M. C. Lutterodt, K. Mollgard, and M. Moller. 2010. 'Expression of the homeobox genes OTX2 and OTX1 in the early developing human brain', *J Histochem Cytochem*, 58: 669-78.

Lau, J., C. Schmidt, S. L. Markant, M. D. Taylor, R. J. Wechsler-Reya, and W. A. Weiss. 2012. 'Matching mice to malignancy: molecular subgroups and models of medulloblastoma', *Childs Nerv Syst*, 28: 521-32.

Le, T. N., G. Du, M. Fonseca, Q. P. Zhou, J. T. Wigle, and D. D. Eisenstat. 2007. 'Dlx homeobox genes promote cortical interneuron migration from the basal forebrain by direct repression of the semaphorin receptor neuropilin-2', *J Biol Chem*, 282: 19071-81.

Lee, M. J., B. A. Hatton, E. H. Villavicencio, P. C. Khanna, S. D. Friedman, S. Ditzler, B. Pullar, K. Robison, K. F. White, C. Tunkey, M. LeBlanc, J. Randolph-Habecker, S. E. Knoblaugh, S. Hansen, A. Richards, B. J. Wainwright, K. McGovern, and J. M. Olson.

2012. 'Hedgehog pathway inhibitor saridegib (IPI-926) increases lifespan in a mouse medulloblastoma model', *Proc Natl Acad Sci U S A*, 109: 7859-64.

Lee, Y., H. L. Miller, H. R. Russell, K. Boyd, T. Curran, and P. J. McKinnon. 2006. 'Patched2 modulates tumorigenesis in patched1 heterozygous mice', *Cancer Res*, 66: 6964-71.

Leung, C., M. Lingbeek, O. Shakhova, J. Liu, E. Tanger, P. Saremaslani, M. Van Lohuizen, and S. Marino. 2004. 'Bmi1 is essential for cerebellar development and is overexpressed in human medulloblastomas', *Nature*, 428: 337-41.

Liang, L., C. Aiken, R. McClelland, L. C. Morrison, N. Tatari, M. Remke, V. Ramaswamy, M. Issaivanan, T. Ryken, M. R. Del Bigio, M. D. Taylor, and T. E. Werbowetski-Ogilvie. 2015. 'Characterization of novel biomarkers in selecting for subtype specific medulloblastoma phenotypes', *Oncotarget*, 6: 38881-900.

Lie, D. C., S. A. Colamarino, H. J. Song, L. Desire, H. Mira, A. Consiglio, E. S. Lein, S. Jessberger, H. Lansford, A. R. Dearie, and F. H. Gage. 2005. 'Wnt signalling regulates adult hippocampal neurogenesis', *Nature*, 437: 1370-5.

Lin, C. Y., S. Erkek, Y. Tong, L. Yin, A. J. Federation, M. Zapatka, P. Haldipur, D. Kawauchi, T. Risch, H. J. Warnatz, B. C. Worst, B. Ju, B. A. Orr, R. Zeid, D. R. Polaski, M. Segura-Wang, S. M. Waszak, D. T. Jones, M. Kool, V. Hovestadt, I. Buchhalter, L. Sieber, P. Johann, L. Chavez, S. Groschel, M. Ryzhova, A. Korshunov, W. Chen, V. V. Chizhikov, K. J. Millen, V. Amstislavskiy, H. Lehrach, M. L. Yaspo, R. Eils, P. Lichter, J. O. Korbel, S. M. Pfister, J. E. Bradner, and P. A. Northcott. 2016. 'Active medulloblastoma enhancers reveal subgroup-specific cellular origins', *Nature*, 530: 57-62.

Lisabeth, E. M., G. Falivelli, and E. B. Pasquale. 2013. 'Eph receptor signaling and ephrins', *Cold Spring Harb Perspect Biol*, 5.

Liu, Z., L. Chi, Y. Fang, L. Liu, and X. Zhang. 2013. 'Specific expression pattern of a novel Otx2 splicing variant during neural differentiation', *Gene*, 523: 33-8.

LoRusso, P. M., C. M. Rudin, J. C. Reddy, R. Tibes, G. J. Weiss, M. J. Borad, C. L. Hann, J. R. Brahmer, I. Chang, W. C. Darbonne, R. A. Graham, K. L. Zerivitz, J. A. Low, and D. D. Von Hoff. 2011. 'Phase I trial of hedgehog pathway inhibitor vismodegib (GDC-0449) in patients with refractory, locally advanced or metastatic solid tumors', *Clin Cancer Res*, 17: 2502-11.

Louis, D. N., H. Ohgaki, O. D. Wiestler, W. K. Cavenee, P. C. Burger, A. Jouvet, B. W. Scheithauer, and P. Kleihues. 2007. 'The 2007 WHO classification of tumours of the central nervous system', *Acta Neuropathol*, 114: 97-109.

Louis, D. N., A. Perry, G. Reifenberger, A. von Deimling, D. Figarella-Branger, W. K. Cavenee, H. Ohgaki, O. D. Wiestler, P. Kleihues, and D. W. Ellison. 2016. 'The 2016 World Health Organization Classification of Tumors of the Central Nervous System: a summary', *Acta Neuropathol*, 131: 803-20.

Lu, M., H. Breyssens, V. Salter, S. Zhong, Y. Hu, C. Baer, I. Ratnayaka, A. Sullivan, N. R. Brown, J. Endicott, S. Knapp, B. M. Kessler, M. R. Middleton, C. Siebold, E. Y. Jones, E. V. Sviderskaya, J. Cebon, T. John, O. L. Caballero, C. R. Goding, and X. Lu. 2013. 'Restoring p53 function in human melanoma cells by inhibiting MDM2 and cyclin B1/CDK1-phosphorylated nuclear iASPP', *Cancer Cell*, 23: 618-33.

Ma, J., D. G. Lanza, I. Guest, C. Uk-Lim, A. Glinskii, G. Glinsky, and S. Sell. 2012. 'Characterization of mammary cancer stem cells in the MMTV-PyMT mouse model', *Tumour Biol*, 33: 1983-96.

Manoranjan, B., C. Venugopal, N. McFarlane, B. W. Doble, S. E. Dunn, K. Scheinemann, and S. K. Singh. 2012. 'Medulloblastoma stem cells: where development and cancer cross pathways', *Pediatr Res*, 71: 516-22.

Marino, S., M. Vooijs, H. van Der Gulden, J. Jonkers, and A. Berns. 2000. 'Induction of medulloblastomas in p53-null mutant mice by somatic inactivation of Rb in the external granular layer cells of the cerebellum', *Genes Dev*, 14: 994-1004.

Martinez-Morales, J. R., M. Signore, D. Acampora, A. Simeone, and P. Bovolenta. 2001. 'Otx genes are required for tissue specification in the developing eye', *Development*, 128: 2019-30.

Masuda, S., J. Wu, T. Hishida, G. N. Pandian, H. Sugiyama, and J. C. Izpisua Belmonte. 2013. 'Chemically induced pluripotent stem cells (CiPSCs): a transgene-free approach', *J Mol Cell Biol*, 5: 354-5.

Matsuo, I., S. Kuratani, C. Kimura, N. Takeda, and S. Aizawa. 1995. 'Mouse Otx2 functions in the formation and patterning of rostral head', *Genes Dev*, 9: 2646-58.

Maurer, D., and T. K. Hensch. 2012. 'Amblyopia: background to the special issue on stroke recovery', *Dev Psychobiol*, 54: 224-38.

McMahon, A. P., A. L. Joyner, A. Bradley, and J. A. McMahon. 1992. 'The midbrain-hindbrain phenotype of Wnt-1-/Wnt-1-mice results from stepwise deletion of engrailed-expressing cells by 9.5 days postcoitum. ', *Cell*, 69: 581-95.

Mehta, M.P.; Chang S.M.; Newton, H.B; and Vogelbaum, M.A. 2011. *Principles and Practice of Neuro-Oncology : A Multidisciplinary Approach*.

Mehta, MP., Chang S., Newton H., Guha A., and Vogelbaum M. 2011. *Principles and Practice of Neuro-oncology: A multidisciplinary approach* (Demos Medical Publishing; 1 edition (Oct 21 2010)).

Metcalfe, C., B. Alicke, A. Crow, M. Lamoureux, G. J. Dijkgraaf, F. Peale, S. E. Gould, and F. J. de Sauvage. 2013. 'PTEN loss mitigates the response of medulloblastoma to Hedgehog pathway inhibition', *Cancer Res*, 73: 7034-42.

Metzler, M., A. Forster, R. Pannell, M. J. Arends, A. Daser, M. N. Lobato, and T. H. Rabbitts. 2006. 'A conditional model of MLL-AF4 B-cell tumourigenesis using invertor technology', *Oncogene*, 25: 3093-103.

Michiels, E. M., E. Oussoren, M. Van Groenigen, E. Pauws, P. M. Bossuyt, P. A. Voute, and F. Baas. 1999. 'Genes differentially expressed in medulloblastoma and fetal brain', *Physiol Genomics*, 1: 83-91.

Mizuno, H., B. T. Spike, G. M. Wahl, and A. J. Levine. 2010. 'Inactivation of p53 in breast cancers correlates with stem cell transcriptional signatures', *Proc Natl Acad Sci U S A*, 107: 22745-50.

Moretti, A., K. L. Laugwitz, T. Dorn, D. Sinnecker, and C. Mummery. 2013. 'Pluripotent stem cell models of human heart disease', *Cold Spring Harb Perspect Med*, 3.

Morfouace, M., A. Shelat, M. Jacus, B. B. Freeman, 3rd, D. Turner, S. Robinson, F. Zindy, Y. D. Wang, D. Finkelstein, O. Ayrault, L. Bihannic, S. Puget, X. N. Li, J. M. Olson, G. W. Robinson, R. K. Guy, C. F. Stewart, A. Gajjar, and M. F. Roussel. 2014. 'Pemetrexed and gemcitabine as combination therapy for the treatment of Group3 medulloblastoma', *Cancer Cell*, 25: 516-29.

Morrison, L. C., R. McClelland, C. Aiken, M. Bridges, L. Liang, X. Wang, D. Di Curzio, M. R. Del Bigio, M. D. Taylor, and T. E. Werbowetski-Ogilvie. 2013. 'Deconstruction of

medulloblastoma cellular heterogeneity reveals differences between the most highly invasive and self-renewing phenotypes', *Neoplasia*, 15: 384-98.

Muller, P. A., and K. H. Vousden. 2014. 'Mutant p53 in cancer: new functions and therapeutic opportunities', *Cancer Cell*, 25: 304-17.

Nakagawa, M., M. Koyanagi, K. Tanabe, K. Takahashi, T. Ichisaka, T. Aoi, K. Okita, Y. Mochiduki, N. Takizawa, and S. Yamanaka. 2008. 'Generation of induced pluripotent stem cells without Myc from mouse and human fibroblasts', *Nat Biotechnol*, 26: 101-6.

Niclis, J. C., A. Pinar, J. M. Haynes, W. Alsanie, R. Jenny, M. Dottori, and D. S. Cram. 2013. 'Characterization of forebrain neurons derived from late-onset Huntington's disease human embryonic stem cell lines', *Front Cell Neurosci*, 7: 37.

Niclis, J., A. O. Trounson, M. Dottori, A. Ellisdon, S. P. Bottomley, Y. Verlinsky, and D. Cram. 2009. 'Human embryonic stem cell models of Huntington disease', *Reprod Biomed Online*, 19: 106-13.

Nishida, A., A. Furukawa, C. Koike, Y. Tano, S. Aizawa, I. Matsuo, and T. Furukawa. 2003. 'Otx2 homeobox gene controls retinal photoreceptor cell fate and pineal gland development', *Nat Neurosci*, 6: 1255-63.

Nishihara, D., I. Yajima, H. Tabata, M. Nakai, N. Tsukiji, T. Katahira, K. Takeda, S. Shibahara, H. Nakamura, and H. Yamamoto. 2012. 'Otx2 is involved in the regional specification of the developing retinal pigment epithelium by preventing the expression of sox2 and fgf8, factors that induce neural retina differentiation', *PLoS One*, 7: e48879.

Niu, C. S., D. X. Li, Y. H. Liu, X. M. Fu, S. F. Tang, and J. Li. 2011. 'Expression of NANOG in human gliomas and its relationship with undifferentiated glioma cells', *Oncol Rep*, 26: 593-601.

Niwa, H., J. Miyazaki, and A. G. Smith. 2000. 'Quantitative expression of Oct-3/4 defines differentiation, dedifferentiation or self-renewal of ES cells', *Nat Genet*, 24: 372-6.

Northcott, P. A., A. Korshunov, H. Witt, T. Hielscher, C. G. Eberhart, S. Mack, E. Bouffet, S. C. Clifford, C. E. Hawkins, P. French, J. T. Rutka, S. Pfister, and M. D. Taylor. 2011. 'Medulloblastoma comprises four distinct molecular variants', *J Clin Oncol*, 29: 1408-14.

Northcott, P. A., D. J. Shih, J. Peacock, L. Garzia, A. S. Morrissy, T. Zichner, A. M. Stutz, A. Korshunov, J. Reimand, S. E. Schumacher, R. Beroukhim, D. W. Ellison, C. R. Marshall, A. C. Lionel, S. Mack, A. Dubuc, Y. Yao, V. Ramaswamy, B. Luu, A. Rolider, F. M. Cavalli, X. Wang, M. Remke, X. Wu, R. Y. Chiu, A. Chu, E. Chuah, R. D. Corbett, G. R. Hoad, S. D. Jackman, Y. Li, A. Lo, K. L. Mungall, K. M. Nip, J. Q. Qian, A. G. Raymond, N. T. Thiessen, R. J. Varhol, I. Birol, R. A. Moore, A. J. Mungall, R. Holt, D. Kawauchi, M. F. Roussel, M. Kool, D. T. Jones, H. Witt, L. A. Fernandez, A. M. Kenney, R. J. Wechsler-Reya, P. Dirks, T. Aviv, W. A. Grajkowska, M. Perek-Polnik, C. C. Haberler, O. Delattre, S. S. Reynaud, F. F. Doz, S. S. Pernet-Fattet, B. K. Cho, S. K. Kim, K. C. Wang, W. Scheurlen, C. G. Eberhart, M. Fevre-Montange, A. Jouvet, I. F. Pollack, X. Fan, K. M. Muraszko, G. Y. Gillespie, C. Di Rocco, L. Massimi, E. M. Michiels, N. K. Kloosterhof, P. J. French, J. M. Kros, J. M. Olson, R. G. Ellenbogen, K. Zitterbart, L. Kren, R. C. Thompson, M. K. Cooper, B. Lach, R. E. McLendon, D. D. Bigner, A. Fontebasso, S. Albrecht, N. Jabado, J. C. Lindsey, S. Bailey, N. Gupta, W. A. Weiss, L. Bognar, A. Klekner, T. E. Van Meter, T. Kumabe, T. Tominaga, S. K. Elbabaa, J. R. Leonard, J. B. Rubin, L. M. Liau, E. G. Van Meir, M. Fouladi, H. Nakamura, G. Cinalli, M. Garami, P. Hauser, A. G. Saad, A. Iolascon, S. Jung, C. G. Carlotti, R. Vibhakar, Y. S. Ra, S. Robinson, M. Zollo, C. C. Faria, J. A. Chan, M. L. Levy, P. H.

Sorensen, M. Meyerson, S. L. Pomeroy, Y. J. Cho, G. D. Bader, U. Tabori, C. E. Hawkins, E. Bouffet, S. W. Scherer, J. T. Rutka, D. Malkin, S. C. Clifford, S. J. Jones, J. O. Korbel, S. M. Pfister, M. A. Marra, and M. D. Taylor. 2012. 'Subgroup-specific structural variation across 1,000 medulloblastoma genomes', *Nature*, 488: 49-56.

Okumura-Nakanishi, S., M. Saito, H. Niwa, and F. Ishikawa. 2005. 'Oct-3/4 and Sox2 regulate Oct-3/4 gene in embryonic stem cells', *J Biol Chem*, 280: 5307-17.

Oliver, T. G., T. A. Read, J. D. Kessler, A. Mehmeti, J. F. Wells, T. T. Huynh, S. M. Lin, and R. J. Wechsler-Reya. 2005. 'Loss of patched and disruption of granule cell development in a pre-neoplastic stage of medulloblastoma', *Development*, 132: 2425-39.

Omodei, D., D. Acampora, P. Mancuso, N. Prakash, L. G. Di Giovannantonio, W. Wurst, and A. Simeone. 2008. 'Anterior-posterior graded response to Otx2 controls proliferation and differentiation of dopaminergic progenitors in the ventral mesencephalon', *Development*, 135: 3459-70.

Ono, Y., T. Nakatani, Y. Sakamoto, E. Mizuhara, Y. Minaki, M. Kumai, A. Hamaguchi, M. Nishimura, Y. Inoue, H. Hayashi, J. Takahashi, and T. Imai. 2007. 'Differences in neurogenic potential in floor plate cells along an anteroposterior location: midbrain dopaminergic neurons originate from mesencephalic floor plate cells', *Development*, 134: 3213-25.

Packer, R. J., A. Gajjar, G. Vezina, L. Rorke-Adams, P. C. Burger, P. L. Robertson, L. Bayer, D. LaFond, B. R. Donahue, M. H. Marymont, K. Muraszko, J. Langston, and R. Sposto. 2006. 'Phase III study of craniospinal radiation therapy followed by adjuvant chemotherapy for newly diagnosed average-risk medulloblastoma', *J Clin Oncol*, 24: 4202-8.

Palmer, S. L., W. E. Reddick, and A. Gajjar. 2007. 'Understanding the cognitive impact on children who are treated for medulloblastoma', *J Pediatr Psychol*, 32: 1040-9.

Panhuysen, M., D. M. Vogt Weisenhorn, V. Blanquet, C. Brodski, U. Heinzmann, W. Beisker, and W. Wurst. 2004. 'Effects of Wnt1 signaling on proliferation in the developing mid-/hindbrain region', *Mol Cell Neurosci*, 26: 101-11.

Panman, L., M. Papathanou, A. Laguna, T. Oosterveen, N. Volakakis, D. Acampora, I. Kurtsdotter, T. Yoshitake, J. Kehr, E. Joodmardi, J. Muhr, A. Simeone, J. Ericson, and T. Perlmann. 2014. 'Sox6 and Otx2 control the specification of substantia nigra and ventral tegmental area dopamine neurons', *Cell Rep*, 8: 1018-25.

Park, I. H., P. H. Lerou, R. Zhao, H. Huo, and G. Q. Daley. 2008. 'Generation of human-induced pluripotent stem cells', *Nat Protoc*, 3: 1180-6.

Pei, Y., C. E. Moore, J. Wang, A. K. Tewari, A. Eroshkin, Y. J. Cho, H. Witt, A. Korshunov, T. A. Read, J. L. Sun, E. M. Schmitt, C. R. Miller, A. F. Buckley, R. E. McLendon, T. F. Westbrook, P. A. Northcott, M. D. Taylor, S. M. Pfister, P. G. Febbo, and R. J. Wechsler-Reya. 2012. 'An animal model of MYC-driven medulloblastoma', *Cancer Cell*, 21: 155-67.

Perea-Gomez, A., K. A. Lawson, M. Rhinn, L. Zakin, P. Brulet, S. Mazan, and S. L. Ang. 2001. 'Otx2 is required for visceral endoderm movement and for the restriction of posterior signals in the epiblast of the mouse embryo', *Development*, 128: 753-65.

Perrier, A. L., V. Tabar, T. Barberi, M. E. Rubio, J. Bruses, N. Topf, N. L. Harrison, and L. Studer. 2004. 'Derivation of midbrain dopamine neurons from human embryonic stem cells', *Proc Natl Acad Sci U S A*, 101: 12543-8.

Pfister, S., M. Remke, A. Benner, F. Mendrzyk, G. Toedt, J. Felsberg, A. Wittmann, F. Devens, N. U. Gerber, S. Joos, A. Kulozik, G. Reifenberger, S. Rutkowski, O. D. Wiestler, B. Radlwimmer, W. Scheurlen, P. Lichter, and A. Korshunov. 2009. 'Outcome prediction in pediatric medulloblastoma based on DNA copy-number aberrations of chromosomes 6q and 17q and the MYC and MYCN loci', *J Clin Oncol*, 27: 1627-36.

Philipova, T., N. Baryawno, W. Hartmann, T. Pietsch, H. Druid, J. I. Johnsen, and T. J. Ekstrom. 2011. 'Differential forms of p53 in medulloblastoma primary tumors, cell lines and xenografts', *Int J Oncol*, 38: 843-9.

Piao, J., T. Major, G. Auyeung, E. Policarpio, J. Menon, L. Droms, P. Gutin, K. Uryu, J. Tchieu, D. Soulet, and V. Tabar. 2015. 'Human embryonic stem cell-derived oligodendrocyte progenitors remyelinate the brain and rescue behavioral deficits following radiation', *Cell Stem Cell*, 16: 198-210.

Pietsch, T., A. Waha, A. Koch, J. Kraus, S. Albrecht, J. Tonn, N. Sorensen, F. Berthold, B. Henk, N. Schmandt, H. K. Wolf, A. von Deimling, B. Wainwright, G. Chenevix-Trench, O. D. Wiestler, and C. Wicking. 1997. 'Medulloblastomas of the desmoplastic variant carry mutations of the human homologue of Drosophila patched', *Cancer Res*, 57: 2085-8.

Pizer, B.L., and S.C. Clifford. 2009. 'The potential impact of tumour biology on improved clinical practice for medulloblastoma: progress towards biologically driven clinical trials', *British Journal of Neurosurgery*, 23: 364-75.

Po, A., E. Ferretti, E. Miele, E. De Smaele, A. Paganelli, G. Canettieri, S. Coni, L. Di Marcotullio, M. Biffoni, L. Massimi, C. Di Rocco, I. Screpanti, and A. Gulino. 2010. 'Hedgehog controls neural stem cells through p53-independent regulation of Nanog', *Embo j*, 29: 2646-58.

Prakash, N., and W. Wurst. 2006. 'Genetic networks controlling the development of midbrain dopaminergic neurons', *J Physiol*, 575: 403-10.

Prusky, G. T., and R. M. Douglas. 2003. 'Developmental plasticity of mouse visual acuity', *Eur J Neurosci*, 17: 167-73.

Puelles, E., D. Acampora, R. Gogoi, F. Tuorto, A. Papalia, F. Guillemot, S. L. Ang, and A. Simeone. 2006. 'Otx2 controls identity and fate of glutamatergic progenitors of the thalamus by repressing GABAergic differentiation', *J Neurosci*, 26: 5955-64.

Puelles, E., A. Annino, F. Tuorto, A. Usiello, D. Acampora, T. Czerny, C. Brodski, S. L. Ang, W. Wurst, and A. Simeone. 2004. 'Otx2 regulates the extent, identity and fate of neuronal progenitor domains in the ventral midbrain', *Development*, 131: 2037-48.

Puelles, L., and J. L. Rubenstein. 2003. 'Forebrain gene expression domains and the evolving prosomeric model', *Trends Neurosci*, 26: 469-76.

Pugh, T. J., S. D. Weeraratne, T. C. Archer, D. A. Pomeranz Krummel, D. Auclair, J. Bochicchio, M. O. Carneiro, S. L. Carter, K. Cibulskis, R. L. Erlich, H. Greulich, M. S. Lawrence, N. J. Lennon, A. McKenna, J. Meldrim, A. H. Ramos, M. G. Ross, C. Russ, E. Shefler, A. Sivachenko, B. Sogoloff, P. Stojanov, P. Tamayo, J. P. Mesirov, V. Amani, N. Teider, S. Sengupta, J. P. Francois, P. A. Northcott, M. D. Taylor, F. Yu, G. R. Crabtree, A. G. Kautzman, S. B. Gabriel, G. Getz, N. Jager, D. T. Jones, P. Lichter, S. M. Pfister, T. M. Roberts, M. Meyerson, S. L. Pomeroy, and Y. J. Cho. 2012. 'Medulloblastoma exome sequencing uncovers subtype-specific somatic mutations', *Nature*, 488: 106-10.

Pui, C. H., A. J. Gajjar, J. R. Kane, I. A. Qaddoumi, and A. S. Pappo. 2011. 'Challenging issues in pediatric oncology', *Nat Rev Clin Oncol*, 8: 540-9.

Ragge, N. K., A. G. Brown, C. M. Poloschek, B. Lorenz, R. A. Henderson, M. P. Clarke, I. Russell-Eggitt, A. Fielder, D. Gerrelli, J. P. Martinez-Barbera, P. Ruddle, J. Hurst, J. R. Collin, A. Salt, S. T. Cooper, P. J. Thompson, S. M. Sisodiya, K. A. Williamson, D. R. Fitzpatrick, V. van Heyningen, and I. M. Hanson. 2005. 'Heterozygous mutations of OTX2 cause severe ocular malformations', *Am J Hum Genet*, 76: 1008-22.

Ramaswamy, V., M. Remke, E. Bouffet, C. C. Faria, S. Perreault, Y. J. Cho, D. J. Shih, B. Luu, A. M. Dubuc, P. A. Northcott, U. Schuller, S. Gururangan, R. McLendon, D. Bigner, M. Fouladi, K. L. Ligon, S. L. Pomeroy, S. Dunn, J. Triscott, N. Jabado, A. Fontebasso, D. T. Jones, M. Kool, M. A. Karajannis, S. L. Gardner, D. Zagzag, S. Nunes, J. Pimentel, J. Mora, E. Lipp, A. W. Walter, M. Ryzhova, O. Zheludkova, E. Kumirova, J. Alshami, S. E. Croul, J. T. Rutka, C. Hawkins, U. Tabori, K. E. Codispoti, R. J. Packer, S. M. Pfister, A. Korshunov, and M. D. Taylor. 2013. 'Recurrence patterns across medulloblastoma subgroups: an integrated clinical and molecular analysis', *Lancet Oncol*, 14: 1200-7.

Rao, R. A., N. Dhele, S. Cheemadan, A. Ketkar, G. R. Jayandharan, D. Palakodeti, and S. Rampalli. 2015. 'Ezh2 mediated H3K27me3 activity facilitates somatic transition during human pluripotent reprogramming', *Sci Rep*, 5: 8229.

Ray, A., M. Ho, J. Ma, R. K. Parkes, T. G. Mainprize, S. Ueda, J. McLaughlin, E. Bouffet, J. T. Rutka, and C. E. Hawkins. 2004. 'A clinicobiological model predicting survival in medulloblastoma', *Clin Cancer Res*, 10: 7613-20.

Real, P. J., G. Ligero, V. Ayllon, V. Ramos-Mejia, C. Bueno, I. Gutierrez-Aranda, O. Navarro-Montero, M. Lako, and P. Menendez. 2012. 'SCL/TAL1 regulates hematopoietic specification from human embryonic stem cells', *Mol Ther*, 20: 1443-53.

Remke, M., T. Hielscher, P. A. Northcott, H. Witt, M. Ryzhova, A. Wittmann, A. Benner, A. von Deimling, W. Scheurlen, A. Perry, S. Croul, A. E. Kulozik, P. Lichter, M. D. Taylor, S. M. Pfister, and A. Korshunov. 2011. 'Adult medulloblastoma comprises three major molecular variants', *J Clin Oncol*, 29: 2717-23.

Reubinoff, B. E., P. Itsykson, T. Turetsky, M. F. Pera, E. Reinhartz, A. Itzik, and T. Ben-Hur. 2001. 'Neural progenitors from human embryonic stem cells', *Nat Biotechnol*, 19: 1134-40.

Rhinn, M., A. Dierich, W. Shawlot, R. R. Behringer, M. Le Meur, and S. L. Ang. 1998. 'Sequential roles for Otx2 in visceral endoderm and neuroectoderm for forebrain and midbrain induction and specification', *Development*, 125: 845-56.

Robarge, K. D., S. A. Brunton, G. M. Castanedo, Y. Cui, M. S. Dina, R. Goldsmith, S. E. Gould, O. Guichert, J. L. Gunzner, J. Halladay, W. Jia, C. Khojasteh, M. F. Koehler, K. Kotkow, H. La, R. L. Lalonde, K. Lau, L. Lee, D. Marshall, J. C. Marsters, Jr., L. J. Murray, C. Qian, L. L. Rubin, L. Salphati, M. S. Stanley, J. H. Stibbard, D. P. Sutherlin, S. Ubhayaker, S. Wang, S. Wong, and M. Xie. 2009. 'GDC-0449-a potent inhibitor of the hedgehog pathway', *Bioorg Med Chem Lett*, 19: 5576-81.

Robinson, G., M. Parker, T. A. Kranenburg, C. Lu, X. Chen, L. Ding, T. N. Phoenix, E. Hedlund, L. Wei, X. Zhu, N. Chalhoub, S. J. Baker, R. Huether, R. Kriwacki, N. Curley, R. Thiruvenkatam, J. Wang, G. Wu, M. Rusch, X. Hong, J. Becksfort, P. Gupta, J. Ma, J. Easton, B. Vadodaria, A. Onar-Thomas, T. Lin, S. Li, S. Pounds, S. Paugh, D. Zhao, D. Kawauchi, M. F. Roussel, D. Finkelstein, D. W. Ellison, C. C. Lau, E. Bouffet, T. Hassall, S. Gururangan, R. Cohn, R. S. Fulton, L. L. Fulton, D. J. Dooling, K. Ochoa, A.

Gajjar, E. R. Mardis, R. K. Wilson, J. R. Downing, J. Zhang, and R. J. Gilbertson. 2012. 'Novel mutations target distinct subgroups of medulloblastoma', *Nature*, 488: 43-8.

Robinson, G. W., B. A. Orr, G. Wu, S. Gururangan, T. Lin, I. Qaddoumi, R. J. Packer, S. Goldman, M. D. Prados, A. Desjardins, M. Chintagumpala, N. Takebe, S. C. Kaste, M. Rusch, S. J. Allen, A. Onar-Thomas, C. F. Stewart, M. Fouladi, J. M. Boyett, R. J. Gilbertson, T. Curran, D. W. Ellison, and A. Gajjar. 2015. 'Vismodegib Exerts Targeted Efficacy Against Recurrent Sonic Hedgehog-Subgroup Medulloblastoma: Results From Phase II Pediatric Brain Tumor Consortium Studies PBTC-025B and PBTC-032', *J Clin Oncol*, 33: 2646-54.

Romer, J., and T. Curran. 2005. 'Targeting medulloblastoma: small-molecule inhibitors of the Sonic Hedgehog pathway as potential cancer therapeutics', *Cancer Res*, 65: 4975-8.

Romer, J. T., H. Kimura, S. Magdaleno, K. Sasai, C. Fuller, H. Baines, M. Connelly, C. F. Stewart, S. Gould, L. L. Rubin, and T. Curran. 2004. 'Suppression of the Shh pathway using a small molecule inhibitor eliminates medulloblastoma in Ptc1(+/-)p53(-/-) mice', *Cancer Cell*, 6: 229-40.

Rosso, S. B., and N. C. Inestrosa. 2013. 'WNT signaling in neuronal maturation and synaptogenesis', *Front Cell Neurosci*, 7: 103.

Roussel, M. F., and G. W. Robinson. 2013. 'Role of MYC in Medulloblastoma', *Cold Spring Harb Perspect Med*, 3.

Roy, N. S., C. Cleren, S. K. Singh, L. Yang, M. F. Beal, and S. A. Goldman. 2006. 'Functional engraftment of human ES cell-derived dopaminergic neurons enriched by coculture with telomerase-immortalized midbrain astrocytes', *Nat Med*, 12: 1259-68.

Royet, J., and R. Finkelstein. 1995. 'Pattern formation in Drosophila head development: the role of the orthodenticle homeobox gene', *Development*, 121: 3561-72.

Sachlos, E., R. M. Risueno, S. Laronde, Z. Shapovalova, J. H. Lee, J. Russell, M. Malig, J. D. McNicol, A. Fiebig-Comyn, M. Graham, M. Levadoux-Martin, J. B. Lee, A. O. Giacomelli, J. A. Hassell, D. Fischer-Russell, M. R. Trus, R. Foley, B. Leber, A. Xenocostas, E. D. Brown, T. J. Collins, and M. Bhatia. 2012. 'Identification of drugs including a dopamine receptor antagonist that selectively target cancer stem cells', *Cell*, 149: 1284-97.

Sanchez-Danes, A., Y. Richaud-Patin, I. Carballo-Carbajal, S. Jimenez-Delgado, C. Caig, S. Mora, C. Di Guglielmo, M. Ezquerra, B. Patel, A. Giralt, J. M. Canals, M. Memo, J. Alberch, J. Lopez-Barneo, M. Vila, A. M. Cuervo, E. Tolosa, A. Consiglio, and A. Raya. 2012. 'Disease-specific phenotypes in dopamine neurons from human iPS-based models of genetic and sporadic Parkinson's disease', *EMBO Mol Med*, 4: 380-95.

Sato, S., T. Inoue, K. Terada, I. Matsuo, S. Aizawa, Y. Tano, T. Fujikado, and T. Furukawa. 2007. 'Dkk3-Cre BAC transgenic mouse line: a tool for highly efficient gene deletion in retinal progenitor cells', *Genesis*, 45: 502-7.

Schilter, K. F., A. Schneider, T. Bardakjian, J. F. Soucy, R. C. Tyler, L. M. Reis, and E. V. Semina. 2011. 'OTX2 microphthalmia syndrome: four novel mutations and delineation of a phenotype', *Clin Genet*, 79: 158-68.

Schmitz, M., A. Temme, V. Senner, R. Ebner, S. Schwind, S. Stevanovic, R. Wehner, G. Schackert, H. K. Schackert, M. Fussel, M. Bachmann, E. P. Rieber, and B. Weigle. 2007. 'Identification of SOX2 as a novel glioma-associated antigen and potential target for T cell-based immunotherapy', *Br J Cancer*, 96: 1293-301.

Schroeder, K., and S. Gururangan. 2014. 'Molecular variants and mutations in medulloblastoma', *Pharmgenomics Pers Med*, 7: 43-51.

Schuller, U., V. M. Heine, J. Mao, A. T. Kho, A. K. Dillon, Y. G. Han, E. Huillard, T. Sun, A. H. Ligon, Y. Qian, Q. Ma, A. Alvarez-Buylla, A. P. McMahon, D. H. Rowitch, and K. L. Ligon. 2008. 'Acquisition of granule neuron precursor identity is a critical determinant of progenitor cell competence to form Shh-induced medulloblastoma', *Cancer Cell*, 14: 123-34.

Schwartzentruber, J., A. Korshunov, X. Y. Liu, D. T. Jones, E. Pfaff, K. Jacob, D. Sturm, A. M. Fontebasso, D. A. Quang, M. Tonjes, V. Hovestadt, S. Albrecht, M. Kool, A. Nantel, C. Konermann, A. Lindroth, N. Jager, T. Rausch, M. Ryzhova, J. O. Korbel, T. Hielscher, P. Hauser, M. Garami, A. Klekner, L. Bognar, M. Ebinger, M. U. Schuhmann, W. Scheurlen, A. Pekrun, M. C. Fruhwald, W. Roggendorf, C. Kramm, M. Durken, J. Atkinson, P. Lepage, A. Montpetit, M. Zakrzewska, K. Zakrzewski, P. P. Liberski, Z. Dong, P. Siegel, A. E. Kulozik, M. Zapatka, A. Guha, D. Malkin, J. Felsberg, G. Reifenberger, A. von Deimling, K. Ichimura, V. P. Collins, H. Witt, T. Milde, O. Witt, C. Zhang, P. Castelo-Branco, P. Lichter, D. Faury, U. Tabori, C. Plass, J. Majewski, S. M. Pfister, and N. Jabado. 2012. 'Driver mutations in histone H3.3 and chromatin remodelling genes in paediatric glioblastoma', *Nature*, 482: 226-31.

Sharpe, H. J., G. Pau, G. J. Dijkgraaf, N. Basset-Seguin, Z. Modrusan, T. Januario, V. Tsui, A. B. Durham, A. A. Dlugosz, P. M. Haverty, R. Bourgon, J. Y. Tang, K. Y. Sarin, L. Dirix, D. C. Fisher, C. M. Rudin, H. Sofen, M. R. Migden, R. L. Yauch, and F. J. de Sauvage. 2015. 'Genomic analysis of smoothened inhibitor resistance in basal cell carcinoma', *Cancer Cell*, 27: 327-41.

Shih, D. J., P. A. Northcott, M. Remke, A. Korshunov, V. Ramaswamy, M. Kool, B. Luu, Y. Yao, X. Wang, A. M. Dubuc, L. Garzia, J. Peacock, S. C. Mack, X. Wu, A. Rolider, A. S. Morrissy, F. M. Cavalli, D. T. Jones, K. Zitterbart, C. C. Faria, U. Schuller, L. Kren, T. Kumabe, T. Tominaga, Y. Shin Ra, M. Garami, P. Hauser, J. A. Chan, S. Robinson, L. Bognar, A. Klekner, A. G. Saad, L. M. Liau, S. Albrecht, A. Fontebasso, G. Cinalli, P. De Antonellis, M. Zollo, M. K. Cooper, R. C. Thompson, S. Bailey, J. C. Lindsey, C. Di Rocco, L. Massimi, E. M. Michiels, S. W. Scherer, J. J. Phillips, N. Gupta, X. Fan, K. M. Muraszko, R. Vibhakar, C. G. Eberhart, M. Fouladi, B. Lach, S. Jung, R. J. Wechsler-Reya, M. Fevre-Montange, A. Jouvet, N. Jabado, I. F. Pollack, W. A. Weiss, J. Y. Lee, B. K. Cho, S. K. Kim, K. C. Wang, J. R. Leonard, J. B. Rubin, C. de Torres, C. Lavarino, J. Mora, Y. J. Cho, U. Tabori, J. M. Olson, A. Gajjar, R. J. Packer, S. Rutkowski, S. L. Pomeroy, P. J. French, N. K. Kloosterhof, J. M. Kros, E. G. Van Meir, S. C. Clifford, F. Bourdeaut, O. Delattre, F. F. Doz, C. E. Hawkins, D. Malkin, W. A. Grajkowska, M. Perek-Polnik, E. Bouffet, J. T. Rutka, S. M. Pfister, and M. D. Taylor. 2014. 'Cytogenetic prognostication within medulloblastoma subgroups', *J Clin Oncol*, 32: 886-96.

Shtutman, M., J. Zhurinsky, I Simcha, C. Albanese, M. D'Amico, R. Pestell, and Ben-Ze'ev A. 1999. 'The cyclin D1 gene is a target of the beta-catenin/LEF-1 pathway', *Proc. Natl. Acad. Sci. USA*, 96: pp. 5522–27.

Siegel, R., D. Naishadham, and A. Jemal. 2012. 'Cancer statistics, 2012', *C cancer Journal for Clinicians*, 62: 10-29.

Sikkema, A. H., W. F. den Dunnen, E. Hulleman, D. G. van Vuurden, G. Garcia-Manero, H. Yang, F. J. Scherpen, K. R. Kampen, E. W. Hoving, W. A. Kamps, S. H. Diks, M. P.

Peppelenbosch, and E. S. de Bont. 2012. 'EphB2 activity plays a pivotal role in pediatric medulloblastoma cell adhesion and invasion', *Neuro Oncol*, 14: 1125-35.

Simeone, A. 1998. 'Otx1 and Otx2 in the development and evolution of the mammalian brain', *Embo j*, 17: 6790-8.

Simeone, A., E. Puelles, and D. Acampora. 2002. 'The Otx family', *Curr Opin Genet Dev*, 12: 409-15.

Simeone, A., E. Puelles, D. Omodei, D. Acampora, L. G. Di Giovannantonio, M. Di Salvio, P. Mancuso, and C. Tomasetti. 2011. 'Otx genes in neurogenesis of mesencephalic dopaminergic neurons', *Dev Neurobiol*, 71: 665-79.

Singh, S. K., I. D. Clarke, M. Terasaki, V. E. Bonn, C. Hawkins, J. Squire, and P. B. Dirks. 2003. 'Identification of a cancer stem cell in human brain tumors', *Cancer Res*, 63: 5821-8.

Singh, S. K., C. Hawkins, I. D. Clarke, J. A. Squire, J. Bayani, T. Hide, R. M. Henkelman, M. D. Cusimano, and P. B. Dirks. 2004. 'Identification of human brain tumour initiating cells', *Nature*, 432: 396-401.

Snuderl, M., A. Batista, N. D. Kirkpatrick, C. Ruiz de Almodovar, L. Riedemann, E. C. Walsh, R. Anolik, Y. Huang, J. D. Martin, W. Kamoun, E. Knevels, T. Schmidt, C. T. Farrar, B. J. Vakoc, N. Mohan, E. Chung, S. Roberge, T. Peterson, C. Bais, B. H. Zhelyazkova, S. Yip, M. Hasselblatt, C. Rossig, E. Niemeyer, N. Ferrara, M. Klagsbrun, D. G. Duda, D. Fukumura, L. Xu, P. Carmeliet, and R. K. Jain. 2013. 'Targeting placental growth factor/neuropilin 1 pathway inhibits growth and spread of medulloblastoma', *Cell*, 152: 1065-76.

Song, H., M. Hollstein, and Y. Xu. 2007. 'p53 gain-of-function cancer mutants induce genetic instability by inactivating ATM', *Nat Cell Biol*, 9: 573-80.

Spatazza, J., H. H. Lee, A. A. Di Nardo, L. Tibaldi, A. Joliot, T. K. Hensch, and A. Prochiantz. 2013. 'Choroid-plexus-derived Otx2 homeoprotein constrains adult cortical plasticity', *Cell Rep*, 3: 1815-23.

Stecca, B., and A. Ruiz i Altaba. 2005. 'Brain as a paradigm of organ growth: Hedgehog-Gli signaling in neural stem cells and brain tumors', *J Neurobiol*, 64: 476-90.

Sugiyama, S., A. A. Di Nardo, S. Aizawa, I. Matsuo, M. Volovitch, A. Prochiantz, and T. K. Hensch. 2008. 'Experience-dependent transfer of Otx2 homeoprotein into the visual cortex activates postnatal plasticity', *Cell*, 134: 508-20.

Swartling, F. J. 2012. 'Myc proteins in brain tumor development and maintenance', *Ups J Med Sci*, 117: 122-31.

Tabori, U., B. Baskin, M. Shago, N. Alon, M. D. Taylor, P. N. Ray, E. Bouffet, D. Malkin, and C. Hawkins. 2010. 'Universal poor survival in children with medulloblastoma harboring somatic TP53 mutations', *J Clin Oncol*, 28: 1345-50.

Taipale, J., J. K. Chen, M. K. Cooper, B. Wang, R. K. Mann, L. Milenkovic, M. P. Scott, and P. A. Beachy. 2000. 'Effects of oncogenic mutations in Smoothened and Patched can be reversed by cyclopamine', *Nature*, 406: 1005-9.

Takahashi, K., K. Tanabe, M. Ohnuki, M. Narita, T. Ichisaka, K. Tomoda, and S. Yamanaka. 2007. 'Induction of pluripotent stem cells from adult human fibroblasts by defined factors', *Cell*, 131: 861-72.

Takahashi, K., and S. Yamanaka. 2006. 'Induction of pluripotent stem cells from mouse embryonic and adult fibroblast cultures by defined factors', *Cell*, 126: 663-76.

Takasato, M., P. X. Er, M. Becroft, J. M. Vanslambrouck, E. G. Stanley, A. G. Elefanty, and M. H. Little. 2014. 'Directing human embryonic stem cell differentiation towards a renal lineage generates a self-organizing kidney', *Nat Cell Biol*, 16: 118-26.

Takayama, K., M. Inamura, K. Kawabata, K. Katayama, M. Higuchi, K. Tashiro, A. Nonaka, F. Sakurai, T. Hayakawa, M. K. Furue, and H. Mizuguchi. 2012. 'Efficient generation of functional hepatocytes from human embryonic stem cells and induced pluripotent stem cells by HNF4alpha transduction', *Mol Ther*, 20: 127-37.

Tam, P. P. 1989. 'Regionalisation of the mouse embryonic ectoderm: allocation of prospective ectodermal tissues during gastrulation', *Development*, 107: 55-67.

Tang, M., Y. Miyamoto, and E. J. Huang. 2009. 'Multiple roles of beta-catenin in controlling the neurogenic niche for midbrain dopamine neurons', *Development*, 136: 2027-38.

Tarbell, N.J., H. Friedman, W.R. Polkinghorn, T. Yock, T. Zhou, Z. Chen, P. Burger, P. Barnes, and L. Kun. 2013. 'High-Risk Medulloblastoma: A Pediatric Oncology Group
Randomized Trial of Chemotherapy Before or After
Radiation Therapy (POG 9031)', *Journal of Clinical Oncology*, 31: 2936.

Taylor, M. D., L. Liu, C. Raffel, C. C. Hui, T. G. Mainprize, X. Zhang, R. Agatep, S. Chiappa, L. Gao, A. Lowrance, A. Hao, A. M. Goldstein, T. Stavrou, S. W. Scherer, W. T. Dura, B. Wainwright, J. A. Squire, J. T. Rutka, and D. Hogg. 2002. 'Mutations in SUFU predispose to medulloblastoma', *Nat Genet*, 31: 306-10.

Taylor, M. D., P. A. Northcott, A. Korshunov, M. Remke, Y. J. Cho, S. C. Clifford, C. G. Eberhart, D. W. Parsons, S. Rutkowski, A. Gajjar, D. W. Ellison, P. Lichter, R. J. Gilbertson, S. L. Pomeroy, M. Kool, and S. M. Pfister. 2012. 'Molecular subgroups of medulloblastoma: the current consensus', *Acta Neuropathol*, 123: 465-72.

Taylor, R. E., C. C. Bailey, K. J. Robinson, C. L. Weston, D. A. Walker, D. Ellison, J. Ironside, B. L. Pizer, and L. S. Lashford. 2005. 'Outcome for patients with metastatic (M2-3) medulloblastoma treated with SIOP/UKCCSG PNET-3 chemotherapy', *Eur J Cancer*, 41: 727-34.

ten Donkelaar, H. J., M. Lammens, P. Wesseling, H. O. Thijssen, and W. O. Renier. 2003. 'Development and developmental disorders of the human cerebellum', *J Neurol*, 250: 1025-36.

Tetsu, O., and F. McCormick. 1999. 'Beta-catenin regulates expression of cyclin D1 in colon carcinoma cells', *Nature*, 398: 422-6.

Thomas, K. R., and M. R. Capecchi. 1990. 'Targeted disruption of the murine int-1 proto-oncogene resulting in severe abnormalities in midbrain and cerebellar development', *Nature*, 346: 847-50.

Thomson, J. A., J. Itskovitz-Eldor, S. S. Shapiro, M. A. Waknitz, J. J. Swiergiel, V. S. Marshall, and J. M. Jones. 1998. 'Embryonic stem cell lines derived from human blastocysts', *Science*, 282: 1145-7.

Triscott, J., C. Lee, C. Foster, B. Manoranjan, M. R. Pambid, R. Berns, A. Fotovati, C. Venugopal, K. O'Halloran, A. Narendran, C. Hawkins, V. Ramaswamy, E. Bouffet, M. D. Taylor, A. Singhal, J. Hukin, R. Rassekh, S. Yip, P. Northcott, S. K. Singh, C. Dunham, and S. E. Dunn. 2013. 'Personalizing the treatment of pediatric medulloblastoma: Polo-like kinase 1 as a molecular target in high-risk children', *Cancer Res*, 73: 6734-44.

Unternaehrer, J. J., and G. Q. Daley. 2011. 'Induced pluripotent stem cells for modelling human diseases', *Philos Trans R Soc Lond B Biol Sci*, 366: 2274-85.

Vaillant, C., and D. Monard. 2009. 'SHH pathway and cerebellar development', *Cerebellum*, 8: 291-301.

Vandendries, E. R., D. Johnson, and R. Reinke. 1996. 'orthodenticle is required for photoreceptor cell development in the Drosophila eye', *Dev Biol*, 173: 243-55.

Vanner, R. J., M. Remke, M. Gallo, H. J. Selvadurai, F. Coutinho, L. Lee, M. Kushida, R. Head, S. Morrissy, X. Zhu, T. Aviv, V. Voisin, I. D. Clarke, Y. Li, A. J. Mungall, R. A. Moore, Y. Ma, S. J. Jones, M. A. Marra, D. Malkin, P. A. Northcott, M. Kool, S. M. Pfister, G. Bader, K. Hochedlinger, A. Korshunov, M. D. Taylor, and P. B. Dirks. 2014. 'Quiescent sox2(+) cells drive hierarchical growth and relapse in sonic hedgehog subgroup medulloblastoma', *Cancer Cell*, 26: 33-47.

Vernay, B., M. Koch, F. Vaccarino, J. Briscoe, A. Simeone, R. Kageyama, and S. L. Ang. 2005. 'Otx2 regulates subtype specification and neurogenesis in the midbrain', *J Neurosci*, 25: 4856-67.

Viswanathan, S. R., and G. Q. Daley. 2010. 'Lin28: A microRNA regulator with a macro role', *Cell*, 140: 445-9.

Vivanco, I., and C. L. Sawyers. 2002. 'The phosphatidylinositol 3-Kinase AKT pathway in human cancer', *Nat Rev Cancer*, 2: 489-501.

Von Hoff, D. D., P. M. LoRusso, C. M. Rudin, J. C. Reddy, R. L. Yauch, R. Tibes, G. J. Weiss, M. J. Borad, C. L. Hann, J. R. Brahmer, H. M. Mackey, B. L. Lum, W. C. Darbonne, J. C. Marsters, Jr., F. J. de Sauvage, and J. A. Low. 2009. 'Inhibition of the hedgehog pathway in advanced basal-cell carcinoma', *N Engl J Med*, 361: 1164-72.

Wang, G., H. Zhang, Y. Zhao, J. Li, J. Cai, P. Wang, S. Meng, J. Feng, C. Miao, M. Ding, D. Li, and H. Deng. 2005. 'Noggin and bFGF cooperate to maintain the pluripotency of human embryonic stem cells in the absence of feeder layers', *Biochem Biophys Res Commun*, 330: 934-42.

Wang, X., C. Venugopal, B. Manoranjan, N. McFarlane, E. O'Farrell, S. Nolte, T. Gunnarsson, R. Hollenberg, J. Kwiecien, P. Northcott, M. D. Taylor, C. Hawkins, and S. K. Singh. 2012. 'Sonic hedgehog regulates Bmi1 in human medulloblastoma brain tumor-initiating cells', *Oncogene*, 31: 187-99.

Wassarman, K. M., M. Lewandoski, K. Campbell, A. L. Joyner, J. L. Rubenstein, S. Martinez, and G. R. Martin. 1997. 'Specification of the anterior hindbrain and establishment of a normal mid/hindbrain organizer is dependent on Gbx2 gene function', *Development*, 124: 2923-34.

Wechsler-Reya, R. J., and M. P. Scott. 1999. 'Control of neuronal precursor proliferation in the cerebellum by Sonic Hedgehog', *Neuron*, 22: 103-14.

Werbowetski-Ogilvie, T. and McClelland, R. 2014. 'Human embryonic stem cells and cancer: modeling disease in a dish.' in, *Cancer Stem Cells* (John Wiley and Sons, Hoboken, NJ: V. K. Rajaskhar).

Werbowetski-Ogilvie, T. E., M. Bosse, M. Stewart, A. Schnerch, V. Ramos-Mejia, A. Rouleau, T. Wynder, M. J. Smith, S. Dingwall, T. Carter, C. Williams, C. Harris, J. Dolling, C. Wynder, D. Boreham, and M. Bhatia. 2009. 'Characterization of human embryonic stem cells with features of neoplastic progression', *Nat Biotechnol*, 27: 91-7.

Werbowetski-Ogilvie, T. E., L. C. Morrison, A. Fiebig-Comyn, and M. Bhatia. 2012. 'In vivo generation of neural tumors from neoplastic pluripotent stem cells models early human pediatric brain tumor formation', *Stem Cells*, 30: 392-404.

Werbowetski-Ogilvie, T. E., M. Seyed Sadr, N. Jabado, A. Angers-Loustau, N. Y. Agar, J. Wu, R. Bjerkvig, J. P. Antel, D. Faury, Y. Rao, and R. F. Del Maestro. 2006. 'Inhibition of medulloblastoma cell invasion by Slit', *Oncogene*, 25: 5103-12.

Wetmore, C., D. E. Eberhart, and T. Curran. 2000. 'The normal patched allele is expressed in medulloblastomas from mice with heterozygous germ-line mutation of patched', *Cancer Res*, 60: 2239-46.

Wiesel, T. N., and D. H. Hubel. 1963. 'SINGLE-CELL RESPONSES IN STRIATE CORTEX OF KITTENS DEPRIVED OF VISION IN ONE EYE', *J Neurophysiol*, 26: 1003-17.

Woodburn, R. T., B. Azzarelli, J. F. Montebello, and I. E. Goss. 2001. 'Intense p53 staining is a valuable prognostic indicator for poor prognosis in medulloblastoma/central nervous system primitive neuroectodermal tumors', *J Neurooncol*, 52: 57-62.

Wortham, M., G. Jin, J. L. Sun, D. D. Bigner, Y. He, and H. Yan. 2012. 'Aberrant Otx2 expression enhances migration and induces ectopic proliferation of hindbrain neuronal progenitor cells', *PLoS One*, 7: e36211.

Wu, G., A. Broniscer, T. A. McEachron, C. Lu, B. S. Paugh, J. Becksfort, C. Qu, L. Ding, R. Huether, M. Parker, J. Zhang, A. Gajjar, M. A. Dyer, C. G. Mullighan, R. J. Gilbertson, E. R. Mardis, R. K. Wilson, J. R. Downing, D. W. Ellison, J. Zhang, and S. J. Baker. 2012. 'Somatic histone H3 alterations in pediatric diffuse intrinsic pontine gliomas and non-brainstem glioblastomas', *Nat Genet*, 44: 251-3.

Wyatt, A., P. Bakrania, D. J. Bunyan, R. J. Osborne, J. A. Crolla, A. Salt, C. Ayuso, R. Newbury-Ecob, Y. Abou-Rayyah, J. R. Collin, D. Robinson, and N. Ragge. 2008. 'Novel heterozygous OTX2 mutations and whole gene deletions in anophthalmia, microphthalmia and coloboma', *Hum Mutat*, 29: E278-83.

Xie, J., R. L. Johnson, X. Zhang, J. W. Bare, F. M. Waldman, P. H. Cogen, A. G. Menon, R. S. Warren, L. C. Chen, M. P. Scott, and E. H. Epstein, Jr. 1997. 'Mutations of the PATCHED gene in several types of sporadic extracutaneous tumors', *Cancer Res*, 57: 2369-72.

Yagi, T., D. Ito, Y. Okada, W. Akamatsu, Y. Nihei, T. Yoshizaki, S. Yamanaka, H. Okano, and N. Suzuki. 2011. 'Modeling familial Alzheimer's disease with induced pluripotent stem cells', *Hum Mol Genet*, 20: 4530-9.

Yang, J., J. Wu, C. Tan, and P. S. Klein. 2003. 'PP2A:B56epsilon is required for Wnt/beta-catenin signaling during embryonic development', *Development*, 130: 5569-78.

Yang, Z. J., T. Ellis, S. L. Markant, T. A. Read, J. D. Kessler, M. Bourboulas, U. Schuller, R. Machold, G. Fishell, D. H. Rowitch, B. J. Wainwright, and R. J. Wechsler-Reya. 2008. 'Medulloblastoma can be initiated by deletion of Patched in lineage-restricted progenitors or stem cells', *Cancer Cell*, 14: 135-45.

Yokota, N., T. G. Mainprize, M. D. Taylor, T. Kohata, M. Loreto, S. Ueda, W. Dura, W. Grajkowska, J. S. Kuo, and J. T. Rutka. 2004. 'Identification of differentially expressed and developmentally regulated genes in medulloblastoma using suppression subtraction hybridization', *Oncogene*, 23: 3444-53.

Zbinden, M., A. Duquet, A. Lorente-Trigos, S. N. Ngwabyt, I. Borges, and A. Ruiz i Altaba. 2010. 'NANOG regulates glioma stem cells and is essential in vivo acting in a cross-functional network with GLI1 and p53', *Embo j*, 29: 2659-74.

Zeltzer, L. K., Q. Lu, W. Leisenring, J. C. Tsao, C. Recklitis, G. Armstrong, A. C. Mertens, L. L. Robison, and K. K. Ness. 2008. 'Psychosocial outcomes and health-related quality of life

in adult childhood cancer survivors: a report from the childhood cancer survivor study', *Cancer Epidemiol Biomarkers Prev*, 17: 435-46.

Zhang, J., G. Wu, C. P. Miller, R. G. Tatevossian, J. D. Dalton, B. Tang, W. Orisme, C. Punchihewa, M. Parker, I. Qaddoumi, F. A. Boop, C. Lu, C. Kandoth, L. Ding, R. Lee, R. Huether, X. Chen, E. Hedlund, P. Nagahawatte, M. Rusch, K. Boggs, J. Cheng, J. Becksfort, J. Ma, G. Song, Y. Li, L. Wei, J. Wang, S. Shurtleff, J. Easton, D. Zhao, R. S. Fulton, L. L. Fulton, D. J. Dooling, B. Vadodaria, H. L. Mulder, C. Tang, K. Ochoa, C. G. Mullighan, A. Gajjar, R. Kriwacki, D. Sheer, R. J. Gilbertson, E. R. Mardis, R. K. Wilson, J. R. Downing, S. J. Baker, and D. W. Ellison. 2013. 'Whole-genome sequencing identifies genetic alterations in pediatric low-grade gliomas', *Nat Genet*, 45: 602-12.

Zhang, Q., and D. D. Eisenstat. 2012. 'Roles of homeobox genes in retinal ganglion cell differentiation and axonal guidance', *Adv Exp Med Biol*, 723: 685-91.

Zhang, Y., J. Laterra, and M. G. Pomper. 2009. 'Hedgehog pathway inhibitor HhAntag691 is a potent inhibitor of ABCG2/BCRP and ABCB1/Pgp', *Neoplasia*, 11: 96-101.

Zhou, H., S. Wu, J. Y. Joo, S. Zhu, D. W. Han, T. Lin, S. Trauger, G. Bien, S. Yao, Y. Zhu, G. Siuzdak, H. R. Scholer, L. Duan, and S. Ding. 2009. 'Generation of induced pluripotent stem cells using recombinant proteins', *Cell Stem Cell*, 4: 381-4.